DEVELOPMENT OF A DOUBLE-SHOOT SYSTEM ON A DISC DRILL

A Thesis Submitted to the College of

Graduate Studies and Research

In Partial Fulfillment of the Requirements

For the Degree of Master of Science

In the Department of Chemical and Biological Engineering

University of Saskatchewan

Saskatoon

By

GUILLAUME CLOUTIER BOILY

PERMISSION TO USE

In presenting this thesis in partial fulfillment of the requirements for a degree of Master of Science from the University of Saskatchewan, I agree that the Libraries of this University may make it freely available for inspection. I further agree that permission for copying of this thesis in any manner, in whole or in part, for scholarly purposes may be granted by the professor or professors who supervised my thesis work or, in their absence, by the Head of the Department or the Dean of the College in which my thesis work was done. It is understood that any copying or publication or use of this thesis or parts thereof for financial gain shall not be allowed without my written permission. It is also understood that due recognition shall be given to me and to the University of Saskatchewan in any scholarly use which may be made of any material in my thesis.

Requests for permission to copy or to make other uses of materials in this thesis/dissertation in whole or part should be addressed to:

Head of the Department of Chemical and Biological Engineering
University of Saskatchewan
57 Campus Drive
Saskatoon, Saskatchewan, S7N 5A9
Canada

OR

Dean
College of Graduate Studies and Research
University of Saskatchewan
107 Administration Place
Saskatoon, Saskatchewan, S7N 5A2
Canada

ABSTRACT

This research project developed a double-shoot apparatus to distribute seeds and fertilizer at an optimal agronomically and widely accepted placement. The research developed different concepts based on the study of the dynamics of the seeding implement affected by the addition of the double-shoot capability to the system. The capabilities were characterized with several field tests to evaluate their performances on different essential aspects of a disc drill. The selected concepts from the field results were validated using Discrete Element Method (DEM) simulations, specially developed and validated with data obtained from the project.

The field tests included the measurements of: seed-to-fertilizer vertical/horizontal separation, 3-D forces, and trials with crop residues. The field tests differed in the number of apparatuses tested, the number of locations used and the period of the year in which they were performed. The validations were based on DEM simulations, which were developed in parallel to an analytical soil mechanics model. The analytical model determined the draft forces on an analytical knife, which was also used into DEM simulations with first-generation soil bins. The drafts measured in first-generation soil bins were compared to the values predicted by the analytical model in order to determine the desired soil properties. The virtual disc drill was used to determine the seed-to-fertilizer reference values for the experiments, to predict the wear pattern of steel ground-engaging tools, and to predict the compressive forces, which were used to predict the wear rate of the knife. The analytical disc drill simulations were performed at two ground speeds prior to wheat sowing.

The analyses that were made on the field results, have demonstrated that the Concept No. 2, and 3 (from a list of 7 concepts) had significant better product placements than the openers used as benchmark single-shoot and double-shoot. Also, these field results highlighted the fact that the

Concepts No. 2, and No. 3 had a slightly better placement than the opener used as benchmark double-shoot from CNH Industrial Ltd. The 3-D force measurement experiments revealed significant difference between the openers depending on the direction (vertical load, side load, draft) of force tested. The forces could be statically different, but not in any major ways, except for the Concept No. 2 side load, which was constantly lower than any other side load forces. The field trials with crop residues revealed that the implements using the Concept No. 2, and 3 had superior performance to manage residues. The implements equipped with these two concepts were the only ones to pass through the varieties of residue and extreme conditions without plugging.

The seed-to-fertilizer values extracted from the simulations were similar to the values from field experiments. Simulations confirmed the positions of high resistance sections (carbides) on the soil/residue scraper and predicted high wear locations on the knife. The simulated wear patterns on the scraper and on the knife were visually confirmed and validated throughout field tests. Furthermore, the knife wear rate prediction was determined using the Archard equation with the simulated compressive forces that requires protection for durability requirements.

ACKNOWLEDGMENTS

I would like to sincerely acknowledge Dr. Martin Roberge, my co-supervisor, for his endless support, technical assistance, and advice throughout the project. I would also like to acknowledge my supervisor Dr. Venkatesh Meda, my Committee Chair Dr. Lope Tabil, and the third member of my Graduate Advisory Committee Dr. Akindele Odeshi, for their valuable inputs.

Special thanks to CNH Industrial Ltd. for their funding, the technical knowledge they provided to me, and for letting me use their facilities and equipment. I would also like to thank the Saskatoon Research & Development department for their technical support, particularly Joel Gervais for his assistance throughout this project.

I would like to thank the University of Saskatchewan, the College of Graduate Studies, the College of Engineering, and the Department of Chemical and Biological Engineering for their funding and support.

I would also like to thank all summer students who helped during the field tests, who are, unfortunately, too numerous to name.

Lastly, I would like to express my deepest thanks to my family and friends for their continuous support and encouragement.

TABLE OF CONTENTS

LIST OF TABLES

LIST OF FIGURES

LIST OF SYMBOLS (NOMENCLATURE)

A_c = Contact area (m^2)

c = Soil cohesion (kPa)

c_a = Calculated soil-to-tool adhesion strength, independent of normal pressure (kPa)

d = Tool depth (m)

F_e = Applied normal load (g)

$F_{c/a}$ = Cohesion and/or adhesion force (N)

F_i = Resultant normal or shear force calculated on the i^{th} element (N)

g = Acceleration due to gravity (9.81 $m \cdot s^{-2}$)

g_i = Gravity acceleration ($m \cdot s^{-2}$)

H = Total draft (kN)

H_g = Material hardness ($10^6 \cdot g \cdot cm^{-2}$)

k = Spring stiffness (contact stiffness)

K = Normal or shear stiffness ($N \cdot m^{-1}$)

K_a = Constant related to the probability per unit encounter of production of a wear particle

m = Total mass of the particle (kg)

m = Mass of the point mass (entire particle) (kg)

N_a = N factor related to the apparatus velocity

N_c = N factor related to soil cohesion

N_{ca} = N factor related to the soil tool adhesion strength

N_q = N factor related to the surcharge pressure vertically acting on the soil surface

N_γ = N factor related to soil density

P = Total ground engaging tool force (kN)

q = Surcharge pressure vertically acting on the soil surface (kPa)

r = Horizontal radius of soil fracture (m)

r/d = Ratio of the horizontal radius of soil fracture on the tool depth ($r/d = \cot\alpha + \cot\beta$)

s = Ultimate width of each side crescent (m)

t_{crit} = Critical time step (s)

U = Overlap (m)

v = Apparatus velocity ($m \cdot s^{-1}$)

v_{ma} = Maximal apparatus velocity parameter ($m \cdot s^{-1}$)

v_{mi} = Minimal apparatus velocity parameter ($m \cdot s^{-1}$)

v_p = Relative velocity ($cm \cdot s^{-1}$)

V_h = Void volume (cm^3)

V_s = Solid volume (cm^3)

V_t = Total volume($V_t = V_h + V_s$), (cm^3)

w = Tool width (m)

W = Wear rate ($cm^3 \cdot s^{-1}$)

$\ddot{x}_i$ = Particle acceleration ($m \cdot s\text{-}^2$)

$\%_{ps}$ = Straw pore space percentage (%)

α = Tool rake angle (degrees) from the horizontal (˚)

β = Wedge angle degrees (˚)

γ = Soil density ($t \cdot m^{-3}$) or ($kN \cdot m^{-3}$)

δ = Angle of friction between soil and the tool material (degrees) (˚)

ξ = Cohesion energy density ($J \cdot m^{-3}$)

φ = Angle of internal friction (degrees) (˚)

1.0 INTRODUCTION

The development of this project will be realized in agricultural mechanization, specifically on air seeders. A seeder is a farm implement that creates soil furrows where grains can be deposited with an optimal placement favoring seed growth.

The seeders from the first horse-drawn mechanical Seed Drill machine in 1701 by Jethro Tull to the 1960 seeders comprised almost the same key components: a seed box on top of the metering system and a seed tube under it. The seed in the seed box goes through the metering system, dropping through the seed tube by gravity and going into the soil by a furrow opener. This type of seeder which is named Seed Drill, Grain Drill, or Box Seeder can perform greatly, but has some limitations.

Box seeders are limited to a maximum width of around 13.72 m (45 ft.). For this specific width, it is often composed of three 4.47 m (15 ft.) seeders with heavy linkage to allow the motion of the two seeders on the extremities. The seed reserve covers the entire metering system and needs to be filled in its entire width, which makes the filling tedious. Also, the seed reserve is limited in volume due to its placement on the top of the drill. The seeds are distributed from the tank through the seed meter and then from a tube into the ground by gravity. By using gravity only, it is easier to create a wad in the seed tubes compared to an air seeder. The ground opener of the box seeders can project soil particles into the tube and cause seed pile-up, which plugs the system. Furthermore, the spacing between two units of seeding or furrow openers cannot be modified compared to delivering seed and/or fertilizer to any type of air drills with various spacing of ground engaging tools.

Air seeders are more complex than box seeders and normally require more electronics and controllers. The air seeder distributes the seeds with a flow of air; when properly adjusted, air flow

prevents soil particles from accumulating into the seed tube and greatly reduces the chances of plugging the product delivery system. Moreover, the air seeder has almost no limit for width until the traction of the tractor to pull the air seeder and air drill becomes an issue. An air seeder consists of a seed tank, a metering system, a fan, an assembly of hoses or tubes connected to an air drill (frame, linkages, and wheels), and some furrow openers. The tank can be mounted on the air drill directly, or it can be on a cart which is either towed between the tractor and the drill or towed behind the drill. The mounted seed tank on an air drill can have a capacity of up to 3524 liters (100 bushels), whereas a tank mounted on an air cart can have a capacity of 33477 L (950 bushels). The geometries and settings of the seed/fertilizer metering system is similar to a box seeder; however, the metering system delivers the seeds into an air flow inlet, which in some cases features a Venturi section that minimizes the risk of plugging. The hoses transport the products from the metering system to the furrow openers by passing through the air drill. The air drill is a wheeled structure that holds the furrow openers and allows a vertical movement from the ground. Furrow openers are available in many different types, but mainly (passive) hoe openers and single/double disc openers.

Hoe openers look like a modified shovel from a cultivator, which are designed to introduce one, two, or more products into the ground; all these products are in different furrows. The disc drill is an assembly of static and dynamic parts, a lot more complicated than a hoe opener, but allows for faster seeding ground speed. However, disc openers can more often sow directly without primary or secondary tillage on the field, which is often not the case for hoe openers due to the obstruction of residues left by the last growing season. The disc opener assembly is offered in many geometries by farm equipment manufacturers. The assembly is normally made up of a linkage, a main structure, a gauge wheel, a tillage disc (either with a scraper or a second disc), a

system to adjust the seeding depth, and a packing wheel to close the furrow. The linkages allow the rotation of the assembly to allow seeding or a transport position. The linkage is often formed by two armed parallel linkages or by only one arm for a single linkage. The main structure is normally an iron cast piece which maintains all the different parts together. The gauge wheel determines the depth where the seed or fertilizer is placed. Moreover, the gauge wheel can be used like a dirt/mud remover on the disc. The disc components are primarily used as a rotating soil opener. The packing wheel compresses the ground around and on top of the seeds and/or fertilizer to optimize the emergence of the crops.

Fertilizer mid-row banders (seeding a single row of fertilizer at a higher rate in between two rows of seeds) can be installed on a disc drill to minimize the number of fertilizer ground engaging tools, but the fertilizer is placed far from the seed and could make it available late in the growth of the crop. Using an integrated double-shoot system, the fertilizer is close to the seed to provide nutrients at the beginning of the crop growth (critical moment). Using such seeding geometry, the fertilizer is close to the seed but not in the same furrow, to avoid burning the seed.

2.0 OBJECTIVES

Research Objectives:

The research objective is to determine the best method of placing fertilizer precisely in the ground at an optimal distance away from the seeds without causing any damage to the seed or disrupting the seed bed. The overall objective is to study the dynamics of the seeding implement affected by the addition of double-shoot capabilities to the system.

Main Objective:

- To develop a seed-row unit for placing fertilizer and seeds simultaneously in the soil in a single pass as function of crop types and yield residues from the previous year.

Specific Objectives:

The specific objectives are to Develop and validate a Discrete Element Method (DEM) model that can be used to:

1. Develop a concept of seed-row unit that minimizes the variance of the seed and fertilizer spatial distribution into the soil compared to a predetermined agronomically widely accepted seed/fertilizer placement.
2. Minimize the horizontal draft (and corresponding fuel consumption) to pull the seeding row units, using an analytical model of soil mechanics to predict the soil fracture and draft forces on the ground engaging tool.
3. Minimize the wear characteristics of the tillage tools (knife and disc mud/residue scraper) in order to maximize the life expectancy of the seeding row unit and lower the maintenance costs.

2.1 Organization of the Thesis

The thesis is divided in eight chapters as follows: Introduction, Objectives, Literature Review, Material and Methods, Results and Discussion, Summary and Conclusions, Recommendations, References, and Appendices.

The Introduction chapter introduces seeders from the first horse-drawn mechanical seed machine to a modern air seeder. The seeders are introduced by describing their general operation methods, and the parts involved throughout the seeding flow. In addition, the introduction presents the different types of air seeders with their characteristics and introduces the importance of having the fertilizer close to the seed furrow.

The Objectives chapter describes precisely the project research objectives, the main objectives, and the specific objectives.

The Literature Review chapter presents the patents related to the disc drill, which have a double-shoot function on the seed row units (single-shoot operation means seeding one product only (usually seeds) and double-shoot means delivering seeds and fertilizer). This section relates the importance of fertilizer placement versus the seed, and the consequence of a poor fertilizer distribution. Also, this section presents the direct seeding advantages and general characteristics of wheat, canola, and ammonia fertilizer, which are the products used during the field tests. Furthermore, the Literature Review section details the discrete element method (DEM) by providing short descriptions of the method of field applications, by detailing the physical properties of the products employed during the simulations, and by illustrating the possible physical interactions with the method. Moreover, this section presents the different wear characterization techniques that can be employed to characterize wear on ground engaging tools.

The Material and Methods chapter describes all the important characteristics of the apparatus and locations, in addition to detailing the methodologies for the field and validation experiments. This section presents the methodology for the seed/fertilizer placement experiment, the 3-D force experiment, and the experimental field trials with crop residues effect on thrash flow. Also, this section presents the parameters and the formulas used to create the analytical model. Furthermore, the elements used to elaborate the DEM simulations, and the development of the simulations themselves are presented at the end of the Material and Methods section.

The Results and Discussion chapter presents the results collected to characterize the fields. This section describes and comments on the statistical results obtained for the seed-to-fertilizer experiment and the 3-D force experiment. Also, this section provides the DEM validation results for the analytical model and the seed/fertilizer placement experiment. Furthermore, the DEM validation subsection provides wear rates predictions and wear rates estimations based on the DEM validation results.

The Conclusion and Recommendations chapter includes conclusions directly related to the objectives from the tests and analyses realized throughout the project. These recommendations are made to refine the use of the apparatus and improve its mechanical performance.

The reference section presents a complete list of references used throughout the text.

The Appendix section displays the totality of figures or graphs created for the experiments or the validations. Also, Section A presents raw data graphs for soil characterization.

3.0 LITERATURE REVIEW

The Literature Review chapter presents the following: the patents regarding disc drill double-shoot openers, the importance of placing the fertilizer at an optimal distance from the seeds, the advantages of direct seeding, the general characteristics of the products used during field testing, the introduction to the discrete element method (DEM), and the wear characteristic of ground engaging tools. The wear characteristic section presents the different techniques to characterize the wear such as laboratory methods, ASTM standard procedures, soil bin trial, and field testing. Also, the wear characterization section describes the DEM method applied to predict the amount of wear on implements.

3.1 Disc Drill Double-Shoot Openers Patents

This section presents the patents related closely to a system using discs to provide two different granular agricultural products (seeds or fertilizer) into the ground on the same assembly. Furthermore, this section describes the characteristics of each system and how implements work to distribute these products.

3.1.1 Allis Chalmers

The patent attributed to Allis Chalmers Manufacturing Company (U.S. Patent No. 2,869,489, 1959) describes a double-seed boots assisted by a curved disc (Figure 3.1). The edge of the curve disc is aligned in the direction of travel to create a furrow with the boot located on the convex side, which keeps the trench opened. The fertilizer (28) is placed using the first section of the boot and pushed to the side by an angled wall. The angled wall is the beginning of the second section of the seed boot, where the seed (29) is deposited. The products are placed on both sides of a single trench at the same level as shown in Figure 3.2.

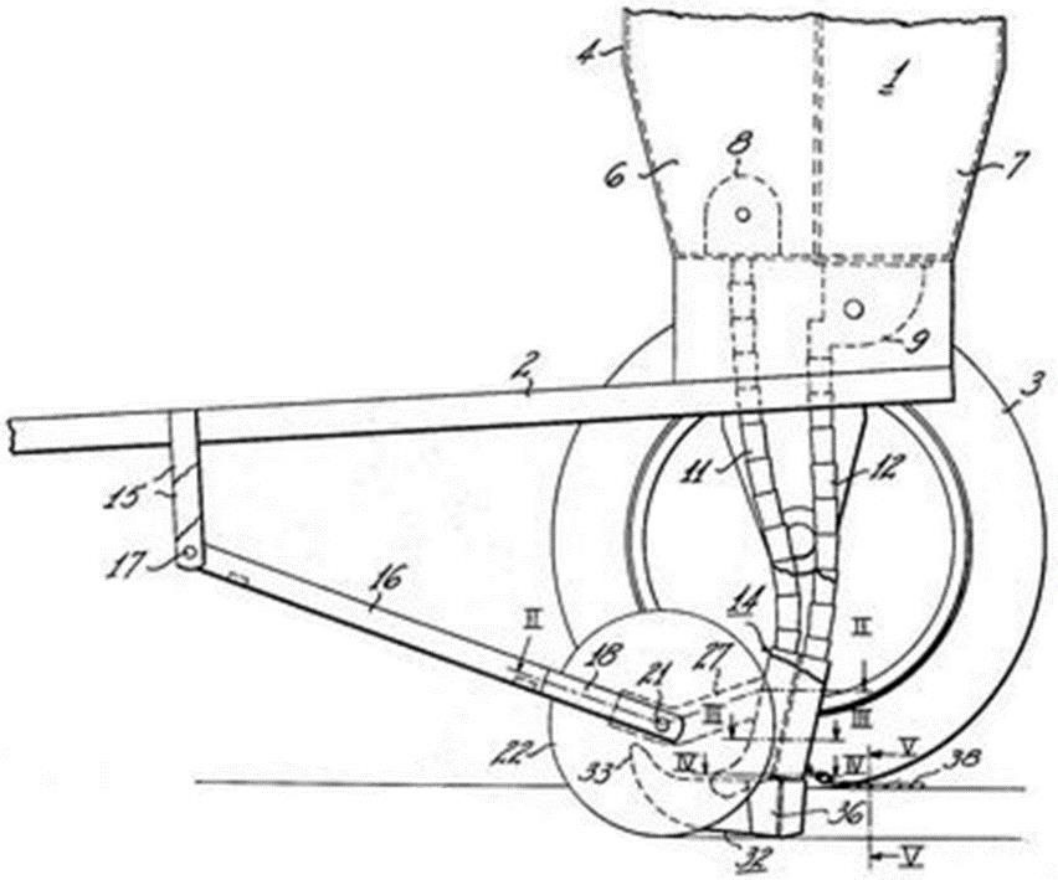

Figure 3.1. Allis Chalmers Manufacturing Company opener (U.S. Patent No. 2,869,489, 1959).

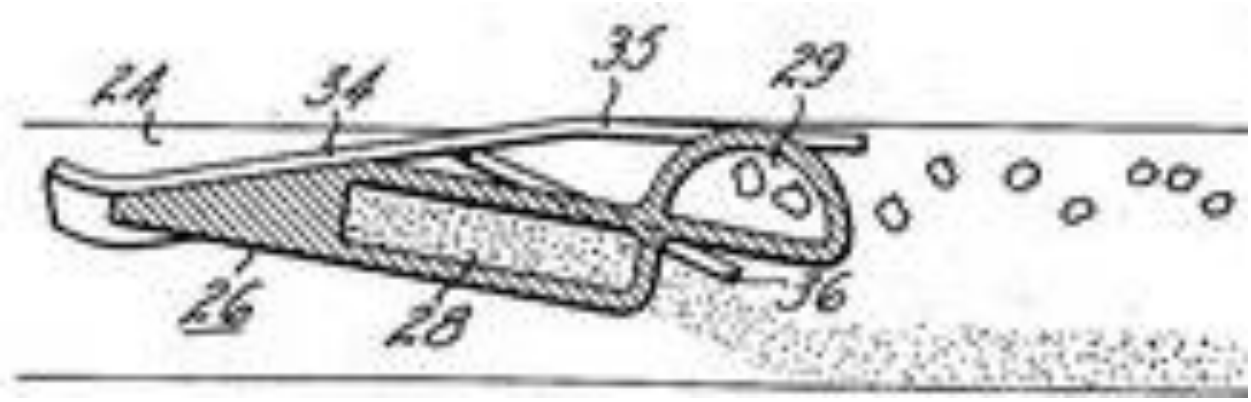

Figure 3.2. Allis Chalmers Manufacturing Company seed (29) and fertilizer (28) placement (U.S. Patent No. 2,869,489, 1959).

3.1.2 Aspinwall Manufacturing

The patent assigned to Aspinwall Manufacturing Company (U.S. Patent No. 1,012,118, 1911) defines a straight disc (α) assisted by a mouldboard on each side (Figure 3.3). The fertilizer is distributed on each side of the opener disc (α) to be mixed with the ground at the trench bottom. The opener can only distribute a mixture of seed/fertilizer or single product due to its single distribution tube, which is divided in two before the disc (α) as displayed in Figure 3.4.

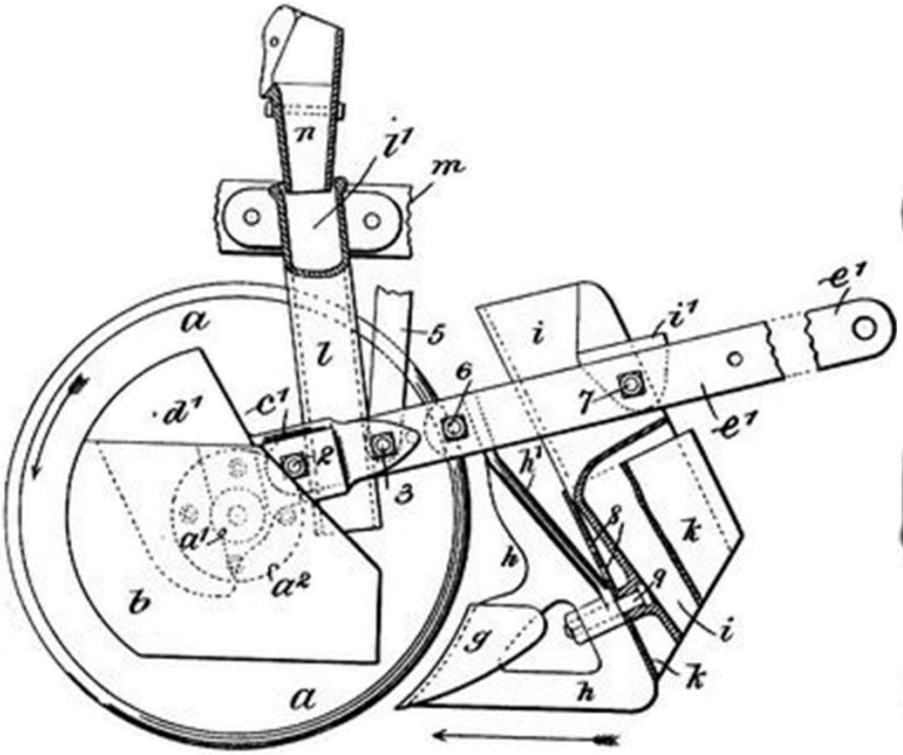

Figure 3.3. Aspinwall Manufacturing Company Opener (U.S. Patent No. 1,012,118, 1911).

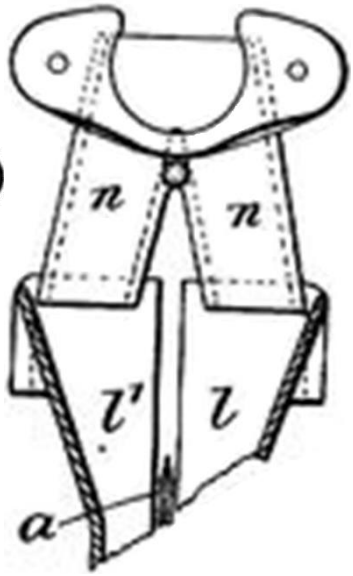

Figure 3.4. Aspinwall Manufacturing Company delivery system (U.S. Patent No. 1,012,118, 1911).

3.1.3 Atom-Jet SDX Double-Shoot System

The patent related to the SDX Double-Shoot System attributed to Atom-Jet Industries (U.S., Patent No. 7,568,438, 2009) characterizes a modified scraper from a Case IH SDX™ opener (Figure 3.5). The scraper has the same dimensions as the original, but a supplementary tube is added at the scraper end to create the double-shoot function. The fertilizer (110) is distributed first and deeper by the main apparatus (Disc and Scraper) instead of the seed (104), which is delivered on the side by the scraper double-shoot function (Figure 3.6).

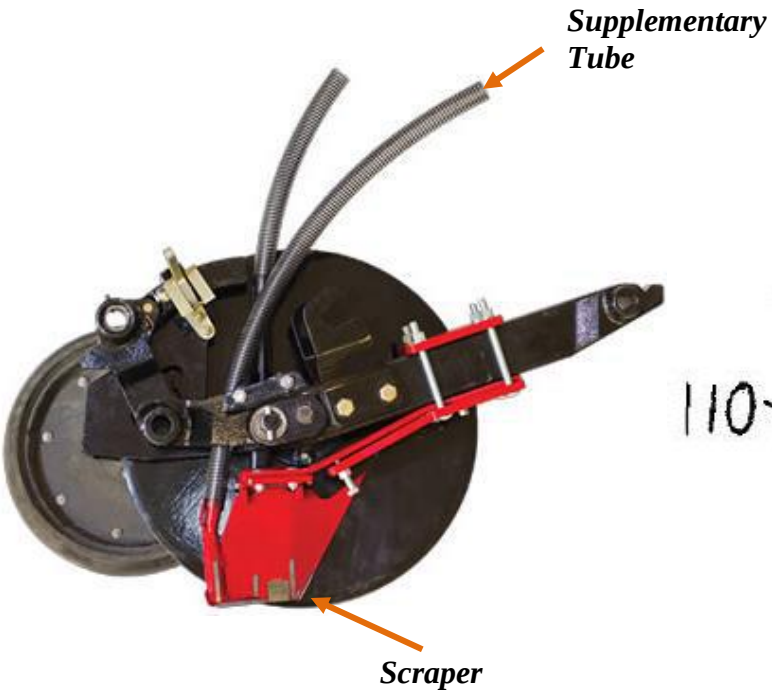

Figure 3.5. Atom-Jet scraper on a CASE IH SDX opener (Courtesy of Atom-Jet Industries website-http://agriculture.atomjet.com/sdx-series/).

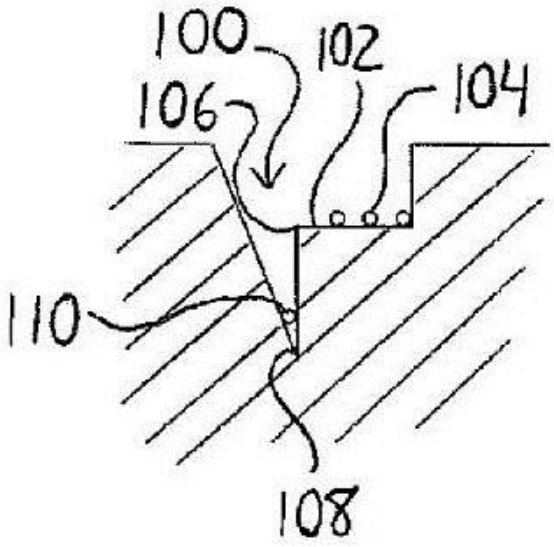

Figure 3.6. Atom-Jet seed (104) and fertilizer (110) placement (U.S., Patent No. 7,568,438, 2009).

3.1.4 Barton™ Double-Shoot Opener

Figure 3.7 shows a drawing of the patented Barton™ Double-shoot Opener by Flexicoil (European Patent No. 1,002,457, 2000), (U.S. Patent No. 5,609,114, 1997) (European Patent No. 0,677,239, 1995). It comprises an assembly of two straight staggered discs assisted by residue scrapers (Figure 3.7). The first disc dispenses the fertilizer (80) deeper and offset from the seed (84) row created by the second disc, as presented in Figure 3.8. The two discs are driven through the ground with a compound angles from the vertical and the direction of travel as displayed in Figure 3.8

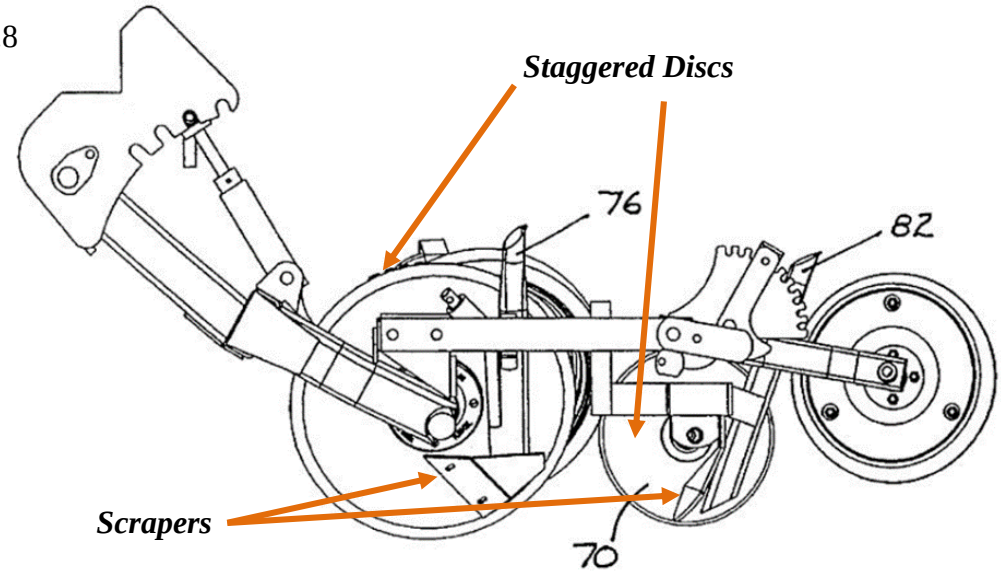

Figure 3.7. Barton™ Double-Shoot opener by Flexicoil (U.S. Patent No. 5,609,114, 1997).

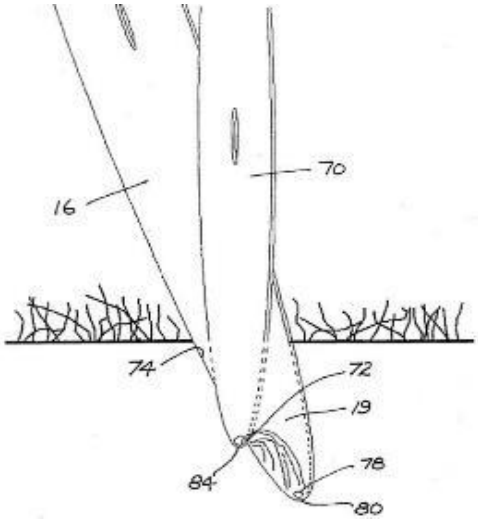

Figure 3.8. Drawing of Barton™ Double-Shoot Opener by Flexicoil showing seed (84) and fertilizer (80) placement (U.S. Patent No. 5,609,114, 1997).

3.1.5 Concept of Bogachev et al.

The patent attributed to Bogachev, V. D., Bogachev, K. D. and Bogachyova V. D. (Soviet Union Patent No. 491,340, 1975) illustrates a double disc opener with two independent seed boots (Figure 3.9). The two discs of different size use the same axis to distribute the products. The fertilizer (5) is distributed by the tube on the side of the biggest disc instead of the seed (4), which is delivered by the tube on the side of the smallest disc (Figure 3.10). The biggest disc allows deeper penetration into the ground to place the fertilizer lower than the seed. The fertilizer while being below creates a reasonable separation between the fertilizer furrow and the seed furrow. The two seed boots (4 and 5) are inside the shadow created by the disc assembly (Figure 3.10).

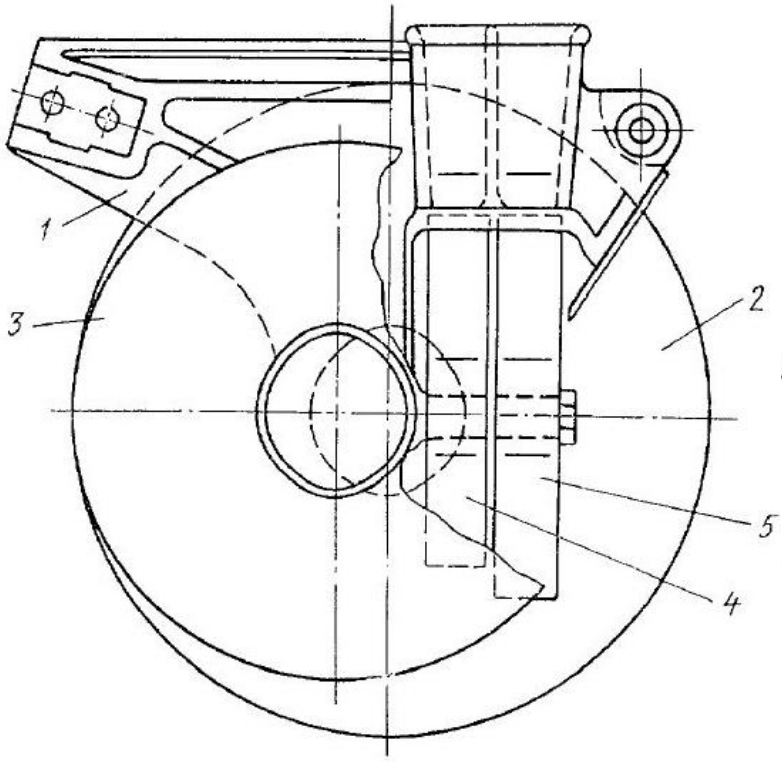

Figure 3.9. Concept of Bogachev, V. D., Bogachev, K. D. and Bogachyiva, V. D. Opener Side View (Soviet Union Patent No. 491,340, 1975)

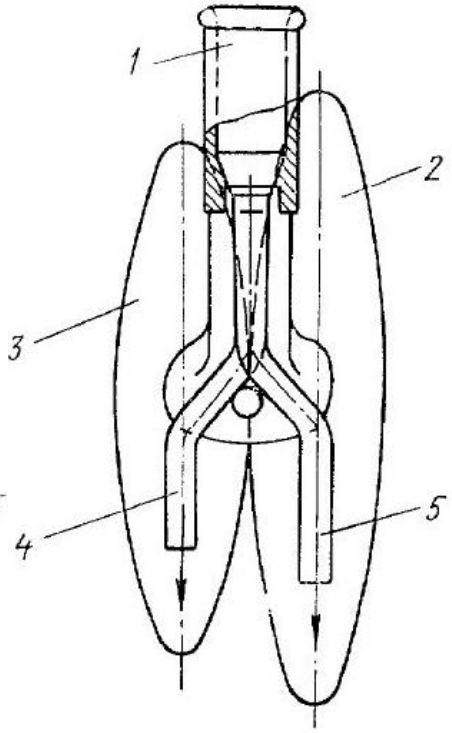

Figure 3.10. Concept of Bogachev, V. D., Bogachev, K. D. and Bogachyova, V. D. Opener Rear View, Seed (4) and Fertilizer (5) Placement (Soviet Union Patent No. 491,340, 1975)

3.1.6 Bourgault Industries Seed Boot/Scraper

The patent granted to Bourgault Industries Ltd. (U.S. Patent No. 7,681,656, 2010) describes a single-shoot disc opener with the possibility of installing a winged seed boot/scraper to replace the standard scraper (Figure 3.11). The seed boot/scraper is a double function scraper exactly like the Pillar Laser Disc/Hoe Opener. The fertilizer is placed into the furrow created by the disc and the scraper instead of the seed, which is introduced by the winged scraper. The wing of the scraper creates a furrow on the side of the fertilizer furrow, which is specially placed shallower and following the fertilizer distribution, to not disturb the seed placement (Figure 3.12). The disc operates with an angle from the vertical and the travel direction (compound angle) to create furrows. The winged boot/scraper cannot be used with spacing under twelve inches, due to the increase of force caused by the scraper wing.

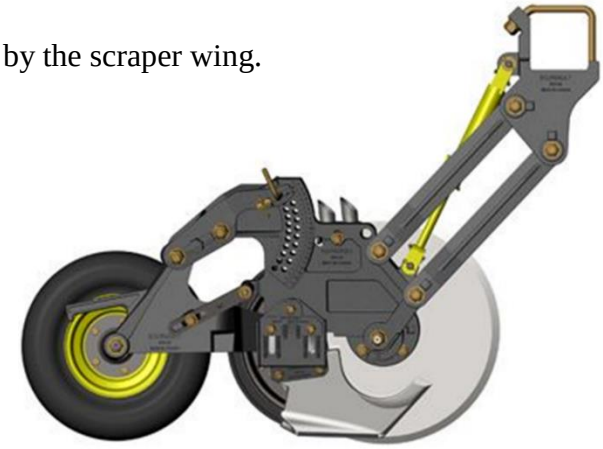

Figure 3.11. Bourgault Industries Ltd. opener with the winged seed boot/scraper (Courtesy of Bourgault North America website-http://www.bourgault.com/SearchProduct/ViewProduct/tabid/168/language/en-US/Default.aspx?docid=709&New=true&IsSearch=false).

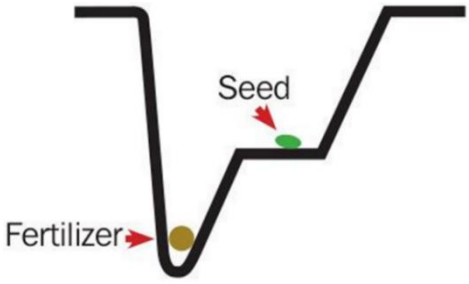

Figure 3.12. Bourgault Industries Ltd. Seed and fertilizer placement with the winged seed boot/scraper (Courtesy of Bourgault North America website-http://www.bourgault.com/SearchProduct/View Product/tabid/168/language/en-US/Default.aspx?docid=709&New=true&IsSearch=false).

3.1.7 Charles E. Patric (1918)

The patent attributed to Charles E. Patric (U.S. Patent No. 1,254,266, 1918) describes a two-shoe/runner (section of the opener sliding on the ground) opener, assisted by a curved disc (15) and a steel wheel (10) (Figure 3.13). The curved disc is maintained in place by the nose of the first runner, which is connected at its center to the main seeding unit frame. The shape of the first runner follows the curved disc to finalize the fertilizer furrow. The second shoe (4) is in line with the first runner (3) (Figure 3.14), but behind the empty space (void) between the numbers 1 and 2, displayed in Figure 3.13. According to the patent, the void between the runners allows enough time to cover the fertilizer with a soil layer, before the second runner distributes the seeds on top. The output of the second runner is larger and shallower than the first to keep the protective layer of soil between the seeds and the fertilizer. The layer is supposed to be uniform and thick enough to protect the seeds from ammonia burning.

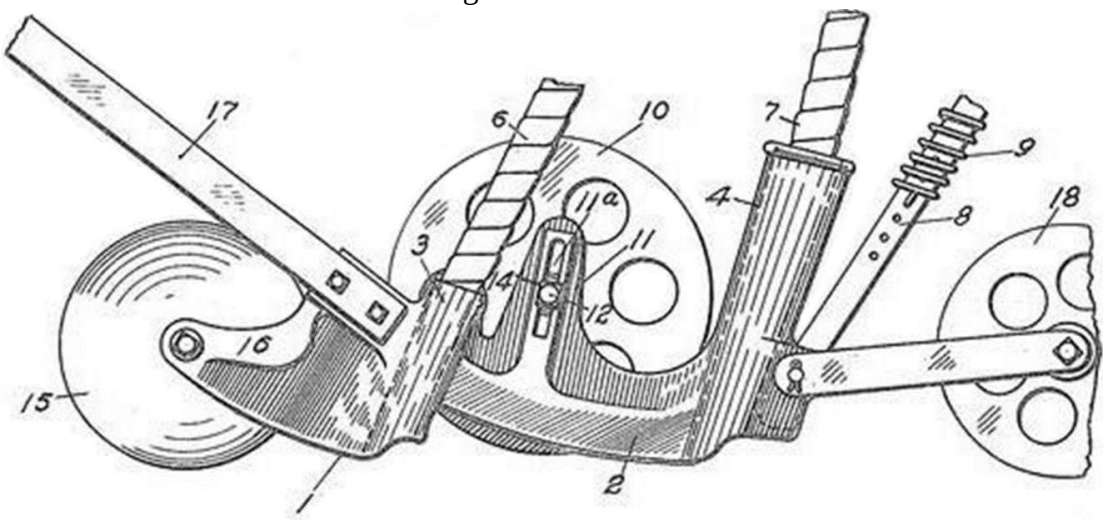

Figure 3.13. Charles E. Patric opener 1918 (U.S. Patent No. 1,254,266, 1918).

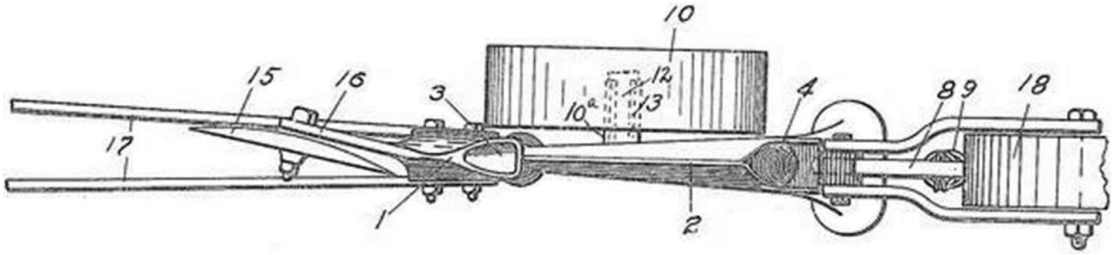

Figure 3.14. Charles E. Patric opener 1918 bottom view, seed (3) and fertilizer (4) outputs (U.S. Patent No. 1,254,266, 1918).

3.1.8 Charles E. Patric (1917)

The patent attributed to Charles E. Patric (U.S. Patent No. 1,229,194, 1917) shows a disc drill opener assisted by a double function runner (section of the opener sliding on the ground). The concave-convex disc located in the front of the opener creates the fertilizer furrow in collaboration with the runner nose (Figure 3.15). The heel of the runner creates the seed furrow staggered with respect to the fertilizer furrow. The fertilizer furrow (12) is created around 50 mm deep, whereas the seed furrow (5) is formed at a 12.7mm depth, approximately (Figure 3.16).

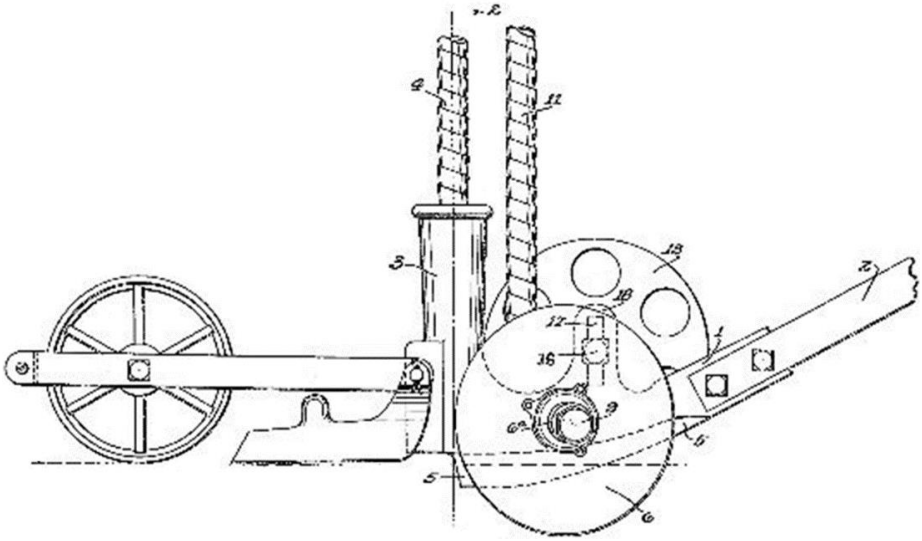

Figure 3.15. Charles E. Patric opener 1917 (U.S. Patent No. 1,229,194, 1917).

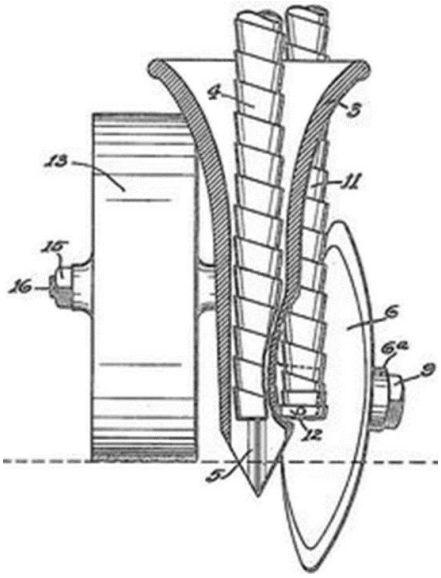

Figure 3.16. Charles E. Patric opener 1917 rear view, seed (5) and fertilizer (12) outputs (U.S. Patent No. 1,229,194, 1917).

3.1.9 Clean Seed

The patent for the Clean Seed Capital Group Ltd. (World Intellectual Property Organization Patent No. 2014/183,182, 2014) describes an entire sowing machine. The furrows are created by a straight notch disc aligned with the direction of travel, followed by a hoe opener (Figure 3.17). The hoe opener shovel delivers the products in three independent furrows created by three separate outputs: back, side, and middle (Figure 3.18). The back output and side output are on the same level, and the middle output is lower than the two other outputs. The three holes are managed by six independent wireless meters, which deliver products at independent rates in the chosen output. The six meter rates can be managed independently from six different gradient maps, which are combined with the tractor Global Positioning System (GPS).

Figure 3.17. Clean Seed Capital Group Ltd. Opener assembly (Courtesy of Clean Seed Capital Group website-http://www.cleanseedcapital.com/cx-6tridenttechnology.html).

Figure 3.18. Clean Seed Capital Group Ltd. Triple output hoe (Courtesy of Clean Seed Capital Group website-http://www.cleanseedcapital.com/cx-6tridenttechnology.html).

3.1.10 CNH (2014, 2012, 2010)

The patents attributed to CNH Canada Ltd. (U.S. Patent No. 8,646,395, 2014), (U.S. Patent No. 8,272,339, 2012), (U.S. Patent No. 8,015,933, 2011), (U.S. Patent No. 7,814,847, 2010) shows a disc opener assembly, which delivers the seed and fertilizer at the same time (Figure 3.19). The disc of the opener, assisted by a scraper, operates with an angle from the travel direction to create the fertilizer furrow. The fertilizer furrow (22) is formed first and is deeper than the seed furrow (62) (Figure 3.20). The seed is delivered into an independent furrow (62) created by the side of the fertilizer furrow (Figure 3.20) with a knife (44) behind the scraper (36) (Figure 3.19). The knife depth and the scraper depth can be adjusted independently to provide an optimal seed versus fertilizer placement. Furthermore, the seed and fertilizer furrows are compacted by a threaded packing wheel, which is adjustable in pressure to provide the best emergence rate possible.

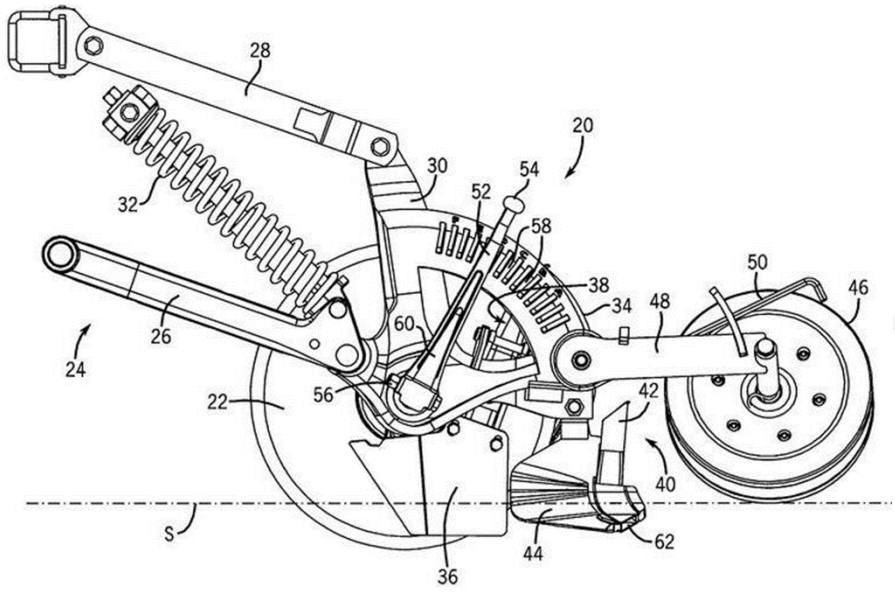

Figure 3.19. CNH Canada Ltd. opener (U.S. Patent No. 8,646,395, 2014).

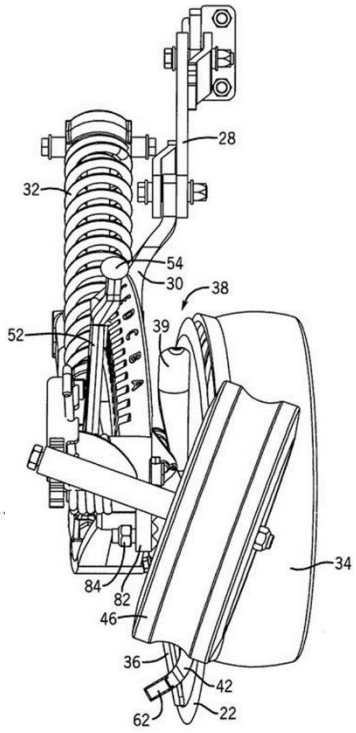

Figure 3.20. CNH Canada Ltd. seed (62) and fertilizer (22) placement (U.S. Patent No. 8,646,395, 2014).

3.1.11 CNH (2007)

The patent accredited to CNH Canada Ltd. (U.S. Patent No. 7,673,571, 2007) illustrates a double-shoot apparatus where the fertilizer furrow is created first with a large disc in collaboration with a residue scraper (Figure 3.21). The seeds are introduced in a furrow created by the side of the fertilizer furrow by a firming wheel, which acts as an opener with a scraper for this concept (Figure 3.22). The firming wheel partially covers the fertilizer furrow (244) when it creates the seed furrow (252), as shown in Figure 3.22. The packing wheel covers the furrows, and at the same time compresses the soil to facilitate seed emergence.

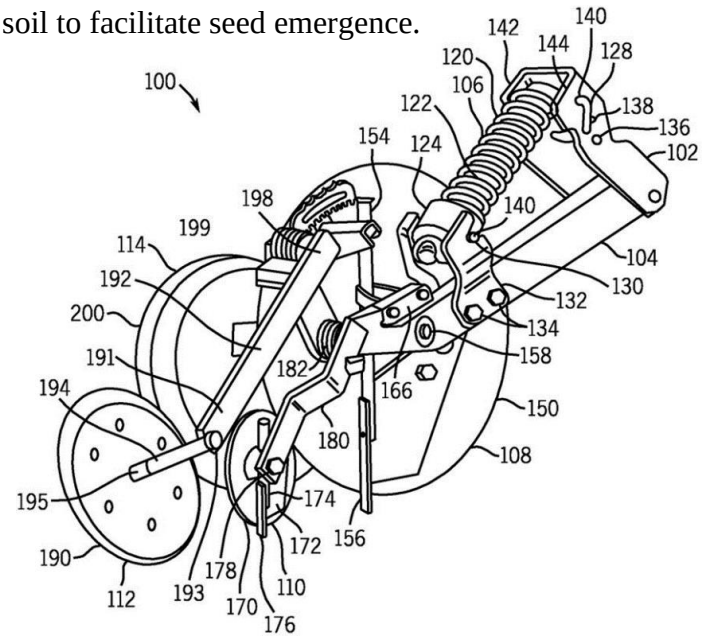

Figure 3.21. CNH Canada Ltd. SDX Double-Shoot Concept (U.S. Patent No. 7,673,571, 2007).

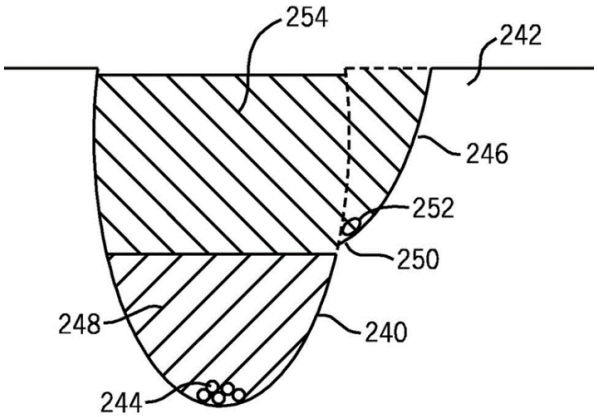

Figure 3.22. CNH Canada Ltd. SDX Double-Shoot Concept, seed (252) and fertilizer (244) placement (U.S. Patent No. 7,673,571, 2007).

3.1.12 Concord

The patent accredited to Concord, Inc. (U. S. Patent No. 4,611,545, 1986) details a layout of three double-disc openers (Figure 3.23). Two openers deliver the seeds (120, 122) while one opener distributes the fertilizer (80) centrally in a front row (Figure 3.24 Each opener distributes the seed at a similar depth and equivalent distance of the fertilizer to provide a homogeneous access to the nutrients. This patent presents the possibility to provide the fertilizer with an independent implement, and it is the only patent described in this literature review representing this method of depositing the product.

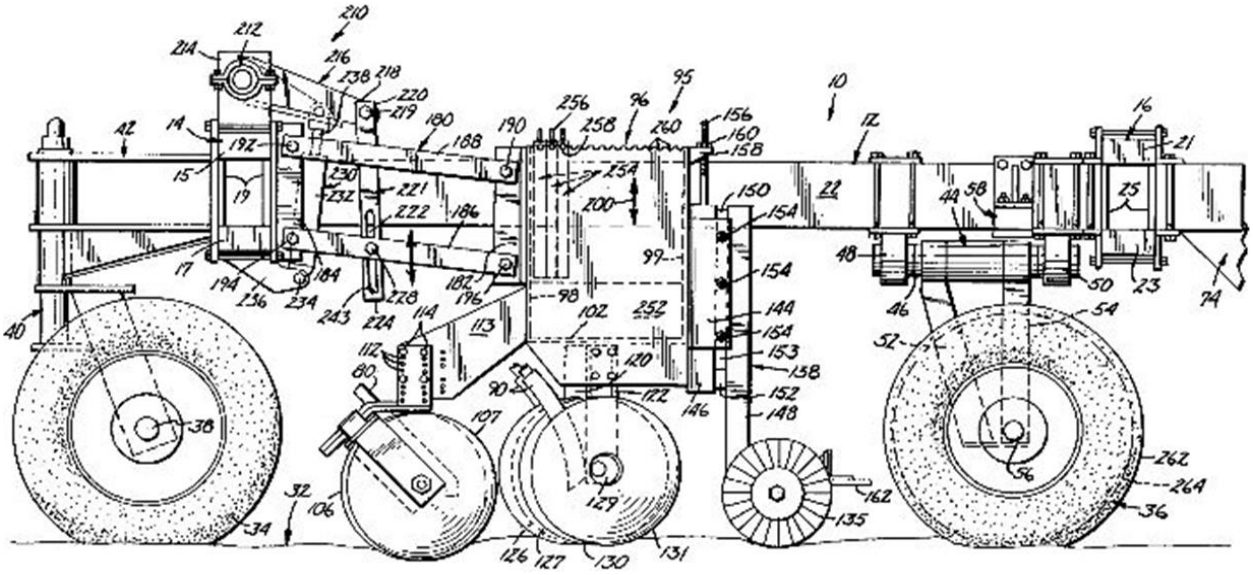

Figure 3.23. Concord Inc. complete drill (U. S. Patent No. 4,611,545, 1986).

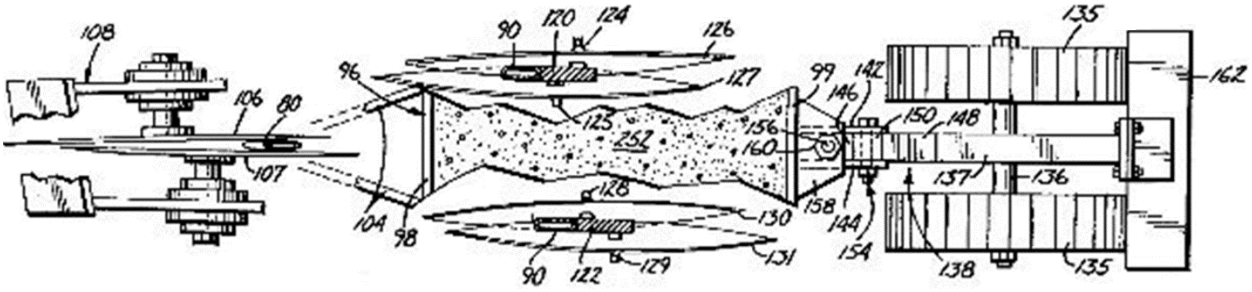

Figure 3.24. Concord Inc. opener seed (120 and 122) and fertilizer (80) placement (U. S. Patent No. 4,611,545, 1986).

3.1.13 Cross Slot No-Tillage

The patent granted to Cross Slot No-Tillage System™ (U.S. Patent No. 5,269,237, 1993) illustrates a tine opener divided in two on each side of a disc (Figure 3.25). The notched disc is straight, aligned into the direction of travel to increase the success of going through the field residues. One tine distributes the seeds and the other one distributes the fertilizer as shown in Figure 3.25. The tines can be adjusted in depth to provide an optimized seed/fertilizer separation or removed as displayed in Figure 3.26.

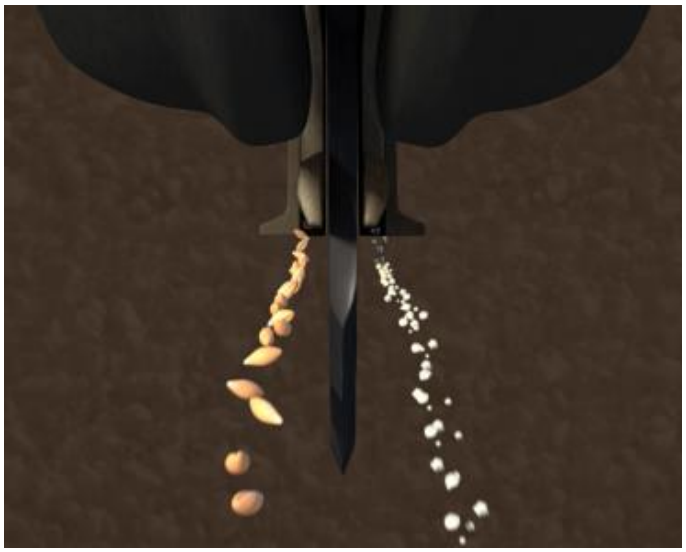

Figure 3.25. Cross Slot No-Tillage System seed and fertilizer placement (Courtesy of Cross Slot No-Tillage Systems website- http://www.crossslot.com/modules/SP_Gallery/gallery.php?gallery=1).

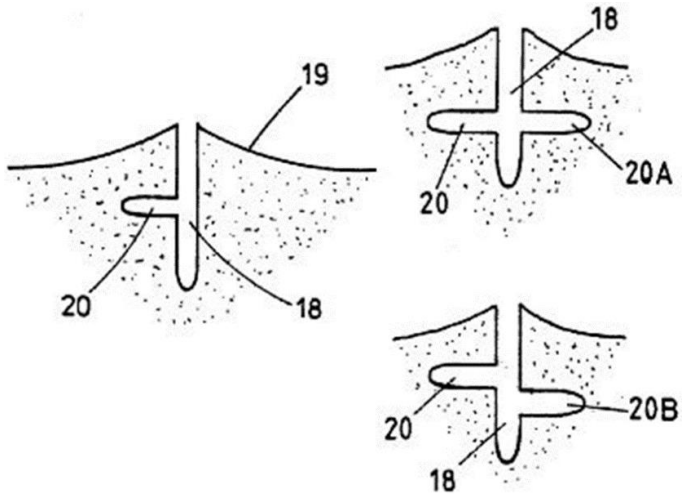

Figure 3.26. Cross Slot No-Tillage System configuration of the furrow (U.S. Patent No. 5,269,237, 1993).

3.1.14 International Harvester™

The patent attributed to International Harvester Company (U.S. Patent No. 3,213,812, 1965) describes a single disc angled into the direction of travel, which is assisted by a dual-purpose scraper (Figure 3.27). The front of the scraper dispenses the fertilizer (31) deeper, and staggered from the seeds (30), which are delivered by the second section (rear) of the scraper (Figure 3.28). There is a notch between the first and the second parts of the scraper to allow the soil to pass through and cover the first furrow created by the scrapper nose.

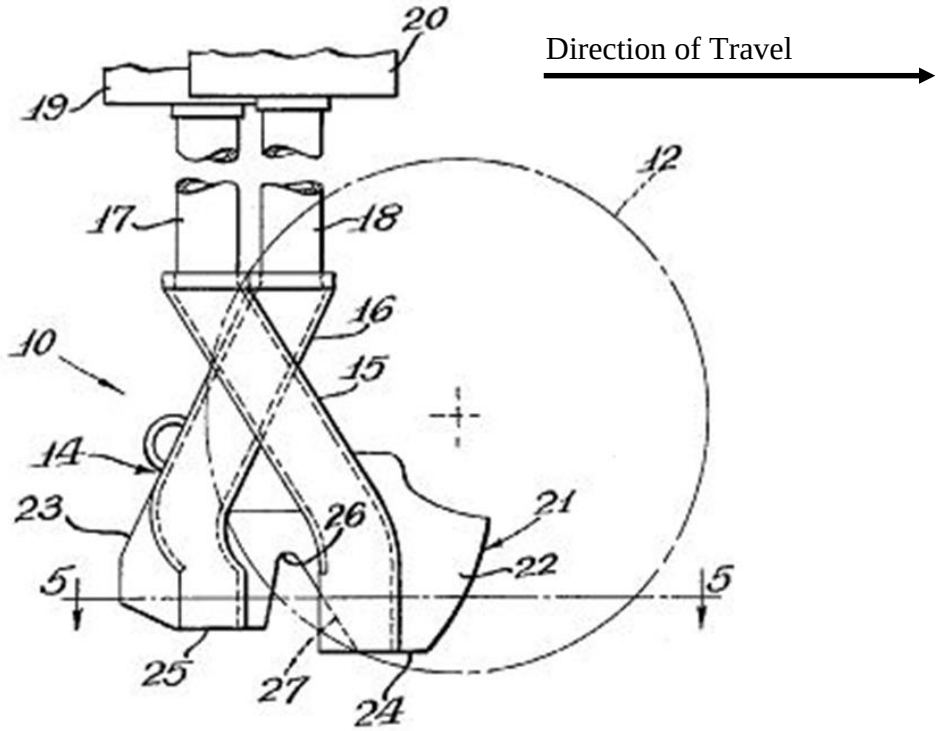

Figure 3.27. International Harvester Company opener (U.S. Patent No. 3,213,812, 1965).

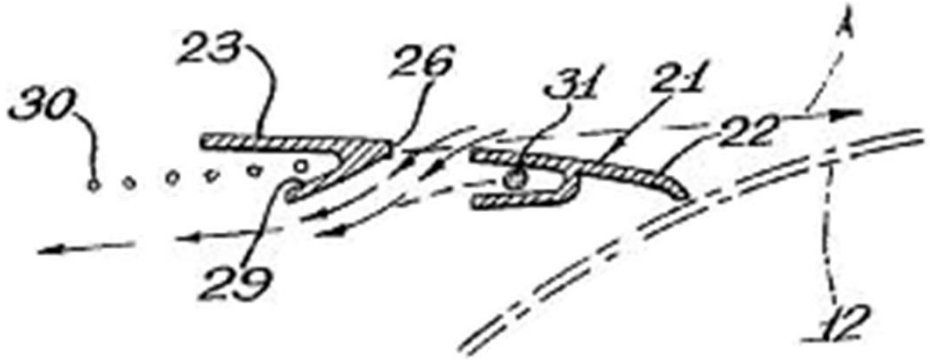

Figure 3.28. International Harvester Company seed (30) and fertilizer (31) placement (U.S. Patent No. 3,213,812, 1965).

3.1.15 John Deere (2000)

The patents credited to the John Deere Company (U.S. Patent No. 6,032,593, 2000) (European Patent No. 0,956,755, 1999) characterizes a double-shoot apparatus composed of a straight (24) and curved disc (70) (Figure 3.29). The straight disc creates the fertilizer furrow with a scraper and its compound angle. The curved disc covers the fertilizer furrow while simultaneously creating the seed furrow. The curved disc, assisted by a scraper, distributes the seed (S) shallower and staggered from the fertilizer (F) (Figure 3.30). The seed furrow is covered and compressed by an angled packing wheel.

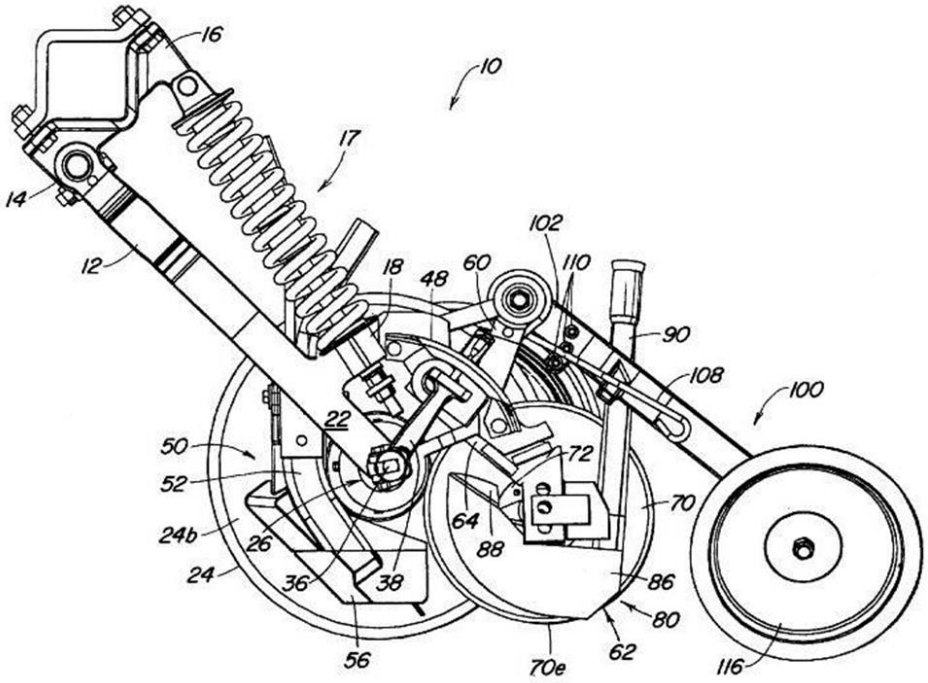

Figure 3.29. Deere and Company double-shoot opener (U.S. Patent No. 6,032,593, 2000).

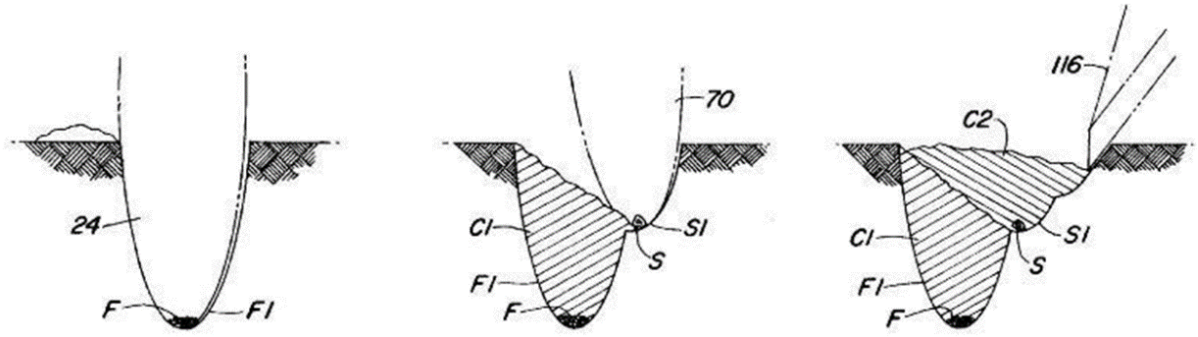

Figure 3.30. Deere and company double-shoot steps, seed (S) and fertilizer (F) placement (U.S. Patent No. 6,032,593, 2000).

3.1.16 John Deere (1960)

Figure 3.31 shows the patent accredited to John Deere Company (U.S. Patent No. 2,920,587, 1960) characterizes a dual disc opener assembly composed of two discs (36,18) with two scrapers (42, 23). Both discs are assisted by a scraper, and are at an angle with the travel direction to create two furrows. The first disc is staggered and of larger diameter in order to place the fertilizer deeper, but the second disc has a more acute angle to cover the first furrow filled with fertilizer while creating the seed furrow (Figure 3.32). The packing wheel then covers the seed furrow and compresses the soil on both furrows to allow a better soil particle contact.

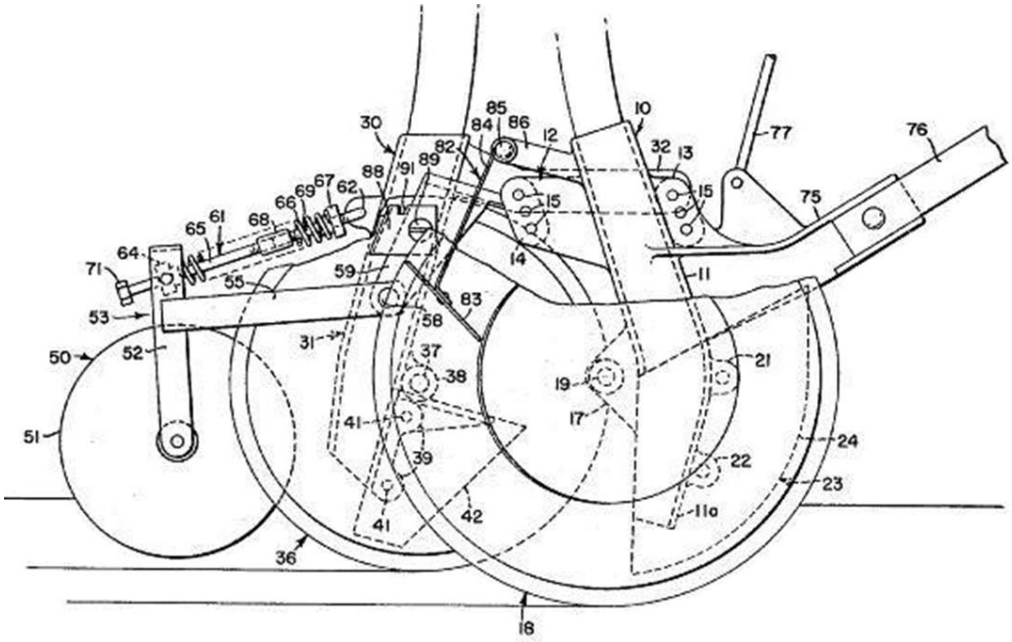

Figure 3.31. Deere and Company dual disc furrow opener (U.S. Patent No. 2,920,587, 1960).

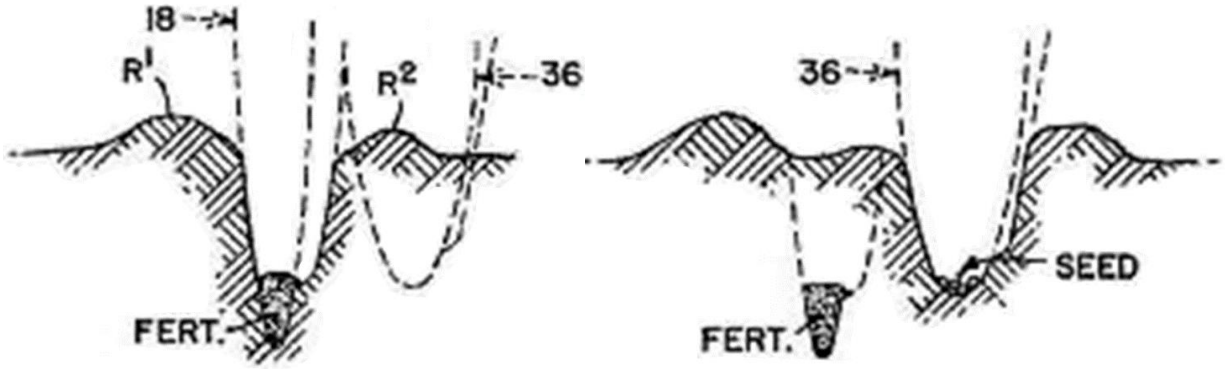

Figure 3.32. Deere and Company dual disc furrow opener seed and fertilizer placement (U.S. Patent No. 2,920,587, 1960).

3.1.17 John Deere (1958)

Figure 3.33 shows the patent attributed to John Deere Company (U.S. Patent No. 2,842,078, 1958), which describes a runner (section of the opener sliding on the ground) opener (13) assisted by a disc/scraper opener (18, 19). As shown in Figure 3.34, the curved disc, assisted by the scraper, distributes the fertilizer (19) in a staggered way and at the same depth as the seeds (37), which are delivered by the runner. The curved disc helped by the scraper covers the seed trench while creating the fertilizer furrow. Moreover, the packing wheel compacts the soil above the furrows for a better emergence rate.

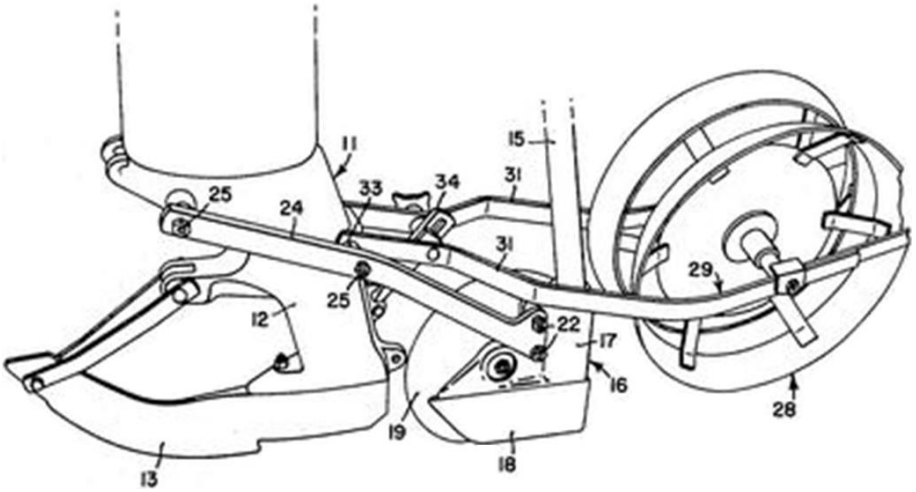

Figure 3.33. John Deere Company runner opener (U.S. Patent No. 2,842,078, 1958).

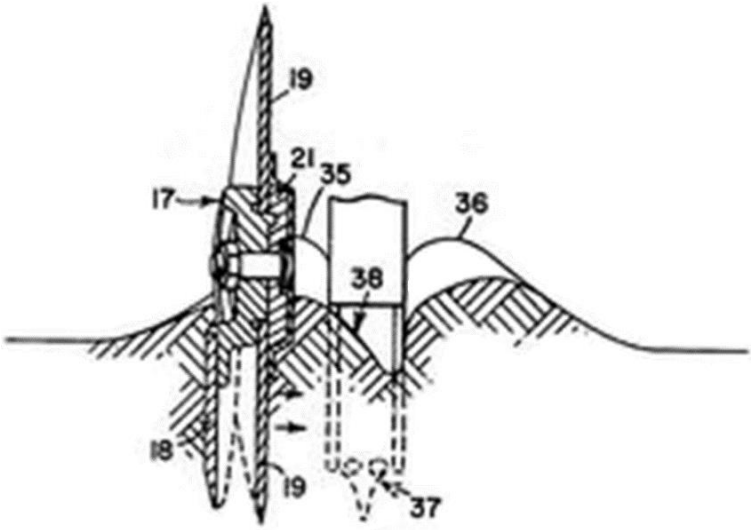

Figure 3.34. John Deere Company runner opener, seed (37) and fertilizer (19) placement (U.S. Patent No. 2,842,078, 1958).

3.1.18 Kurt Hanson

The patent associated with Kurt Hansson (U.S. Patent No. 4,998,488, 1991) defines a straight notched disc aligned with the travel direction, helped by a dual-purpose scraper (Figure 3.35). The scraper edge of the disc makes the seed furrow (16), and the angled wing creates a deeper staggered fertilizer furrow (17) (Figure 3.36). The seed is distributed before the fertilizer, which can potentially disturb the seed placement, and affects the emergence rate. The concept was essentially developed for liquid fertilizer, but can be easily adapted to granular fertilizer.

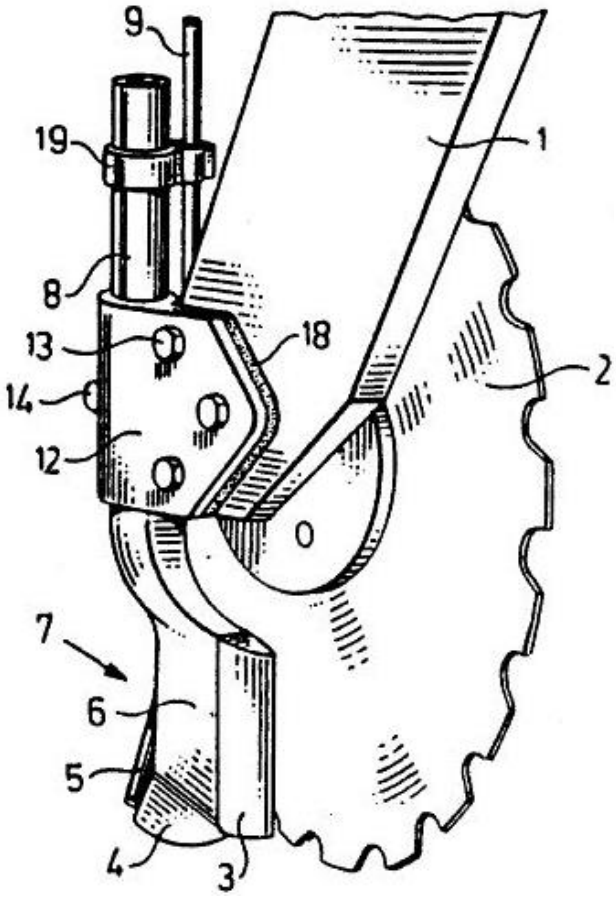

Figure 3.35. Kurt Hanson concept for an agricultural combined drill dispenser opener (U.S. Patent No. 4,998,488, 1991).

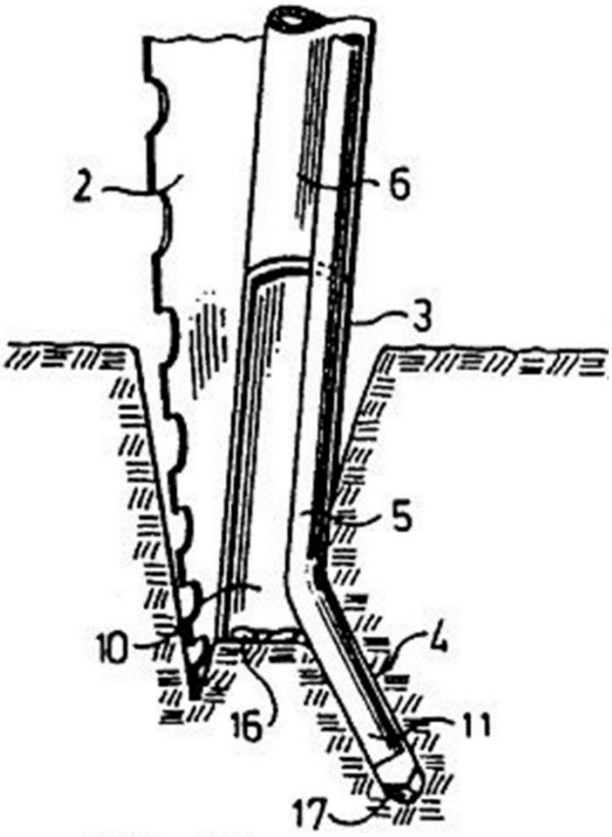

Figure 3.36. Kurt Hanson, seed (16) and Fertilizer (17) placement by the concept for an agricultural combined drill dispenser opener (U.S. Patent No. 4,998,488, 1991).

3.1.19 Massey Fergusson

The patent granted to Massey Fergusson Service N.V. (U.S. Patent No. 3,507,233, 1970) characterizes a double-disc seeder assisted in the front by a disc or a coulter (Figure 3.37). The seed (56) and the fertilizer (53) are distributed in the same furrow with the same opener, but they are carried by two separate hoses (17, 18). Finally, the seeds and fertilizer are mixed together into the furrow, which can cause some seed burning from the ammonia.

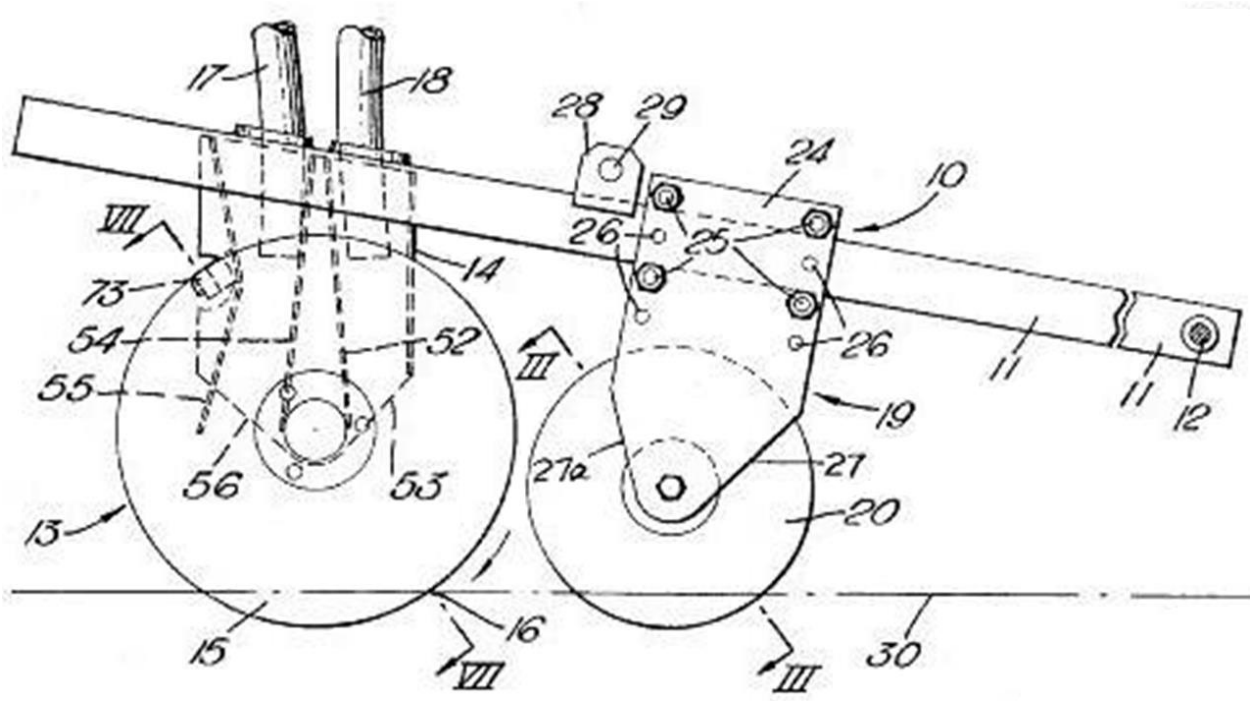

Figure 3.37. Massey Fergusson Service N.V. opener with the seed and fertilizer tube (17 & 18) (U.S. Patent No. 3,507,233, 1970).

3.1.20 Peter Martin Metzler

The patent attributed to Peter Martin Metzler (U.S. Patent No. 1,006,771, 1911) details a curved disc opener assisted by a scraper, and followed by an independent hoe opener (Figure 3.38). The scraper is positioned on the convex side of the disc, which creates the deepest furrow where the fertilizer is deposited. The seeds (10) are distributed by a hoe opener located behind and offset from the fertilizer (8) apparatus, to avoid any disturbance that the fertilizer placement could cause to the seed placement (Figure 3.39). Moreover, the hoe opener dispenses the seeds in a furrow shallower than the fertilizer furrow, as displayed in Figure 3.38.

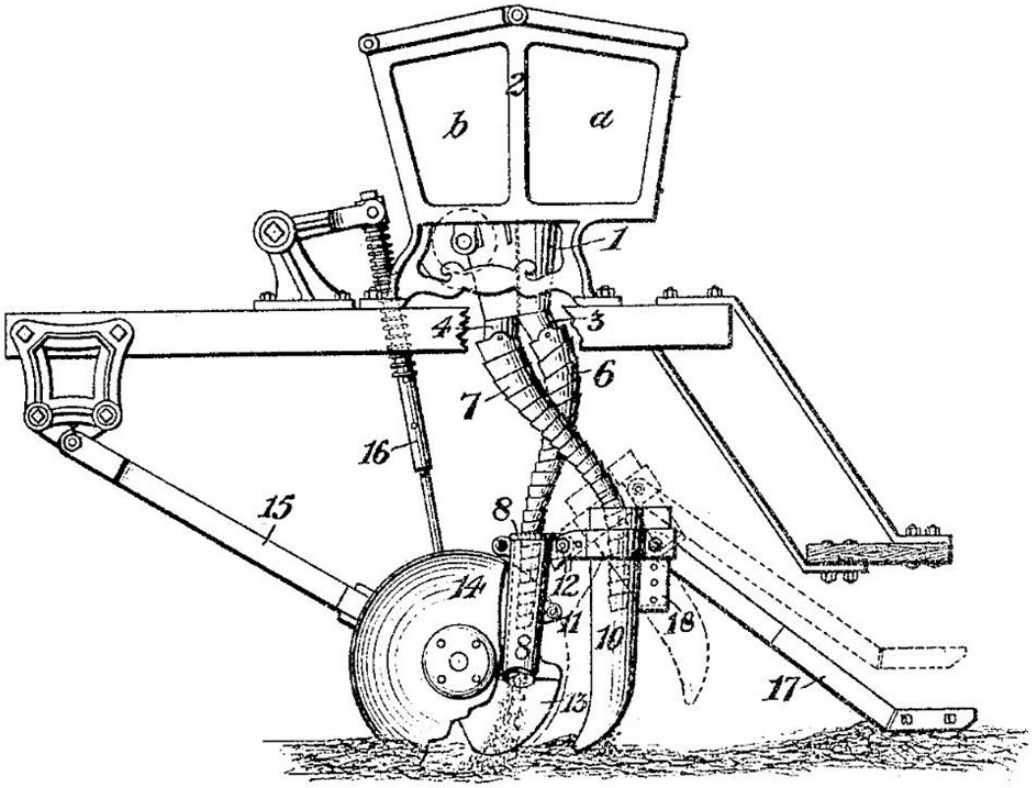

Figure 3.38. Peter Martin Metzler opener (U.S. Patent No. 1,006,771, 1911).

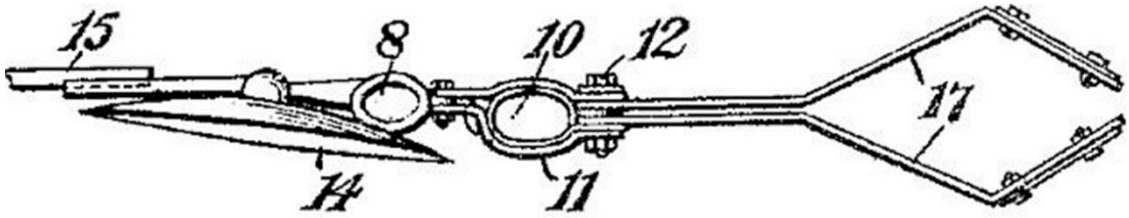

Figure 3.39. Peter Martin Metzler, seed (10) and fertilizer (10) placement (U.S. Patent No. 1,006,771, 1911).

3.1.21 Pillar Laser Disc/Hoe Opener

The patent associated with Pillar Laser™ disc/hoe opener (U.S. Patent No. 7,540,246, 2009) describes an apparatus composed of a compound angled disc, a double function scraper, and a packing wheel (Figure 3.40). The fertilizer is deposited into the furrow created by the compound angled disc and the front edge of the double function scraper. The seeds (64) are introduced in the soil to the side of the fertilizer furrow with the wing of the dual-purpose scraper (Figure 3.41). Also, the fertilizer is distributed before the seeds to ensure that the seedbed will not be disturbed.

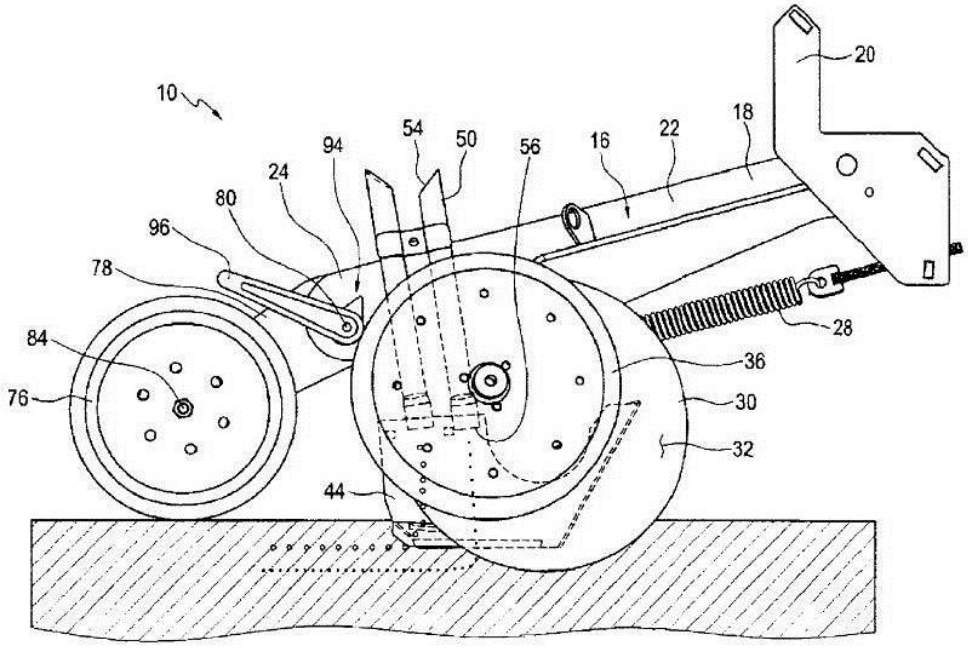

Figure 3.40. Pillar Lasers Inc. Disc/Hoe opener (U.S. Patent No. 7,540,246, 2009).

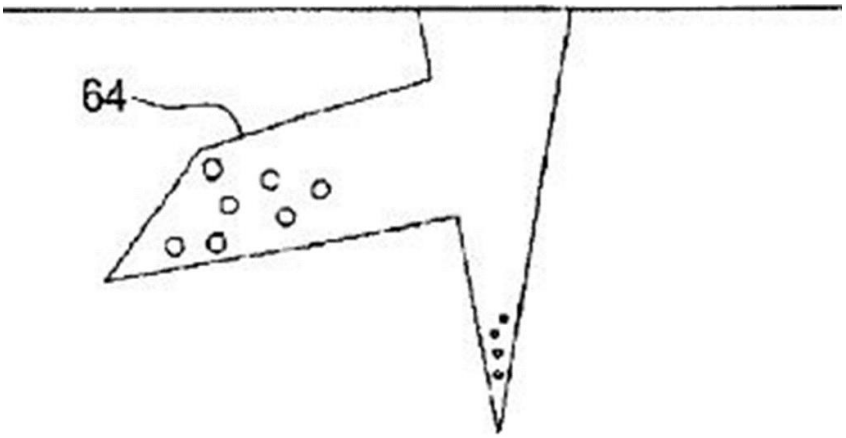

Figure 3.41. Pilar Lasers Inc. Disc/Hoe opener seed (64) and fertilizer placement (U.S. Patent No. 7,540,246, 2009).

3.1.22 Specialty No Till (SNT)

The patent related to the Specialty No Till (SNT)™ opener (U.S. Patent No. 6,978,727, 2005) characterizes an apparatus composed of a compound angled disc, a scraper/stub runner, and a packing wheel (Figure 3.42). The fertilizer furrow is created by the disc and the scraper/runner (section of the opener sliding on the ground (14)) in front of the double-shoot system. The double-shoot system is composed of a tube attached to the packing-wheel arm (Figure 3.43). This tube sprays a band of seeds on the surface of the ground, which is incorporated in the first few millimetres of the ground by the scrubbing action of the offset packer wheel.

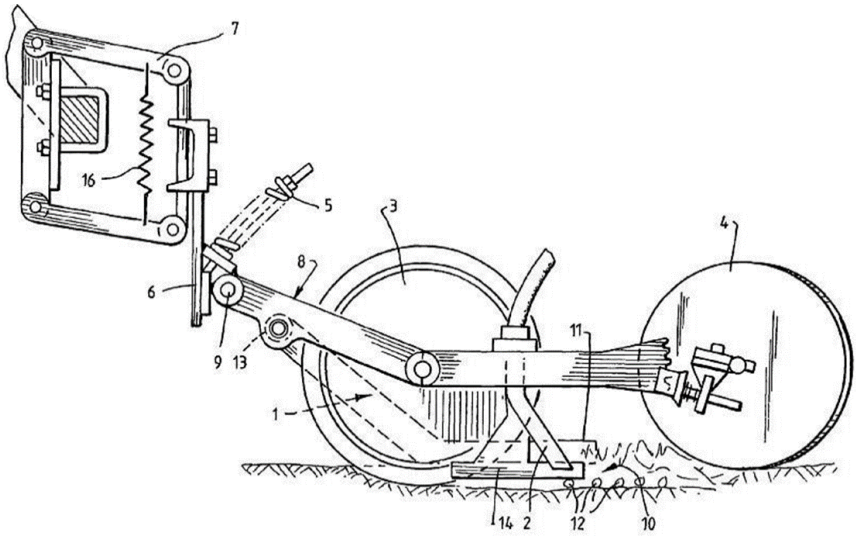

Figure 3.42. Specialty No Till (SNT) opener (U.S. Patent No. 7,540,246, 2009).

Figure 3.43. Specialty No Till (SNT) Double-Shoot System (Courtesy of Specialty No Till SNT website-http://www.specialtynotill.com.au/).

3.1.23 Thermoid

The patent ascribed to the Thermoid™ Company (U.S. Patent No. 2,861,527,1958) represents an angled flat disc opener assisted by a scraper and a fertilizer hose (Figure 3.44). The disc opener is assisted by the scraper to create the seed furrow in front of the fertilizer dispenser. The fertilizer is thrown over the seed furrow from a tube hooked on the back of the scraper, which can create ammonia burns on the seed.

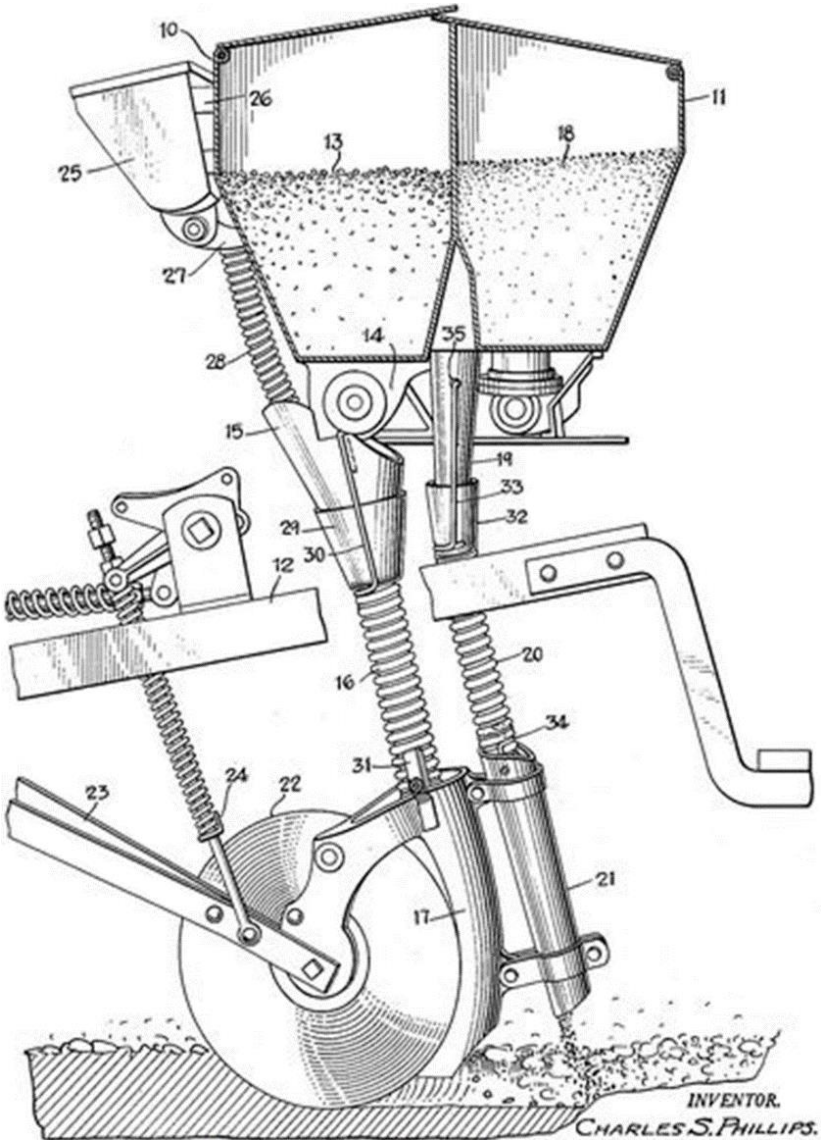

Figure 3.44. Thermoid Company opener (U.S. Patent No. 2,861,527,1958).

3.1.24 Thomas Charles Sargeant

The patent attributed to Thomas Charles Sargeant (G.B. Patent No. 1900/09,933, 1901) describes a seeding implement that uses two curved disc openers one after another (Figure 3.45). The curved discs are the same diameter and distribute the products at the same depth. The first disc creates the furrow for the seed (22), while the second disc covers the first furrow and creates the fertilizer furrow at the same time (35) (Figure 3.46). The fertilizer furrow is covered by the packing wheel, which compresses the seed and fertilizer furrow.

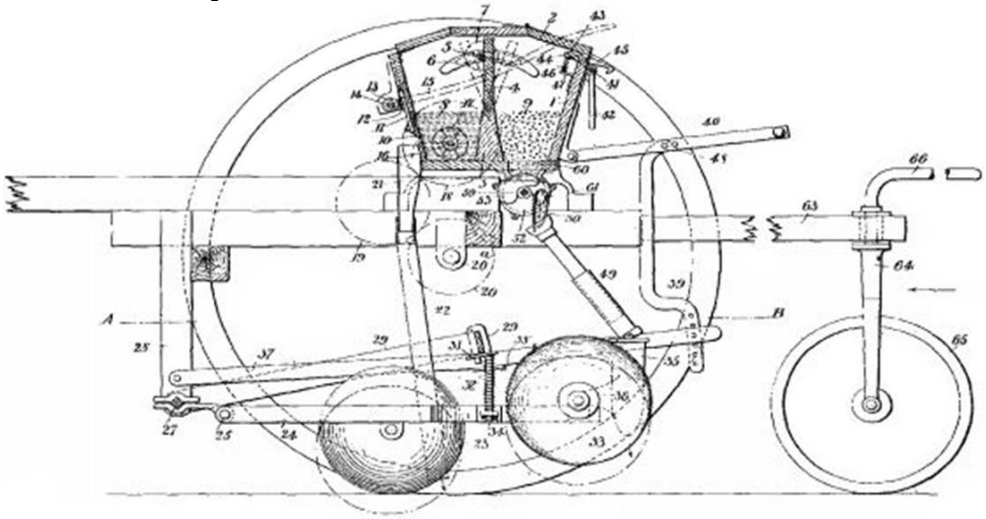

Figure 3.45. Thomas Charles Sargeant opener (G.B. Patent No. 1900/09,933, 1901).

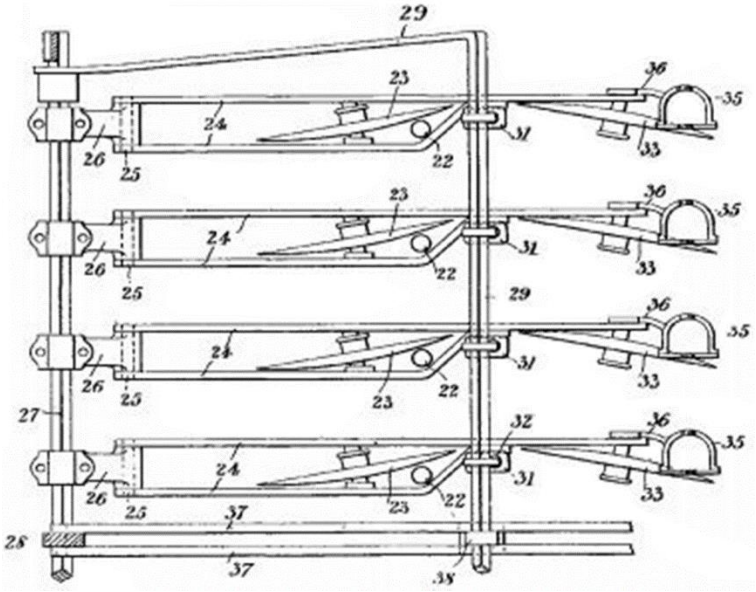

Figure 3.46. Thomas Charles Sargeant opener top view seed (22) and fertilizer (35) placement (G.B. Patent No. 1900/09,933, 1901).

3.1.25 Vieskan Metalli

The patents associated with Vieskan Metalli (Canadian Patent. No. 2,275,124, 2000) (Canadian Patent No.2,326,204, 2002) define two similar types of disc opener, displayed in Figure 3.47 and Figure 3.48. They both use a double-disc opener to create the furrow and they both carry their products separately. The fertilizer is delivered before the seeds and deposited at the bottom of the furrow, while the seeds are distributed over and pushed by the coulter pin into the fertilizer. However, the furrow is compressed by the packing wheel to provide better contact between the soil and the products. Providing the seeds and the fertilizer in the same row could potentially increase the risk of ammonia burning.

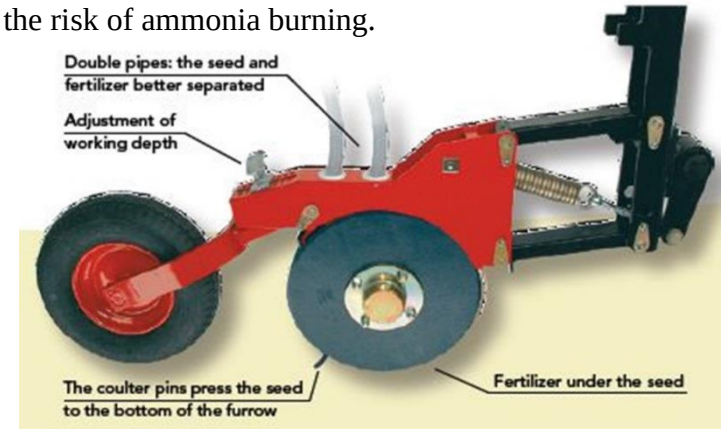

Figure 3.47. Vieskan Metalli standard coulter (Courtesy of Vieskan Metalli 2012 VM Real Direct Seeding Brochure- http://www.vm-koneet.fi/eng/esitteet/vm-2012-eng-www.pdf).

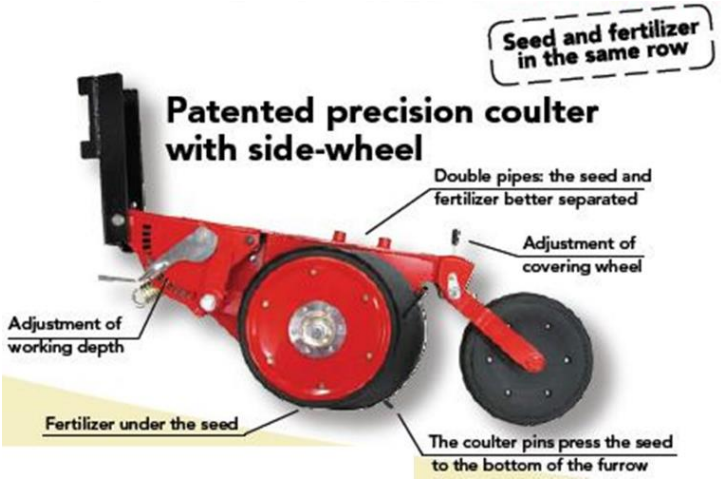

Figure 3.48. Vieskan Metalli precision coulter (Courtesy of Vieskan Metalli 2012 VM Real Direct Seeding Brochure- http://www.vm-koneet.fi/eng/esitteet/vm-2012-eng-www.pdf).

3.1.26 Summary of the Disc Drill Double-Shoot Openers Patents

This section summarizes the main features of the openers and the characteristics of seed versus fertilizer distribution. Moreover, I rated the openers on a base 10 from their main features, their seed versus seed distribution, and their expected overall performance. The opener main features, the seed versus fertilizer distribution characteristic, and the overall performance score are presented in the summary Table 3.1.

Table 3.1. Summary of the disc drill double-shoot openers patents.

Opener Brand	**Opener Main Features**	**Seed vs Fertilizer Distribution**	**Score** (X/10)
Allis Chalmers	Double seed boot assisted by a curved disc	Seed and fertilizer in the same trench both on their side	3
Aspinwall Manufacturing	Straight disc assisted by a mouldboard on each side of the disc	Mixture of seed and fertilizer	1
Atom-Jet SDX Double-shoot System	Modified scraper from a Case IH SDX™ opener	Fertilizer deeper and offset of the seed, independent furrows	6
Barton™	Two staggered discs assisted by residue scrapers	Fertilizer deeper and offset of the seed, independent furrows	9
Bogachev et al.	Two different sized discs on a same axis with two independent distribution tube	Fertilizer deeper and offset of the seed, independent furrows	5
Bourgault Industries Seed Boot/Scraper	Disc opener assisted by a winged seed boot/scraper	Fertilizer deeper and offset of the seed, independent furrows	7
Charles E. Patric (1918)	Two shoes/runner opener assisted by a curved disc or steel wheel	Seed above the fertilizer protected by a layer of soil	3
Charles E. Patric (1917)	Disc opener assisted by a double function runner	Fertilizer deeper and offset of the seed, independent furrows	6
Clean Seed	Straight notch disc followed by a hoe opener	Fertilizer and seed can be distributed in three independent furrows	7
CNH (2014, 2012, 2010)	Disc opener assisted by a scraper followed by a knife on the side	Fertilizer deeper and offset of the seed, independent furrows	9

CNH (2007)	Two different sized discs assisted by scraper	Fertilizer deeper and offset of the seed, independent furrows	6
Concord	Layout of three double disc openers (fertilizer deliver centrally in the front row)	Fertilizer centrally distributed between two seed rows at the seed depth	4
Cross Slot No-Tillage	Tine opener devised on each side of a straight notched disc	Seed and fertilizer distributed in independent furrow, which can be at different height	9
International Harvester™	Disc opener assisted by a dual-purpose scraper	Fertilizer deeper and offset of the seed, independent furrows	3
John Deere (2000)	Two different sized discs (one curve, one straight) both assisted by a scraper	Fertilizer deeper and offset of the seed, independent furrows	9
John Deere (1960)	Two straight discs of different size assisted by a scraper	Fertilizer deeper and offset of the seed, independent furrows	8
John Deere (1958)	Runner opener assisted by a disc/scraper opener	Fertilizer and seed distributed in two independent furrow at the same depth	7
Kurt Hanson	Straight notched disc assisted by a dual-purpose scraper	Fertilizer deeper and offset of the seed, independent furrows	6
Massey Fergusson	Double disc opener assisted by a disc coulter	Mixture of seed and fertilizer	1
Peter Martin Metzler	Curved disc assisted by a scraper followed by an independent hoe opener	Fertilizer deeper and offset of the seed, independent furrows	3
Pillar Laser Disc/Hoe Opener	Disc opener assisted by a double function scraper	Fertilizer deeper and offset of the seed, independent furrows	7
Specialty No Till (SNT)	Disc opener assisted by a scraper/stub runner	Seed spread above the fertilizer protected by a layer of soil	2
Thermoid	Disc assisted by a scraper followed by a fertilizer hose	Fertilizer thrown over the seed furrow, mixture of soil, seed, and fertilizer	2
Thomas Charles Sargeant	Two curved discs almost in line	Seed and fertilizer at the same depth in independent furrow	7
Vieskan Metalli	Double disc opener	Mixture of seed and fertilizer	1

3.2 Fertilizer Placement

The fertilizer and the seed distribution are the most important criteria to consider with a double-shoot seeder. Grant (2004) demonstrated that the use of side-band or mid-row band of P and/or N can be efficient and safe techniques at a high rate, as long as the separation between the products is adequate. The separation between the fertilizer and the seed determines the quantity of fertilizer that can be safely applied (Grant, 2004).

Placing nutrients closer to the crop allows their use earlier in the growing season, according to Grant and Bailey (1993). Also, according to Kalra and Soper (1968), and Bailey and Grant (1990), the distribution of phosphorus (P) directly in the seed furrow or near the crop promotes their use earlier in the season. The placement of fertilizers in the row allows an increment of yield but a reduction of rapeseed emergence by one-third, unlike side banding which increases the yield while maintaining the emergence of the rapeseed, in accordance with Grant and Bailey (1993). This is directly related to the observation made by Nyborg and Hennig (1969) during field trials in Alberta (AB, Canada) with rapeseed. They increased the crop yield by adding l0 kg by hectare (ha) of phosphorus (P) in the row and/or at 2.5 cm below the seed row, however the emergence was reduced by one third for the experiments with the fertilizer directly distributed in the row. Furthermore, an application of 10 $kg \cdot ha^{-1}$ of P 2.5 cm below or 2.5 cm at a downward angle of the seed row does not reduce the emergence but increases the yield of rapeseed, according to Grant and Bailey (1993), Bailey and Grant (1990), Nyborg (196l), Nyborg and Hennie (1969).

3.3 Direct Seeding Advantages

Direct sowing techniques require less agricultural machinery operations compared to the conventional method, while reducing the cost of the seeding operations. Direct sowing requires fewer field passes, reducing the time required to sow, while decreasing the production of greenhouse gases by using less fuel. Furthermore, direct seeding decreases the erosion caused by an uncovered field, by leaving the covered of crop residues. The savings realized with direct seeding is greater if the direct sowing machine is able to manage seeds and fertilizers at the same time (double-shoot system).

The most popular type of openers for the no-till drill in western Canada is named a hoe opener (Chen et al., 2004). Hoe openers are the simplest no-till openers; they are similar to modified cultivator shovels. Hoe openers have the lightest maintenance requirements of all types of openers, but they do not handle heavy residue fields well in comparison to disc drills. Disc drills, unlike hoe openers, create less soil disturbance and allow a better seed placement (Janelle et al., 1995; MNZTFA, 1998; Parent et al., 1993). A disc opener is a more complex apparatus than a hoe opener, but it allows a faster seeding ground speed, while being able to pass through a larger quantity of crop residue. The disc drill requires an accurate design to avoid pushing field residues into the furrow without being previously cut (Payton et al., 1985). The residues introduced into the ground without being cut can be described as the phenomenon of hairpinning. Hairpinning prevents the creation of adequate seedbeds, which stop seeds on the top of the uncut residue, and provides poor seed-to-soil contacts (Chen et al., 2014). The hairpinning phenomenon is more likely to happen when the apparatus is settled at a shallower depth, in soft soil, with a high percentage of moisture content, compared to an implement working deeper in hard soil, with a more usual percentage of moisture content during seeding operations (PAMI, 1995).

3.4 General Agricultural Products Characteristics

The general products characteristics section presents the principal characteristics of the products used during the seed/fertilizer separation experiment, which are wheat, canola (rapeseed), and granular ammonia fertilizer.

3.4.1 Wheat

According to Encyclopedia Britannica 2015, today's three types of wheat make up the major part of the food market: *Triticum vulgare* (or aestivum), *Triticum durum*, and *Triticum compactum* (Singh, 2015). Wheat grains have large variability in their physical properties through the different varieties. The general characteristics are described in Table 3.2, which are combined with their standard deviations and their ranges from Gegas et al. (2010). Wheat seeds have an approximate bulk density of 772 kgm^{-3} (ANSI/ASAE., 1993). The weight of 1000 wheat kernels is in the range of 30 to 50 grams, which corresponds to 19,800 to 33,000 seeds per kilogram (Adgex, 2007). However, wheat seeds are normally provided with a moisture content range of 6.20 to 8.50 percent (dry base), according to Mohsenin (1986). However, wheat kernels are characterized by a range of terminal velocity of 5.8 to 9.15 $m \cdot s^{-1}$, as described by Uhl and Lamp (1966).

Table 3.2. Wheat grains physical properties (Gegas et al, 2010).

Physical Property	Average	Standard deviation	Range
Sample Area (mm^2)	22.8	± 3.6	18.4
Length (mm)	8.5	± 1.1	5.6
Width (mm)	3.3	± 0.4	1.94
Length/ Width (L/W) ratio	8.5	± 0.6	2.64

3.4.2 Canola (Rapeseed)

The physical properties used for canola seeds are taken from a paper, about the discharge of rapeseeds from a model silo, by Parafiniuk et al. (2013). The properties measured were performed on the Suzy variety under two different moisture content levels, 5.5% and 15% (Parafiniuk et al., 2013), as displayed in Table 3.3 with their standard deviation. Canola has an approximate bulk density of 669 $kg \cdot m^{-3}$ (ANSI/ASAE., 1993) and a weight between 2 and 6.5 grams for 1,000 kernels, which corresponds to 154,000 to 499,400 seeds per kilogram (Adgex, 2007).

Table 3.3. Canola (Rapeseed) grains physical properties (Parafiniuk et al., 2013).

Physical Property	5.5% Moisture Content		15% Moisture Content	
	Average	Standard Deviation	Value	Standard Deviation
Length (mm)	2.025	± 0.008	2.05	± 0.01
Width (mm)	1.82	± 0.02	1.82	± 0.01
Volume (mm^3)	3.6	± 0.07	3.71	± 0.08
Diameter (mm)	1.90	± 0.01	1.91	± 0.01
Aspect Ratio (AR)	0.90	± 0.09	0.890	± 0.002
Circularity[1]	0.978	± 0.001	0.95	± 0.05

[1] The circularity parameter formula is: Circularity = $2(Pi*Area)^{1/2}$/Perimeter (Parafiniuk et al., 2013).

3.4.3 Ammonia Fertilizer

The dimensions of ammonia fertilizer particles are determined by a sieve-shaker test. The urea particles have sizes from 3.36 mm (Sieve No. 6) to 1.68 mm (Sieve No. 14) (Smith et al., 2005). The physical properties for granular urea are described in Table 3.4 from UNIDO and IFDC. (1998). Moreover, according to Klenin et al. (1986), the dispersibility of mineral fertilizer is regulated by the fertilizer moisture content, which is an indirect indicator of hygroscopicity.

Table 3.4. Granular urea physical properties (UNIDO and IFDC. 1998).

Physical Property	Low Range Value	High Range Value
Bulk Density (kgm^{-3})	720	820
Apparent Density (kgm^{-3})	1220	1300
Angle of Repose (degree)	34	38
Porosity (%)	5	8

3.5 Discrete Element Method (DEM)

The first known documentation about the application of the Discrete Element Method, or Distinct Element Method (DEM), applied to soil was published by the Géotechnique journal: A discrete numerical model for granular assemblies, authored by Cundall and Strack (1979). The distinct element method determines numerically the equilibrium contact force, and the displacement caused to a system by tracking all the contacts regardless of whether the interactions are between particles or particles to geometry.

The DEM concept uses a time step small enough to assume that the velocity and acceleration are constant. Also, the time step, by being sufficiently small, avoids disturbance being propagated from any particles farther than its immediate neighbors during a single time step. These features allow the DEM to resolve the non-linear interaction of a large group of particles without requiring an excessive memory capability or iterative procedure (Cundall and Strack, 1979).

The calculations provided by the discrete element method are executed by alternating between Newton's second law of motion applied to the particles and the force-displacement law (Hooke's law) applied to the contacts. Newton's second law determines the motion of the particles from the resultant forces on the particles. The force-displacement law defines the forces formed on the particles from the contacts created during particle displacement (Cundall and Strack, 1979). The performance of these two laws creates some deformation on the particles due to the method used to calculate the movement, even if they are considered rigid bodies. The particle deformation itself is minimal compared to the deformation caused to the assembly of particles as a whole. The deformations are created by an overlap between particles, which only occur from contact points (Cundall and Strack, 1979). However, these overlaps are small in comparison to the particle size.

The calculation cycle can be repeated infinitely: the forces are determined by using the force-displacement law as function of the particle overlap at the contact point (Graff, 2010).

The force-displacement general equation:

$$F_i = KU \tag{3.1}$$

where,

F_i = Normal or shear force calculated on the i^{th} element (N)

K = Normal or shear stiffness ($N \cdot m^{-1}$)

U = Overlap (m).

Once the forces are determined, the calculation cycle continues with the application of the Newton's second law.

The Newton's second law equation:

$$F_i = m(\ddot{x}_i - g_i) \tag{3.2}$$

where,

F_i = Resultant force (Normal or Shears) on i^{th} element (N)

m = Total mass of the particle (kg)

$\ddot{x}_i$ = Particle acceleration ($m \cdot s^{-2}$)

g_i = Gravity acceleration ($m \cdot s^{-2}$).

The modern software that uses DEM to simulate particle behaviour is based on models applied at each contact point. The model applied on each contact point is made up of three parts: a stiffness model, a slip model, and a bonding model. The contact stiffness model offers an elastic relationship between the relative displacement and the contact force related to the shear and normal direction. The contact stiffness can be calculated linearly by assuming two contacting stiffness of entities acting in series, or non-linearly by using the Hertz-Mindlin contact model, which calculates

the stiffness coefficient by using the shear modulus and the Poisson's ratio (Itasca, 2003). The slip model is an intrinsic property between two elements in contact, which determines if slip occurs by using the friction contact force (Itasca, 2003). The bonding model is divided into two different types: parallel-bond model, and contact-bond model. Both bond models can be imagined as a glue link between two particles. The contact-bond model can be illustrated as a glue link applied only on an extremely small location at the contact point, which can only transmit forces. The parallel-bond can be illustrated as glue applied on a predetermined cross-section between two particles, which can transmit forces and moments.

3.5.1 DEM SOFTWARE

DEM software collects data by tracking interactions associated with each particle, and their energies can be traced (Graff, 2010). Different types of energy can be recorded, like frictional work, bond energy, strain energy, body work, kinetic energy, and boundary work (Itasca, 2003).

The critical parameter in DEM software is the selection of the right time step size. The time step size determines the accuracy and the computational power required in the simulations. The time step is a compromise between the accuracy required and the computational power available. The compromise is necessary because a smaller time step requires more iterations to complete the simulation, which is directly related to the total time necessary to complete the simulation. The time step chosen needs to keep the acceleration, velocity, and the forces constant over the time to be considered appropriate (Graff, 2010). The simulation remains stable if the critical time step is not exceeded (Itasca, 2005). The critical time step is calculated from a mass-spring system, which in the first instance is considered as a single spring attached to a single mass moving to create infinite combinations.

The critical time step is determined by solving equation (3.3):

$$t_{crit} = \sqrt{\frac{m}{k}} \tag{3.3}$$

where,

t_{crit} = Critical time step (s)

m = Mass of the point mass (entire particle), (kg) and

k = Spring stiffness (contact stiffness).

The DEM requires entry of certain parameters to calculate all the desired values. These values are essentially the particle physical characteristics and the magnitude of their contacts (Graff, 2010). Table 3.5, which is adapted from Graff (2010), summarizes all particle parameters required for the different types of contacts.

Table 3.5. Crop and general properties used in DEM (Graff, 2010).

Particle Parameters	**Contact models**	**Slip models**	**Bonds**
Particle density	Normal stiffness	Coefficient of rolling friction	Critical normal stress
Radius	Shear stiffness	Coefficient of static friction	Critical shears stress
	Poisson's ratio		
	Shear modulus		
	Coefficient of restitution		

The success of a DEM simulation is determined by the ability to select the right input value for each parameter, in order to recreate as realistically as possible the natural particle behaviour observed in a controlled environment for model validation.

3.5.1.1 *Physical Properties of Simulated Materials*

According to George (2008), typical soil true densities of the particles are distributed within a common range from 2550 to 2700 $kg \cdot m^{-3}$. The general value of 2650 $kg \cdot m^{-3}$ is commonly accepted for any soil particle types (sand, silt, and clay) (George, 2008). Also, some precise soil particle density values are provided on various websites. Stone particle densities and steel particle densities are provided on various websites. The low-end straw particle density value is provided by the ASABE presentation paper of Lam et al. (2007). The high-end straw particle value is provided from a study about the compaction characteristics of barley, canola, oat, and wheat straw from Adapa et al. (2009). The particle densities are available in Table 3.6.

The bulk density for sand and silt particles are provided by AgriInfo's (2015) website, and the clay bulk density values were extracted from the SI metric (2014) chart website. The stone and the steel bulk densities are assumed to be the same as their particle density, due to the fact that no voids are assumed during the bulk density measurement. The straw bulk density values are provided by an ASABE Meeting Presentation paper about the physical characterization of wet and dry wheat straw and switchgrass from Lam et al. (2007). Bulk density values are available in Table 3.6.

The pore space typical percentage values for the sand, silt, and clay are provided by AgriInfo's (2015) website. The stone pore space percentage and the steel pore space percentage are assumed to be zero. The pore space percentage for the straw is calculated from Table 3 in the ASABE Meeting Presentation paper: Physical characterization of wet and dry wheat straw and switchgrass - bulk and specific density, by Lam et al. (2007). The wheat volume of void is added to the volume of solid to generate the total volume. The volume of void is divided by the total volume, and multiplied by 100 to create the pore space percentage.

Calculate the straw pore space material as follows:

$$\%_{ps} = \left[\frac{V_h}{(V_h+V_s)}\right] * 100 = \left(\frac{V_h}{V_t}\right) * 100 \quad (3.4)$$

where,

$\%_{ps}$ = Straw pore space percentage (%)

V_h = Void volume (cm^3)

V_s = Solid volume (cm^3)

V_t = Total volume, ($V_t = V_h + V_s$) (cm^3)

All the pore volume percentage values are available in Table 3.6.

The diameters of the sand, silt, and clay particles were sourced from the USDA (2014); Soil Physical and Chemical Properties website. However, many other classifications of size limit for soil exist, such as that of the International Society of Soil Mechanics (ISSS), Federal Aviation Agency (FAA), and Massachusetts Institute of Technology, to name a few. The major classification of size limits was summarized by Brajas (2008). The stone diameters were chosen to be representative of the stones that were observed in a typical field. The diameters of the straw were measured from the fields during experiments. The values of different materials are shown in Table 3.6.

The Poisson's ratios for the sand, silt, clay, and rock particles were obtained from a textbook by Subramanian, N. (2008, p. 1398). The Poisson's ratio of steel was obtained from Engineers Edge's (2015). The high-end range value for the Poisson's ratio of wheat straw was obtained from Afzalinia (2005). The high-end range value for the Poisson's ratio of wheat straw was estimated by Afzalinia from the pressure range encountered in a large square baler in order to minimize the square summation of certain parameters. The low range value for the Poisson's ratio

of wheat straw was taken from Sitkei (1986). Futhermore, the Poisson's ratio values for other forage materials are available from Sitkei (1986) for forage material.

The shear modulus range for the soil particles (sand, silt, and clay), and the shear modulus range for the stone particles were provided by the report No. FHWA-SA-97-076 (Kavazanjian et al., 1997) from the U.S. Department of Transport, Federal Highway Administration. The shear modulus range provided for the stone was determined with gravel. The shear modulus of steel was sourced from a materials science and engineering book (Callister, 2007).

The shear modulus values for the straw particles were extracted from a paper by Kushwaha et al. (1983). The shear modulus values for straw from the paper was used to create an average, which was made with two, five, and ten straws. The shear modulus averages for straw displayed in the table is expressed for the equivalent of one straw. The shear straw moduli were measured on the straw diameter cross-section, which had 6.0 to 27.0 percent moisture content. Shear modulus values are available in Table 3.6.

Table 3.6. Physical properties of simulated materials.

Physical Properties	Sand	Silt	Clay	Stone	Steel	Straw
True Particle Density (kgm^{-3})	2655 to 2659	2798	2837	2300 to 2800	7820	930 to 1585
Bulk Density (kgm^{-3})	1400 to 1600	1300 to 1400	1100 to 1800	2300 to 2800	7820	99 to 290
Pore Space (%)	40	47 to 50	58	0	0	15 to 21
Diameter (mm)	2 to 0.05	0.05 to 0.002	Less Than 0.002	24.5 to 79.2	N.a.	3 to 5
Poisson's Ratio	0.15 to 04	0.3 to 0.35	0.1 to 0.5	0.1 to 0.4	0.265 to 0.303	0.25 to 0.38
Shear Modulus (kPa)	27600 to 345000	27600 to 138000	2750 to 34500	69000 to 345000	83000000	7040 to 22830

3.5.1.2 ***Physical Interaction***

The physical interactions available with EDEM are described under one of these categories: particle-to-particle contact models, particle-to-geometry contact models, and particle body forces (DEM Solutions, 2015). Also, it is under one of these categories that the contact model is applied; the contact model explanations were taken from the EDEM User Guide (DEM Solutions, 2015), and some extra clarifications are provided in the PFC3D User's Manual, Version 2.0 (Itasca, 2003).

3.5.1.2.1 Hertz-Mindlin (No Slip)

The Hertz-Mindlin is the contact model used by default for particle-to-particle and particle-to-geometry contacts. The Hertz-Mindlin is a non-linear contact model based on the approximation of a theory developed by Mindlin and Deresiewicz (1953), which was described by Cundal (1988) (Itasca, 2003). The contacts created between particles and geometries can be recorded to estimate relative wear by activating the relative wear recording option in DEM software. The relative wear option facilitates the determination of locations of high pressure/high wear on simulated apparatus. The relative wear option uses the relative velocity between the bulk material and the device with the force generated for its calculations (DEM Solutions, 2015). The relative wear option provides additional data, which can be used to determine the high-risk locations of wear, and/or can be used to compare quantitatively the geometries between them, but cannot be used to determine a specific material removal rate (DEM Solutions, 2015).

3.5.1.2.2 Hertz-Mindlin (No Slip) with RVD Rolling Friction

The Hertz-Mindlin (no slip) with RVD Rolling Friction model uses the same method as the Hertz-Mindlin (no slip) model to determine the contact forces, but proposes a different technique to calculate rolling friction contacts (DEM Solutions, 2015). The Hertz-Mindlin (no slip) contact model can record the relative wear contact as well.

3.5.1.2.3 Hertz-Mindlin with Archard Wear

The Hertz-Mindlin with Archard Wear model, combined with the process of sliding/abrasive wear on the apparatus surfaces, determines explicitly the amount of material removed due to the handling of bulk materials (DEM Solutions, 2015). The apparatus pieces are characterized through simulation by specific wear resistance values, according to the type of material they are made of. These specific wear resistance values will establish the intensity of wear caused by particle interactions on the geometries.

3.5.1.2.4 Hertz-Mindlin with Heat Conduction

The Hertz-Mindlin with Heat Conduction model determines the heat flow interactions between particles. The model uses particle overlaps and particle temperatures to calculate the heat flux (DEM Solutions, 2015). The model requires using updated temperatures to let external heat sources create effects on particles. Since the thermal effect from a warm ground-engaging tool at work was considered negligible, the heat conduction in DEM was not considered as part of the project.

3.5.1.2.5 Hertz-Mindlin with Bonding

The Hertz-Mindlin with Bonding model creates links between particles or between particle and geometry. The model does not link directly the particle to the geometry, due to the fact that the bonding occurs on the particle physical radius, and not on the contact radius as many other DEM models (DEM Solutions, 2015). To operate the contact bond model, some parameters need to be specified, such as the normal stiffness, the shear stiffness, the critical normal stress, the critical shear stress, and the bonded disc radius. These parameters are determined to reproduce the material behaviour as realistically as possible. Moreover, the bonds are created when the particle collides with other elements, and their strengths are directly related to the stiffness value. The strong force generated by the bonds will require a lower simulation time step to seize all the high energy. The particle behaviour is determined by the Hertz-Mindlin model prior to the first contact.

3.5.1.2.6 Hertz-Mindlin with JKR Cohesion

The Hertz-Mindlin with JKR (Johnson-Kendall-Roberts) Cohesion model was initially created to simulate the influence of Van der Waals forces during a flow of dry and/or fine powders. The model is currently used to illustrate the cohesive behaviour of fine and moist materials (DEM Solutions, 2015). Also, the model is applied on materials with larger-scaled particles, in order to reproduce the moisture interactions on bulk materials (DEM Solutions, 2015). The interactions are implemented with selected material properties to maintain the moisture charge at its surfaces, which is known as surface energy. The surface energy values are determined for interactions between particles and/or particle-to-geometry. The abundance of surface energy added in the simulations will affect the material adhesions (DEM Solutions, 2015).

3.5.1.2.7 Linear Cohesion

The Linear Cohesion contact model interacts with the default Hertz-Mindlin contact model to add normal cohesion forces on the contact point between two particles and one particle with a geometry (DEM Solutions, 2015). Linear cohesion strength is determined by material cohesiveness, which is harmonized to the simulation by adjusting the energy density for each interaction.

3.5.1.2.8 Linear Spring

The Linear Spring contact force model can be visually represented by a damped linear spring (DEM Solutions, 2015). The linear spring model requires establishing the spring velocity, which must be identical for the interactions between particles and interactions between a particle and a geometry.

3.5.1.2.9 Hysteretic Spring

The Hysteretic Spring model allows bulk elasto-plastic deformation behaviour directly from its contact mechanic equations (DEM Solutions, 2015). The Hysteretic Spring model acts like the Linear Spring model by allowing elastic comportment until a predetermined stress value, which is the limit before the material begins to be deformed plastically. The plastic deformations can appear without large forces applied on the materials. The deformations are illustrated by the huge encroachment, what characterizes the compressible materials (DEM Solutions, 2015). The characterization of compressible materials is mostly fashioned by the coefficients of restitution, which are used to dissipate the energy instead of the Hertz-Mindlin method. The restitution coefficients determine the portion of the compressed energy restituted by the particle during the decompression. The low restitution coefficients allow larger material deformation under the same pressure.

The Hysteretic Spring model requires defining the damping factor to determine the damping velocity (DEM Solutions, 2015). The damping factor removes the possibilities of small vibrations between particles, which may persist nearly infinitely. Also, the model requires defining the stiffness factor, which determines the ratio between the normal loading stiffness versus tangential stiffness. The stiffness factor is included in the model to determine the forces applied tangentially to the contact. Also, the stiffness factors are usually within the range of 0.7 to 1 in accordance to the literature (DEM Solutions, 2015). Furthermore, the model must have a yield strength parameters determined for any interaction types, which are normally estimated from the shear moduli.

3.5.1.2.10 Moving Plane

The Moving Plane contact model is applied on specific geometries to mimic the particle behaviour in contact with the plane in motion (DEM Solutions, 2015). Moreover, the moving plane contact model transfers the movement to the particles by friction at the surface of the designated geometries.

3.5.1.2.11 Particle Body Forces

The Particle Body Forces model becomes involved when specific conditions are reached. The body force can be applied on particles travelling at a specific speed, and/or on particles at a specific position, and/or on particles that reach specific temperatures, and much more. The temperature of particles is not considered a body force, but the model allows for peripheral heat sources to create heat influence on particles (DEM Solutions, 2015). The particle body force applied as temperature requires using the Hertz-Mindlin with Heat Conduction contact model, which is essential to complete the calculation related to the heat transfer between the elements in

interaction (DEM Solutions, 2015). However, it is required to attribute heat capacity for each particle type.

3.6 Wear Characteristics

The wear processes on seeding implements are mostly associated with soil displacement, which follows erratic patterns. These irregular patterns make it difficult to determine or predict the wear rates and the locations thereof. The manner in which wear appears depends directly on soil properties and conditions. Furthermore, agricultural tools are made from a large selection of materials, and each one of them responds differently to field conditions. The addition of each of these parameters increases the level of difficulty for determining the wear pattern (Graff, 2010).

Abrasive wear is the most common type of wear occurring on agricultural implements, which appears when the hardness between two materials is different. The material typically used in the fabrication of agricultural implements is two to five times softer than the soil abrading particles (sand, silt, clay, and rock) as reported by Graff (2011), and Swanson (1993). Harder materials wear softer materials by forming grooves into it (Breaux and Keska, 2002). The grooves created in the softer material can be the result of plastic deformation or micro-cutting. Plastic deformations do not directly remove chips or fragments from the material as opposed to a micro-cutting operation. The subsequent plastic deformations result in fatigue, which ultimately tears the material surface.

Soil conditions are the principal parameters influencing wear rate. Soil moisture and soil texture are the two parameters that have the most influence. The proportion of the soil particles, for example sand and clay, creates variations in wear rates due to the specific hardness of each particle type (Graff, 2010). The wear rates are also affected by angularity of the particles, the

working ground speed, and the working seed depth. Angular particles, according to the study by Swanson (1993), wear five to eight times more the materials than round particles (Graff, 2010). The implements are exposed to soil pressure along their surface as a function of the working depth and the working speed. The wear rates are directly related to the pressure applied by the soil on the implement; the higher the soil pressures are, the higher the wear rates will be. The variations of soil pressure against the implements will be more important with an increase of working depth than with an increase of working speed, according to Srivastava et al. (2006).

3.6.1 Wear Characterization Techniques

The wear characterization techniques section is extracted from Section 2.4 of Graff (2010). The methods described in this section are the up-to-date version, and a wrap-up of the methods described by Graff (2010). For detailed information about the majority of the techniques described in the section below, the reader should consult the reference (Graff, 2010). This is based on the description and determination of the wear patterns on soil-tool interactions (research project from the same research group).

Wear characterization techniques were developed to evaluate the performances of materials on the same basis in a controlled environment. Most of the methods were developed for specific cases and particular circumstances. Furthermore, only a few of these techniques are adaptable to a wide spectrum of conditions.

This section presents the wear characterization by laboratory methods and by soil bin trials. The sub-section "3.6.2.1 ASTM Standard Procedures," describes specific ASTM standard procedures adaptable to the project.

3.6.2 Wear Characterization by Laboratory Methods

Laboratory methods are useful to reproduce a specific field condition at a real scale. Also, laboratory methods are often at lower cost than field tests, and their results provided for specific conditions are often more accurate, due to the controlled environment.

3.6.2.1 ***ASTM Standard Procedures***

The standard procedures developed by the American Society for Testing and Materials (ASTM) provides controlled conditions to evaluate materials wear on the same basis. The procedures presented below were developed to quantify the abrasive wear produced on tool materials specimens.

3.6.2.1.1 Wet Sand/Rubber Wheel Abrasion Test (ASTM Test Method G 105-02)

The "Wet Sand/Rubber Wheel Abrasion Test" (ASTM, 2007) generates wear by creating pressure on a test specimen with a spinning neoprene rubber tire. Abrading particles are mixed with de-ionized water in a container, wherein the wheel and the specimen are also partially immersed in the same container. The rotating wheel has stirring paddles to keep the slurry, and de-ionized water mixture agitated during the entire test duration.

3.6.2.1.2 Dry Sand/Rubber Wheel Abrasion Test (ASTM Test Method G 65 – 04)

The "Dry Sand/Rubber Wheel Abrasion Test" (ASTM, 2010b) uses the same apparatus as the "Wet Sand/Rubber Wheel Abrasion Test" (ASTM, 2007), but in dry conditions. A rotating chlorobutyl rubber tire creates abrasion on the test specimen by applying force against the sample with sand (Ottawa type) introduced directly above the point where the rotating wheel applies pressure on the sample.

3.6.2.1.3 Pin-on-Disc Wear Test (ASTM Test Method G 99 – 05)

The material tested with the Pin-on-Disc test (ASTM, 2010c), can be either the disc or the pin. Usually the pin is the sample tested, which can be cylindrical shaped with a spherical end or sphere-shaped. A typical pin sample has a diameter between two and ten millimetres. The pin is normally loaded against the disc with an arm and a mass to keep the pressure constant. The disc has a diameter between 30 and 100 mm with a thickness ranging from 2 to 10 mm. The disc can be positioned vertically or horizontally for the experimentation, but the wear result may differ between the vertical and the horizontal orientation. The test is performed by impregnating the pin or the disc, a rotating movement around the disc centre axis. The test is concluded after the completion of a pre-determined number of rotations. Moreover, the sample wear can be measured either by weight loss or by dimension attenuation.

3.6.2.1.4 Abrasive Loop Contact Test (ASTM Test Method G 174 - 04)

The abrasive loop contact test (ASTM, 2009) uses a small metal piece characterized by a length of 32 mm, a width of 8 mm, and a thickness of 4 mm. Also, the specimens should have a roughness less than 0.2 µm. The piece is placed above a 16 mm diameter drive spindle with 200 g centered between the pivot and the drive spindle. The spindle drives an abrasive tape at the precise rhythm of 300 rpm. The abrasive belts are only used for a period of one hour in connection with a one-hour test. The test can be extended over one hour, but the belt needs to be changed every hour. The wear can be measured by the weight lost and by several physical measurements such as optical and profilometer.

3.6.2.1.5 Rotary Abraser Platform Test (ASTM Test Method G 195 – 13 a)

The rotary abraser platform test (ASTM, 2013) can be used on both rigid and flexible samples. The samples accepted on the rotating platform of the apparatus are characterized by a thickness

from 6.35 mm to 40 mm. The samples are worn by a pair of abrasive wheels attached on two movable arms, which are located opposite the samples. The abrading wheels are commonly loaded with 250, 500, or 1000 g depending on the durability of the materials. The material worn by the two wheels creates an amount of debris mixed with abrasive particles, which are removed by two vacuum nozzles. The vacuum nozzles are placed diametrically opposite over the wear pattern to provide a clean sample for the abrading wheels. The wear is evaluated over a number of pre-determined cycles and determined by the weight loss. Moreover, the measures can be displayed in milligrams lost per thousand abrasion cycles or in many other different units detailed in section 12 of the standard.

3.6.2.2 ***Soil Bin Trials***

Soil bin experiments have the objective of imitating the soil behaviour observed in specific fields and recreating the wear conditions for that type of soil. Soil bin trials can provide more accurate results for a specific environment than field tests, due to the fact that the soil parameters and the soil conditions are controlled and the experiment environment is regulated. The tests can be conducted during any season in any weather condition, which allows more flexibility compared to other tests. Experiments carried out with soil bins allows for the study of a higher number of parameters more efficiently, and with more sophisticated acquisition equipment than field tests. Soil bin trials are usually performed with smaller and less expensive machinery models that can predict the performances of full-size and more costly prototypes (Gill et al. 1994). The wear soil bin trials are preferably made in circular soil bins to allow continuous travel distance, but the soil bins can be in an assortment of shapes, lengths, and dimensions, depending on their planned functions (Graff, 2010).

3.6.3 Field Testing

Field tests are used to determine actual wear reactions on the implements. The experiments can be completed on a partial or total range of conditions expected during the life expectancy of the devices. The field tests are more time consuming and expensive than the soil bin test or other simple tests, but they provide a data set of the different apparatuses at the same time, for the same experimental conditions. However, the field tests can determine wear rates and accurate wear performance for each apparatus under the same experimental conditions (Graff, 2010). According to Er and Par (2006), field environments could not be simply reproduced with test machines and/or an abrasive device due to the impacts or contacts with hard soil particles. Moreover, field conditions, working depth, and working speed all affect wear rates (Graff, 2010).

Field tests can be required to compare different implements under the same conditions to evaluate their performances. For benchmarking purposes, different implements are usually installed on a single apparatus to collect data under the same conditions and at the same time. In order to reduce the environmental disparity incidence and the wear rate variation due to the mounting placement, the apparatus has to be randomly relocated on the testing device between the repetitions (Wingate-Hill et al., 1979). As described by Graff et al. (2007), the wear rate will be different between an apparatus mounted on the first row (or rank) and an apparatus mounted on a second row (or rank) of given ground engaging tools.

Soil field condition measurements provide the information required to characterize the soil in order to compare or predict the results of future experimentations (Graff, 2010). The representative measurements of the soil contents are soil moisture contents and soil texture while incorporating the relative soil stoniness (Wingate-Hill et al., 1979). Soil cone index measurements can be used as complementary values to determine the compaction difference between untouched soils and

fields compacted by machines or implement tires (Owsiak; 1997, 1999). Soil bulk density such as the cone index value can be determined like complementary value (Wingate-Hill et al. 1979). The complementary value facilitates data predictions or comparisons for future experimentations. Furthermore, fields are heterogeneous media, which makes them too delicate to be represented with a single sample (Graff, 2010).

Field tests are generally chosen to represent a medium or an environment that imitates realistic conditions, where the production apparatuses are expected to perform a tillage or seeding/planting operation. The main objectives of the field tests are to collect results in order to obtain generic conclusions (Graff, 2010). Field testing results are usually described reactions of predetermined materials under specific environments, and/or reactions between different conditions. The data collected from the field tests are normally not collected with an extreme precision with intent to develop mathematical models (Graff, 2010). The wear on the apparatuses is usually determined by weight loss, due to the data acquisition methods and the measurement procedures required, which is a simple method that can be used directly at the testing area (Graff, 2010).

3.6.4 DEM

The wear rate is a process very difficult to simulate due to its time and environment dependence, in addition to a slow evolution rates. It is already assumed that the apparatus could be created from an amount of particles bonded by the DEM bonding model. The particles are bonded together with a predetermined strength, and when the force exerted on them exceeds the limit, the particles are liberated from their bonds. The particles liberated from their links slowly change the tool shape and reproduce the wear rate in the simulation. Unfortunately, current technology is still too limited to provide with high precision the wear of parts within a reasonable time. The number of particles required to create a realistic wear rate on simulated ground engaging

tools are in the order of 10^{35}, so the number of particles removed during one cycle is small enough to reproduce a realistic wear rate (Graff, 2010).

Other approaches can be used to determine the wear rate with DEM simulations such as Kalala et al. (2005) and/or Cleary (1998), which use pressure force collected on devices or other parameters provided from DEM software to predict wear rates. Furthermore, Archard and Hirst (1956) elaborated a formula that describes the sliding wear as a function of the pressure employed on the sliding interval, and inversely proportional to the composition of the element hardness (Graff, 2010). The relation developed by Archard and Hirst is commonly known as the Archard equation, which is generally abridged as:

$$W = \frac{K_a * \mathrm{F}_e * v_p}{H_g} \tag{3.5}$$

where,

W = Wear rate ($cm^3 \cdot s^{-1}$)

K_a = Constant related to the probability per unit encounter of production of a wear particle

F_e = Applied normal load (g)

v_p = Relative velocity ($cm \cdot s^{-1}$)

H_g = Material hardness ($10^6 \cdot g \cdot cm^{-2}$)

3.7 Literature Review Summary

The literature review chapter summarized the following: review of the patents concerning disc drill double-shoot opener, the effect of distributing the fertilizer at an ideal location from the seeds, the benefit of no-till seeding, the general aspect of the different products used in field experiments, the fundamentals of Discrete Element Method (DEM), and wear characterization techniques of ground-engaging tools. The wear characteristic section presented methods to characterize tool wear such as the laboratory methods, the ASTM standard procedures, the soil bin trials, and field experiments. Moreover, the wear characterization chapter described the DEM techniques used to estimate the intensity of wear on apparatuses. However, in order to minimize operations required by producers during seeding, and to optimize the fertilizer placement versus the seeds, a double-shoot system on a disc drill will be developed based on the knowledge introduced in the Literature Review chapter.

4.0 MATERIALS AND METHODS

The material and methods chapter describes the fields and the soil openers used for the different field tests conducted. It details the procedures employed for the field experiments: seed-to-fertilizer separation, 3-D force experiments, and field trials with crop residues. It also presents formulas and parameters used to create the analytical model, and elaborates on DEM simulations.

4.1 Fields

The different locations used to perform the experiments are all located within 50 km of the city of Saskatoon in the province of Saskatchewan, Canada, as displayed in Figure 4.1. The field-soil composition varied from loamy sand to silty clay, as shown in Figure 4.2. The precise soil compositions are presented in section 5.1.7 Soil Texture. The fields usually had either canola or wheat residues lying on the ground, except for the Asquith Summer Fallow Loamy Sand Field, which had no residue. Table 4.1 provides the type of crop residues, with the straw density (per surface) determined by the yield of the last harvesting season. Each field was treated with liquid herbicide, except the Lutheran Loamy Sand Field with wheat residue, and the Lutheran Loamy Sand Field #2 (See Table 4.1). The fields were treated with herbicide before the experiment to control the weed grass to ensure that the conditions were identical to the spring seeding conditions. The Lutheran Loamy Sand Field with wheat residue and the Lutheran Loamy Sand Field #2 were used at the post-harvest season, which did not require chemical treatment. All the field characteristics (i.e. soil temperature, soil compaction, etc.) are presented in Section 5.1 Soil Characterization.

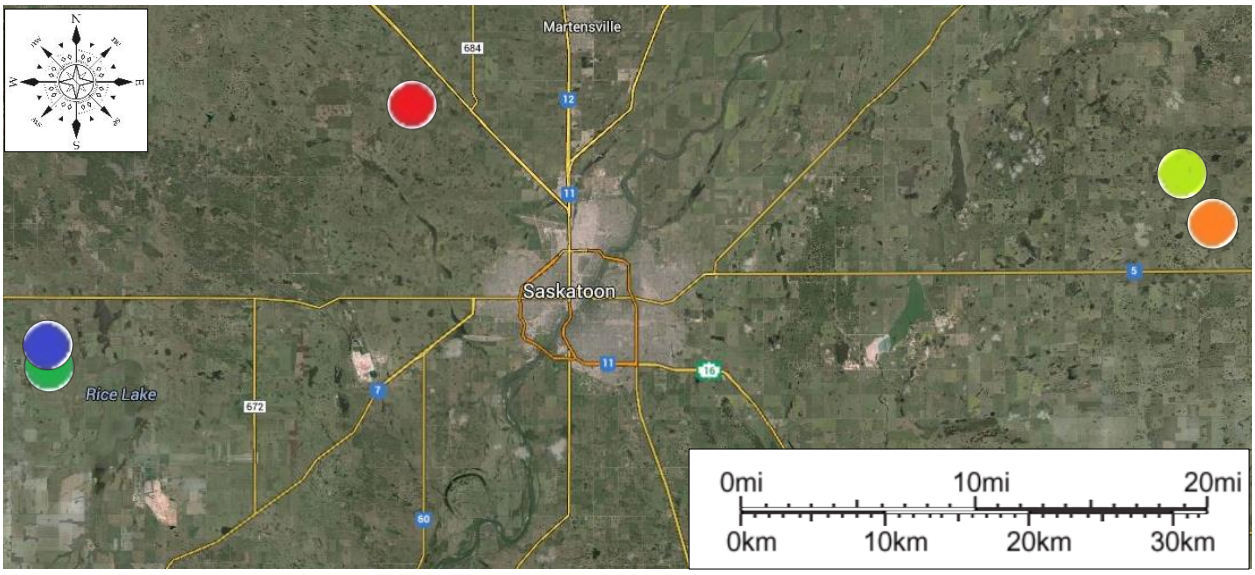

*See legend Table 4.1.

Figure 4.1. Field Locations.

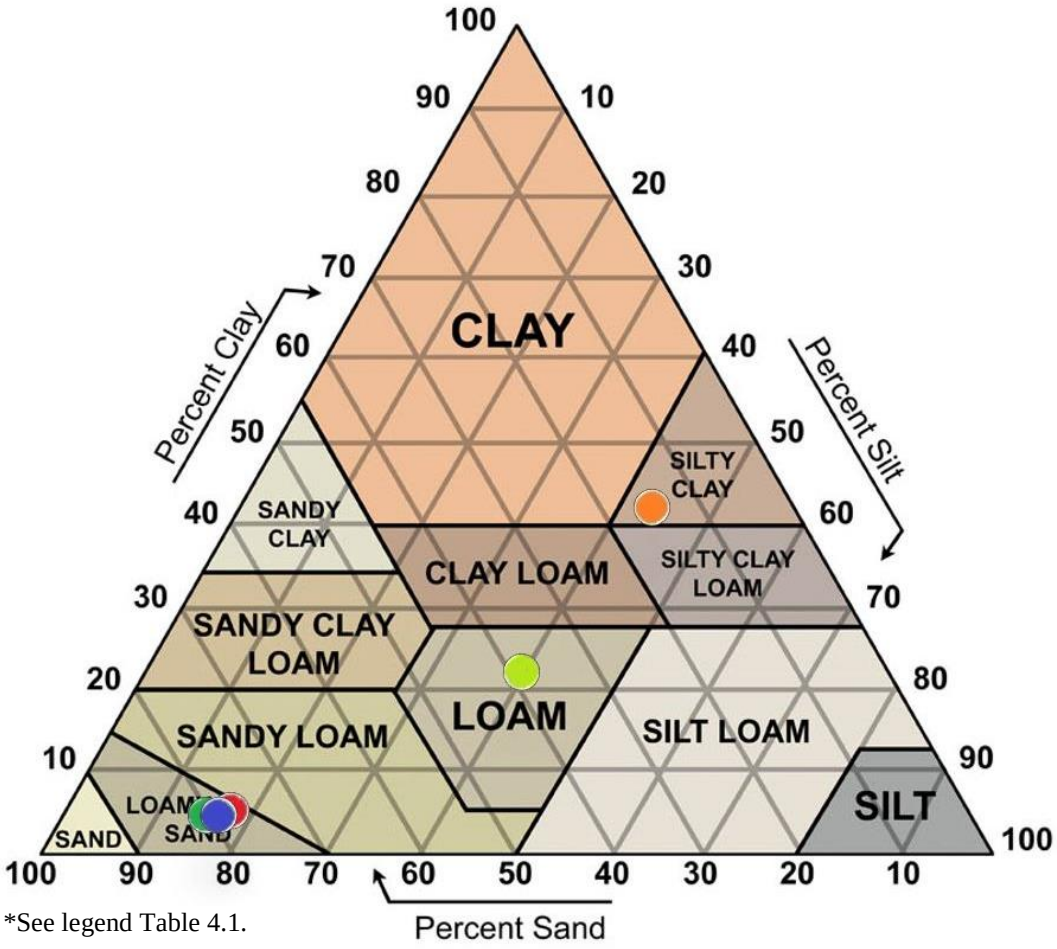

*See legend Table 4.1.

Figure 4.2. Soils triangle.

Table 4.1. Summary of the composition of test fields.

Colour Code	Fields Name and Soil Type	Type of Crop	Amount of Crop Residues ($bu \cdot A^{-1}$)	Type of Chemical Used
	Lutheran Loamy Sand Field	Canola	45	Roundup Weather Max with Amitrol 240
		Wheat	50	None
	Lutheran Loamy Sand Field No.2	Canola	45	None
	Asquith Loamy Sand Field	Canola	30	Roundup Weather Max with Amitrol 240
	Asquith Summer Fallow Loamy Sand Field	None	None	Roundup Weather Max with Amitrol 240
	St-Denis Loam Field	Wheat	55	Roundup Weather Max
	St-Denis Silty Clay Field	Wheat	55	Roundup Weather Max

4.1.1 Lutheran Loamy Sand Field

The Lutheran Loamy Sand Field is located at the intersection of range road 3064 and the township road 382 near the city of Saskatoon. The Lutheran Loamy Sand Field #2 is located one kilometre north of the Lutheran Loamy Sand Field. The Lutheran Loamy Field was used for the seed-to-fertilizer separation experiment and the experimental field trials with crop residues, except the Lutheran Loamy Sand #2, which was only used for the experimental field trials with crop residues. The Lutheran Loamy Sand Field is composed of two different plots, which are located side-by-side, as shown in Figure 4.3. The rectangular section is used for the seed-to-fertilizer experiments, and their dimensions are 91.5 m by 442.8 m. Also, the plot is subdivided into four sub-plots of 61 m by 40.7 m displayed in Figure 4.4. The larger plot in an L shape is the segment

used for the trials with crop residues; it has a square dimension of 550m by 550m. The L-shaped plot is subdivided into three sub-plots of 183.3 m by 292.2 m, 183.3 m by 257.8 m, and 183.3 m by 257.8 m, as described in Figure 4.5. The Lutheran Loamy Sand #2 field is not described on the pictures due to the fact that the field was only used for the trials with crop residues, with the objective of determining the capacity of the openers to pass through a substantial amount of crop residues.

Figure 4.3. Lutheran Loamy Sand Field location.

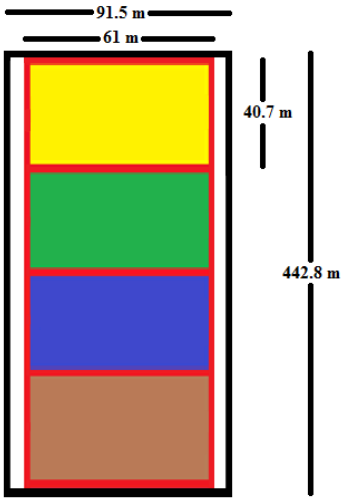

Figure 4.4. Lutheran Loamy Sand Field subdivision plot for seed and fertilizer separation experiment.

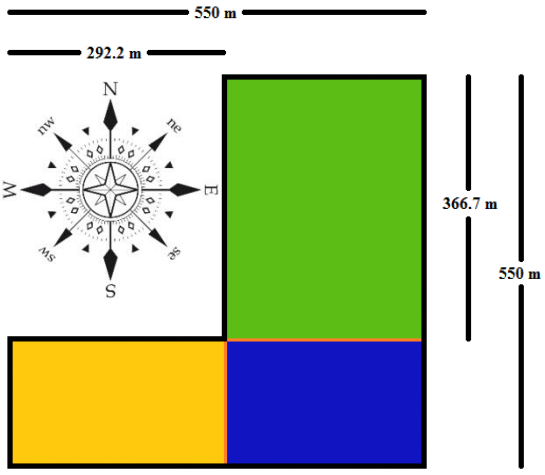

Figure 4.5. Lutheran Loamy Sand subdivision plot for residue characteristics experiments.

The seed and fertilizer separation experiment at the Lutheran Loamy Sand Field was performed in late spring/beginning of the summer 2014, with 1586 L (45 bushels) per acre of canola residues, as shown in Figure 4.6. The experimental field trials with crop residues at the Lutheran Loamy Sand Field were done at the beginning of autumn with 1762 L (50 bushels) per acres of fresh wheat residue lying on the ground, as displayed in Figure 4.7. The wheat swaths that served for the extreme condition portion of the experimental field trials with crop residues are displayed in Figure 4.7. The Lutheran Loamy Sand #2 field was used during the fall with a coverage of canola residue similar to Figure 4.6.

Figure 4.6. Lutheran Loamy Sand Field Seed and fertilizer placement general plot view.

Figure 4.7. Lutheran Loamy Sand Field residue characteristics general plot view.

4.1.2 Asquith Loamy Sand Field

Asquith Loamy Sand Field is located 800 m east of SK-673 Road and 1.6 km south of SK-14 Road near the town of Asquith (See Figure 4.8).

Figure 4.8. Asquith Loamy Sand Field Location.

This field was used for the seed and fertilizer placement experiment, and the 3-D forces experiment. The seed and fertilizer separation experiment was performed in late spring/beginning of the summer 2014, and the 3-D forces experiment was performed in the fall 2014. Both experiments were completed with 1057 L (30 bushels) per acres of canola residue as shown in Figure 4.10. The plot has a rectangular dimension of 115.2m by 232.8m, which is sub-divided into four subplots of 84.7m by 58.2m for the seed-to-fertilizer experiment as displayed in Figure 4.9. The plot for the 3-D force experiment was used on its entire length of 232.8 m.

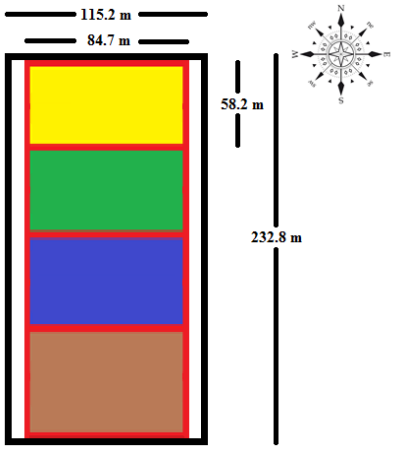

Figure 4.9. Asquith Loamy Sand Field seed and fertilizer placement subdivision plot.

Figure 4.10. Asquith Loamy Sand Field general plot view.

4.1.3 Asquith Summer Fallow Loamy Sand Field

Asquith Loamy Sand Field is located 800m east of SK-673 Road and 1.6 km south of SK-14 Road close near the town of Asquith, beside the Asquith Loamy Sand Field (See Figure 4.11).

Figure 4.11. Asquith Summer Fallow Loamy Sand Field location.

This field was only used for the seed and fertilizer experiment. The plot has a rectangular dimension of 115.2 m by 356.6 m, which is sub-divided into four subplots of 84.7m by 89.2 m (See Figure 4.12). The seed and fertilizer separation experiment was performed in the late spring/beginning of the summer 2014, without residue, as shown in Figure 4.13.

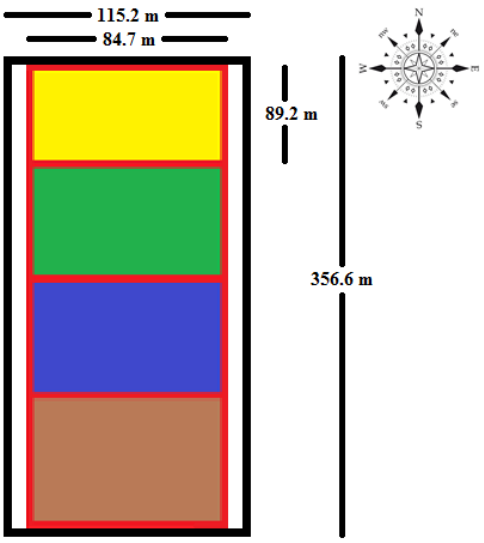

Figure 4.12. Asquith Summer Fallow Loamy Sand Field seed and fertilizer placement subdivision plot.

Figure 4.13. Asquith Summer Fallow Loamy Sand Field general plot view.

4.1.4 Saint-Denis Loam Field

The St- Denis Loam Field is situated 4 km east of SK-671 Road (Lerew Street), and 6.4 km north of SK-5 Road near the town of St-Denis as displayed in Figure 4.14.

Figure 4.14. St-Denis Loam Field location.

The field was only used for the seed and fertilizer experiment. The plot has rectangular dimensions of 91.4 m by 442.6 m, which is sub-divided in four subplots of 61 m by 110.6 m as shown in Figure 4.15. The seed and fertilizer separation experiment was performed in the late spring/beginning of the summer 2014 with 1938 L (55 bushels) of wheat residue per acre (see Figure 4.16).

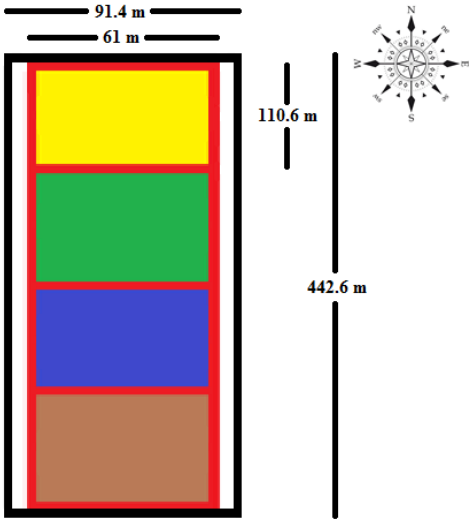

Figure 4.15. St-Denis Loam Field Seed and fertilizer placement subdivision plot.

Figure 4.16. St-Denis Loam Field general plot view.

4.1.5 St-Denis Silty Clay Field

Figure 4.17 shows the St- Denis Silty Clay field, which is located 6.4 km east of SK-671 Road (Lerew Street) and 4 km north of SK-5 Road, near the town of St-Denis.

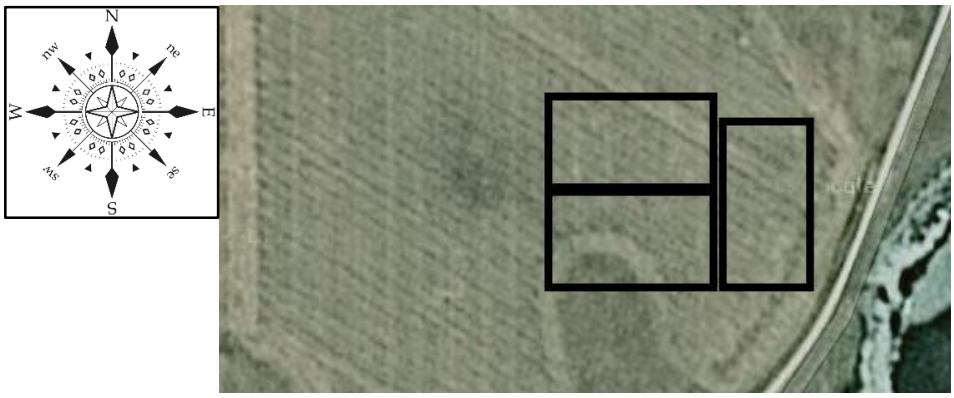

Figure 4.17. St-Denis Silty Clay Field location.

This field was only used for the seed and fertilizer experiment. The plot is divided into three rectangular plots of the same dimensions (91.4 m by 152.4 m), which are sub-divided into four subplots of 38.1 m by 61 m as shown in Figure 4.18. The seed/fertilizer separation experiment was performed in the late spring/beginning of the summer 2014, with 1938 L (55 bushels) per acre of wheat residue. Figure 4.19 shows the wheat residue.

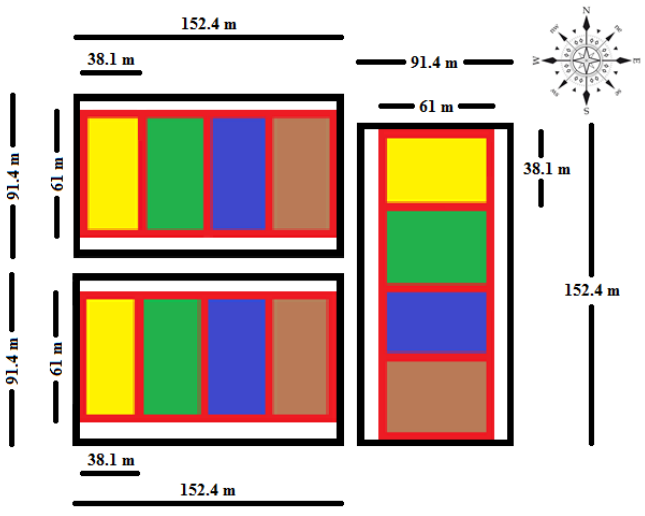

Figure 4.18. St-Denis Silty Clay Field Seed and fertilizer placement subdivision plot arrangement.

Figure 4.19. St-Denis Silty Clay Field Seed and fertilizer placement subdivision plot.

4.2 Soil Characterization and Classification

The soil characterization section uses a variety of measurements to classify the results in order to make them comparable over time. A proper soil characterization requires the determination of the soil temperature, the determination of the soil compaction, the characterization of the ground residue, the determination of soil moisture content, and a precise soil texture analysis. Soil characterizations were performed on each field before the seed-to-fertilizer separation experiments.

4.2.1 Determination of Soil Temperature

The soil temperature was taken on the plots only a few minutes before the beginning of the tests, in order to provide the most representative ground temperature. The soil temperature measurements were taken five times on each field subdivision, for a total of 20 measurements per field. The measurements were collected by a 9836 Taylor® Pro Adjustable Head Digital Thermometer (Taylor Precision Products, Oak Brook, IL). The thermometer has an operational range of – 40°C to 232°C, it is equipped with a 125 mm stainless steel steam, and a 25.4 mm liquid crystal display. The depth of the measurements was taken from 100 mm to the surface, which represents the working zone of the apparatuses. In order to take the measurements correctly, the 125 mm steam was lowered to 100 mm into the ground for a period of 30 s to stabilize the thermometer measurements.

4.2.2 Soil Compaction

The soil compaction test was accomplished by taking five measurements on each field subdivision, for a total of 20 per field. The compaction measurements were taken by the soil compaction tester serial number 1347-23665 REV E model 155850003D (Dickey-John®

Corporation, Auburn, IL). The penetrometer can be used with two different tips: 12.7 mm (1/2 inch) and 19.05 mm (3/4 inch). The penetrometer have pressure ranging from 0 to 4137 kPa (600 psi) with the 12.7 mm (1/2 inch) tip, and a range from 0 to 2758 kPa (400 psi) with the 19.05 mm (3/4 inch) tip. The tests were accomplished with the 19.05 mm (3/4) tip to provide more accurate results. The locations where the compaction tests were completed presented the most representative field conditions, so low and high locations were avoided, as well as tire prints. The soil compaction tester was driven vertically into the soil at the rate of 25.4 mm per second (1 inch per second), until it reached 152.4 mm (6 inches) deep. The highest value reached during the test was recorded as the soil compaction value.

4.2.3 Crop Residues

The tests made for ground residue were related to stubble thickness, stubble height, and ground cover percentage. These measurements were used to characterize the residues from the last harvesting seasons, and to estimate the quantity of crop residues lying on the ground.

4.2.3.1 *Stubble Thickness*

The stubble thicknesses were measured by a transparent ruler NO R-405-30 ACME made in China. The ruler was 30 cm long (12 inches) with a smallest scale unit of one millimetre. To have a good estimate of the stubble thickness, the diameter of the stems was measured to the closest millimetre for a total of ten measurements per field.

4.2.3.2 *Stubble Height*

The stubble heights were measured by a 1316 Lufkin® Cooper Tools measuring tape, made in the U.S.A. The measuring tape was equipped with a 19.05 mm (3/4 inch) steel band REPL ORDER NO. 3374 10 7 RY316 2. The stubble height measurements were taken from the ground

to the head of the stubble. Also, in order to have a good estimate of the stubble height, all measurements were taken at the closest 0.79375 mm (1/32 inch), for a total of ten measurements per field.

4.2.3.3 *Ground Cover Percentage*

Ground cover percentages are the estimated quantities of straw on the ground on predetermined surfaces. The predetermined area used for the estimations is 0.09290304 m^2 (1 ft^2), which is defined by a quadrat of 0.3048 m (1 ft.) by 0.3048 m (1 ft.). Ten measurements were taken per field to give a general idea of the ground cover percentage.

4.2.4 Determination of Water (Moisture) Content of Soil by Mass Basis

The determination of the soil moisture content is made in two different steps, namely, the soil sampling and the analyses. Soil samplings must be representative of the general field conditions. The analyses require a repeatable accurate procedure, which is provided by an ASTM standard.

4.2.4.1 *Soil Sampling*

Soil samplings were effectuated once per subdivision, for a total of four samples per field. The soil samples were taken at a depth between 25 mm to 75 mm, which represents the working depth of the disc drills during the experimentations. Each sample had a mass over 700 g, and was stored in a sealed plastic bag until analyzed. The samples were stored in a cooler for the field period, and in a refrigerator until they were analyzed in the laboratory.

4.2.4.2 *Determination of Water (Moisture) Content of Soil by Mass Basis*

The soil moisture content by mass was determined independently for each field subdivision by following the ASTM standard D2216-10 (ASTM, 2010 a). Method A was performed in

accordance with the equipment used and the precision required. Method A is precise at the closest 1% of moisture content level. Method A required a GP2 model scale type with 0.1 g readability for samples over 200 g. Also, the method required a dryer able to maintain a constant temperature of 110°C ± 5°C during the entire drying period. The balance used was a PLG 15001 (Adam Equipment, Oxford, CT) with a maximum load of 15 kg and precision of 0.1 g. The dryer used was a 2800 Thermotron (Thermotron Industries, Holland, MI) with a temperature range from -87°C to 190°C. Tin plates were used as containers during the drying period.

The first step was to weigh the container, which needed to be cleaned every time, and emptied of any residue (M_c). The second step was to weigh approximately 300 g of wet soil in a tin plate (M_{cms}). An amount of 300 g of soil was chosen so that enough soil would be left in the sample to allow for a second analysis in case of erroneous results, thus respecting the minimum 200 g of soil required by method A. The third step was to place the samples in the oven at 110°C ± 5°C for 24 h. The sample weight recorded after 24 h of drying included the tin plate with the dry soil weight (M_{cds}). The period of drying was longer than the 12 to 16 h suggested by the method in order to limit the sample manipulation and ensure that the samples were dry. Another method to verify the humidity of the samples is to record their weight after 12 hours of drying as reference values, and record the weight at 16 hours of drying. The two values are compared to determine if there is a significant difference. If a significant difference is found, another 4 hours of drying is added. After the 4 extra hours, the samples are weighed and are compared to their own weight from 4 hours earlier. If a significant difference is determined, another 4 hours of drying is required and the cycle is repeated until the difference is non-significant. If no significant difference is found, the value is recorded as the mass of the tin plate with the dry soil (M_{cds}).

Calculate the water content of the material as follows:

$$w = \left[\frac{(M_{cms} - M_{cds})}{(M_{cds} - M_c)}\right] \cdot 100 = \left(\frac{M_w}{M_s}\right) \cdot 100 \quad (4.1)$$

where,

w = water content (%)

M_{cms} = mass of container and moist specimen (g)

M_{cds} = mass of container and oven-dry specimen (g)

M_c = mass of container (g),

M_w = mass of water ($M_w = M_{cms} - M_{cds}$) (g)

M_s = mass of oven-dry specimen ($M_s = M_{cds} - M_c$)

4.2.5 Soil Texture Analysis

The soil texture analysis was performed in two different steps namely, the soil sampling and the soil analysis. The soil texture sampling, just like the soil sampling section in the determination of soil moisture, required being representative of the general field conditions. The soil texture analyses, like the soil water analyses, required high precision and repeatability. Unlike the water determination analyses, the soil texture analyses required lots of time, trained staff, and specialized laboratory and field equipment.

4.2.5.1 ***Soil Sampling***

Soil samplings were effectuated four times per subdivision for a total of 16 times per field. All 16 samples were mixed together in a large pail to create a unique representative soil sample, which was sent to a specialized laboratory for particle size analysis. The organic material which covered the soil surface was removed from the soil samples prior to being introduced in the pail. Soil samples were taken between 0 mm to 152.4 mm (6 inches) with a PN012 from JMC Soil Samplers (Newton, Iowa, U.S.A.) of 12 inches large diameter sampling tube. The sampling tube has a diameter of 31.75 mm (1.25 inches). Each sample has a mass over 700 g and was stored in a

plastic bag. The samples were stored in a cooler for the field period and in a refrigerator until they were analyzed by Australian Laboratory Services (ALS).

4.2.5.2 ***Soil Analysis***

The particle size analyses were performed by the Australian Laboratory Services (ALS) located in Saskatoon. They prepared the samples by drying and grinding them to ensure that no too large aggregates were used. They performed the Mini-Pipet method according to the SSIR-51 Method 3.2.1.2.2 (Burt et al., 2014) to analyze the soil samples, and they environmentally disposed of the samples. The Mini-Pipet method is only usable with particles with a diameter less than 2 mm. According to Burt et al. in the SSIR-51 (Method 3.2.1.2.2), the summary of the procedures are as follows: "Water-dispersible clay is analyzed by mechanical means in distilled water without the removal of organic matter and soluble salts and use of a chemical dispersant. The clay percentage is determined gravimetrically by pipetting a 2.5 – mL aliquot from a sample tube at 2.5-cm after the appropriate settling times. Calculated settling times for specific temperatures are determined using Stokes's Law. The sand fractions are analyzed for the remaining sample by sieving through a nest of sieves."

4.2.6 Date of the Experiments

The field experiments were performed from May 20th to October 31st, 2014, inclusively. The summary Table 4.2 displays the dates when the experiments were performed by field and by type of experiment. Moreover, the texture analysis experiment is provided with the sampling, extraction, and analysis dates, contrary to the other experiments, which are implemented with the performed date only.

Table 4.2. Summary of experiment, field and date performed.

Experiments	**Fields**	**Date** (2014)
Determination of Soil Temperature	Lutheran Loamy Sand Field	July, 16, 17, 21, 22
	Asquith Loamy Sand Field	July, 23 August, 06, 07
	Asquith Summer Fallow Loamy Sand Field	July, 22, 23, 29 August, 06
	Saint-Denis Loam Field	August, 11,13
	Saint-Denis Silty Clay Field	August, 11, 12
Soil Compaction	Lutheran Loamy Sand Field	July, 16, 17, 21, 22
	Asquith Loamy Sand Field	July, 23 August, 06, 07
	Asquith Summer Fallow Loamy Sand Field	July, 22,23, 29 August, 06
	Saint-Denis Loam Field	August, 11,13
	Saint-Denis Silty Clay Field	August, 11, 12
Crop Residues Characterization	Lutheran Loamy Sand Field	July, 16
	Asquith Loamy Sand Field	July, 23
	Asquith Summer Fallow Loamy Sand Field	July, 22
	Saint-Denis Loam Field	August, 11
	Saint-Denis Silty Clay Field	August, 11

Determination of Water (Moisture) Content of Soil by Mass Basis	Lutheran Loamy Sand Field	July, 16, 17, 21, 22
	Asquith Loamy Sand Field	July, 23 August, 06, 07
	Asquith Summer Fallow Loamy Sand Field	July, 22, 23, 29 August, 06
	Saint-Denis Loam Field	August, 11, 13
	Saint-Denis Silty Clay Field	August, 11, 12
Texture Analysis	Lutheran Loamy Sand Field	May, 16 (Sampling) June, 02 (Extraction) June, 03 (Analysis)
	Asquith Loamy Sand Field	May, 16 (Sampling) June, 02 (Extraction) June, 03 (Analysis)
	Asquith Summer Fallow Loamy Sand Field	May, 16 (Sampling) June, 02 (Extraction) June, 03 (Analysis)
	Saint-Denis Loam Field	May, 20 (Sampling) June, 02 (Extraction) June, 03 (Analysis)
	Saint-Denis Silty Clay Field	May, 20 (Sampling) June, 02 (Extraction) June, 03 (Analysis)
Seed-to-Fertilizer Separation	Lutheran Loamy Sand Field	July, 16, 17, 21, 22
	Asquith Loamy Sand Field	July, 23 August, 06, 07
	Asquith Summer Fallow Loamy Sand Field	July, 22, 23, 29 August, 06
	Saint-Denis Loam Field	August, 11,13
	Saint-Denis Silty Clay Field	August, 11, 12
3-D Force Experimentation	Asquith Summer Fallow Loamy Sand Field	October, 03
Experimental Field trials with Crop Residues	Lutheran Loamy Sand Field	October, 20, 21, 31
	Lutheran Loamy Sand Field #2	October, 31

4.3 Openers

The opener section describes the apparatuses used during the field experimentations. The experimentations were performed with a total of six openers, which are described in detail to provide an understanding of the operating mechanism. Three of the six openers are concepts (Concept No.1, Concept No.2, and Concept No.3) especially developed for this work, which are based on a concept developed by CNHi prior to the beginning this thesis. The last version of the concept developed by CNHi was used as BenchMark Double-Shoot CNHi (BMDS CNH) to establish a base line to compare the performance of the concepts. The performances of the concepts are also compared with the Pillar Laser Inc. disc/hoe opener, which was selected as the BenchMark Double-Shoot (BMDS). The Pillar Laser Inc. disc/hoe opener allows comparison of double-shoot efficiency of the concepts versus a manufactured opener that used a similar double-shoot process. Moreover, the seeding performance of the concepts is compared to the John Deere 90 series opener, which is the single-shoot disc drill selected to be the BenchMark Single-Shoot (BMSS) due to its good reputation for seed placement. The BMSS was used to compare the seeding accuracy between manufactured single-shoot disc drills and the double-shoot concepts.

Furthermore, the last segment of the Openers section presents the development of the knife designs and their specific characteristics. Finally, the development of the knife design section displays the characteristics and provides the designs selected as concepts.

4.3.1 BMDS (BenchMark Double-Shoot)

The opener used as the BMDS is the Disc Hoe opener from Pillar Laser Inc. (U.S. Patent No. 7,540,246, 2009). This opener was selected because it uses a comparable process to the knife concept to distribute product. It was also selected because it is a popular seeding drill for local farmers due to its accuracy in the placement of the products. The BMDS uses a 457 mm (18 inch)

disc with a dual-purpose scraper/boot (Figure 4.22). The openers have two different adjustments: the main adjustment sets the disc depth, and the secondary adjustment sets the scraper/boot depth. The disc depth is the depth where the fertilizer is introduced into the ground (fertilizer depth in this situation). The scraper/boot depth is the distance between the fertilizer depth and the seed depth. Furthermore, the secondary adjustment is dependent on the main adjustment; the seed depth cannot be set directly. The opener only uses a single linkage between the frame and the opener with a spring in tension to create the down pressure (Figure 4.21). The BMDS is offered with three different types of rubber packing wheel: Standard, Smooth, and Pillar (Figure 4.20). The standard packing wheel is characterized by a thin double shoulder tread and a system of bearings to link the packing wheel to the opener. The Sooth and Pillar packing wheels use a system of hub and spindle to link the packing wheel to the opener combined with a tick tread. The Sooth packing wheel is characterized by a convex shape in contrast to the Pillar, which is equipped by a double shoulder tread similar to the Standard tread. The Pillar Laser Inc. opener was equipped with the Pillar packing wheel during the experiments. For more information about the Disc Hoe opener from Pillar Laser Inc., see subsection 3.1.21.

Figure 4.20. Pillar Laser $_{Inc.}$ three types of packing wheels (Courtesy of Pillar Disc/hoe Drill 2014 Brochure-http://www.pillarlasers.com/uploads/2013/08/1pagetoolbar%20copy.pdf).

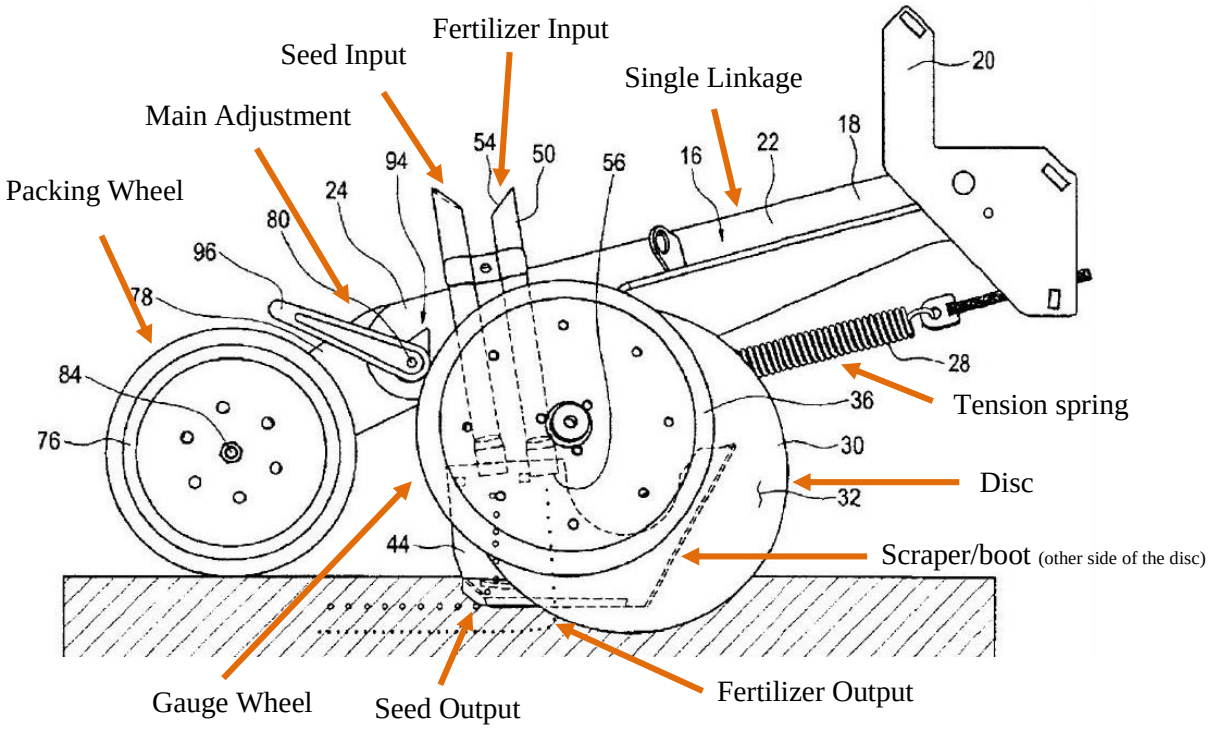

Figure 4.21. Side view Pillar Laser Inc. Disc/hoe opener (U.S. Patent No. 7,540,246, 2009).

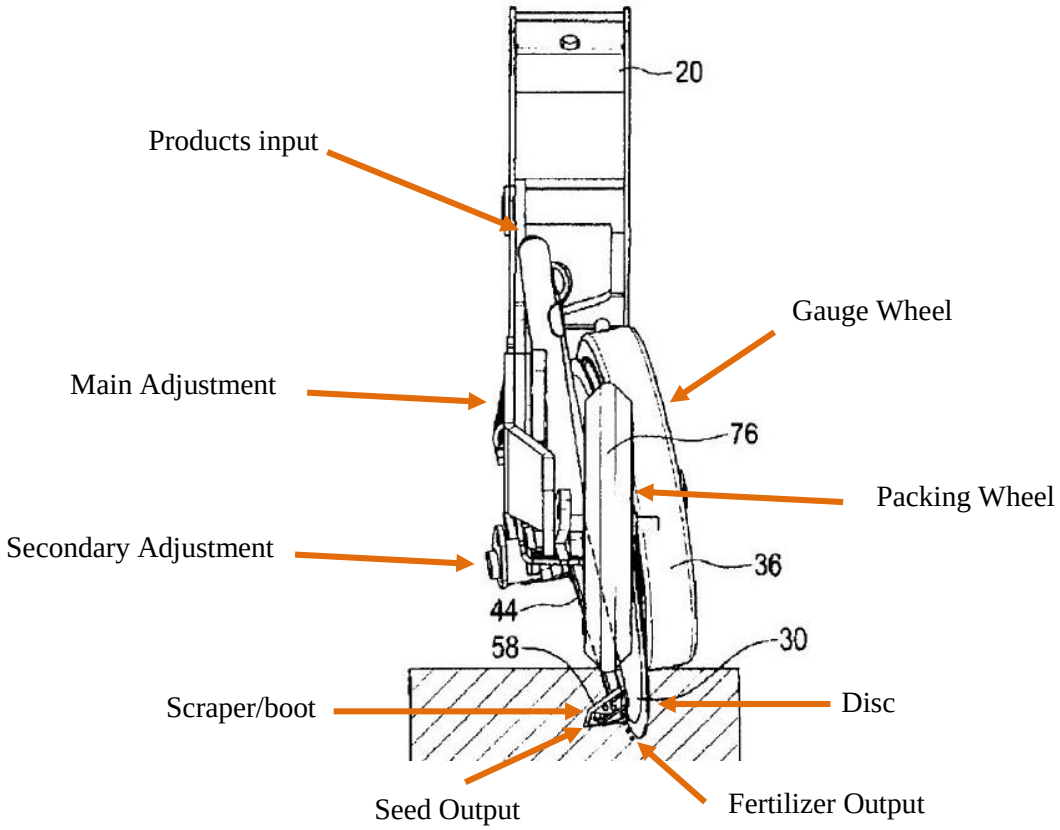

Figure 4.22. Rear view Pillar Laser Inc. Disc/hoe opener (U.S. Patent No. 7,540,246, 2009).

4.3.2 BMSS (Benchmark Single-Shoot)

The opener selected to be the BMSS is the John Deere 90 series opener (U.S. Patent No. 6,209,466, 2001), (U.S. Patent No. 4,760,806, 2001). The John Deere 90 series opener uses a disc of 457 mm (18 inches), which operates with a compound angle. The first angle is from the vertical and the second angle is from the direction of travel, in order to create the least possible soil disturbance. The opener only uses a single linkage between the frame and the opener, which is assisted by a compression spring to create the down pressure (Figure 4.23). The BMSS features a firming wheel to ensure that the seeds are correctly placed on the bottom of the furrow. Additionally, only the cast packing wheel is available for this opener.

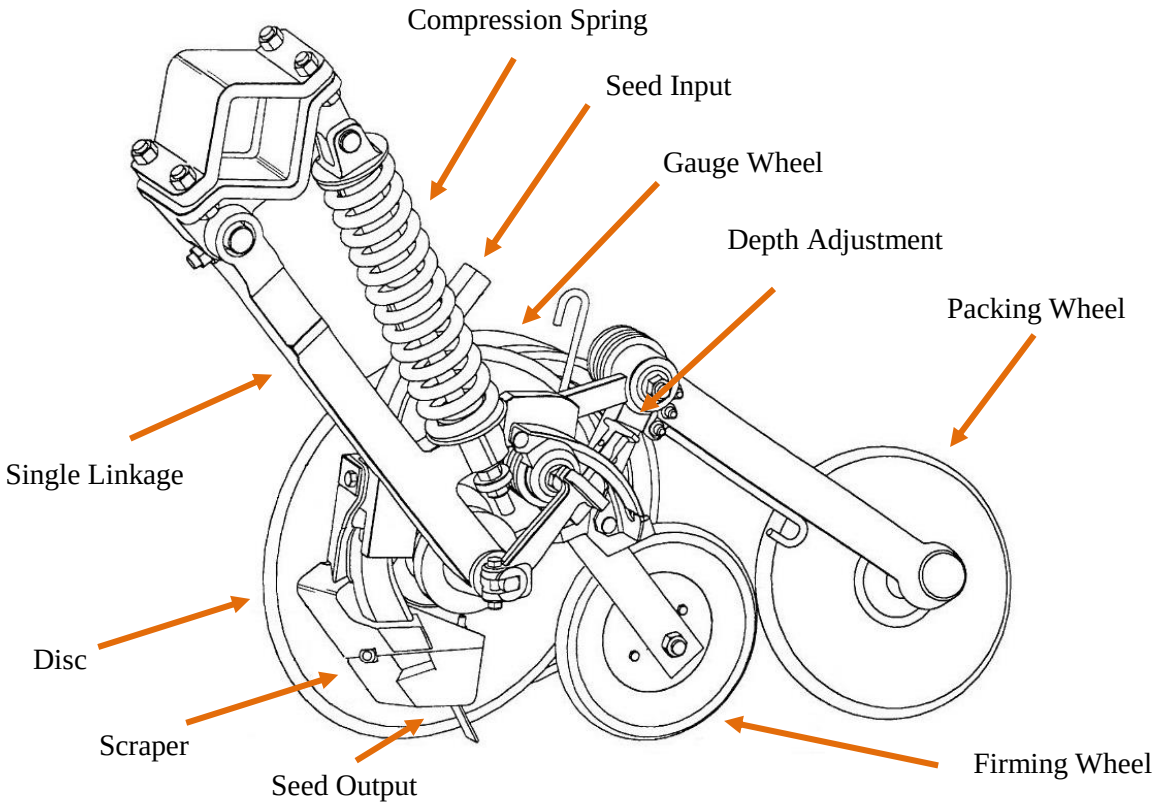

Figure 4.23. Side View John Deere 90 series openers (U.S. Patent No. 6,209,466, 2001).

4.3.3 CNH (Case New Holland) Openers

The CNH openers section includes the BMDS CNH, Concept No. 1, Concept No. 2, and Concept No. 3. They are all based on the CNHi double-shoot disc opener prototype (U.S. Patent No. 8,646,395, 2014). They use a 457 mm (18 in) disc with a scraper to put down the fertilizer followed by a knife, which introduces the seeds into the ground. The double-shoot disc opener from CNHi uses a system of parallel linkage made of one upper arm, and one lower arm (Figure 4.24). The parallel linkage allows the opener to be, at all times, correctly positioned according to the ground level, as opposed to the BMDS and BMSS, which can be positioned correctly at only one angle. Moreover, the parallel linkage allows the opener to keep an optimized seed/fertilizer placement during the ground level variation. Furthermore, the draft for the double linkage remains the same as on the flat ground during the ground level variation. The CNHi openers use a single compression spring to create the down force required to maintain the disc drill correctly in the ground. The openers have two adjustments: one main adjustment that sets the disc depth, and one secondary adjustment that sets the knife depth. The disc depth set by the main adjustment is the depth where the fertilizer is introduced into the ground (fertilizer depth). The knife depth set by the secondary adjustment is the distance between the fertilizer depth and the seed depth. Furthermore, the secondary adjustment is dependent on the main adjustment, which cannot set the seed depth directly from the ground surface. The openers use a straight packing wheel aligned in the direction of travel instead of the angular packing wheel shown in Figure 4.25. The BMDS CNH and the three concepts are different in terms of knife shape and interaction with the scraper. The knife front edge is different in terms of angle and length. The seed outlet of each knife is located at the same relative position in relation to the scraper.

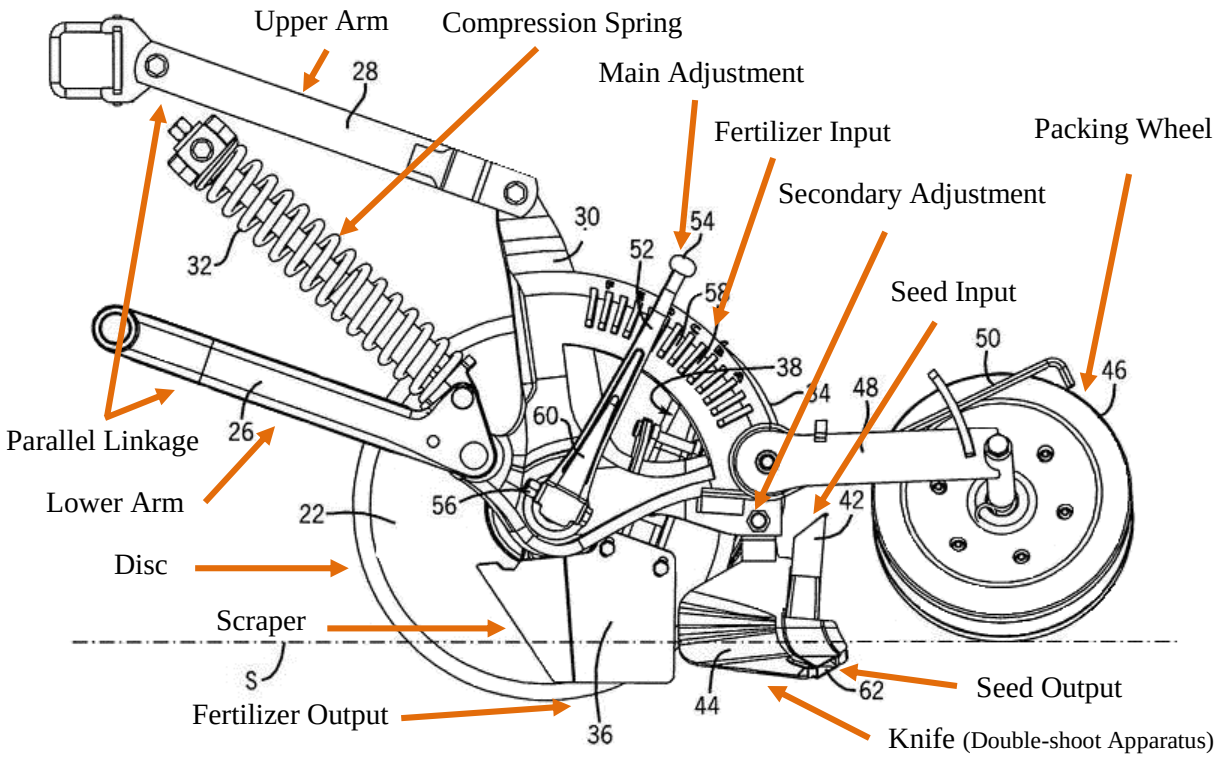

Figure 4.24. Side view CNH opener (U.S. Patent No. 8,646,395, 2014).

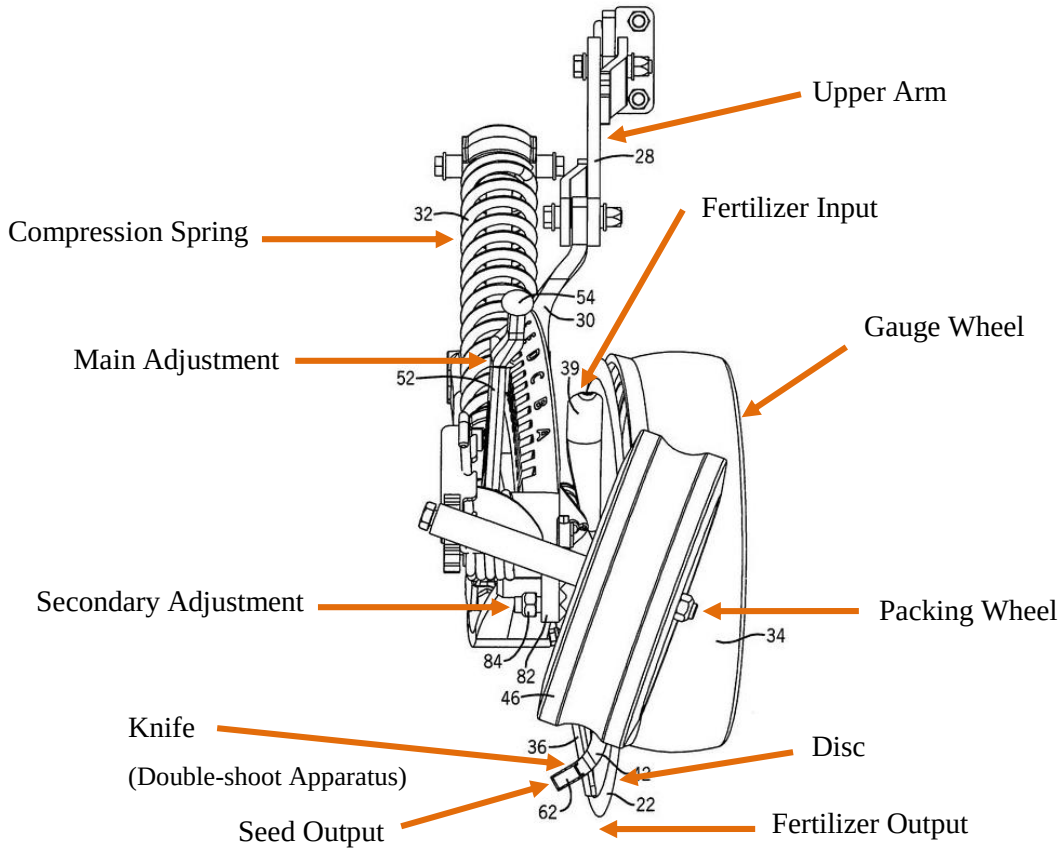

Figure 4.25. Rear view CNH opener (U.S. Patent No. 8,646,395, 2014).

The scrapers have two sets of parallel holes to follow the disc wear, as displayed in Figure 4.26, Figure 4.27, Figure 4.28, and Figure 4.29. The scrapers are installed on the upper set of holes (low position) when the discs are new, and when the disc wear is sufficient, the scrapers are moved to the lower set of holes (high position). The scrapers create a backwards movement when they move from their upper to their lower set of holes. The knives are located directly behind the scrapers while the scrapers are at their lower position. Then an overlap occurs while the scrapers move to their high position.

The knife heads (Figure 4.26) have a width of 76.2 mm (3 inches), a thickness of 25.4 mm (1 inch), a maximum depth notch (Figure 4.26), and 14 or 15 notches of 3.175 mm (1/8 inch), which allows a depth adjustment by increments of 6.35 mm (1/4 inch). The measurements from the side views, between the center of the knife heads and the closest scraper's edge, are 94.2 mm when the scrapers are at their low position and 88.5 mm when they are at their high position. Also, a horizontal distance of 28.2 mm is measured between the middle of the knife heads and the closest edge of the scrapers on the front view, as presented in Figure 4.30. The horizontal distance from the front view between the scrapers and the middle of the knives does not change at any of the scrapers' positions. Furthermore, in Figure 4.30, the reader needs to consider that all scrapers are unbent to allow a better view of the knives; only the end of the scrapers are at the right position, which determines the limit of the scrapers' shadow.

4.3.3.1 *BMDS CNH (Benchmark Double-Shoot Case New-Holland)*

The BMDS CNH is a prototype knife developed a few years prior to the project. The knife was developed in order to create an optimized product placement with a minimal increase of drafts. The BMDS CNH knife is mainly located in the shadow of the scraper, as shown in Figure 4.30 under the label BMDS CNH.

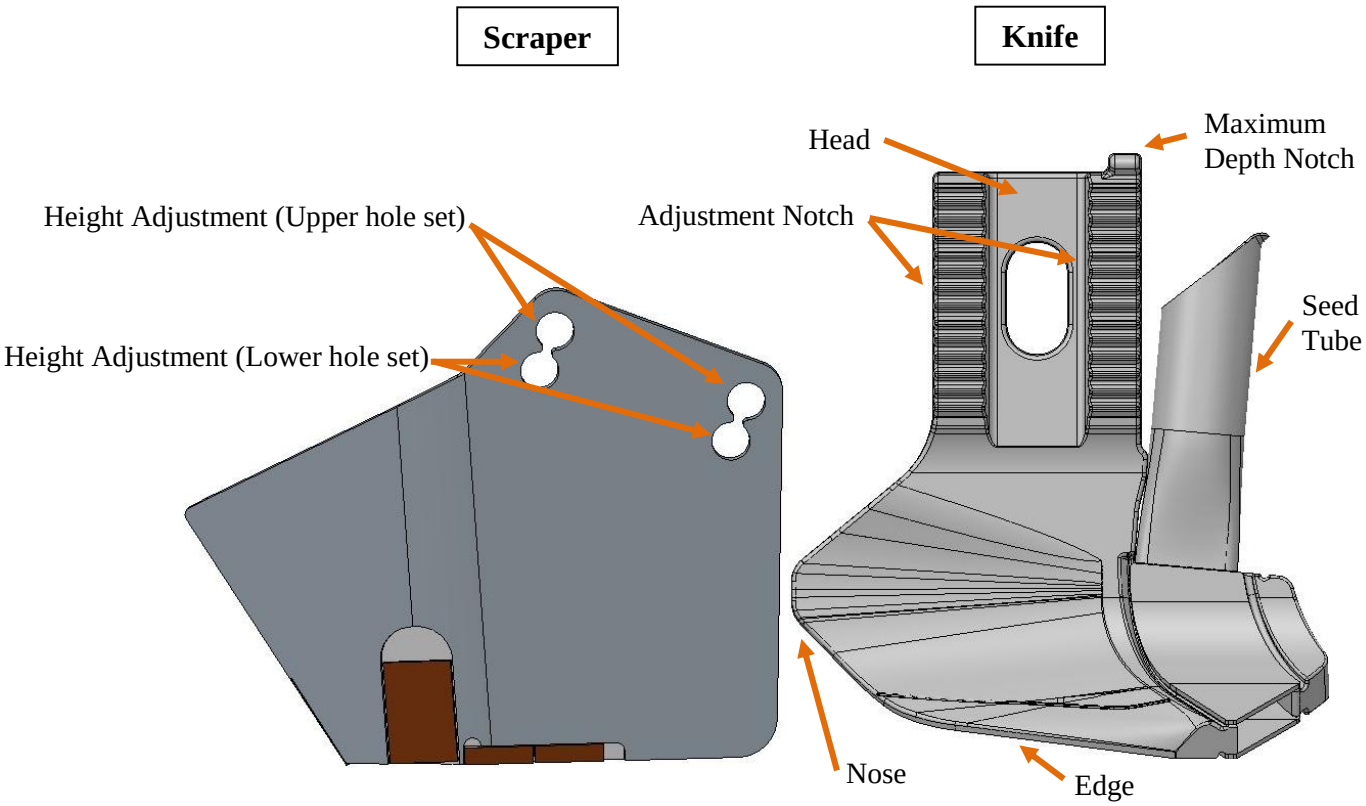

Figure 4.26. Side view BMDS CNH with the scraper.

The knife has a gap of 5 mm between the closest scraper edge and its nose when the scraper is at its low position. The distance on the side view (Figure 4.26) between the knife's nose and the closest edge of the scraper changes from a gap to an overlap of 1.2 mm when the scraper is at its high position. Also, in the front view, in Figure 4.30 under the BMDS CNH label, the knife has a horizontal distance of 15 mm between the knife's nose and the scraper's back high corner.

The knife has overall dimensions of 200 mm long by 225 mm high and 67 mm wide, including the seed tube. The nose thickness progressively increases from 5 mm to 16.5 mm before the seed tube. The edge thickness is approximately 3.2 mm, and increases to 16.5 mm before the seed tube as well.

The BMDS CNH is a double-shoot apparatus that has a knife curvature that begins from the back of the knife's head and goes outside of the scraper shadow (See Figure 4.30 under the

label BMDS CNH). Also, the back of the nose is directly aligned with the back of knife's head (Figure 4.30 under the label BMDS CNH). Furthermore, the BMDS CNH allows a gap of 47 mm between the scraper's end and the point where the knife edge begins to be outside of the scraper shadow (Figure 4.26).

4.3.3.2 ***Concept No. 1***

Concept No. 1 is a prototype knife developed a few years prior to the project. The knife was developed in order to keep the BMDS CNH ideal product placement with similar draft. Concept No. 1 knife is almost totally located in the shadow of the scraper as shown in Figure 4.30. under the label, Concept No. 1.

The knife has a gap of 5 mm between the closest edge of the scraper and its nose when the scraper is at its low position. The distance on the side view between the knife's nose and the closest edge of the scraper changes from a gap to an overlap of 1.2 mm when the scraper moves to its high position (Figure 4.27). Also, in Figure 4.30 under the Concept No. 1 label, the knife has a horizontal distance of 31 mm between the knife's nose and the scraper's back high corner.

The knife has an overall size of 200 mm long by 225 mm high and 67 mm wide, including the seed tube. The thickness of the nose's lowest part progressively increases from 5 mm to 16.5 mm before the seed tube. The nose's highest part keeps a thickness of 5 mm until the head increases drastically to 16.5 mm (Figure 4.27). The edge thickness is approximately 2.5 mm and increases to 16.5 mm before the seed tube.

Concept No. 1 is a double-shoot apparatus with a knife curvature that begins from the back of the knife's head and goes outside of the shadow of the scraper (Figure 4.30 under the label Concept No. 1). Also, the back of the nose is aligned with the back of the knife's head (Figure 4.30 under the label Concept No. 1). Furthermore, Concept No. 1 allows a gap of 47 mm between the

scraper's end and the point where the knife edge begins to be outside of the scraper shadow (Figure 4.27).

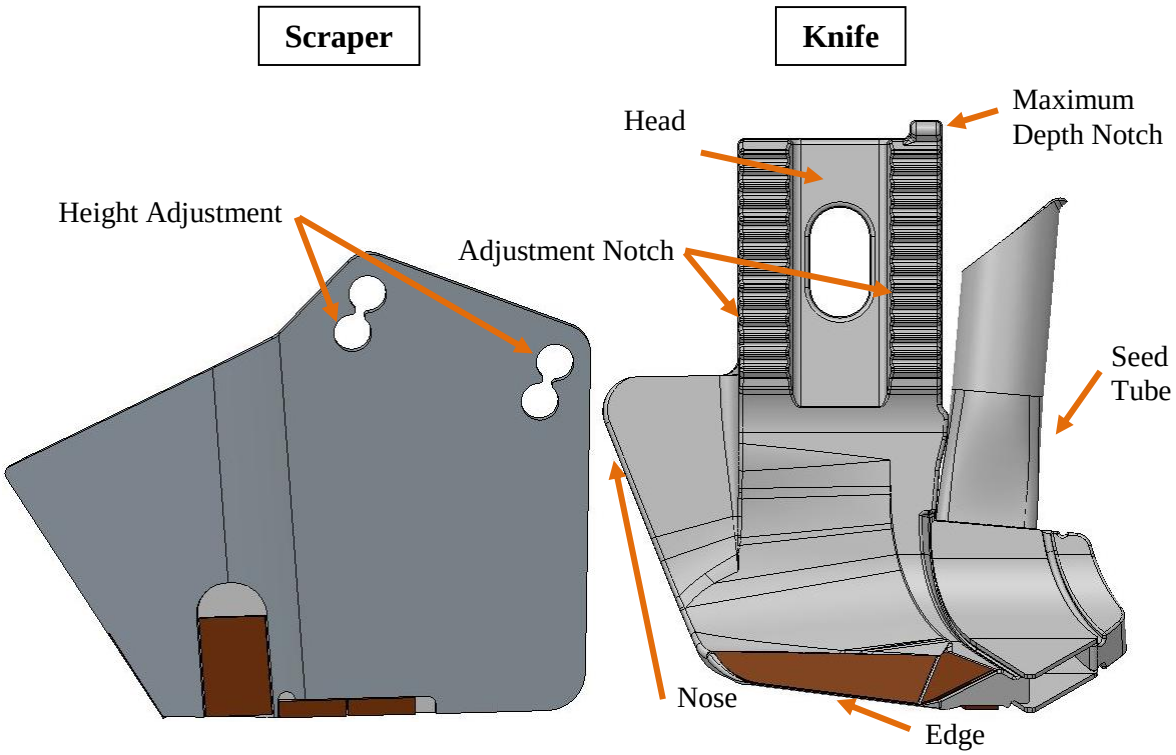

Figure 4.27. Side view Concept No. 1 with the scraper.

4.3.3.3 ***Concept No. 2***

Concept No. 2 is a prototype knife developed specifically for this project. The knife is developed in order to keep the same ideal product placement of the BMDS CNH with similar draft. The Concept No. 2 knife is almost wholly located in the scraper shadow as shown in Figure 4.30 under the label Concept No. 2.

The knife is completely located behind the scraper when the scraper is in the low position, but when the scraper moves to its high position, the knife needs to move backward to follow the horizontal scraper displacement. The displacement system is only expected on the last version of the knife, and not on the knife used during the project. The system uses a head and head hole wider

than the head currently used, to allow lateral displacement. Also, an eccentric or cross-shaped washer is required with the wide head/head hole system to maintain the knife in place.

The knife has an overlap of 15.5 mm between the knife's nose and the scraper end edge notwithstanding the scraper's position. The overlap between the knife and the scraper is described as a lip; it is displayed in blue in Figure 4.28. Also, in the front view of Figure 4.30 under the Concept No. 2 label, the knife is almost touching the scraper, which helps to retain the deformation created on the scraper by the ground force.

The knife has overall dimensions of 221 mm long, by 225 mm high, and 57.5 mm wide, including the seed tube. The lip (blue section in Figure 4.28) is 5 mm thick until the edge of the scraper, which increases by 6.3 mm as the scraper thickens. The knife thickness from the scraper end increases from 11.3 mm to 16.5 mm before the seed tube (Figure 4.28). The edge thickness increases from approximately 3.5 mm to 16.5 mm before the seed tube.

Concept No. 2 is a double-shoot apparatus knife with two curvatures beginning at each side of the nose until the end of the knife (Figure 4.30 under the label Concept No. 2). The outside curvature (the curvature coming outside of the scraper's shadow) begins at the scraper's edge to facilitate the transition between the scraper and the knife. The inside curvature begins on the lip and goes directly to the end of the knife. Also, the knife's nose is positioned near the scraper's end, which closes the space during the use of the disc drill. The space left between the scraper and the knife is considered as tolerance to adjust the knife as close as possible to the scraper. The Concept No. 2 configuration does not allow any gap between the scraper's end and the point where the knife edge begins to be outside of the scraper shadow (Figure 4.28). Furthermore, the seed output is located at the same position as the BMDS CNH to keep the same optimal seed distribution.

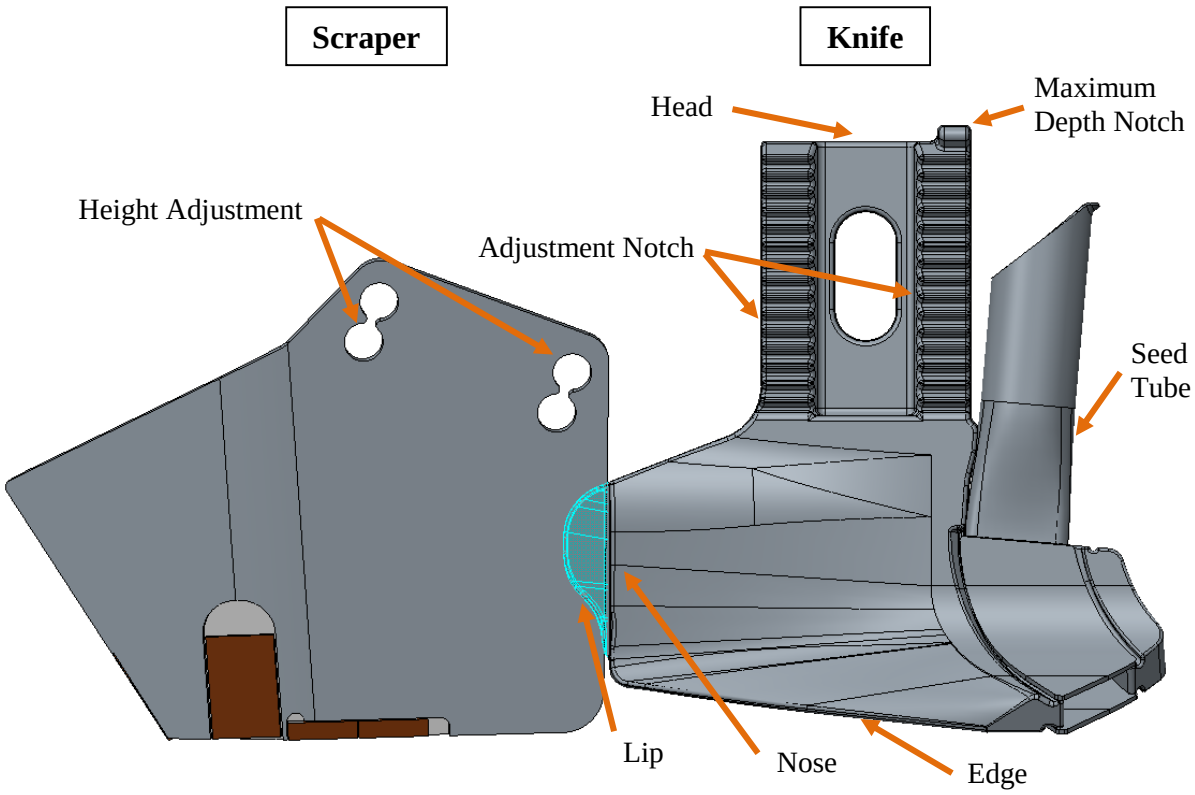

Figure 4.28. Side view Concept No. 2 with the scraper.

4.3.3.4 ***Concept No. 3***

Concept No. 3 is a prototype knife that was developed specifically for this project. The knife was developed in order to keep the ideal product placement of the BMDS CNH with equivalent draft. The concept No. 3 knife is almost entirely located in the shadow of the scraper, as revealed in Figure 4.30 under the label Concept No. 3.

The knife is completely located behind the scraper when the scraper is in its low position, but when the scraper moves to its high position, the knife needs to move backward to follow the horizontal scraper displacement. The displacement system is only presented on the last version of the knife, and not on the knife used during the project. The system uses a wider head and head hole than the current head, to allow the lateral displacement. Also, an eccentric or cross-shaped washer is required with the wide head/head hole system to maintain the knife in place.

The knife's nose is located directly behind the end of the scraper, which has the same curvature as the scraper. The knife's nose stays hidden behind the scraper notwithstanding the scraper's position (Figure 4.30 under the Concept No. 3 label). The knife has overall dimensions of 205 mm long by 225 mm high and 57.5 mm wide, including the seed tube (Figure 4.29). The scraper nose is 6.4 mm thick, and becomes thicker at the two curves, until 16.5 mm before the seed tube. The edge thickness is approximately 3.5 mm and increases to 16.5 mm before the seed tube.

Concept No. 3 is a double-shoot apparatus knife with two curvatures, which begin on each side of the nose and goes through the end of the knife (Figure 4.30 under the label Concept No. 3). The outside curvature (the curvature that comes outside of the scraper's shadow) begins directly on the external scraper's edge to facilitate the transition between the scraper and the knife. The inside curvature begins directly on the inside scraper's edge to facilitate the product's transition. Also, the knife's nose is positioned near the scraper end, which closes the space during the use of the disc drill. The space left between the scraper and the knife is considered as tolerance to adjust the knife as close as possible to the scraper. The Concept No. 3 configuration does not allow any gap between the scraper's end and the point where the knife's edge begins to be outside of the scraper shadow (Figure 4.29). Furthermore, the seed output is located at the same position as the BMDS CNH to keep the same optimum seed distribution.

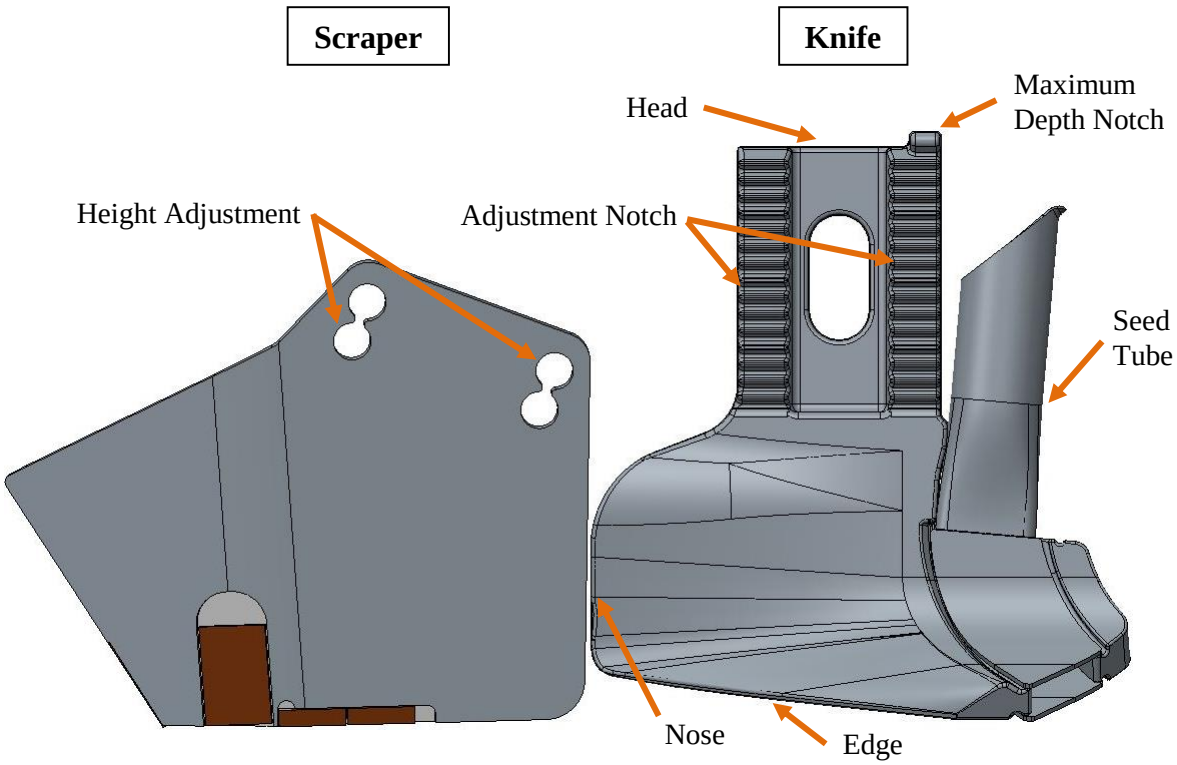

Figure 4.29. Side view Concept No. 3 with the scraper.

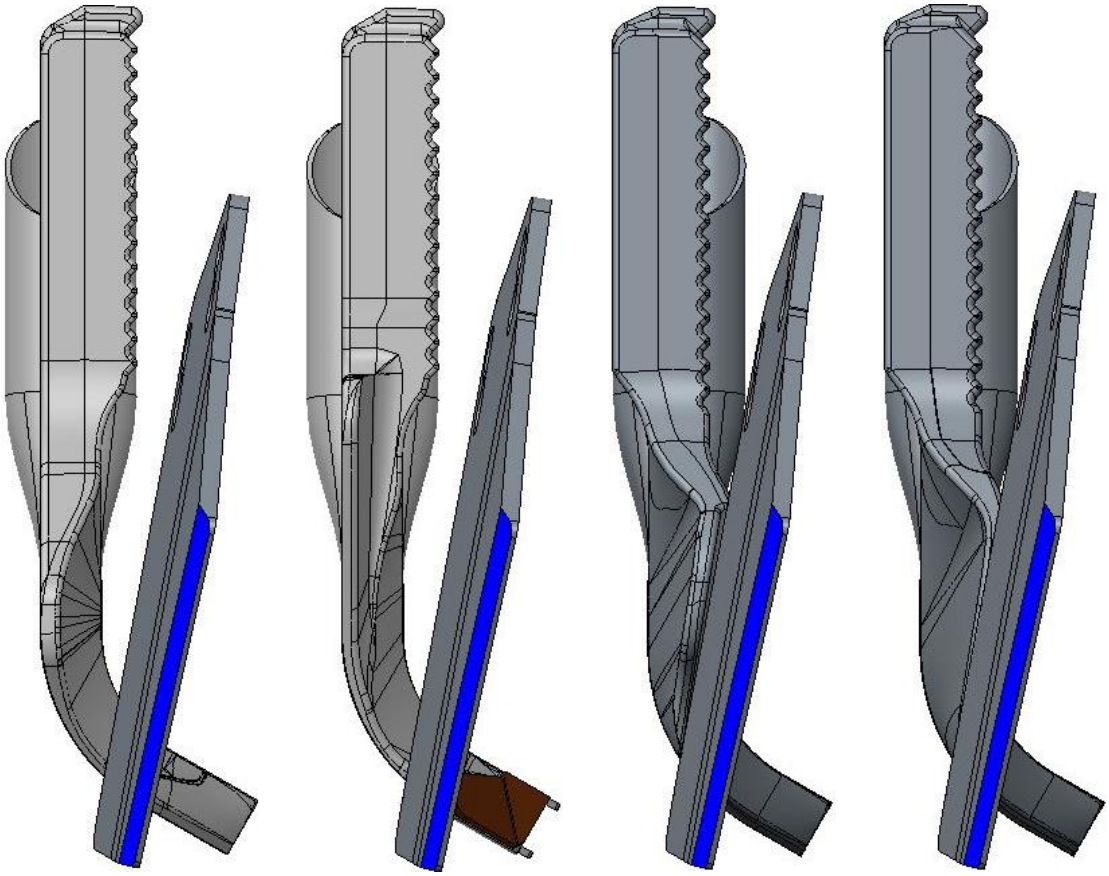

Figure 4.30. Front view of the knives with the scraper unbend.

4.3.4 Knife Designs Development

The concepts were selected through knife design development, which were elaborated from the BMDS CNH. Design No.00 use the same characteristics as the BMDS CNH except for its nose, which is higher (Figure 4.31. Design No.00) to provide more room between the end of the scraper and the knife (Figure 4.33. Design No.00). Design No.01 reuses the same curvature as the BMDS CNH (Figure 4.32. Design No.01), but its nose is extended (See Figure 4.33. Design No.01) with a notch (Figure 4.31. Design No.01), which prevents the scraper from bending excessively to maintain it in an ideal position. Furthermore, the notch of Design No. 01 allows a smoother attack edge angle and transition between the scraper and the knife (Figure 4.33. Design No.01). Design No.02 reuses the characteristics of Design No.01 (Figure 4.33. Design No.02) with an improved nose and notch (Figure 4.31. Design No.02). Design No.03 incorporates the characteristics of the Design No.02, with a nose curve towards the scraper (Figure 4.31. Design No.03), which closes the gap between the scraper and the knife (Figure 4.33. Design No.03). Design No.04 reuses the peculiarity of Design No.03, in addition to shifting the mounted location of the knife main part from the back to the notched side of the knife head (Figure 4.32. Design No.04). The shifted position of the knife main part improves the soil flow between the scraper and the knife (Figure 4.33. Design No.04). Design No.05 resumes the characteristics of Design No.4, improved by a notched nose (Figure 4.31 and Figure 4.32. Design No.05), which protects the scraper against excessive deformation and maintains it at optimal position. The notch in the nose of Design No.05 is created to merge with the scraper (Figure 4.33. Design No.05), to provide an optimal soil flow between the scraper and the knife. Design No.06, as the other knives, reuses the characteristics of the previous knife design augmented by an improved feature. Design No.06 is directly positioned behind the scraper (Figure 4.33. Design No.06), with a nose cut straight (Figure 4.31. Design

No.06). The Design No.06 nose shape and its positioning behind the scraper allow an optimum soil flow between the scraper and the knife. However, three concepts were selected from the characteristics enumerated above to be the experimental concepts. Design No.00 was selected as Concept No.1 to evaluate the alternative to provide more space between the end of the scraper and the edge of the knife. Design No.05 was designated as Concept No.2 to determine the efficiency of the knife shape and its notch. Finally, Design No.06 was selected as Concept No.03 to conclude on the performance of the knife shape, and the option of closing the gap between the scraper and the knife. Furthermore, Figure 4.31 to Figure 4.33 are displayed with fuchsia arrows, which display the specific characteristics of the different designs. Moreover, the specific characteristics and the designs selected are compiled in the knife development summary Table 4.3.

Table 4.3. Knife design development summary table.

Design	Specific Characteristic	Design Selected
BMDS CNH	• Knife used as the starting point for the development of the knife designs	BMDS CNH
Design # 00	• Higher nose and same curvature than the BMDS CNH (Developed prior the project)	Concept No.1
Design # 01	• Longer nose and same curvature than the BMDS CNH • Notch created in the attack edge to retain the scraper	
Design # 02	• Nose and notch are modified from the Design No.1 • Same curvature than the BMDS CNH	
Design # 03	• Nose of the knife closing the gap in between the knife and the scraper	
Design # 04	• Main part of the knife shifted from the back to the notched side of the knife head	
Design # 05	• Notch in the nose of the knife created to merge with the scraper	Concept No.2
Design # 06	• Knife trailing the scraper	Concept No.3

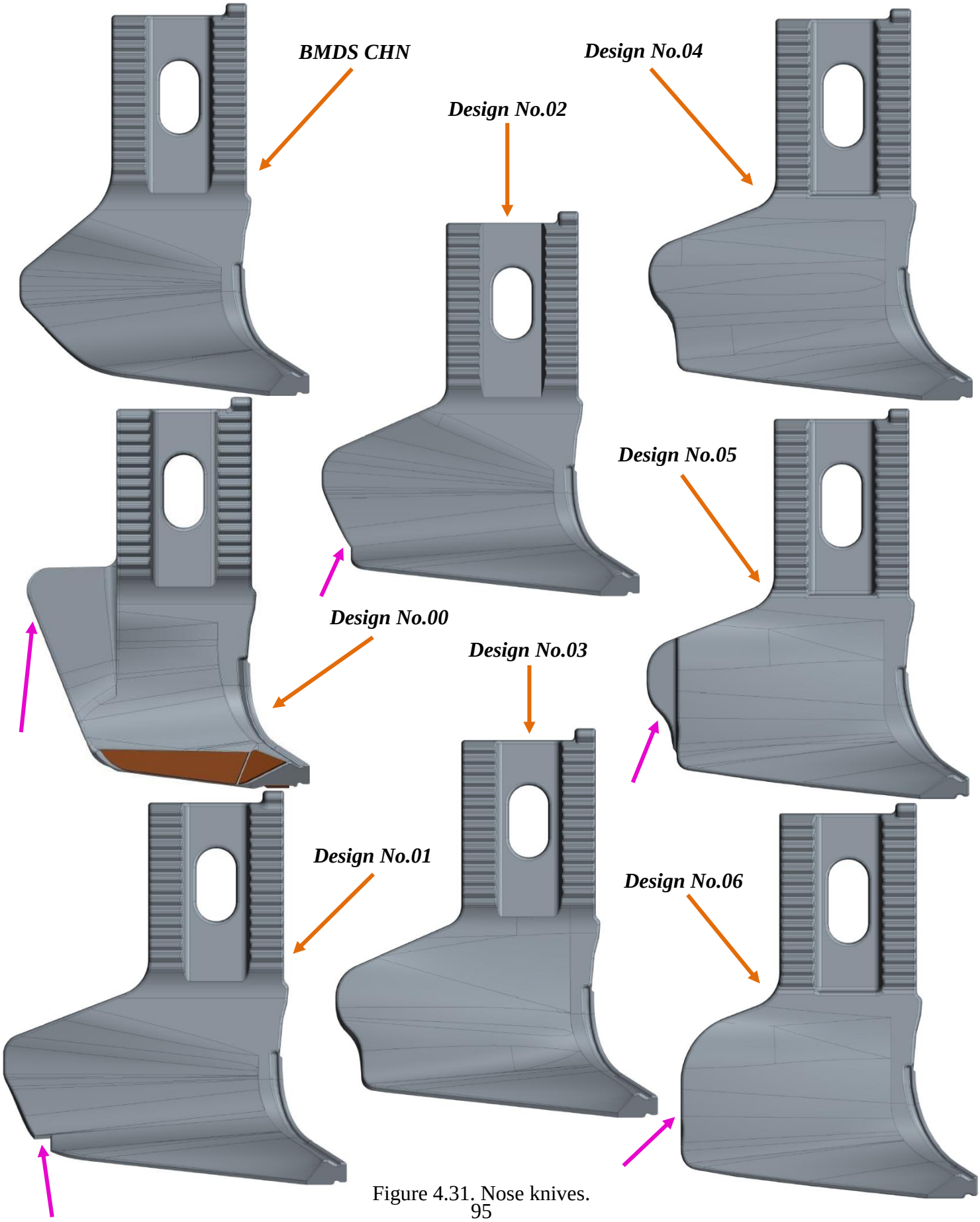

Figure 4.31. Nose knives.

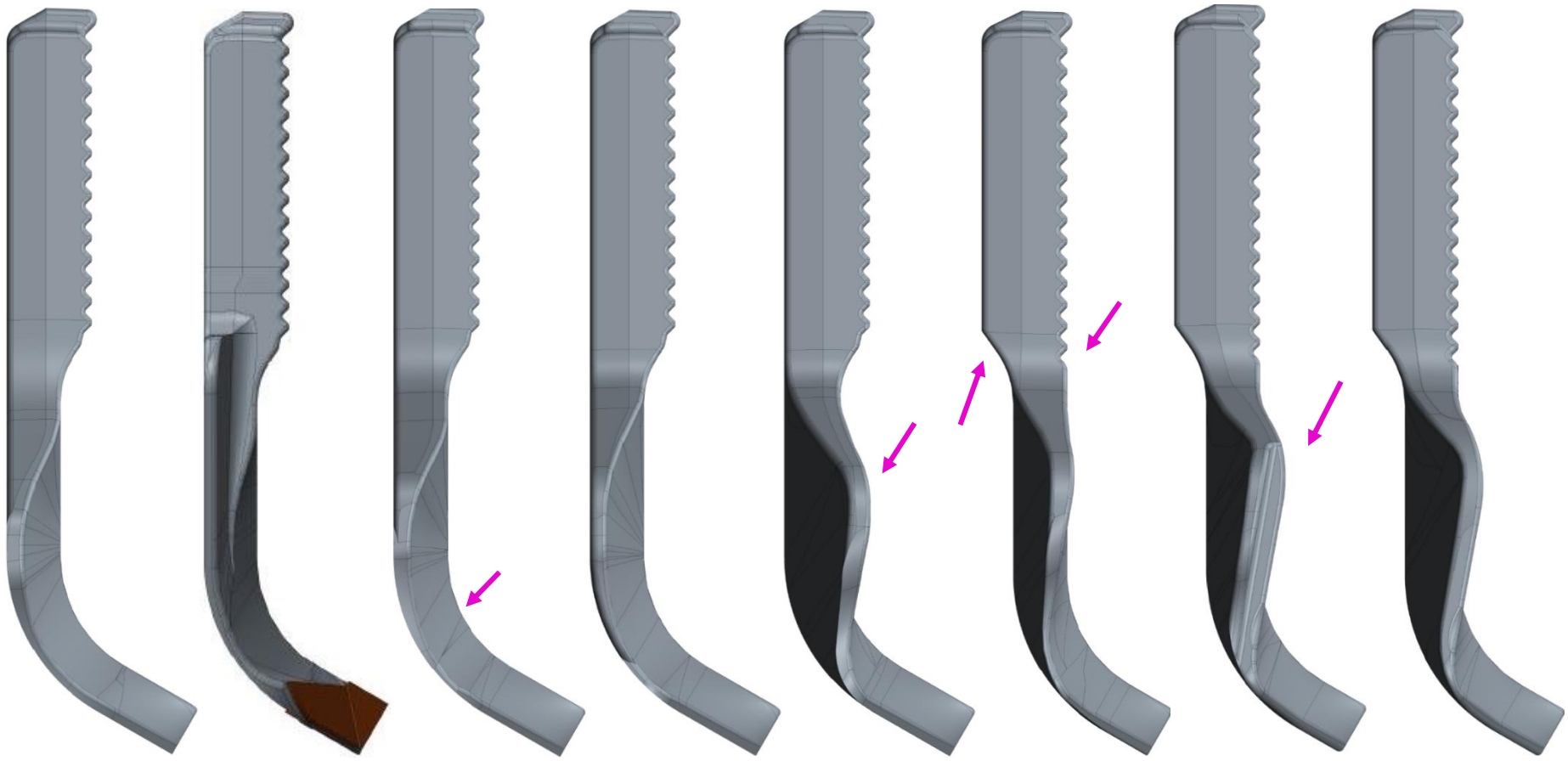

Figure 4.32. Front view of the knives.

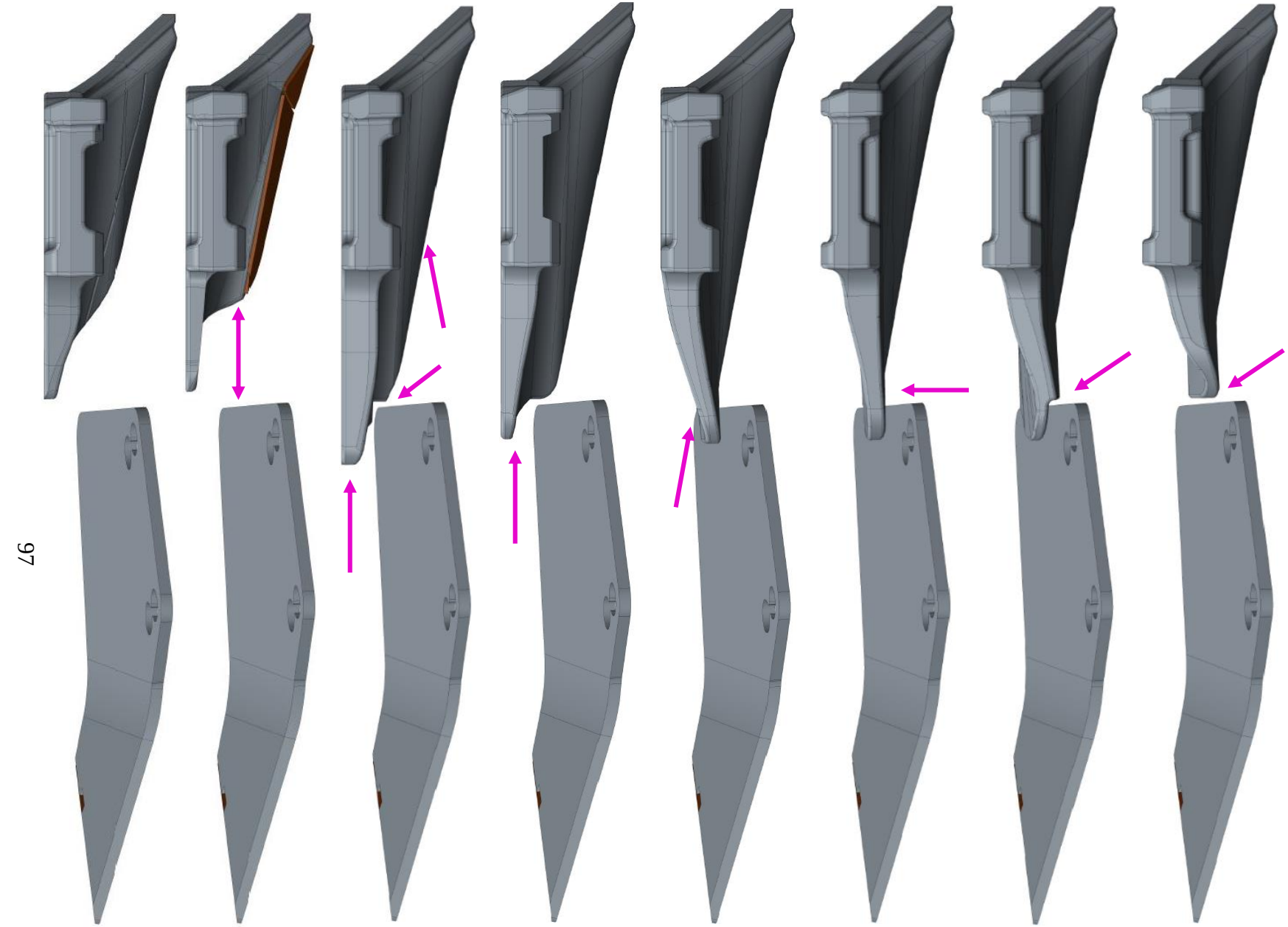

Figure 4.33. Top view of the knives with the scraper.

4.4 Seed-to-Fertilizer Separation

The seed to fertilizer separation experiment required the most planning due to the number of trials performed. The tests required all five fields, which are described in section 4.1. The experiments were conducted with an apparatus that simultaneously operated the six openers. This series of experiments was performed to evaluate their performances in the same conditions. The openers are statistically evaluated on the placement of two products at two velocities. Also, the configurations were repeated three times each (i.e. Lutheran Loamy Sand Field at 8.85 kmh^{-1} (5.5 mph) with the wheat crop).

The subplot colour presented in Figure 4.4, Figure 4.9, Figure 4.12, Figure 4.15, and Figure 4.18 in Section 4.1 Fields represents the different combinations between the crop type and the velocity. The yellow subplot represents the wheat crop at 8.85 $km \cdot h^{-1}$ (5.5 mph), the green subplot designates the wheat crop at 12.87 $km \cdot h^{-1}$ (8.0 mph), the blue subplot defines the canola crop at 8.85 $km \cdot h^{-1}$ (5.5 mph), and the brown subplot belongs to the canola crop at 12.87 $km \cdot h^{-1}$ (8.0 mph).

The seed to fertilizer experiments used one opener of each type, which are the following: a benchmark double-shoot (BMDS), a benchmark double-shoot CNH Industrial (BMDS CNH), a benchmark single-shoot (BMSS), a Concept No. 1, a Concept No. 2, and a Concept No. 3. The openers have a minimum of 510 mm (~20 inches) between them to ensure that no interactions are possible, and to avoid external interferences on the product placement. The openers are positioned on the apparatus the same way as the experimental field trials with crop residues, except the rear row, which includes only the BMDS and the BMSS as disc drill. The opener positions are displayed in Figure 4.48 to Figure 4.50.

The seed/fertilizer separation experiment involves comparing the seeds and the fertilizer placement between the openers. The opener's comparison required the determination of three measurements: the seed depth, the fertilizer depth, and the horizontal distance. These three measurements will be used to determine the entire Section 5.2.1 Seed-to-Fertilizer Separation. The seed depth and the fertilizer depth are taken from the surface of the ground through the products. The ground surface is reproduced with a ruler laid down perpendicularly to the furrow edge, in order to take accurate measurements. The horizontal distance is taken at 90˚ of the seed and the fertilizer furrows between a seed and a fertilizer particle. The measurements and the ruler are displayed in Figure 4.34.

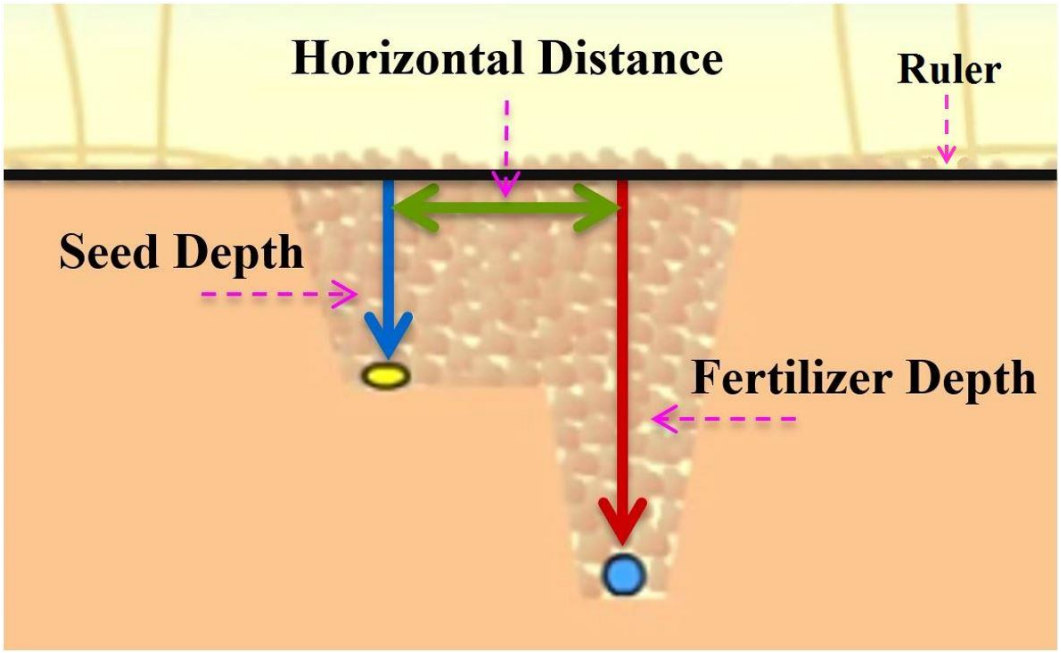

Figure 4.34. Measures taken for the seed and fertilizer separation experiment.

The protocol for the seed/fertilizer separation experiment is developed under nine steps enumerated below with visual support from Figure 4.35 to Figure 4.43, inclusively. Steps 7 through 9 must be repeated at intervals of 50 mm until 1 m long distance. The three different measurements should have 21 inputs each. The nine-step protocol is elaborated as follows:

Step No. 1: Localization of the furrow: the pink line represents the furrow.

Figure 4.35. Step No. 1: Furrow localization.

Step No. 2: Cutting grass on the top of the furrow.

Figure 4.36. Step No. 2: Cutting grass on the top of the furrow.

Step No. 3: Cleaning the furrow surface.

Figure 4.37. Step No. 3: Cleaning the furrow surface.

Step No. 4: Digging the localization hole.

Figure 4.38. Step No. 4: Digging the localization hole.

Step No. 5: Digging the seed furrow for one metre (blue dash line).

Figure 4.39. Step No. 5: Digging the seed furrow.

Step No. 6: Digging the fertilizer furrow for one metre (red dash line).

Figure 4.40. Step No. 6: Digging the fertilizer furrow.

Step No. 7: Seed depth measurement.

Figure 4.41. Step No. 7: Seed depth measurement.

Step No. 8: Fertilizer depth measurement.

Figure 4.42. Step No. 8: Fertilizer depth measurement.

Step No. 9: Measurement at 90˚ between a seed and a fertilizer particle (Green Arrow).

Figure 4.43. Step No. 9: Measurement at 90˚ between a seed and a fertilizer particle.

4.5 3-D Force Experiments

The 3-D force experimental apparatus was developed from a device used for decades at the University of Saskatchewan. This device has undergone some modifications through the years. The version used by Vaishnav (1983) employed six load cells like the modern apparatus, but the load cell geometry was different. The research apparatus used one load cell to measure the draft, two to measure the vertical forces, and three to measure the side forces. The current apparatus was modified to use two load cells to measure the draft forces, three to measure the vertical loads, and one to measure the side load, according to Chandon and Kushwaha (2002). The current apparatus used by the university is displayed in Figure 4.44.

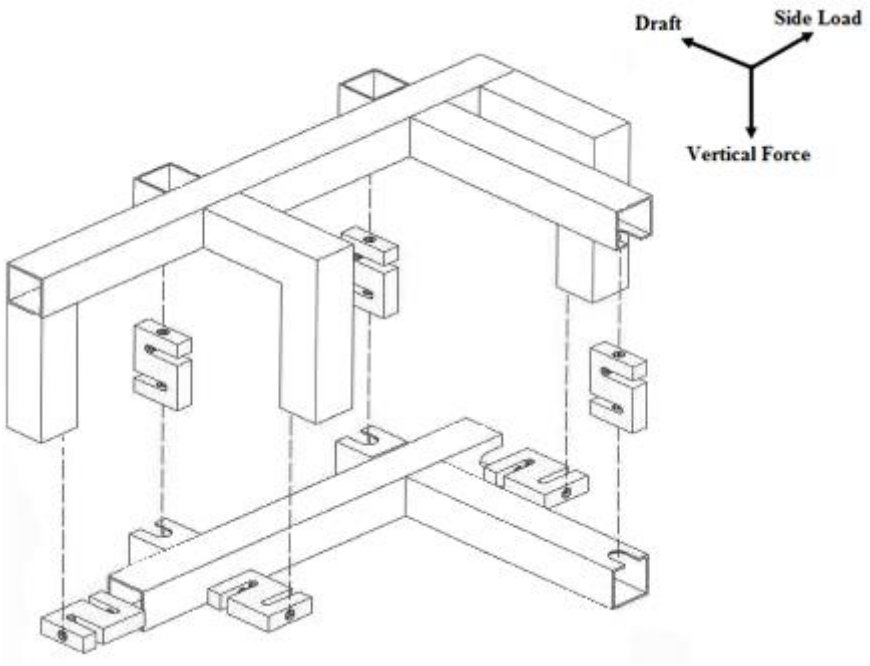

Figure 4.44. 3-D force apparatus developed by Chardon and Kushwaha (2002).

The apparatus used during the field testing in the present research has few adjustments from Figure 4.44, and is shown in Figure 4.45, and Figure 4.46. The third vertical load cell (V3) is aligned with one of the first two vertical load cells (V1, or V2) (see Figure 4.45), but located in

the middle of the two. The third load cell has the same horizontal distance as the university apparatus. The second modification is related to the side load cell (SL) as shown in Figure 4.46. It has the same configuration as the university apparatus, but is transferred to the other side of the device.

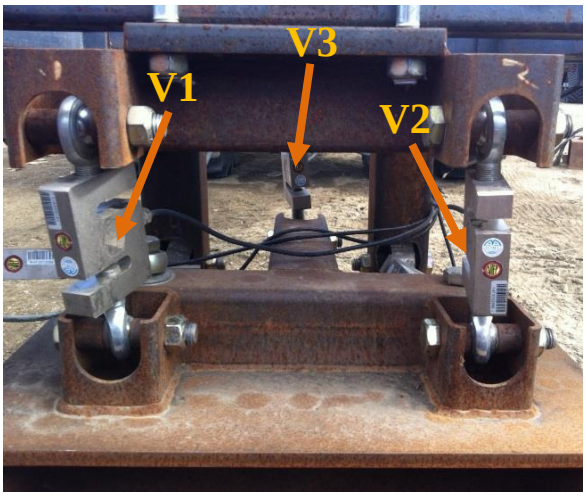

Figure 4.45. 3-D force apparatus vertical load cells.

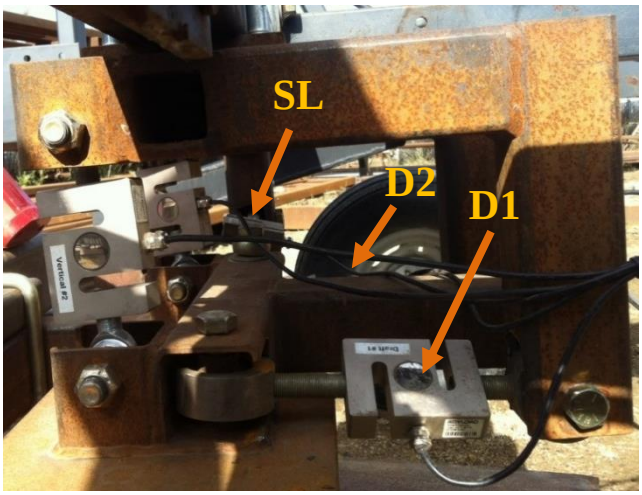

Figure 4.46. 3-D force apparatus draft and side load cells.

The 3-D experimental apparatus used six load cells (101NH ANYLOAD, Hangzhou, Zhejiang, China) with 4545.45 kg (10000 lbs.) capacity. The load cells were connected to a 6 m long 4-core shielded cable, which was linked to a relay box, model NI 9949 (National Instrument, Zhonglu, China). The relay boxes were connected to a recorder unit, model NI 9237 (National Instrument, Debrecen, Hungary), serial number 198859B-01L, by a 2 m long cable Cat-5E Ethernet National Instruments, made in China, serial number 151733A-02. The recorder unit was attached to a data logger, model NI cDAQ-9174 National Instruments made in Hungary, serial number 199FCB7. The data logger and the load cells received 10 V of excitation to be functional.

The load cells were employed at an acquisition rate of 500 Hz. The data were gathered by the data logger and analyzed using Lab View version 9.0.1 software, in order to be saved under

the .lvm file format. The data was refined by MATLAB version 2014b using a low pass Butterworth filter. The filter used a cutoff frequency of 50 Hz to reduce the noise and smoothen the data. Figure 4.47 presents the filtered data coloured in fuchsia versus the raw data in blue. The data was finally saved in a file supported by Excel® version 2013 to be adapted for the required statistical analysis.

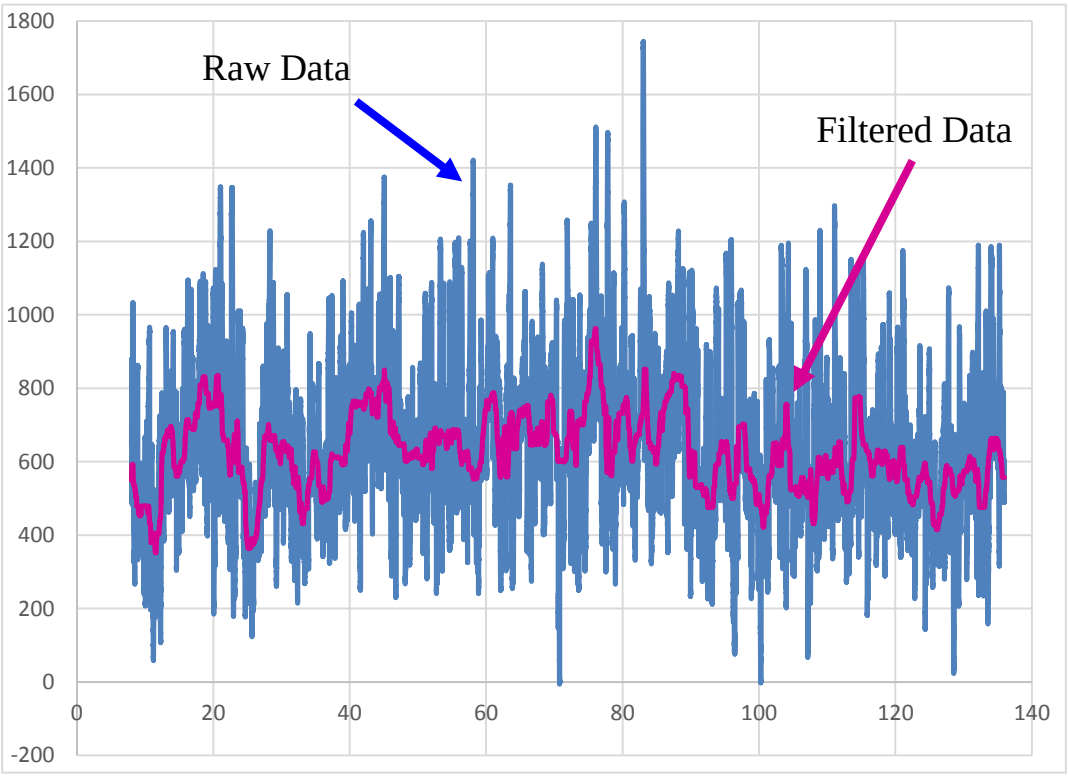

Figure 4.47. Raw data versus filtered data.

The 3-D force experiments were carried out solely at the Asquith Summer Fallow Loamy Sand Field location, with 4 geometries: BMDS CNH, Concept No. 1, Concept No. 2, and Concept No. 3. The openers were adjusted for wheat conditions, which were 50.8 mm (2 inches) deep for the fertilizer and 25.4 mm (1 inch) deep for the seed. The same two ground speeds were used as

during the seed/fertilizer separation experiments, which were 8.85 $km \cdot h^{-1}$ (5.5 mph) and 12.87 $km \cdot h^{-1}$ (8.0 mph). Furthermore, each combination was replicated three times.

4.6 Experimental Field Trials with Crop Residues

The experimental field trials with crop residues was an experiment without data acquisition. The tested openers could only pass or fail (Yes or No test). The experiment determined if the capacity of each opener was sufficient to pass through a field with a critical content of residue without hair pinning or plugging due to crop residue accumulation. These trials determined if the opener behaviour was refined enough to avoid accumulation of crop residues.

The tests were conducted with an experimental plot drill fill with a benchmark single-shoot (BMSS), a benchmark double-shoot (BMDS), two benchmarks double-shoot CNH Industrial (BMDS CNH), two Concepts No. 1, two Concepts No. 2, and two Concepts No. 3. All openers were tested at the same time, on the same experimental plot drill, and on the same location with a minimum distance of 510 mm (~20 inches) between them. The distance between the openers ensured avoiding any interactions between them. The plot drill was divided into two sides: left wing and right wing (in direction of travel). Furthermore, each wing had a front and a rear row. The left wing front row was equipped from the left to the right with a concept No. 1, and a BMDS CNH. The left wing rear row was equipped from the left to the right with a BMDS, a BMDS CNH, and a Concept No. 1. The right wing front row was equipped from the left to the right with a concept No. 2, and a concept No. 3. The right wing rear row was equipped from the left to the right with a concept No. 3, a concept No. 2, and a BMSS. For a visual description of the opener's placement on the plot drill, see Figure 4.48 to Figure 4.50.

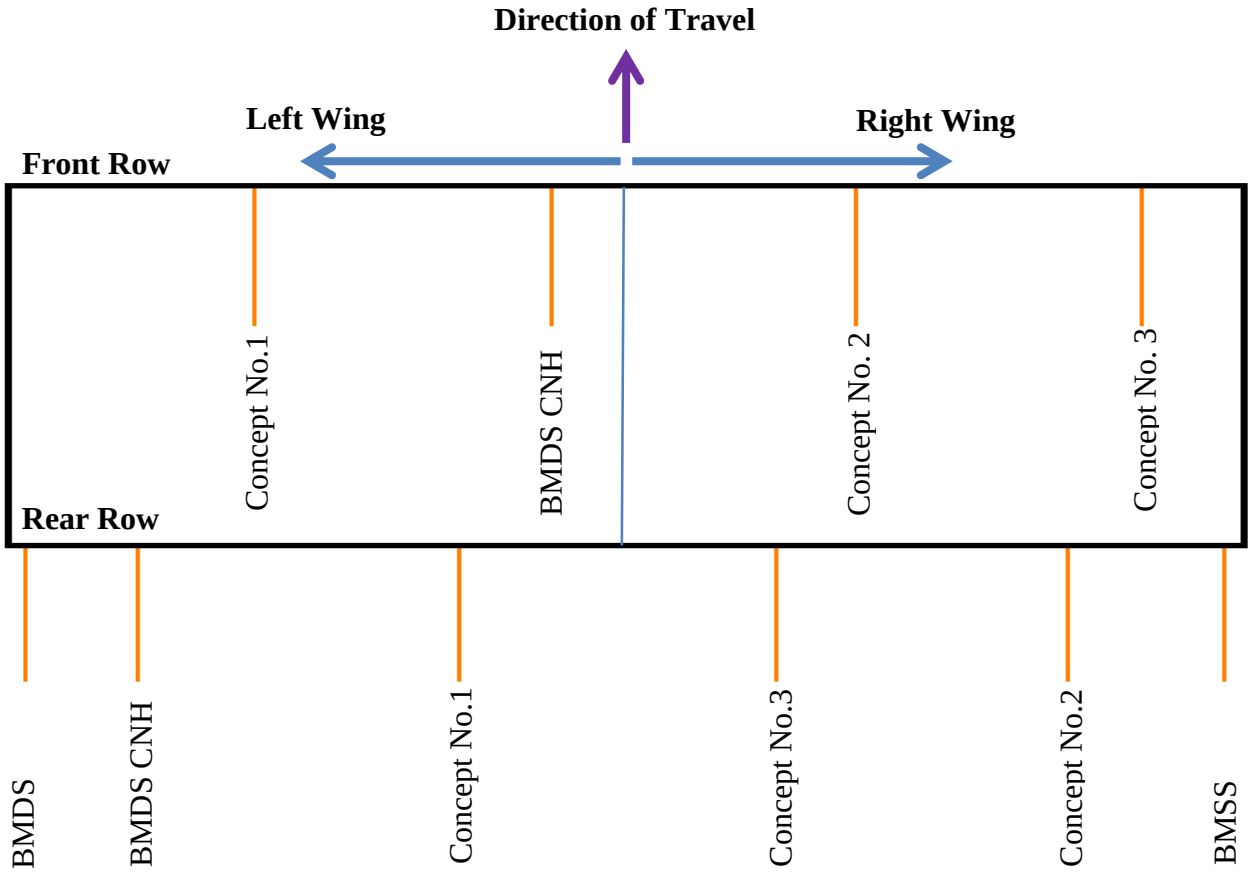

Figure 4.48. Plot drill top view representation.

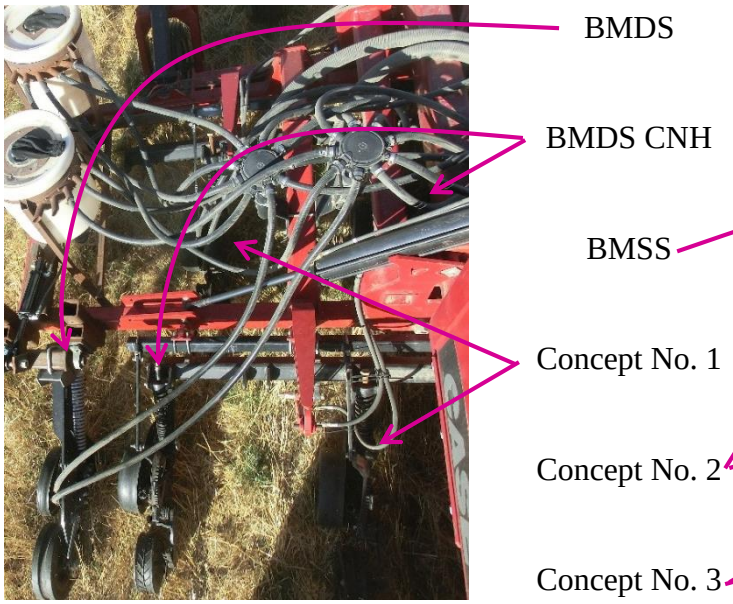

Figure 4.49. Plot drill left wing.

Figure 4.50. Plot drill right wing.

The plot drill was driven through two fields covered by different types and amount of crop residues. The two locations used were the Lutheran Loamy Sand Field and Lutheran Loamy Sand Field No. 2. Lutheran Loamy Sand Field No. 2 was a field close to the Lutheran Loamy Sand Field with a loamy sand soil composition similar to the Lutheran Loamy Sand Field. The major differences between these two fields were the quantity and the types of residue. The Lutheran Loamy Sand Field had a volume of 1938 L (55 bushels) per acre of wheat residues and Lutheran Loamy Sand Field No. 2 had a volume of 1586 L (45 bushels) per acre of canola residues. The quantity of the residues left in the field was determined by the number of bushels harvested during the last harvest. Furthermore, the Lutheran Loamy Sand Field contained an extreme condition, which consisted of a dense wheat straw swath. The plot drill was driven over the dense wheat swath to reproduce intense conditions.

The experimental field trials with crop residues were conducted at two speeds: 8.85 $km \cdot h^{-1}$ (5.5 mph), and 12.87 $km \cdot h^{-1}$ (8.0 mph) on two locations: Lutheran loamy sand, and Lutheran loamy sand No. 2. The Lutheran Loamy Sand Field also contained the extreme condition recreated with the wheat straw swath, which was the third condition. These two fields with their three conditions, combined with the two speeds used, have created six possibilities (i.e. Lutheran loamy sand at 8.85 $km \cdot h^{-1}$ (5.5 mph)). The trials were performed at a single wheat depth setting, which was 50.8 mm (2 inches) and 25.4 mm (1 inch), for the fertilizer and the seed respectively.

4.7 **Data Analysis**

The data analyses were conducted on the data sequence of the Seed/Fertilizer Separation experiments and the 3-D force experiment using R© software version 3.1.3 (R Foundation for Statistical Computing, Vienna, Austria). The statistical procedures used through the analyses of the different experiments were similar, only the code was adapted to the data set. First of all, two libraries were required to be uploaded into the code before beginning the analysis: the Least-Squares means (lsmeans) and the Simultaneous Inference in General Parametric Models (multcomp). The lsmeans library was used to calculate the least-squares means in a linear model about specific factors (Lenth, 2012). The "multcomp" library is a software package that simultaneously produces tests and confidence intervals for general linear hypotheses in parametric models (Horton et al., 2015).

The first step of the statistical analysis was to implement the analysis of variance (ANOVA) on the selected data set. The model was applied on the selected variables in relation to the apparatus required to be compared. The variance results were analyzed by a generic general linear hypothesis method, directly applied by a matrix of linear functions. The matrix of linear functions was developed by a Tukey test, which compares all the possible interactions between the apparatuses. The Tukey test uses an ANOVA to create comparisons between the devices. The Tukey test results were presented at 95% confidence, with a compact letter display of all pairwise comparisons (Figure 4.51). The letters shown in the compact letters display characterize similarities and differences between two openers. The letters in the compact letter display are the same for the openers which have no significant difference, and they are different if the openers have a significant difference. Moreover, the letters are positioned on the top of the graph, which presents the results by apparatus respectively. The data were provided by box plots, which allows the

determination of the type of distribution for each data set (Figure 4.51). A line (blue, orange, fucshia, was provided on the graphs, which is an average line or a target line, depending on the test (See Figure 4.51).

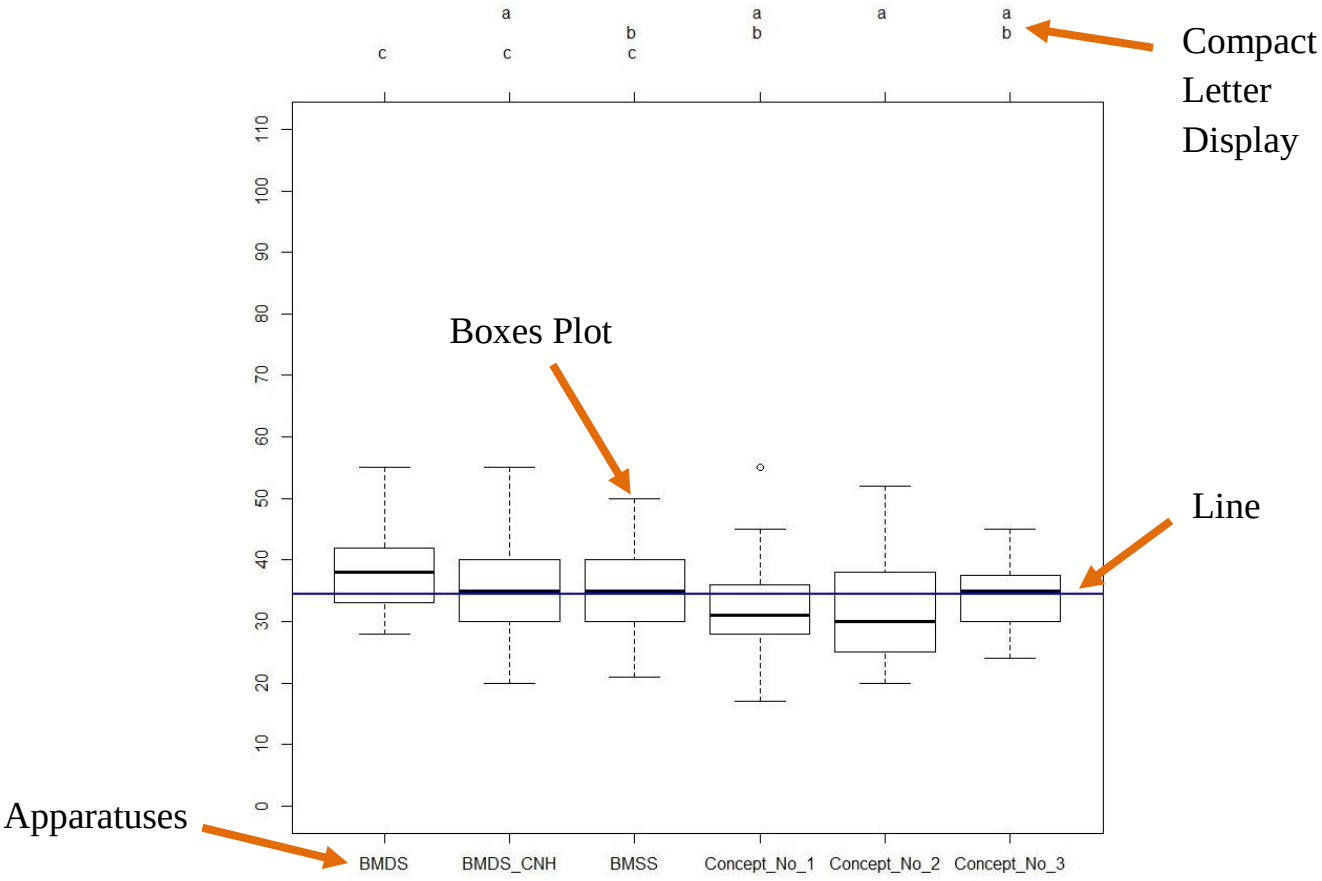

Figure 4.51. Example of statistical analysis result graph.

4.7.1 Data Analysis Applied to the Seed/Fertilizer Separation Experiment

The statistical analyses for this series of experiments was determined by fields, by ground speeds, and by types of crop. Statistical analysis results were provided in two groups: direct measurements and offset distances. The direct measurement group contains the measurements of seed depth (wheat and canola), fertilizer depth, and horizontal separation. The offset distances group contains measurements of vertical difference (delta) and horizontal difference (delta).

However, the direct measurements graphs are displayed with an average line, contrary to the offset distances graphs, which are presented with a target line.

4.7.2 Data Analysis Applied to the 3-D Force Experiments

The statistical analyses applied to the 3-D force experiments were determined only by ground speed. The statistical analyses were displayed on three different types of graph, side load, total draft, and vertical load, which were provided with an average line. However, the vertical reaction is directly related to the penetrability of the disc apparatus, according to Nartov (1985).

The data sets collected at 8.85 km·h-1 (5.5 mph) were reduced from 200 000 to 2500 data, and the data sets collected at 12.87 km·h-1 (8.0 mph) were reduced from 130 000 to 2500 data. The data sets were reduced in order to decrease the analysis sensitivity, due to the fact that larger data sets have more precision. The statistical analyses applied to the 3-D force experiments had a precision range of 0.07 to 0.19% at 200 000 data and 0.61 to 1.59% at 2500 data, which represent an augmentation of the significant value from 1.1 N (200 000 data) to 14 N (2500 data), as displayed in summary Table 4.4. The significant value is the minimal difference between two means of different groups to be considered significantly different. The data sets were reduced prior to being introduced in the statistical R software version 3.1.3. The data sets were reduced by Excel® version 2013, which has created an average for each pre-determined number of variables. The data set made of averaged data was created by taking the first pre-determined number of variables to create the first averaged variable. The second averaged variable was determined by using the second data set of pre-determined variables to create the second variable. The averaged variables are determined until the data set is completely employed. The variables are only used once to keep the weight proportional for each value compared to the original dataset. The amount of data

included in the averaged variable was directly determined by the number of variables included in the original data set, which was divided by the number of values wanted.

Table 4.4. Sensitivity analyses summary.

Parameter	Type of Force								
	Side Load			Draft			Vertical Load		
Number of data points	2500	130000	200000	2500	130000	200000	2500	130000	200000
Significant value (N)	10 ~ 11	1.5	1.3	10 ~ 11	1.7	1.1	12 ~ 14	2.1	1.4
Percentage of precision (%)	1.57 ~ 1.61	0.24	0.19	1.20 ~ 1.29	0.2	0.13	0.61 ~ 0.71	0.1	0.07

4.8 **Analytical Model**

An analytical model was created to validate the draft forces created by the knife in the early virtual soil bins in DEM software, in order to validate the analytical soil compositions. The analytical model was created from the three-dimensional wedge theory developed by McKyes and Ali (1977). The wedge theory was developed for narrow soil-cutting tools without the need for experimental inputs of soil failure geometry (McKyes, 1985, p. 60). The determination of a few parameters was a prerequisite to use the model: the effective rake angle or angle of attack (α), the surcharge pressure vertically acting on the soil surface (q) (normally 0 kPa with that model since this is not a digging tool), the acceleration due to gravity (g = 9.81 ms^{-2}), the tool width (w), and the tool depth (d). Most of these parameters can be visualized in Figure 4.52. According to Negi et al. (1976), and McKyes et al. (1977), no considerable effects were created by the foot sweep angle or the shank angle, as long as the implement remains symmetrical to the x-z plane, as displayed in Figure 4.52 (McKyes, 1985).

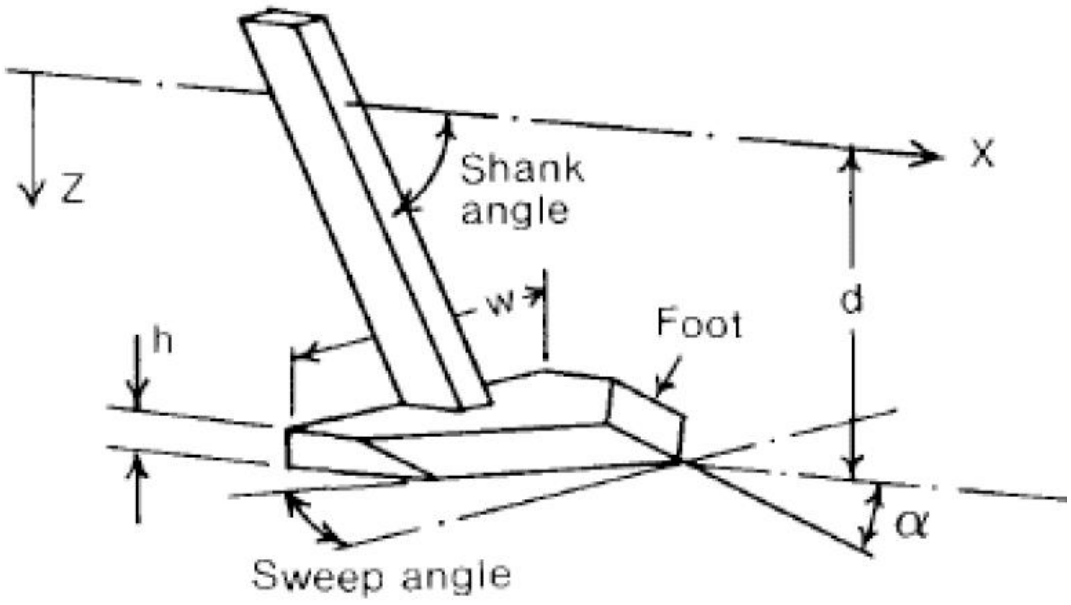

Figure 4.52. Shank and foot tools for the analytical model (Mckyes, 1985).

4.8.1 Analytical Parameters

The analytical model parameters section determines the parameters for the analytical model, which are directly extracted from scientific literature. These parameters were used by the analytical model to estimate the analytical knife draft.

4.8.1.1 ***Soil Density (γ)***

The soil density parameter was determined from the summary paper delivered by Cranfield University (Godwin et al., 2004). The soil density values published in the Typical Soil Properties document (Godwin et al., 2004) must be adapted to the particle size used for the analytical soil bins, due to the difference from the real size of the particles.

4.8.1.2 ***Soil Cohesion (c)***

The soil cohesion parameter can be determined by multiple sources. The spreadsheet from Godwin et al., (2004) proposes an accurate range and typical values of soil cohesion as functions of different soil types. Another source to determine the soil cohesion was the Geotechdata website (Geotechdata, 2014). The section suggests specific soil cohesion values depending on the state of the soil (compacted, saturated, loose, etc.). Furthermore, the table "Typical cohesion and angle of internal friction values," in Section 3 of the Pavement Manual (MnDOT. 2007), offers a large range of soil cohesion values as functions of the general soil compositions. Moreover, some soil cohesion values of precise soil types were provided in Appendix 4 of the Soil Cutting and Tillage book by McKyes (1985).

4.8.1.3 *Angle of Internal Friction (φ)*

The angle of internal friction parameters can be determined by multiple sources. The spreadsheet from Godwin et al., (2004) proposed a range and typical values of angles of internal friction in function of different soil types. Another source to determine the angle of internal friction values was the table provided in the section, Typical values of soil friction angle for different soils, according to USCS from the Geotechdata website (Geotechdata. 2013). The section suggests an angle of internal friction range, depending on the state of the soil (compacted, saturated, loose, etc.). Furthermore, the table "Typical cohesion and angle of internal friction values" in Section 3 of the Pavement Manual (MnDOT. 2007), offers a large range of internal friction angles as functions of the general soil compositions. Additionally, some internal friction angles of precise soil types were provided in Appendix 4 of the Soil Cutting and Tillage book by McKyes (1985).

4.8.1.4 *The angle of friction between soil and the tool material (δ)*

The angle of internal friction can be determined by multiple sources. The spreadsheet from Godwin et al., (2004) proposed an accurate range and typical values of angles of friction in function of different soil types. The spreadsheet from Godwin et al., (2004) recommends a δ value from 0.5 to 0.7 of the φ value. According to McKyes (1985), the angle of friction between soil and the tool material δ can be estimated at two thirds of internal friction angle φ.

4.8.1.5 *Adhesion (c_a)*

The adhesion (c_a) can be considered negligible except when the soil conditions are wet adhesive and/or the soil has a high clay concentration (Godwin et al., 2004). If one of these special circumstances occurs, the adhesion value should be determined for the specific experiment (Godwin et al., 2004).

4.8.1.6 *Wedge angle value (β)*

The wedge angle was calculated experimentally by minimizing the N factor related to soil density N_y formula (Grisso and Perumpral, 1985). The wedge angle was also available in the tables displayed in Appendix No. 3 of the Soil Cutting and Tillage book (McKyes, 1985, pp. 208-211). The values determined by minimizing the N_y formula were compared to the value of the table to ensure they were similar. The wedge angle was essential to the total draft H calculations

4.8.2 Analytical Formula

The analytical formula section describes the formulas used to determine the total draft force and the total draft equation itself. Moreover, the analytical formula section provide the mathematical formulas and details each of their input parameters.

4.8.2.1 *Total Draft Equation (H)*

The total draft was calculated from the formula 3.58 in the Soil Cutting and Tillage (McKyes, 1985) or from the formula 8.2 in the Agricultural Engineering Soil Mechanics (McKyes, 1989). Both formulas were the same.

The total draft was calculated as follows:

$$H = P \cdot \sin(\alpha + \delta) + c_a \cdot d \cdot w \cdot \cot(\alpha) \quad (4.2)$$

where,

H = Total draft (kN)

P = Total ground engaging tool force (kN)

α = Tool rake angle from the horizontal (degrees, ˚)

δ = Angle of friction between soil and the tool material (degrees, ˚)

c_a = Calculated soil to tool adhesion strength (kPa)

d = Tool depth (m)

w = Tool width (m)

4.8.2.2 *Total Force equation (P)*

The total draft (H) equation required the calculation of the total force value (P). The total force was calculated from equation 3.54 from the Soil Cutting and Tillage book (McKyes, 1985) or from formula 8.8 from the Agricultural Engineering Soil Mechanics (McKyes, 1989), if no ground speed was assumed. The two formulas were almost the same, except for the soil density (γ) unit used, which was $t \cdot m^{-3}$ in the book of McKyes, 1985, and $kN \cdot m^{-3}$ in the book of McKyes, 1989. Since the simulations assume a ground speed, formula 3.68 from the Soil Cutting and Tillage book (McKyes, 1985) was used to determine the total force. The formula that assumes speed was required only if the ground speed was above the velocity determined by equation 4.4, and not necessary if the apparatus velocity was below the speed calculated by equation 4.3. Between these two values, the use of the formula that assumes speed was recommended even if the inertia forces have minimal effects on the draft. Equation 4.3 is the conclusion from Schuring and Emori (1964) about the minimal speed required to affect significantly the inertial force of a tool in the soil. Equation 4.4 is an optimization created by Wheeler and Godwin (1996) from the Schuring and Emori (1964) formula, which includes the side effect of the soil failure on narrow tines.

Minimal apparatus velocity parameter was calculated as follows:

$$v_{mi} = \sqrt{5gw} \tag{4.3}$$

Maximal apparatus velocity parameter was calculated as follows:

$$v_{ma} = \sqrt{5g \cdot (w + 0.6d)} \tag{4.4}$$

The total force was calculated as follows:

From equation 3.54 (McKyes, 1985):

$$P = (\gamma g d^2 N_\gamma + c d N_c + q d N_q + C_a d N_{ca}) \cdot w \quad (4.5)$$

From equation 8.8 (McKyes, 1989):

$$P = (\gamma d^2 N_\gamma + c d N_c + q d N_q + c_a d N_{ca}) \cdot w \quad (4.6)$$

From equation 3.68 (McKyes, 1985):

$$P = (\gamma g d^2 N_\gamma + c d N_c + c_a d N_{ca} + q d N_q + \gamma v^2 d N_a) \cdot w \quad (4.7)$$

where,

P = Total tool force (kN)

γ = Soil density ($t \cdot m^{-3}$, eq.3.54) ($kN \cdot m^{-3}$, eq. 8.8)

g = Acceleration due to gravity (9.81 $m \cdot s^{-2}$)

d = Tool depth (m)

N_γ = N factor related to soil density

c = Soil cohesion (kPa)

N_c = N factor related to soil cohesion

q = Surcharge pressure vertically acting on the soil surface (kPa)

N_q = N factor related to the surcharge pressure vertically acting on the soil surface

c_a = Soil tool adhesion strength, independent of normal pressure (kPa)

N_{ca} = N factor related to the soil tool adhesion strength

v = Apparatus velocity ($m \cdot s^{-1}$)

v_{ma} = Maximal apparatus velocity parameter ($m \cdot s^{-1}$)

v_{mi} = Minimal apparatus velocity parameter ($m \cdot s^{-1}$)

Na = N factor related to the apparatus velocity

w = Tool width (m)

4.8.2.3 *N factor related to the soil density (N_y)*

The total tool force (P) required the calculation of the N factor related to the soil density (N_γ). The N factor was calculated with equation 3.57 from the Soil Cutting and Tillage (McKyes, 1985). The values determined by the equation were compared with the Appendix #2 values: Values of N factors in the Universal Earthmoving Equation for narrow flat blade cutting soil in passive failure, in the Soil Cutting and Tillage book (McKyes, 1985).

The N factor related to the soil density (N_γ) was calculated as follows:

$$N_\gamma = \frac{\frac{1}{2}(\cot\alpha + \cot\beta)\cdot\left(1 + \frac{2d}{3w}\cdot(\cot\alpha + \cot\beta)\left(1 - \left(\frac{\cot\alpha}{\cot\alpha + \cot\beta}\right)^2\right)^{1/2}\right)}{\cos(\alpha+\delta) + \sin(\alpha+\delta)\cdot\cot(\beta+\varphi)} \quad (4.8)$$

where,

$N\gamma$ = N factor related to soil density

α = Tool rake angle from the horizontal (degrees, ˚)

β = Wedge angle (degrees, ˚)

d = Tool depth (m)

w = Tool Width (m)

φ = Angle of internal friction (degrees, ˚)

4.8.2.4 *N factor related to the soil cohesion (N_c)*

The total tool force (P) required the calculation of the N factor related to the soil cohesion (N_c). The N factor related to the soil cohesion was calculated with a part of equation 3.54 from the Soil Cutting and Tillage book (McKyes, 1985). The values calculated with the formula were compared to Appendix #2: Values of N factors in the Universal Earthmoving Equation for narrow

flat blade cutting soil in passive failure, in the Soil Cutting and Tillage book (McKyes, 1985, pp. 170 – 207).

The N factor related to the soil cohesion (N_c) was calculated as follows:

$$N_c = \frac{\left(1 + \cot\beta \cdot \cot(\beta + \varphi)\right) \cdot \left(1 + \frac{s}{w}\right)}{\cos(\alpha + \delta) + \sin(\alpha + \delta) \cdot \cot(\beta + \varphi)} \quad (4.9)$$

where,

N_c = N factor related to soil cohesion

β = Wedge angle (degrees, ˚)

φ = Angle of internal friction (degrees, ˚)

s = Ultimate width of each side crescent (m)

w = Tool Width (m)

α = Tool rake angle from the horizontal (degrees, ˚)

δ = Angle of friction between soil and the tool material (degrees, ˚)

4.8.2.5 *N factor related to the surcharge pressure vertically acting on the soil surface (N_q)*

The total tool force (P) required the calculation of the N factor related to the surcharge pressure vertically acting on the soil surface (N_q). The N factor related to the surcharge pressure vertically acting on the soil surface was determined with a part of formula 3.54, from the Soil Cutting and Tillage book (McKyes, 1985). The values calculated by the equation were compared to Appendix #2: Values of N factors in the Universal Earthmoving Equation for narrow flat blade cutting soil in passive failure, in the Soil Cutting and Tillage book (McKyes, 1985, pp. 170 – 207).

The N factor related to the surcharge pressure vertically acting on the soil surface (N_q) was calculated as follows:

$$N_q = \frac{\frac{r}{d}\left(1 + \frac{s}{w}\right)}{\cos(\alpha + \delta) + \sin\left(\alpha + \delta\right) \cdot \cot(\beta + \varphi)} \tag{4.10}$$

where,

N_q = N factor related to the surcharge pressure vertically acting on the soil surface

r = Horizontal radius of soil fracture (m)

d = Tool depth (m)

r/d = Ratio of the horizontal radius of soil fracture on the tool depth (r/d = cot α + cot β)

s = Ultimate width of each side crescent (m)

w = Tool depth (m)

α = Tool rake angle from the horizontal (degrees, ˚)

δ = Angle of friction between soil and the tool material (degrees, ˚)

β = Wedge angle (degrees, ˚)

φ = Angle of internal friction (degrees, ˚)

4.8.2.6 *N factor related to the soil adhesion strength (N_{ca})*

The total tool force (P) required the calculation of the N factor related to the soil tool adhesion strength (N_{ca}). The N factor related to the soil tool adhesion strength was calculated with a part of formula 3.54 from the Soil Cutting and Tillage book (McKyes, 1985). The values determined by the equation were compared to Appendix #2: Values of N factors in the Universal Earthmoving Equation for narrow flat blade cutting soil in passive failure, in the Soil Cutting and Tillage book (McKyes, 1985, pp. 170 – 207).

The N factor related to the soil tool adhesion strength (N_{ca}) was calculated as follows:

$$N_{ca} = \frac{1 - \cot\alpha \cdot \cot(\beta + \varphi)}{\cos(\alpha + \delta) + \sin(\alpha + \delta) \cdot \cot(\beta + \varphi)} \quad (4.11)$$

where,

N_{ca} = N factor related to the soil tool adhesion strength

α = Tool rake angle from the horizontal (degrees, ˚)

β = Wedge angle (degrees, ˚)

φ = Angle of internal friction (degrees, ˚)

δ = Angle of friction between soil and the tool material (degrees, ˚)

4.8.2.7 *N factor related to the apparatus velocity (N_a)*

The N factor related to the apparatus velocity (N_a) had to be calculated to determine the total tool force. The N factor related to the apparatus velocity was calculated from equation 3.69 from the Soil Cutting and Tillage book (McKyes, 1985).

The N factor related to the apparatus velocity (N_a) was calculated as follows:

$$N_a = \frac{\tan\beta + \cot(\beta + \varphi)}{[\cos(\alpha + \delta) + \sin(\alpha + \delta) \cdot \cot(\beta + \varphi)][1 + \tan\beta \cdot cot\alpha]} \quad (4.12)$$

where,

N_a = N factor related to the apparatus velocity

β = Wedge angle (degrees, ˚)

φ = Angle of internal friction (degrees, ˚)

α = Tool rake angle from the horizontal (degrees, ˚)

δ = Angle of friction between soil and the tool material (degrees, ˚)

4.8.2.8 *The soil to tool adhesion strength value (c_a)*

The total tool force (P) equation required the soil to tool adhesion strength value (c_a). The ca value is normally determined directly by observation, or tests done in the fields. The soil-to-tool adhesion may also be estimated from formula 3.23, from the Soil Cutting and Tillage book (McKyes, 1985).

The soil to tool adhesion strength value (c_a) was calculated as follows:

$$c_a = \frac{c \cdot \cot(\varphi)}{\cot(\delta)} \tag{4.13}$$

where,

c_a = Soil to tool adhesion strength, independent of the normal pressure (kPa)

c = Soil Cohesion (kPa)

φ = Angle of internal friction (degrees, ˚)

δ = Angle of friction between soil and the tool material (degrees, ˚)

4.8.2.9 *The ultimate width of each side crescent value (s)*

The total tool force (P) equation required the calculation of the ultimate width of each side value (s). The ultimate width of each side was determined using equation 3.56 from the Soil Cutting and Tillage book (McKyes, 1985).

The ultimate width of each side crescent (s) was calculated as follows:

$$s = \mathrm{d} \cdot (\cot\alpha + \cot\beta) \cdot \left(1 - \left(\frac{\cot\alpha}{\cot\alpha + \cot\beta}\right)^2\right)^{1/2} \tag{4.14}$$

where,

s = Ultimate width of each side crescent (m)

d = Tool depth (m)

α = Tool rake angle from the horizontal (degrees, $^{\circ}$)

β = Wedge angle (degrees, $^{\circ}$)

4.9 DEM Simulation and Validation

The DEM simulations were accomplished using the software EDEM® v. 2.7 from DEM Solutions (Edinburgh, Scotland).

The simulations were conducted with objectives to reproduce the loamy sand fields seeded during the tests. The simulations were created with a few compromises to optimize:

- the required simulation time,
- the size of data stored, and
- the quality of the data collected.

The DEM computer simulation and validation section includes the simulation elements section and the simulation elaboration section, which describes all the implements and techniques used to achieve the simulation purposes.

4.9.1 Simulation Elements

The simulation elements section describes in detail all the essential information about the apparatuses used during the DEM simulations. These descriptions are divided into three sections:

- Analytical Knife,
- Analytical Disc Drill, and
- Analytical Soil Bins.

The Analytical Knife section describes the analytical knife dimensions with a detailed explanation for the assumption made. The Analytical Disc Drill section details all the disc drill

essential parts and their functions/interactions with the environment. The Analytical Soil Bins section describes the composition and the interactions of the soil bins used during the DEM simulation performed by the EDEM®.

4.9.1.1 *Analytical Knife*

The analytical knife was developed to imitate the principal characteristics of the knife edge in a simplified version. The analytical knife has a total length of 120.4 mm (L), which is distributed as 75.4 mm for the slope length (EL), and 45 mm for the seed tube length (SL) as shown in Figure 4.53. The slope length (EL) represents half of the distance of the actual knife edge in order to recreate an average effective rake angle (α), as displayed in Figure 4.53. The seed tube length (SL) recreates the seed tube width in addition to the knife back piece. The nose (NH) of the analytical knife illustrated in Figure 4.53 has a thickness of 3.5 mm, which is the same as the actual knife nose. Moreover, the knife has an attack angle or an effective rake angle (α) (Figure 4.53) of ~ 10° (9.34°), which corresponds to the average attack angle value. The effective rake angle varies throughout the knife edge, due to the fabrication method used to build the knife. The knife end has a thickness of 15.9 mm (H), as shown in Figure 4.53 at the rear extremity of the actual knife. Furthermore, the analytical knife has a width of 52.3 mm (W), as displayed in Figure 4.54, which represents the distance from the farthest point outside of the scraper shadow to the back of the knife.

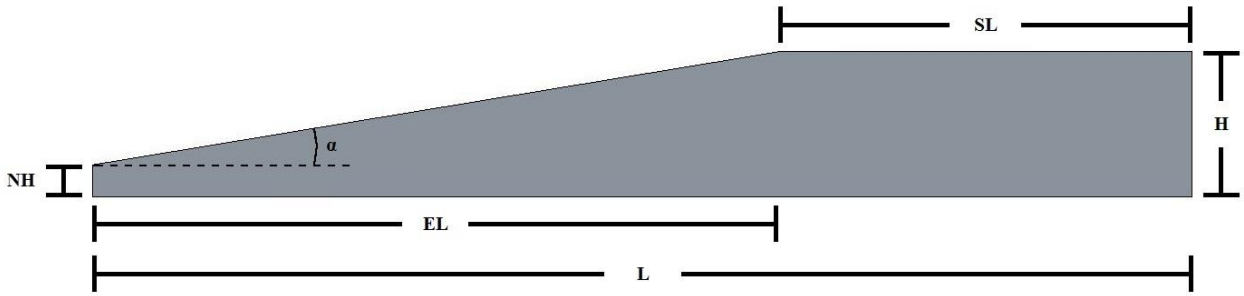

Figure 4.53. Analytical knife side view.

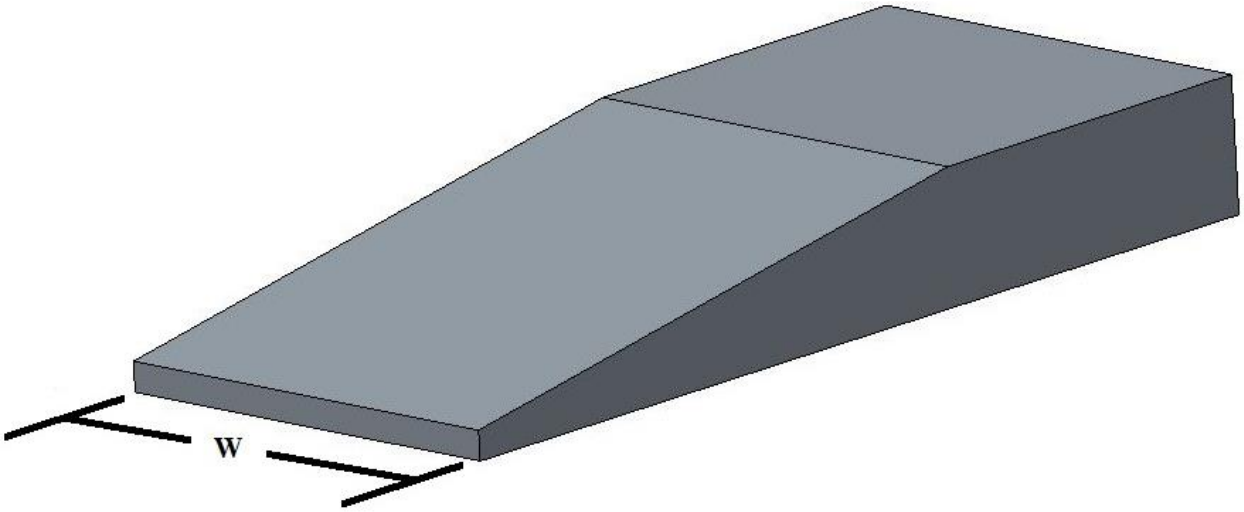

Figure 4.54. Isometric view of the analytical knife.

4.9.1.2 *Analytical Disc Drill*

The virtual disc drill imported in the DEM software is composed of the main parts from the actual disc drill. The main parts have a function directly related to ground engagement and product placement. The main parts are represented in different colours in Figure 4.55 and Figure 4.56, which are the following: green for the disc, cyan for the gauge wheel, orange for the knife, purple for the packing wheel, blue for the seed tube and the scraper. These virtual parts have the same dimensions and functions as their equivalent on the physical disc drill.

The disc cuts through the soil to create the deepest furrow, in collaboration with the scraper. The seed tube distributes the fertilizer in the furrow created by the joint effort of the disc and scraper. The gauge wheel sets the fertilizer depth. The knife creates the seed furrow on the side of the fertilizer furrow to dispense the seed (laterally from a horizontal plane in direction of travel). The knife depth, like the fertilizer depth, is directly related to the depth determined by the gauge wheel, which does not affect the distance between the two distinct furrows. The distance between the fertilizer furrow and the seed furrow can be vertically adjusted by moving the knife up and down by adjusting notches linked to the main frame of the row unit. Furthermore, the packing wheel compacts the soil above the furrows to create a better contact between the seeded products and the soil.

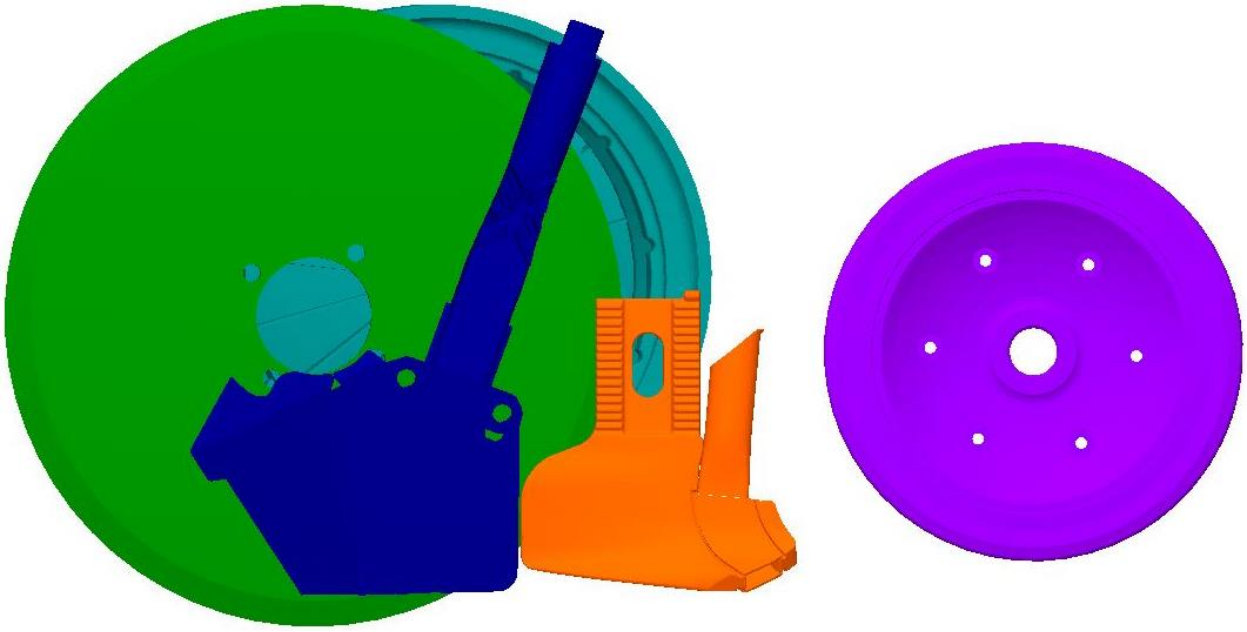

Figure 4.55. Side view of the analytical disc drill.

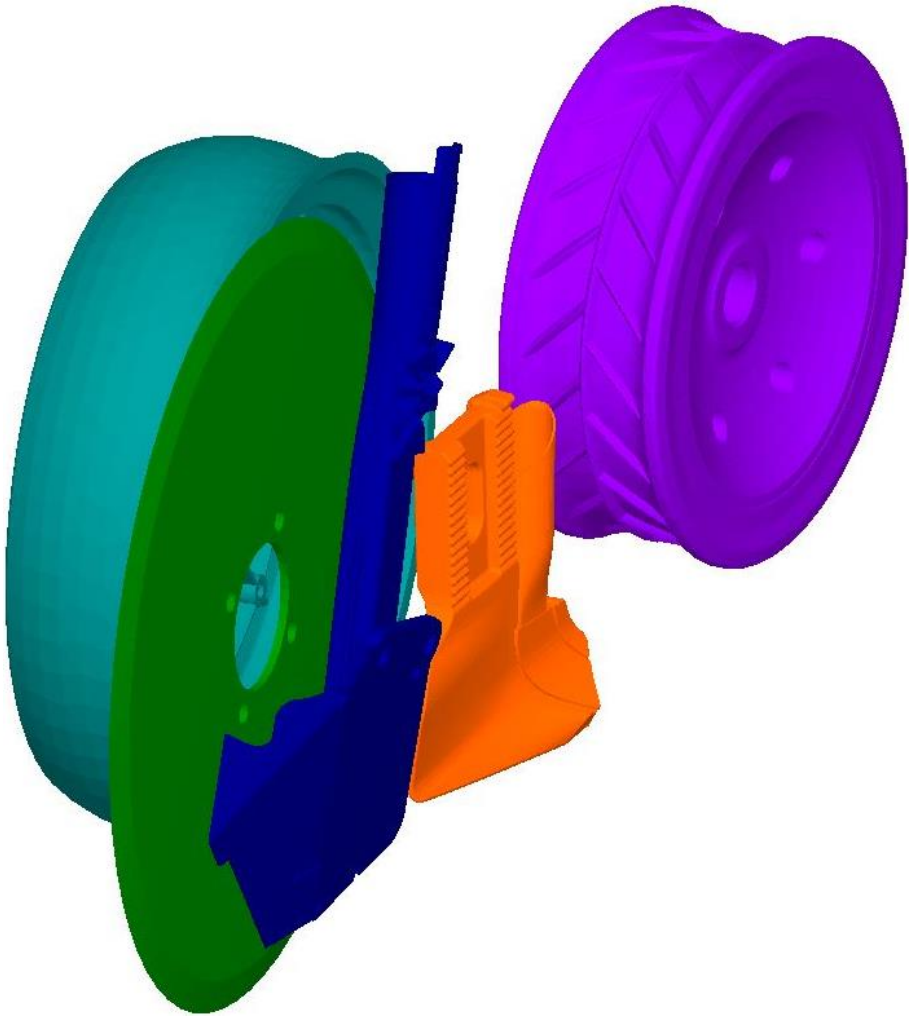

Figure 4.56. Iso front view of the analytical disc drill.

4.9.1.3 *Analytical Soil Bins*

The virtual soil bins section describes the environments used to perform the virtual knife and the complete disc drill simulations in DEM software. The analytical soil bin section is sub-divided into two segments, which are the first-generation soil bins and the second-generation soil bins. These subsections describe the overall dimensions of the soil bins, the particle size used, the soil bin components, two contact models, and the interaction evolving in the virtual soil bins during virtual seeding operations.

The first contact model was the Hertz-Mindlin without slip, which was applied on the interactions between particles and the particle to geometry. The parameters required by the contact model were described in the literature review, Section 3.5.1.1 Physical Properties, except for the restitution coefficients. The base restitution coefficients were provided by the papers and thesis of Ucgul et al. (2015, 2014 a, 2014 b), of Fielke et al. (2013), and Graff (2010). The restitution coefficients were adapted to the desired soil types and soil behaviour wanted.

The second contact model used was the linear cohesion contact model, which reproduces the cohesion effect between particles, and the adhesion effect between the particle and the geometry. The linear cohesion model was used in addition to the Hertz-Mindlin contact model to generate normal cohesion forces. The linear cohesion intensity calculated by EDEM® V2.7 was described by DEM Solutions (2014) and provided in a more thorough form by Ucgul et al. (2015) as follows:

$$F_{c/a} = \xi \cdot A_c \tag{4.15}$$

where,

$F_{c/a}$ = Cohesion and/or adhesion force (N)

ξ = Cohesion energy density ($J \cdot m^{-3}$)

A_c = Contact area (m^2)

The cohesion/adhesion values were adjusted until the simulation stabilized and showed the required behaviour for the selected soil type. The addition of the linear cohesion model provided the extra cohesion necessary between interactions involving wet conditions, or interactions between small particles, like clay soil. In addition, the linear cohesion model addition can provide the cohesion required for sandy environments or powder in dry conditions.

The soil particles used in the virtual (DEM) soil bins are from the USDA (2014) particle size classification, in order to keep the required computational time reasonable. The particle dimensions provided in the analytical soil bins section represents the nominal diameter of the particles. The particles were distributed in the soil bins uniformly, in a predetermined ratio. The difference between the actual soil, and the virtual soil content were compensated by customized interactions for each particle type. The interactions were improved until the virtual soil had comparable behaviours around the implements, as the soil around the apparatus during the field tests. The soil properties of the particles were adjusted to obtain a soil classification in the range of 80 to 82% sand, 12.5 to 13.5% silt, and 4.5 to 6% clay, like the actual fields seeded for this research project.

4.9.1.3.1 First-generation Soil Bins

The first-generation of virtual soil bins had overall dimensions of 2000 mm long by 350 mm wide and 170 mm deep. The various virtual soil bins used for the simulations were created with a maximum of six different particle types: 1 mm clay, 3 mm silt, 5 mm sand, 10 mm sand, rock, and wheat straw. These particles were created with their nominal diameter multiplied by a scale factor to create size variety in a same type of particles. The size varies from 0.7 to 1.3 of the nominal diameter, which was the universal scale factor through the particle types. For example, a 10 mm nominal diameter particle can be represented from 7 mm to 13 mm under a normal

distribution. The scale factor allows each particle type to recreate a soil bin more realistically than a soil bin with only a unique particle size.

The soil particles with a diameter of 1 mm for clay, 3 mm for silt, 5 mm for sand, and 10 mm (largest) were created with only one spherical particle. Stone and wheat straw particles were clusters of particles of four and six spheres respectively. The stone particles used four spheres of 36 mm each and the wheat straw particles used six spheres of 10 mm. The four stone spheres were generated on a same horizontal plane, and distributed symmetrically in the direction of travel. Two of the four spheres were positioned farther from the centerline of the cluster to create extremities, and the two other particles were generated closer to the center to create the main large body of the stone, as displayed in Figure 4.57. The six wheat straw spheres were distributed in line, as shown in Figure 4.58.

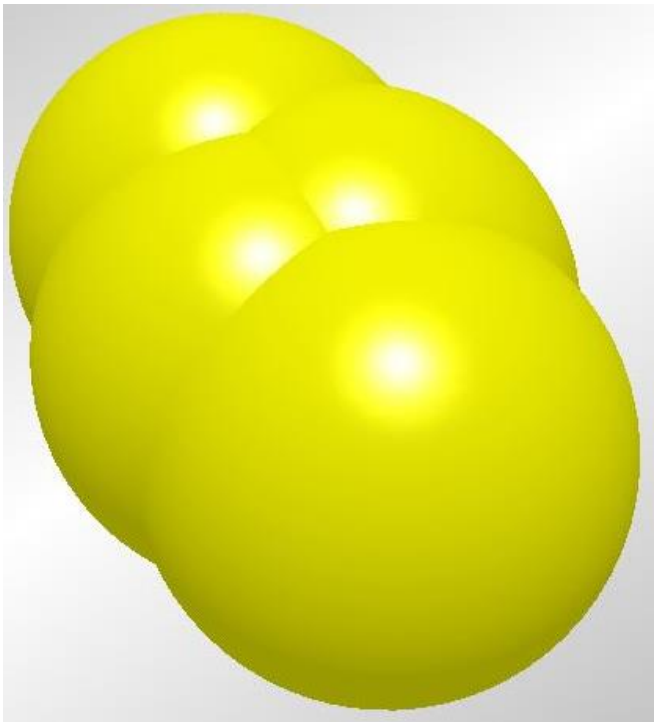

Figure 4.57. Analytical soil bin rock particle.

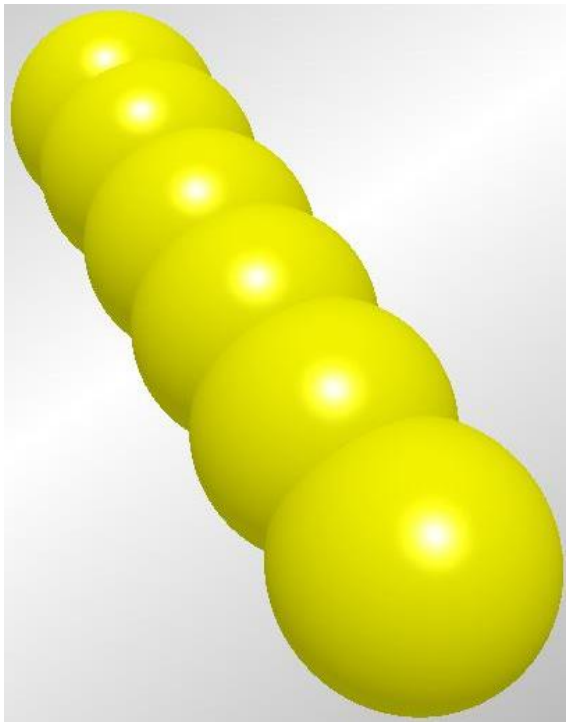

Figure 4.58. Analytical soil bin wheat straw particle.

4.9.1.3.1.1 Virtual Soil Bin with Stone and Wheat Straw Particles

The rock and wheat straw were added to the soil particles to simulate the three loamy sand fields used during the field tests with the chopped wheat residues on the ground. Due to the particle densities and size adaptation used, the analytical soil composition based on the mass of the particle types was 22.7%, sand 5.2% silt, and 72.0% clay.

4.9.1.3.1.2 Virtual Soil Bin with Stones only

The virtual soil bin with stone only used the same particles, but with the exception of the wheat straw particles. This virtual soil bin was created to mimic the actual three loamy sand fields, without wheat residue. Due to the particle size adaptation and the densities used, the virtual soil composition based on the mass of the particle types was 96.2% sand, 3.7% silt, and 0.0% clay.

4.9.1.3.2 Virtual Soil Bin of Second Generation

The second-generation soil bin had overall dimensions of 340 mm wide by 160 mm deep and 14000 mm long. The soil bin was created with two different types of particles: 2 mm silt, and 4 mm sand. The particles were created under a normal distribution with mean equal to the particle diameter, and a standard deviation of 0.05. Generating the particles with a normal distribution allows the creation of soil bins with more realistic behaviour than soil bins created with only nominal diameter particles, but the latest allows the minimization of computational time, which is a significant advantage while running a very large virtual soil bin in a DEM simulation.

The second-generation soil bin was based on the first-generation soil bin results in order to collect accurate data over a longer period of virtual seeding. The second-generation soil bin was created without stones and wheat straw particles to avoid impacts against the rocks (not necessary for these specific simulations) and the voids created by the impacts against the rigid wheat straw

particles. Also, due to the particle size adaptation and the densities used, the virtual soil bin composition (based on the mass of particles) was 43.4% sand, 53.6% silt, and 0% clay.

4.9.2 DEM Simulation

The simulations were developed to

- Determine the draft force on the knife (and compare with the analytical model),
- to validate the seed/fertilizer placements,
- to predict the wear patterns on the knife and scraper, and
- to anticipate the wear rates.

The analytical knife simulations were elaborated to define a soil composition for the second-generation soil bins. The analytical knife simulations were performed in the first-generation soil bins, in order to compare the simulated draft forces values to the draft forces values calculated by the analytical model.

The disc drill simulations were created to reproduce the seed to the fertilizer and the wear experiments at the same time, which were also happening simultaneously in the fields. The knife wear rate estimations were determined using the simulation output of compressive force acting on the knife (from the DEM software).

4.9.2.1 ***Analytical Model (Knife only)***

The analytical simulations of the single knife were performed using the first generation soil bin at two ground speeds: 8.85 $km \cdot h^{-1}$ (5.5 mph) and 12.87 $km \cdot h^{-1}$ (8.0 mph). The two ground speeds correspond to the actual ones used during the field tests. The virtual knife was set at 25.4 mm (one inch) deep, in order to imitate the soil reaction caused by the knife edge outside of the scraper shadow. The virtual knife was simulated to compare the virtual draft force to the analytical

draft force determined by the analytical model, in order to generate a more realistic virtual soil bin in DEM.

4.9.2.2 *Seed-to-Fertilizer Separation Simulations*

The seed-to-fertilizer separation simulations were performed with the second generation soil bin at the two ground speeds (similar to field tests). The complete virtual disc drill was used to validate the product placement, which was effectuated with mechanical settings for wheat seeding. The seeding depth for wheat seeds was 25.4 mm (1 inch) deep and 50.8 mm (2 inches) for the fertilizer. The measurements taken to validate the product placement were the horizontal delta (H, mm), and the vertical delta (V, mm) between seed and fertilizer clouds. The measurements were taken from the centers of mass of the clouds of products, as shown in Figure 4.59. Furthermore, the vertical precision of the seed and fertilizer distribution is displayed in Figure 4.60; likewise, the horizontal distribution accuracy is illustrated in Figure 4.61. Moreover, Figure 4.62 presents an isometric view of the virtual disc drill with the seed and the fertilizer distributed, which gives a general idea of the product placement and accuracy to which they were delivered.

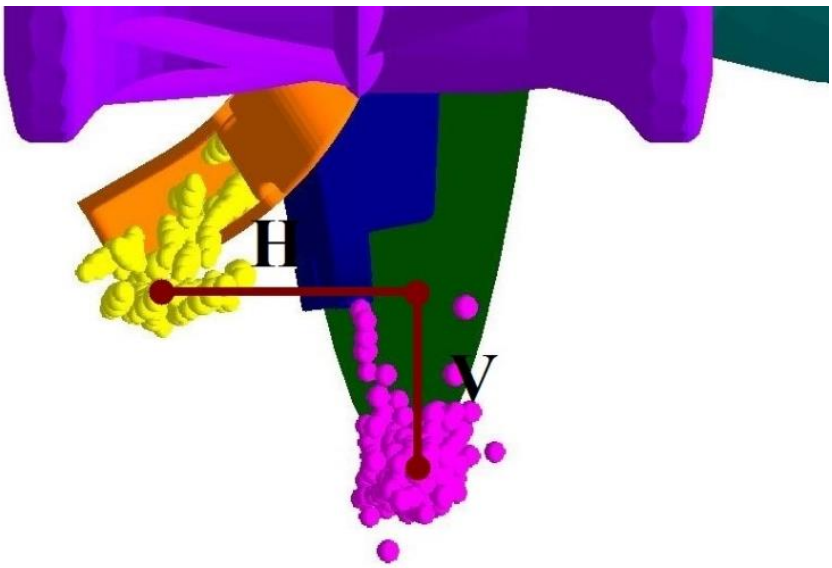

Figure 4.59. Visual representation horizontal and vertical Separation (rear view).

Figure 4.60. Visual representation vertical separation (Side view).

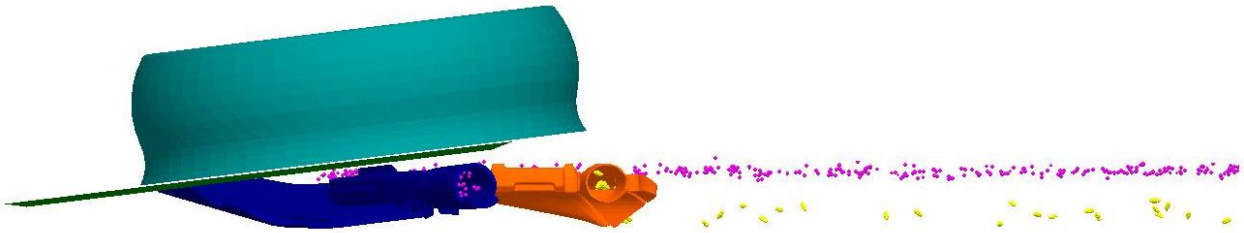

Figure 4.61. Visual representation horizontal separation (Top view, No-Packing Wheel).

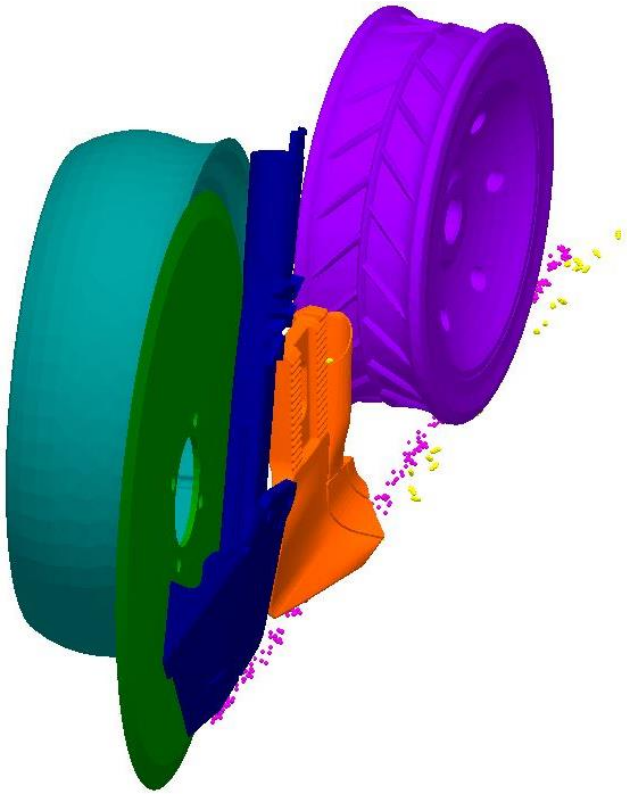

Figure 4.62. Visual representation horizontal and vertical separation (Isometric view).

4.9.2.3 ***Wear Characterization Simulations***

The wear characterization simulations were jointly realized with the seed-to-fertilizer separation. The same ground speeds, apparatus, and depth setting were used, only the type of data collected changed. The following sections include the subsection wear pattern prediction, and wear rate estimation of the knife and scraper.

4.9.2.3.1 Wear Pattern Prediction

The wear pattern prediction was determined by using the software function of "Record Relative Wear" in the Hertz-Mindlin contact model. The intensity of the contacts were directly displayed on the selected geometries with a multicolour gradation system. The wear pattern data were collected by default for each geometry, but only the scraper and the knife were analyzed. The wear patterns were used to validate the positions of the hardening material (often in carbide) welded on the scraper, and to predict the high stress locations during impacts with higher intensity. The high stress locations are most prone to heavy wear, hardening material (solid or welded or sprayed) could be beneficial to increase the lifetime of the ground engaging tools.

4.9.2.3.2 Wear Rate Estimation

The DEM simulations were used to determine the compressive forces caused by the particles on the selected geometry. The analyses were concentrated solely on the knife to determine the range of wear rate, which is related to life expectancy and long-term operational cost. The wear rate ranges were determined by using the Archard Equation, which was described in Section 3.6.4 DEM of this thesis. Moreover, the wear rate prediction will determine the kind of protection the knife could need (i.e. carbide, arc welding, spray etc.).

5.0 RESULTS AND DISCUSSION

This section presents the soil characterization results, the statistically analyzed results for the seed–to-fertilizer separation, the 3-D force experiments, the experimental field trials with crop residues results, and the DEM validation results.

The DEM validation section includes the analytical model validation, the seed-to-fertilizer virtual separation, the wear locations prediction, and the wear rate estimation. Finally, the variations of the results and the fluctuation between the validations are explained in the discussions prior to the summary graph in each section.

5.1 Soil Characterization

The soil characterization section summarizes all the experiments needed for a good characterization of the soil and classification of the results. The soil characterization section displays the results for:

- the soil temperature,
- the soil compaction,
- the stubble thickness,
- the stubble height,
- the ground coverage percentage,
- the soil moisture, and
- the soil texture.

Moreover, the Table 4.2 displays the dates at which the soil characterization measures were taken, by field and by experiment.

5.1.1 Soil Temperature

Raw data for the Lutheran Loamy Sand fields is not available, due to the fact that the measurements were accidentally destroyed. The temperature was mostly steady between the fields, but some soil temperature variations were registered between the plots for the same field. The temperature variation can be attributed to the time elapsed between the measurements and/or the variations of the residue cover with different albedo and sun deflection factors. Table 5.1 summarizes the field soil temperatures, which are the average values of 20 raw data, displayed in Table A. 1.

Table 5.1. Field soil temperature result.

Fields	Lutheran Loamy Sand Field	Asquith Loamy Sand Field	Asquith Summer Fallow Loamy Sand Field	St-Denis Loam Field	St-Denis Silty Clay Field
Average Ground Temperature (°C)	16.6	21.9	21.2	19.9	22.9

5.1.2 Soil Compaction

The compaction tests were conducted before carrying out the experiments. The compaction results demonstrated some variation between values for the same plot. The compaction variation can be caused by previous tire tracks, and/or soil moisture variation. The average compaction data were mainly distributed from 1379.0 kPa (200 psi) to 2068.4 kPa (300 psi). The values were all under the value of 2068.4 kPa (300 psi), which is the critical agronomical limit for an acceptable soil compaction while the value of 1379.0 kPa (200 psi) is the lower limit for an ideal soil compaction. Table 5.2 summarizes the average field compaction values, and Table A. 2 presents the 20 raw data of each average.

Table 5.2. Field compaction result.

Fields	Lutheran Loamy Sand Field	Asquith Loamy Sand Field	Asquith Summer Fallow Loamy Sand Field	St-Denis Loam Field	St-Denis Silty Clay Field
Average Ground Compaction (kPa)	1549.6	1672	1789.2	1347.9	1085.2

5.1.3 Stubble Thickness

The stubble thickness measurements were taken before the tests to keep the stubble intact and similar to the seeding period. The large variation between the diameter values was caused by different crop residue types present in the fields and the varieties of crops used. Both the Lutheran Loamy Sand Field and the Asquith Loamy Sand Field have canola residues, but were seeded with different varieties. The St-Denis fields have similar diameter values due to the fact that both fields have the same owner and the same wheat crop variety. Finally, the Asquith Summer Fallow Loamy Sand Field does not have crop residue, and a slight presence of grass in decomposition on it, which explains the N.A. (Not Available) abbreviation. Table 5.3 summarizes the stubble thickness values, each of which are an average of 10 raw data, shown in Table A. 3.

Table 5.3. Field stubble thickness values result.

Fields	Lutheran Loamy Sand Field	Asquith Loamy Sand Field	Asquith Summer Fallow Loamy Sand Field	St-Denis Loam Field	St-Denis Silty Clay Field
Average Stubble Thickness (mm)	5.98	9.26	N.A.	3.6	3.7

** N.a. = Not Available data*

5.1.4 Stubble Height

The stubble height measurements were taken prior the experiments to provide representative measure. The large variations between the height were caused by the following: the different residue types present on the fields (Wheat vs Canola), the method used to harvest (windrower or straight cut), and the field variations (holes or bumps). Furthermore, certain variations can be attributed to human error or mechanical failure. The St-Denis fields have similar stubble height values because both fields have the same owner, who used the same implements on them. Finally, the Asquith Summer Fallow Loamy Sand Field had no crop residue left on it, which explains the N.A. (Not Available) abbreviation. Table 5.4 summarizes the field stubble height, which are the average values of 10 raw data presented in Table A. 4.

Table 5.4. Field stubble height values result.

Fields	Lutheran Loamy Sand Field	Asquith Loamy Sand Field	Asquith Summer Fallow Loamy Sand Field	St-Denis Loam Field	St-Denis Silty Clay Field
Average Stubble Height (mm)	288	333	N.A.	225	251

** N.a. = Not Available data*

5.1.5 Ground Cover Percentage

The ground cover measures were taken before the tests to keep the residue coverage intact as they were during the seeding period. The variation between the ground coverage values was caused by different residue types (wheat vs canola), crop varieties, yield, type of combine used (rotary vs conventional), and mechanical settings. The Lutheran Loamy Sand Field and the Asquith loamy sand have similar ground coverage value, due to the fact that both fields have canola crop on them and that the type of combine used was the same. The St-Denis fields have a large variation for their ground coverage value, because a rotary and a conventional combine were used at the same time, which created different residue outputs and affected the uniformity of the residue distribution. Also, the Asquith Summer Fallow Loamy Sand Field had no crop residue left on it, but a thin layer of decomposed grass created a slight percentage of ground cover, which did not have significant effects on the seeding apparatus. Table 5.5 summarizes the average field stubble thickness values, and Table A. 5 shows the 10 raw data of each average.

Table 5.5. Field ground coverage values result.

Fields	Lutheran Loamy Sand Field	Asquith Loamy Sand Field	Asquith Summer Fallow Loamy Sand Field	St-Denis Loam Field	St-Denis Silty Clay Field
Average Ground Cover (%)	47.0	47.5	42.0	40.5	49.5

5.1.6 Soil Moisture Content

The soil moisture content measurements were taken before carrying out the experiments to preserve the humidity present in the soil. The soil moisture variations between the different locations were caused by different types of soil, the time elapsed between the sampling, and by human factors. The Lutheran Loamy Sand Field and the Asquith Loamy Sand had similar soil moisture contents, mainly due to the fact that the fields were both used in a short period of time, and because they had a similar soil composition. The St-Denis fields had similar soil moisture in summary Table 5.6, but Table A. 6 presents significant variation between the samples. The soil moisture variation at the St-Denis Loam Field was mostly caused by a hill that creates some dry locations at the peak and wet locations at the base. The soil moisture variation on the St-Denis Silty Clay Field was caused by its proximity to an important pond, which provides moisture by capillarity to a significant part of the plot. The Asquith Summer Fallow Loamy Sand Field moisture variations were mostly caused by the sunshine time variation, which was created by the tree hedgerow adjacent to the field. Also, the moisture content variation between the two Asquith fields was directly related to the delays between the field sampling and to the crop residue covers. Table 5.6 summarizes the soil moisture content values, which are respectively an average of 4 raw data displayed in Table A. 6.

Table 5.6. Soil moisture content result.

Fields	Lutheran Loamy Sand Field	Asquith Loamy Sand Field	Asquith Summer Fallow Loamy Sand Field	St-Denis Loam Field	St-Denis Silty Clay Field
Average Soil Moisture (%)	13.5	13.6	18.0	23.0	24.0

5.1.7 Soil Texture

The soil texture samples were all collected during the same period to keep a steadiness to the soil texture analyses. The samples for the Lutheran field and the Asquith fields were collected on May 16, 2014, while the St-Denis fields were collected on May 20, 2014 (the analytical report is displayed in Table A. 7. Table 5.7 summarizes the soil texture percentages. The Asquith fields had similar soil texture, due to the fact that the fields are adjacent. The similarity of the Asquith fields with the Lutheran field was unexpected, as the fields are separated by 30 kilometres. The two St-Denis fields are separated by less than 5 kilometres and their soil analyses were quite different, especially for the sand and the clay particles. The variation can be caused by the hill at the St-Denis Loam field or simply by a soil texture variation between these two fields.

Table 5.7. Soil texture result.

Fields	ALS No. Identification	Sand (%)	Silt (%)	Clay (%)	Texture
Lutheran Loamy Sand Field	L1462798-1	80.6	13.4	5.92	Loamy Sand
Asquith Loamy Sand Field	L1462798-2	82.5	13.0	4.53	Loamy Sand
Asquith Summer Fallow Loamy Sand Field	L1462798-3	82.0	12.8	5.24	Loamy Sand
St-Denis Loam Field	L1462798-4	38.5	40.7	20.8	Loam
St-Denis Silty Clay Field	L1462798-5	16.2	41.5	42.3	Silty Clay

5.2 Data Analysis

The data analysis section presents the analyzed results of the seed-to-fertilizer separation experiments and the 3-D force experiments. These two experiments were the only ones requiring statistical analysis to compare the apparatuses.

5.2.1 Seed-to-Fertilizer Separation

The seed-to-fertilizer results were divided in two different sections: the direct measurements and the offset seeding distance section. The direct measurements section includes only the measurements taken directly from the fields, such as the seed depth, the fertilizer depth and the horizontal distance. The second section presents the vertical seeding offset distances, and the horizontal seeding offset distances. The vertical seeding offset distances were the measurements between the fertilizer depth and the seed depth, and the horizontal offset distances were the measurements between the seed and the fertilizer furrows at 90 degrees.

5.2.1.1 *Direct Measurements*

The direct measurement combinations are all displayed in APPENDIX B. The Lutheran Loamy Sand Field 12.87 $km \cdot h^{-1}$ Canola, displayed in Figure 5.1 is used as an example because it reflects the general behaviour of each seeding apparatus.

The seed placement experiments was normally dominated by the three different concepts and the BMDS CNH. These four different apparatuses use a knife to introduce the seed, which usually created less variation for their seed placement. Concept No. 2 and No. 3 normally had a slightly better seed placement (non-statistically demonstrated) but observed during the field tests. The BMDS was generally the disc drill which had the second-best seed placement distribution, after the apparatus using a knife. The BMDS had similar seed distribution to the apparatus using a

knife, when the field was flat (no ground variation) and the field conditions were optimal. The BMDS had a wide variation through the different soil types, which are reflected on the box plots of APPENDIX B. The BMDS and the BMSS box plots were sometimes similar to the apparatus using a knife, due to the fact that few fields were considered as optimal. The BMSS was most of the time the opener with the widest variation, and thereby worse for seed placement. The poor consistency of the BMDS and BMSS are explained by the single linkage used by the apparatuses. The single linkage modifies the scraper angle when it compensates for ground variation, in contrast to double linkage, which keeps the same scraper angle when it compensates. The variation of the scraper angle generates a different seeding depth, and creates wide seed distribution.

The fertilizer placement was usually similar between the three concepts and the BMDS CNH, due to the fact that these four openers were using the same distribution system. The box plots of APPENDIX B demonstrate that the fertilizer distributions were normally more grouped with the apparatus using a knife compared to the BMDS. The BMDS had fertilizer distributions more variable to the field conditions than the apparatus using a knife. The variation in the distribution of the BMDS is up to three times the variation of those using a knife. However, fertilizer was typically better placed with the apparatus employing a knife than the BMDS.

The horizontal distances were steady at 30 mm for all openers except for Concept No.1. Concept No.1 had generally significantly less horizontal spacing between the seeds and the fertilizer, due to its shortened edge. The shortened edge does not allow the seeds to be correctly distributed because it creates an irregular furrow. The irregular furrow prevents the seeds from being projected toward the trench edges and thereby creates less horizontal distance between the seed and the fertilizer. Finally, the shortened edge of the Concept No.1 allows a significant amount of soil to flow under the knife nose, which created some disturbance in the fertilizer placement and

affected the horizontal separation. Furthermore, the data distribution associated with the BMDS were usually more scattered than the other apparatuses.

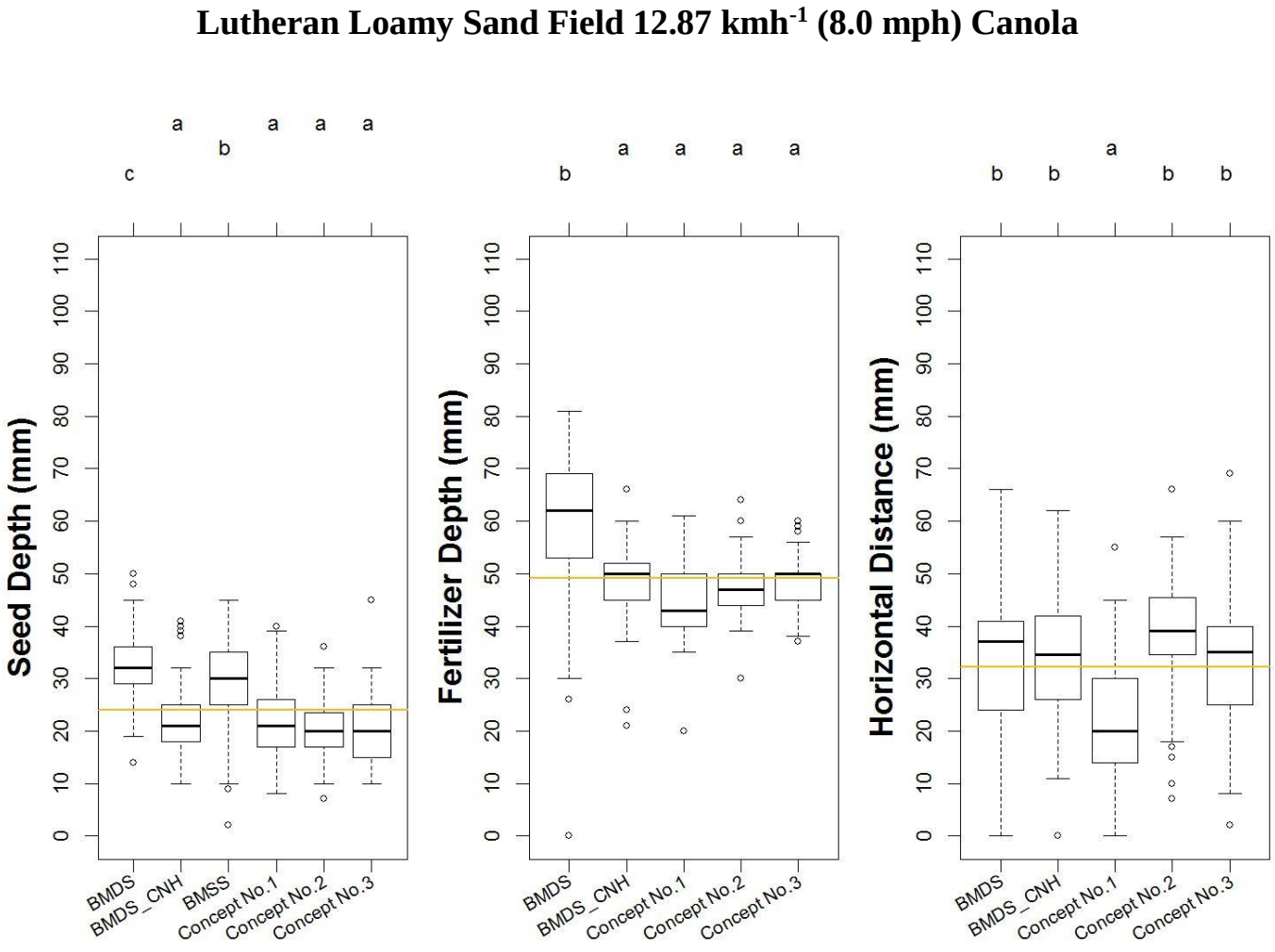

Figure 5.1. Typical seed-to-fertilizer separation result.

5.2.1.2 *Offset Distances*

The offset distances combinations are displayed in APPENDIX C. The Saint-Denis Silty Clay Field 12.87 $km \cdot h^{-1}$ was used as an example because it reflects the typical behaviour of each apparatus (See Figure 5.2).

The vertical delta represents the vertical distance between the seed depth and the fertilizer depth. The data distributions were constant throughout the openers with a few exceptions. The BMDS vertical deltas had less distribution variation compared to its seed-to-fertilizer distributions. The product placement is directly affected by the variation caused by the single linkage, but the single linkage variation does not affect the delta between the two products.

The horizontal delta shows that Concept No. 1 had significantly less horizontal separation than the other openers, which had a median value of not more than 40 mm on a 50 mm scope. The 50 mm horizontal separation was an optimal agronomical objective, but values between 20 and 50 mm were judged acceptable. The opener values were usually distributed between these two limits, except for Concept No. 1, which were occasionally below the minimal acceptable threshold. Finally, the BMDS had, most of the time, a wider horizontal delta distribution than any other openers.

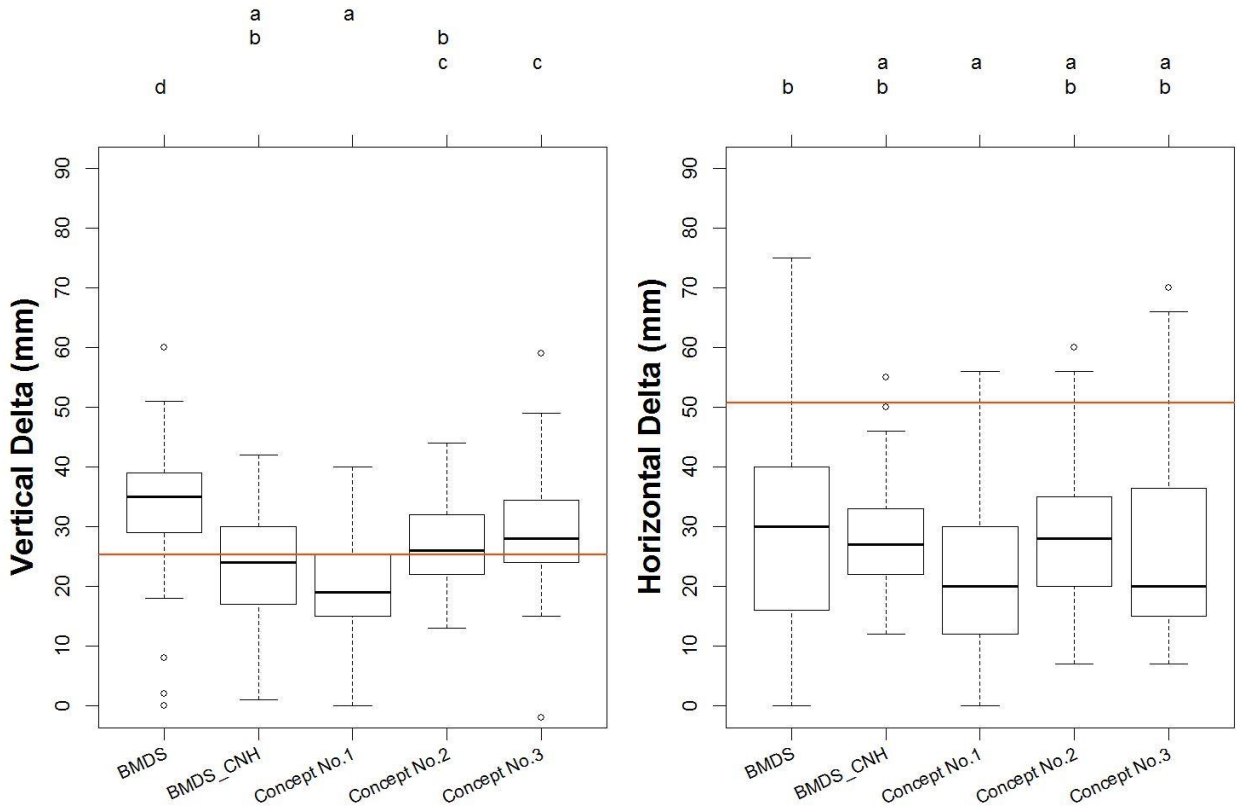

Figure 5.2. Typical example of delta distance result.

5.2.1.3 *Offset Distance Correlation*

The offset distance correlations uses the delta results to determine the interactions between the openers. The letter displayed on the delta figures were used to determine similarities, which are detailed in APPENDIX D. Table 5.8 shows a summary of the vertical and the horizontal delta interactions. Table 5.8 provides the rank of each interaction with the bold number into the brackets. Furthermore, the maximum number of interactions per pair of apparatuses was 20 by type of interaction (Vertical Delta, Horizontal Delta), for a combined total of 40.

Table 5.8. Offset distance correlation results.

Interactions	Vertical Delta (mm)	Horizontal Delta (mm)	Total (mm)
BMDS Vs BMDS CNH	8 (5)	17 (1)	25 (3)
BMDS Vs Concept No.1	11 (4)	5 (4)	16 (5)
BMDS Vs Concept No.2	13 (3)	13 (2)	26 (2)
BMDS Vs Concept No.3	13 (3)	16 (2)	29 (2)
BMDS CNH Vs Concept No.1	15 (2)	5 (4)	20 (5)
BMDS CNH Vs Concept No.2	14 (2)	14 (2)	28 (2)
BMDS CNH Vs Concept No.3	14 (2)	15 (2)	29 (2)
Concept No.1 Vs Concept No.2	13 (3)	11 (3)	24 (4)
Concept No.1 Vs Concept No.3	13 (3)	10 (3)	23 (4)
Concept No.2 Vs Concept No.3	19 (1)	17 (1)	36 (1)

The vertical delta highest number of interactions is created by Concept No. 2 and Concept No. 3, which was explained by the fact that both knives use the same dimension and edge angles to form the trench and distribute the seeds. The second highest number of interactions was created by the BMDS CNH with the three different Concepts, which was also understandable because the apparatus uses the same kind of opener with a different knife shape. The third highest number of

interaction were composed of Concept No. 1 with Concept No. 2 and No. 3, and the BMDS with Concept No. 1 and No. 2. These four pairs of openers all have the same number of significant interactions, because Concept No. 2 and No. 3 was the most constant opener, and the BMDS and Concept No. 1 were the second most constant group of opener. The BMDS has less repeatability caused by its single linkage, as opposed to Concept No. 1, which had some problems with its soil edge interaction. The second-least number of opener interactions was by the BMDS with Concept No. 1, and the smallest number of opener interactions was by the BMDS with the BMDS CNH. The BMDS demonstrates limited repeatability compared to the apparatuses using knives, but the BMDS CNH and Concept No. 1 had residue accumulation issues, which affected repeatability. The second order reliability of the BMDS combined to the residue accumulation issues of the BMDS CNH, and Concept No. 1, created some hazardous interactions.

The horizontal delta interactions were also dominated by the pair comprised of Concept No. 2 and Concept No. 3, but the relation compound of the BMDS and the BMDS CNH had the same number of interactions. The Concept No. 2 and No. 3 vertical delta as the horizontal delta stays reliable, but the BMDS and the BMDS CNH were more reliable for their horizontal separation than their vertical separation. The BMDS had a single linkage to adapt to ground variation, which affects the vertical delta, but not the horizontal delta, due to the solid linkage created by the scraper dual purpose. The fertilizer trench for the BMDS was friable, which allowed an amount of dirt to interfere with vertical positioning. The BMDS CNH distributed the seed at its optimal horizontal location, like Concept No. 2 and No. 3, provided that the amount of residue was not challenging. The BMDS and the BMDS CNH were reliable when the conditions were at their optimum and straightforward. The optimum conditions are summarized by a very flat ground due to the single linkage used by the BMDS, and a field without residues due to the BMDS CNH

accumulation issue. These conditions are not the main purpose and market of a disc drill design. The third-best pairs of apparatus were formed by Concept No. 2 and No. 3, with the BMDS and the BMDS CNH. Concept No. 2 and No. 3 were the most constant pair of openers, and the BMDS and the BMDS CNH were the second best pair of openers for horizontal delta reliability. The second last relationship was a compound of Concept No. 2 and No. 3, with Concept No. 1. Concept No. 2 and No. 3 are the most repeatable openers combined with Concept No. 1 to form two pairs of openers. Concept No. 1 had repeatability issues attributable to a shortened edge, which did not have a uniform seed distribution. The Concept No. 1 horizontal separation issues are clearly demonstrated in Figure 5.1. The least number of interactions involves the second-best pair of openers: BMDS and BMDS CNH, with Concept No. 1.

The summarization of the relationships described above indicates that Concept No. 2 and Concept No. 3 are the most reliable apparatuses. Their reliability was demonstrated by their accuracy in distributing the products combined with the double linkage, which follows the variations of the ground. The second-best combinations were created by the two most predictable apparatuses, Concept No. 2 and No. 3, with the second pair of the most constant openers, the BMDS CNH and the BMDS. The BMDS CNH and the BMDS in optimal conditions had similar repeatability to Concept No. 2 and No. 3. The third-best combination was a compound of BMDS and the BMDS CNH due to their strong performance during the horizontal separation. The vertical interaction between the BMDS and the BMDS CNH was less considerable than their horizontal interaction, mostly due to the different type of linkage used by the apparatus. The fourth-best interaction was composed of the best repeatable pair of openers, Concept No. 2 and Concept No. 3, with Concept No. 1. Concept No. 1 had decent capacities for vertical separation, due to its double linkage, but its horizontal separation capabilities were limited. The combinations of

openers with the least number of interactions were composed of the BMDS and the BMDS CNH, with Concept No. 1. The BMDS and the BMDS CNH were openers with a lesser rate of repeatability and combined with Concept No. 1, which had serious issues, produced the lowest interaction score.

5.2.2 3-D Force Analysis

The 3-D force analysis graphs are all displayed in APPENDIX E. The graph at 12.87 $km \cdot h^{-1}$ is used as an example, because it represents the apparatus behaviour through the different tests (See Figure 5.3).

The side load forces were mostly uniform through the openers, but sometimes they were specific to the openers. The side load median lines of the box plots were normally located between 600 and 800 N, with a similar data distribution through the openers. The variations between the openers were caused by the different knife shapes, but some minor variation could be caused by mechanical and/or human interactions.

The draft data were the critical numbers recorded, due to the fact that the Concepts required to have a draft force similar to the BMD_CNH to be acceptable. Concept No. 2 was the only concept to produce a significantly lower draft than the BMDS CNH. The other Concepts produced a draft force not significantly different than the BMDS CNH. The significantly lower force of the Concept No. 2 is explained by the notch in the nose of the Concept No. 2 knife, which prevents the excessive deformation of the scraper and maintains the back of the scraper at the optimal position. The scraper being maintained by the notch prevents the end of the scraper from bending, which prevents an excessive soil flow on the knife. The optimal soil flow reduced the friction on the knife and created a significant lower draft than for the BMDS CNH.

The vertical force correlations were identical through the different iterations. The openers formed two significant groups. The group with the highest vertical force was formed by Concept No. 1 and Concept No. 3, and the group with the lowest vertical force was formed by the BMDS CNH and Concept No. 2. The vertical forces were statistically significantly different, but the largest difference between the lowest and the highest median value was around 20 Newtons, which is a minor difference for a manufactured opener.

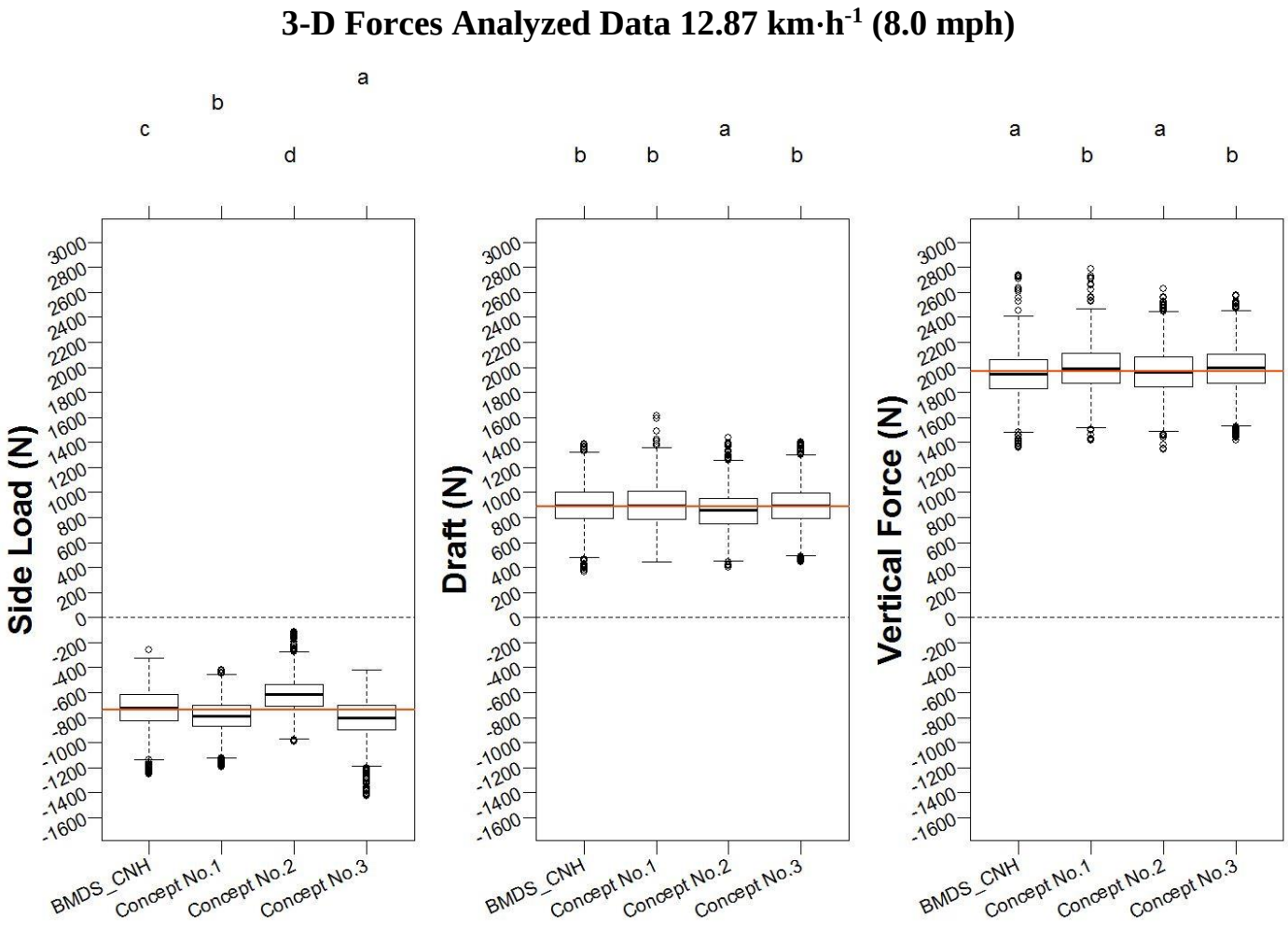

Figure 5.3. Typical example of 3-D force graph result.

5.3 Experimental Field Trials with Crop Residues

The experimental field trial with crop residues was a binary experience ("Yes" or "No"). The test, despite its simplistic results, was one of the most important tests with the seed-to-fertilizer experimentations. This test determines the capacity of the knives to succeed through crop residue conditions considered normal, and one extreme. The apparatus can be rejected with a single "No" in normal conditions, and obtaining a "No" in extreme conditions required a thorough examination. Table 5.9 shows the summary of results, and the detailed results are displayed in APPENDIX F.

The BMDS and the BMSS received only one "No," which was obtained in extreme conditions. The openers did not succeed in passing through a pile of wheat straw residue, which created a wad in its front. The accumulation of straw in front of the opener prevented the discs from rotating.

The BMDS CNH and Concept No. 1 received 2 "Yes" / 7 "No", and 3 "Yes" / 6 "No" respectively, which mean they both failed the test. The BMDS CNH and Concept No. 1 were constantly in a process of residue accumulation and release. Residue accumulations were created between the end of the scraper, the beginning of the knife edge, the nose of the scraper, and the ground. The area described by these four regions can be found in Figure 4.26 and Figure 4.27. These accumulations prevented the apparatuses from succeeding at their seeding functions, because these residue accumulations gradually raised the opener until the aggregations were dislodged by the drag force created by the ground. However, in extreme conditions, the openers were definitively clogged in less than three seconds. Furthermore, only in rare moments, with optimal conditions, were these two disc drills capable of satisfying their duty. Concept No. 2 and Concept No. 3 were the only two apparatuses that did not clog throughout the tests, even at the extreme conditions that stopped the BMDS and the BMSS. Concept No. 2 and No. 3 were able to

pass through any residue conditions, due to the fact that the void between the end of the scraper and the nose of the knife, observable on the BMDS CNH and Concept No. 1, was closed, which does not allow residue accumulation. Moreover, Concepts No. 2 and No.3 had the attack edge extend to the end of the scraper, which creates a better transition between the scraper and the knife and reduces the possibility of creating an accumulation directly on the edge.

All of the results are based on field observations and crop residue accumulation frequency.

Table 5.9. Experimental field trials with crop residues result.

Openers	Test Results		Test Conclusion
	Yes	No	
BMDS	8	1	**Passed**
BMDS CNH	2	7	**Failed**
BMSS	8	1	**Passed**
Concept No.1	3	6	**Failed**
Concept No.2	9	0	**Passed**
Concept No.3	9	0	**Passed**

5.4 Validation of DEM Simulations

The DEM validation section summarizes all the experiments validated by using the Discrete-Element-Method. The analytical forces were validated by the analytical knife at two different ground speeds with the first generation soil bin. The seed-to-fertilizer separation experimentations were validated with the analytical disc drill, at two ground speeds, in the 2nd generation soil bins. The wear predictions were made with the analytical disc drill in the 2nd generation soil bin. The wear pattern predictions were determined by using the cumulative forces collected on the knife and the scraper during the simulations at the two speeds. The wear rate estimations were predicted by using the compressive force determined by EDEM on the knife during the simulations at both speeds. The experimentations using the analytical disc drill were done at the wheat setting, and those using the analytical knife were made at a depth of 25.4 mm (one inch).

5.4.1 Analytical Model Validation

The analytical model validation section compares the force predicted by the analytical model to the draft force collected by the virtual knife in the two first-generation soil bins. The virtual draft forces are displayed in detail in APPENDIX G, and a representative example is provided in Figure 5.4. The drafts collected were displayed in line graphs, where each line represents the draft created by the knife through time. The colours of each line represent a specific condition (i.e. Blue = virtual knife at 8.85 kmh^{-1} into the soil bin with rock only). The graphs have some high peaks caused by impact with rocks, which are highlighted by the orange arrow in Figure 5.4. However, in Figure 5.4 the rectangle in fuchsia represents a stone in front of the virtual knife. The rock pushed by the virtual knife drastically influences the draft, which is displayed in Figure 5.5 under the fuchsia arrow in front of the analytical knife in orange.

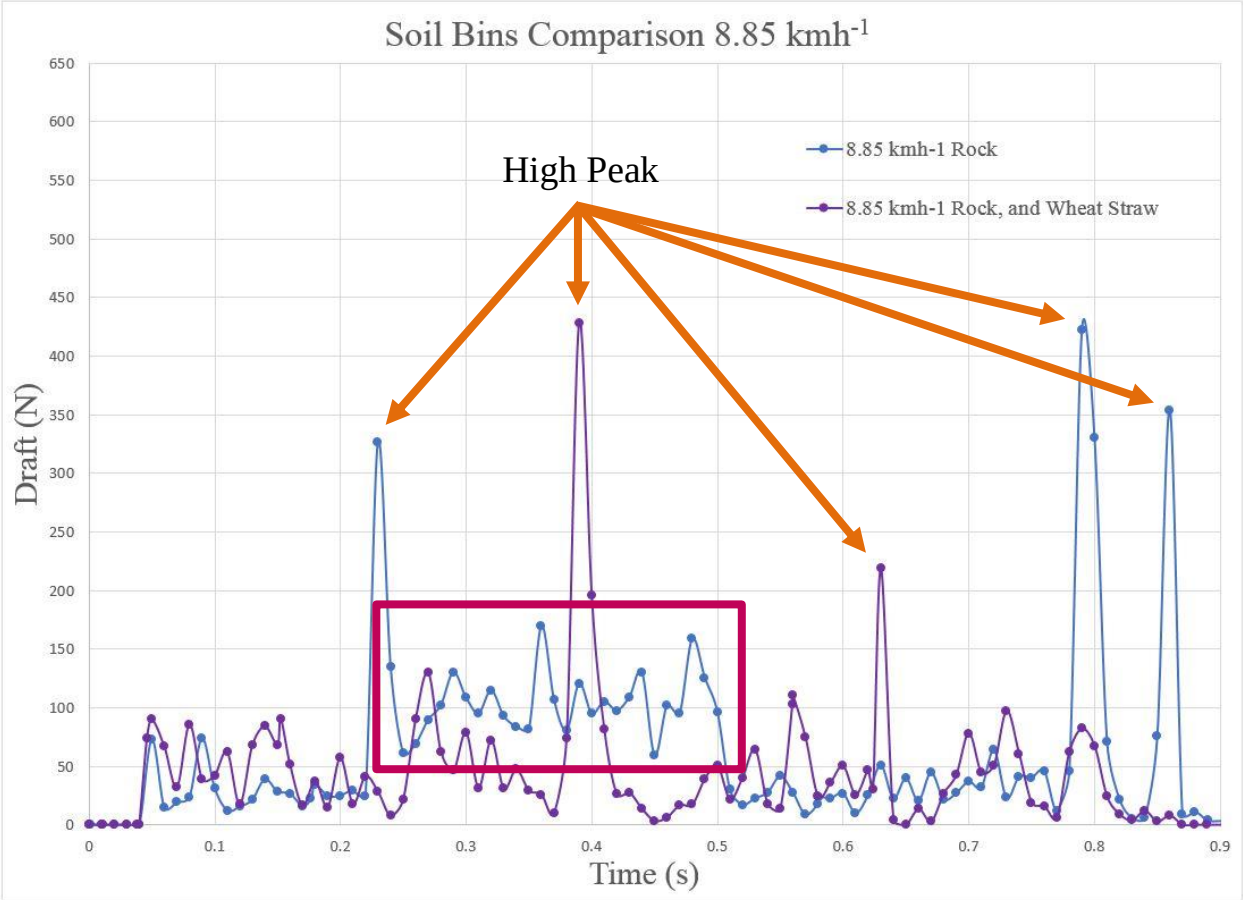

Figure 5.4. Example of analytical force between the two first-generation soil bins.

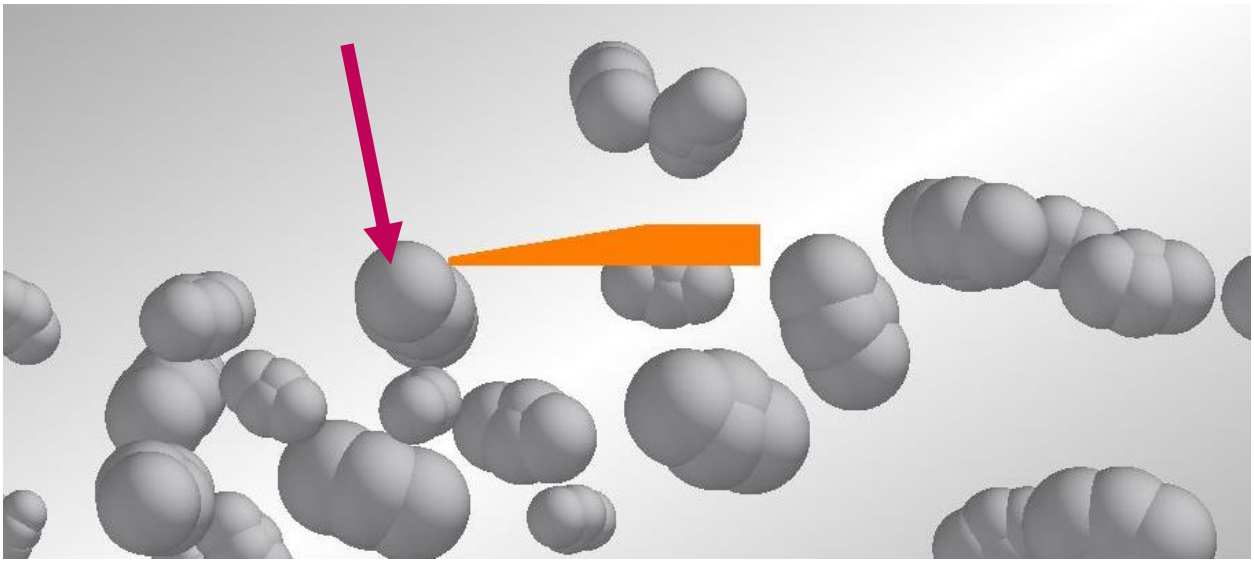

Figure 5.5. Stone in front of the virtual knife.

These irregularities were removed a priori to compute a precise virtual draft average. The virtual draft averages were the measurements used to compare the draft calculated by the analytical model. The values were compared by using error percentages, which were calculated from the difference between the draft measured in DEM (virtual) and the analytical draft divided by the draft. The summary of the draft values and the error percentage are shown in Table 5.10. The soil bins created with the stones and the straws have an unacceptable percentage of 49.5 and 55.2% at 8.85 and 12.87 $km \cdot h^{-1}$, respectively. The high percentage of error was caused directly by the wheat straws, which create a wide variation in the draft. The virtual wheat straw particles were rigid compared to the flexible wheat straw from the field, which created voids in the soil around the apparatus and caused variations in the draft. The soil bins created with only rocks as extra particles, have a 1.4% error percentage at 8.85 $km \cdot h^{-1}$, and 12.1% error percentage at 12.87 $km \cdot h^{-1}$, which is acceptable. The virtual draft at 12.87 kmh^{-1} generated an error percentage of 12.1% versus analytical draft, which is considered precise due to the velocity of the virtual implement in the simulation. Moreover, the accuracy of an analytical model is normally inversely proportional to the apparatus ground velocity, which can explain the increasing error percentage from 8.85 to 12.87 $km \cdot h^{-1}$ for both of the first-generation soil bins.

Table 5.10. Analytical draft summary.

Iterations	DEM Draft (Virtual) Average (N)	Analytical Draft Model (N)	Error (%)
8.85 $km \cdot h^{-1}$ Rock, and Wheat Straw Soil Bins	43.8	29.3	**49.5**
12.87 $km \cdot h^{-1}$ Rock, and Wheat Straw Soil Bins	65.2	42.0	**55.2**
8.85 $km \cdot h^{-1}$ Rock Soil Bins	29.7	29.3	**1.4**
12.87 $km \cdot h^{-1}$ Rock Soil Bins	36.9	42.0	**12.1**

5.4.2 Seed-to-Fertilizer Separation

The seed to fertilizer separation section describes the horizontal and vertical separation results determined analytically by the software EDEM® v. 2.7. The separations were determined by calculating the difference between the centers of mass of the seeds and the fertilizer particles. The raw particles placement, with their centers of mass, are displayed in the figures of APPENDIX H. Also, a visual representation of the analytical horizontal (H) and vertical (V) delta is available in Figure 4.59. Furthermore, the summary of the delta distances are provided in Table 5.11.

The values are provided with and without outliers, due to the fact that the soil used in the simulations can be considered a worst-case scenario for the disc drills. The worst-case scenario for a disc drill is when the trenches are not closing quickly. Prolonged trench closing time allows the seeds to bounce in their furrow and the possibly of the seeds to travel closer of the fertilizer furrow. The seed rarely reached an environment where ammonia burning would be possible, which is less than ten millimetres from the fertilizer cloud depending on soil conditions. Furthermore, the virtual disc drill simulation, even using a worst case scenario soil bin, provided an optimal vertical and horizontal separation, and accurately distributed the seed and fertilizer.

The results were compared between the two speeds, and between the values with and without outliers. The seed particles were considered outliers when they fell into the fertilizer furrow. The seed particles considerably influence the results when they reach this point. The vertical deltas with outliers at 8.85 $km \cdot h^{-1}$ and 12.87 $km \cdot h^{-1}$ have a value of 24.9 mm and 24.8 mm, respectively. The vertical delta measures without outliers have a value of 26.2 mm and 26.4 mm at 8.85 $km \cdot h^{-1}$ and 12.87 $km \cdot h^{-1}$, respectively. The vertical measurements with and without outliers vary a little, due to the fact that only rare particles fall deep enough into the fertilizer trench to

have a significant influence. The horizontal delta measurements with outliers at 8.85 km·h^{-1} and 12.87 km·h^{-1} have a value of 29.2 and 24.4 mm, respectively. Also, the horizontal delta without outliers has values of 34.3 and 33.6 mm at 8.85 kmh^{-1} and 12.87 kmh^{-1}, respectively. Moreover, the horizontal delta measures vary more than the vertical delta measures, due to the fact that seed needs to travel a certain distance before it can fall into the fertilizer furrow, and have some vertical influence. The fertilizer furrow was closed quickly after the introduction of the fertilizer, and only a few rare seeds were able to fall into the furrow. The excessive travel was directly caused by the worst case scenario soil used in the simulation. Also, these falling particles were not in danger of being ammonia burned, except for singular cases. The vertical and horizontal delta measures without outliers were similar to the range described in Section 5.2.1.2 Offset Distances, which means that the products were delivered realistically. Overall, the particle placement was above expectations even for a worst-case scenario soil.

Table 5.11. Analytical seed to fertilizer separation summary.

Velocity	Vertical Delta unit lower (mm)	Vertical Delta without Outliers (mm)	Horizontal Delta (mm)	Horizontal Delta without Outliers (mm)
8.85 km·h^{-1}	24.9	26.2	29.2	34.3
12.87 km·h^{-1}	24.8	26.1	24.4	33.6

5.4.3 Wear Pattern Prediction

The wear pattern predictions were determined for the scraper and the knife at two ground speeds, in order to compare cumulative force intensity during the same time interval. The intensities were directly displayed in Newtons on the apparatus by a multicolour system. The blue represents the lowest values and the red represents the highest values. The green colour fills the gap between the two colours. The low value used for all the implements was set at zero Newtons,

and the high value for the knife was set at 2500 N, compared to 15000 N for the scraper. These values were each determined after 3.5349 s of simulation, which means 8.64 m and 12.56 m travelled for the simulation at 8.85 $km \cdot h^{-1}$ and 12.87 $km \cdot h^{-1}$ respectively. The wear patterns between the slowest and the fastest velocities were distributed similarly; only the intensity of the wear patterns increased proportionally to the ground speed. However, the wear pattern side view and bottom view at the two velocities are displayed in APPENDIX I. The wear patterns are displayed on the figure by using the normal cumulative force or the tangential cumulative force. The normal cumulative force is not displayed in the appendix, due to the fact that they produce the same wear pattern as the cumulative tangential force, but with approximately ten times less intensity than the cumulative tangential force. The low intensity of the normal forces can be caused by the vertical and/or horizontal motionless apparatus in the soil bins. The wear patterns on the scraper were directly located on the carbide pieces. The majority of pressure was absorbed by the large carbide piece (Large), and a less important percentage involved the small carbide piece (Small), as displayed in Figure 5.6. The small carbide piece is located at the bottom of the scraper behind the large carbide piece, as displayed in Figure 5.6. The small carbide piece prevented the bottom of the scraper from wearing and forms a hook in which the residue could accumulate and eventually clog the fertilizer output.

The wear patterns on the knife were mostly distributed on the edge (Edge), and on the knife tip outside of the scraper shadow (Extremity), as shown in Figure 5.6. However, a wear pattern is described on the bottom stress location (Bottom Stress Location), as displayed in Figure 5.7, which is less intense than the patterns displayed on the edge and/or the tip of the knife outside of the scraper shadow. The wear pattern located at the end (End) of the knife, as displayed in Figure 5.7, is less intense than the wear pattern on the edge and the extremity, but it is located on sheet metal.

The End wear pattern could create enough heat and wear to bend the sheet metal to the inside of the seed tube and ultimately obstruct the seed exit, hence the importance of placing a wear protection (i.e. Carbide).

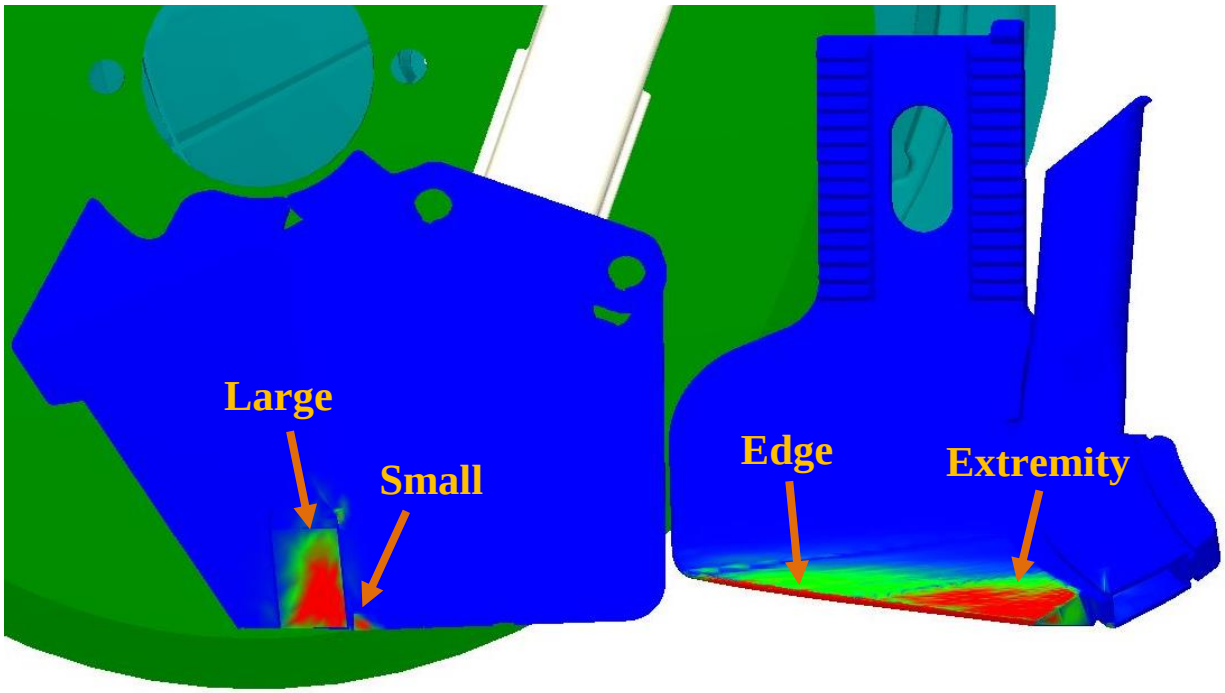

Figure 5.6. Side view of the scraper and knife at 8.85 km·h-[1].

Figure 5.7. Bottom view of the knife at 8.85 km·h-[1].

5.4.4 Wear Rate Estimation

The wear rate estimation section estimates the wear rate at 8.85 $km \cdot h^{-1}$ and 12.87 $km \cdot h^{-1}$, which were the two ground speeds used during field tests. The compressive forces applied on the knife were extracted from DEM simulations. The compressive force raw data with their average line are displayed in APPENDIX J. The average compressive forces were 48.8 N and 53.4 N at 8.85 $km \cdot h^{-1}$ and 12.87 $km \cdot h^{-1}$, respectively. The wear rate estimation range was based on the reference values provided by Archard and Hirst (1956) for mild steel, hardened steel, and tungsten carbide. The cast material used for the knives normally have values between that of mild steel and hardened steel, but given the high wear results, an estimation for tungsten carbide was added. The material hardness ranges were from $18.6 \cdot 10^6$ $g \cdot cm^{-2}$ for mild steel to $130.0 \cdot 10^6$ $g \cdot cm^{-2}$ for tungsten carbide, with the hardened steel value between them of $85.0 \cdot 10^6$ $g \cdot cm^{-2}$. The K values are inversely proportional to material hardness. The materials selected had a K value of 7.0·10-3 for mild steel, $1.3 \cdot 10^{-4}$ for hardened steel, and $1.0 \cdot 10^{-6}$ for tungsten carbide. The wear rate according to the Archard equation is higher for low hardness material with a high K value than for material with high hardness, and a low K value. Furthermore, the ground speed proportionally affects the normal force and the wear rate on the apparatus. The wear rate range was from $728641.14 \cdot 10^{-4}$ $cm^3 \cdot s^{-1}$ for mild steel at 12.87 $km \cdot h^{-1}$, to $9.36 \cdot 10^{-9}$ $cm^3 \cdot s^{-1}$ for tungsten carbide at 8.85 $km \cdot h^{-1}$. The wear rates were converted into days before the materials lost a cubic centimetre of its material, which are displayed in the time column of the summary Table 5.12. The time interval required for an apparatus to lose a cubic centimetre of material is inversely proportional to the wear rate. The shortest amount of time required to lose a cubic centimetre was provided by the mild steel at 12.87 $km \cdot h^{-1}$, which will need 0.016 days (23 minutes), instead of the tungsten carbide at 8.85 $km \cdot h^{-1}$,

which will need 1236.9 days. The wear rate values, the material hardness values, the K values, and the time values are displayed in the summary Table 5.12.

Table 5.12. Wear rate estimation parameters summary.

Relative Velocity	Applied Normal Force (N)	Material Type	Material Hardness (10^6 g·cm^{-2})	K_a Value	Wear Rate (cm^3·s^{-1} ·10^{-9})	Time (Day·cm^{-3})
8.85 km·h^{-1}	48.8	Mild Steel	18.6	$7.0 \cdot 10^{-3}$	457789.05	0.025
		Hardened Steel	85.0	$1.3 \cdot 10^{-4}$	1860.39	6.221
		Tungsten Carbide	130.0	$1.0 \cdot 10^{-6}$	9.36	1236.942
12.87 km·h^{-1}	53.4	Mild Steel	18.6	$7.0 \cdot 10^{-3}$	728641.14	0.016
		Hardened Steel	85.0	$1.3 \cdot 10^{-4}$	2961.10	3.909
		Tungsten Carbide	130.0	$1.0 \cdot 10^{-6}$	14.89	777.143

The cast material had expected hardness values from 60 to 75·10^6 g·cm^{-2}, with a K value around 1.1·10^{-4}. These values provide a wear rate ranging from 1784.07 to 2230.09·10^{-9} cm^3·s^{-1} at 8.85 km·h^{-1}, and wear rates ranging from 2839.62 to 3549.52·10^{-9} cm^3·s^{-1} at 12.87 km·h^{-1}. The wear rate will offer 5.19 to 6.49 days before the apparatus loses 1 cm^3 at 8.85 km·h^{-1}, and 3.26 to 4.08 days at 12.87 km·h^{-1}. The wear rate calculated for the cast material will deform the cast knife shape promptly; the option to add protections (i.e. carbide) on the high pressures/high wear locations needs to be considered to create an accurate/durable seeding knife apparatus.

6.0 SUMMARY, CONCLUSIONS AND RECOMMENDATIONS

6.1 Summary

According to the literature review of scientific articles, the best method to distribute fertilizer without causing any damage to the seeds (damage reducing emergence), while increasing the yield, is to distribute the fertilizer at 2.5 cm on the side, and 2.5 cm under the seed furrow. The method capable of distributing the fertilizer accurately this close to the seed furrow is by using an apparatus directly attached to the seed unit. The knife apparatus was developed to distribute the seeds laterally from fertilizer furrow to ensure an undisturbed seed furrow.

Knife concepts were especially developed to keep or reduce the force required by the seeding implement compared to the BMDS CNH. The concepts compare their performances to the benchmark double-shoot CNH Industrial (BMDS CNH), which was set as the reference for the addition of the double-shoot capability. The BMDS CNH was used as reference for the 3-D forces, due to its minimal draft increase compared to the single-shoot. The BMDS CNH draft increase has been validated prior to the beginning of the project. The field results demonstrated that the concept knives No. 2 and No. 3 had similar or significantly fewer 3-D forces than the BMDS CNH.

The BMDS CNH was also used as reference for the seed-to-fertilizer separation experiments, due to its accurate product placement. Moreover, the BMDS CNH seed-to-fertilizer separation, such as the 3-D forces, were validated before the beginning of the project. The product separation tests were statically evaluated at 95% confidence to compare the opener performances. The seed-to-fertilizer separation correlation demonstrated that the best reliable pair of openers were Concept No. 2 and No. 3. The pairs of openers for the product placement were statistically more accurate

than the BMDS CNH and Concept No. 1, which were the third and fourth-best openers, respectively.

The challenge was to design an opener able to manage an important quantity of crop residues regardless of the crop type. Concept No. 2 and No. 3, according to the experimental field trials with crop residues results, are expected to be as good as a single-shoot opener (at this point in the comparison process). These two knives are the only ones to successfully get through extreme conditions without plugging at all. They also managed field residues with ease during the seed-to-fertilizer separation experiments, unlike the BMDS CNH and Concept No. 1, which were repeatedly plugged.

Knife concept No. 3 was selected in light of the field results to simulate the field experiments with the DEM software. The simulations of the seed to fertilizer separation experiments validated product variances like the distributions observed in hard condition fields. The simulation was performed using a worst-case scenario soil, which allows more seed than normal to travel towards the fertilizer furrow. Overall, the seed to fertilizer separation simulations were accurate and provided exemplary product separations, which was confirmed by predetermined agronomically widely accepted seed/fertilizer placement. Also, the product separations provided by the simulations can be used as a reference for the knife's behaviour in rough conditions.

The analytical soil bins were developed to predict the draft forces, which were determined by an analytical model of soil mechanics. The virtual soil bin with stones only validates the draft forces with an error percentage of 1.4% at 8.85 $km \cdot h^{-1}$ and 12.1% at 12.87 $km \cdot h^{-1}$, which is more than acceptable. The second-generation soil bin was directly based on the virtual soil bin with stones only to provide more accurate results.

The wear pattern simulation validated the wear placement on the scraper and the knife by determining the high pressure/high wear locations. The determination of high pressure/high wear locations combined with the wear prediction allows the determination of ideal kinds of protection at optimal positions. The precise introduction of protections minimizes wear characteristics in order to maximize the life expectancy of the seed-row unit, and reduces maintenance costs.

6.2 Conclusions

To conclude, the project was divided into a research objective, an overall objective, a main objective, and three specific objectives.

1. The research objective was to determine the best method of placing fertilizer at an optimal distance without damaging the seeds or disturbing the seed bed.
    a. The fertilizer was distributed in between the scraper and the disc before and deeper than the seeds, which are delivered by the knife on the side of the fertilizer furrow to ensure that the seed bed was undisturbed.
    b. The optimal fertilizer placement versus the seeds placement to avoid seed damages while providing the fertilizer benefits was fixed at 25 mm on the side and 25 mm under the seed bed, which was confirmed by the literature.
2. The overall objective was to study the dynamics of a disc drill apparatus supplemented with a double-shoot function. The dynamics of the double-shoot disc drills were evaluated for the side load, the draft, and the vertical force. The difference required between two means of different data groups to be significantly different was 10 to 14 N depending on the data distribution, which was very accurate for agricultural machineries.
    a. The statistical analysis results are comparable between the two speeds used during field tests.

b. Concept No. 2 throughout the experiments produce significantly lower 3-D force than BMDS CNH and any other concept.

c. The statistical results demonstrated that the concepts have similar data distributions throughout the different types of force, even if they have significant differences. The significant differences are not considered major in agricultural mechanization field.

3. The main objective was to develop a seed-row unit able to distribute seeds and fertilizer simultaneously as a function of crop types and yield residues from last harvest season.

a. Concept No. 2 and No. 3 distributed seeds and fertilizer into the ground with less variance than the BMDS CNH and Concept No.1. The variance determines the accuracy of each opener, which means Concept No. 2 and No. 3 are more precise.

b. Concept No.2 and No.3 was the pair of openers the most constant through the seed-to fertilizer separation, better than the BMDS CNH and knife No.0, which were the third and fourth-best apparatuses respectively.

c. Concept No.2 and No.3 were the only two openers to get through all the conditions without plugging.

4. The first specific objective was to develop a DEM model that minimizes the seeds and fertilizer spatial distribution, which was validated by the seed to fertilization distribution results.

a. The simulation was developed to recreate a worst-case scenario soil bin, in which Concept No. 3 was used.

b. The DEM model realistically reproduced the vertical and horizontal delta, and the variance in the product distribution comparable to the seed to fertilizer delta results.

5. The second specific objective was to develop a DEM model that was validated by an analytical model of soil mechanics, in order to minimize the horizontal draft.

a. The DEM draft versus the analytical draft, both measured from the analytical knife, had an error percentage of 1.4% at 8.85 $km \cdot h^{-1}$ and 12.1% at 12.87 $km \cdot h^{-1}$, which is more than suitable.

6. The third specific objective was to predict the location of intense wear on the apparatus, in order to minimize the wear characteristic and to maximize the seeding row unit life expectancy.

a. The DEM wear simulations validated the scraper carbide position and shape, in addition to determining the wear intensity.

b. The DEM wear simulations determined potential wear locations on the knife and their intensity, which was used to predict wear rates and the type of protection required.

6.3 Recommendation

Through experimentations and simulations of the development of a double-shoot on a disc drill, knife concepts No. 2 and No. 3 have demonstrated the best capacities. These two candidates are the best prospects to succeed through a wide range of conditions, including some extreme conditions. However, some recommendations are necessary for both of these knives:

1. The two knives offer unexpected performances through the development of the double-shoot disc drill, but some modifications must be made. The head of the knives must allow for a horizontal displacement equivalent to the scraper horizontal displacement, to preserve the same relative positioning between the two implements. The head of the knife must be extended widely to permit a larger slot, which will allow the required horizontal movement.

   The knife vertical movement can be improved by angling the knife mounts and the knife heads to follow the angle of the scraper back edge. The improvement will keep the knife versus the scraper in an ideal position, and will prevent a void when the knife is vertically adjusted.

   The washer maintaining the knives on the mount requires modification in order to be usable at both the low and high scraper position. The washer can be eccentrically shaped, so that it can make a half turn to compensate for the horizontal distance variation. Also, the washer can be cross-shaped with a specific length distribution on each section of the cross to compensate for the horizontal displacement variation.

2. Field experimentation combined with wear simulation results determined that the knives will require some kind of protection on their high pressure/high stress locations. This protection will prevent an excessive wear by reducing the wear characteristics, and will

extend the life expectancy of the seed-row units. The protection might be sufficient with some kind of hard welding, otherwise, the use of carbide inserts will be required.

3. The knives were tested on soil types and crop residues available around Saskatoon, Saskatchewan. The apparatuses need to be tested on a larger range of soil types and crop residues before they satisfy the requirements.

4. The last recommendation concerns the closing system. The system had difficulty adequately closing the furrows on specific field types; this observation was confirmed by the simulations. The closing system, not being able to provide an adequate soil/product contact, can delay emergence and can ultimately reduce yield. The closing system requires more pressure and/or a different design to satisfy the requirements for a larger range of soil conditions.

7.0 REFERENCES

Adapa, P., L. Tabil, and G.Schoenau. 2009. Compaction characteristics of barley, canola, oat and wheat straw. ScienceDirect, Biosystems Engineering 1O4, 335-344. Elsevier Ltd.

Afzalinia, S. 2005. Modeling and validation of the baling process in the compression chamber of a large square baler. PhD diss. Saskatoon, Saskatchewan. University of Saskatchewan, Department of Agricultural and Bioresource Engineering.

Agdex. 2007. Using 1,000 kernel weight for calculating seeding rates and harvest losses. Agdex Reference No. 100/22-1. Alberta, Canada.: Alberta Agriculture and Food

AgriInfo. 2015. Density of Soil: Bulk Density and Particle Density. My Agriculture Information Bank. AgriInfo.in. Available at: http://www.agriinfo.in/?page=topic&superid=4&topicid=271. Accessed 21 May 2015.

ANSI/ASAE. 1993. Density, specific gravity, and mass-moisture relationships of grain for storage. ANSI/ASAE Reference No. D241.4. American National Standards Institute.

Arksey, D. 2009. Disc furrow opener and method for single pass placement of seed and fertilizer. U.S, Patent No. 7,568,438.

Aspinwall, L. A. 1911. Agricultural Implement. U.S. Patent No. 1,012,118

ASTM. 2013. Standard guide for conducting wear tests using a Rotary Platform Abraser, G 195 – 13a. ASTM Annual Book of Standards.

ASTM. 2010a. Standard test method for laboratory determination of water (moisture) content of soil and rock by mass. ASTM Reference No. D 2216-10. American Society for Testing and Materials International.

ASTM. 2010b. Standard test method for measuring abrasion using the dry sand/rubber wheel apparatus, G 65 – 04. Annual Book of Standards.

ASTM. 2010c. Standard test method for wear testing with a pin-on-disk apparatus, G 99 – 05. ASTM Annual Book of Standards.

ASTM. 2009. Standard test method for measuring abrasion resistance of materials by abrasive Loop Contact, G 174 – 04. ASTM Annual Book of Standards.

ASTM. 2007. Standard test method for conducting wet sand/rubber wheel abrasion tests, G 105 – 02. ASTM Annual Book of Standards.

Archard, J. F. and Hirst. W. 1956. The wear of metals under unlubricated conditions. Proceedings of the Royal Society of London. Series A, Mathematical and Physical Sciences. 236(1206): 397 – 410.

Bailey, L. D. and Grant, C. A. 1990b. Fertilizer placement studies on calcareous and non-calcareous chernozemic soils: Growth, P-uptake, oil content and yield of Canadian rape. Commun. Soil Sci. Plant Anaf . 2l: 2089-21O4

Baker, C. J.,Kernohan, D., Robinson, D. J. 1993.Seed sowing apparatus. U.S. Patent No. 5,269,237

Barton, H. 2000. No-till disk opening system. European Patent Mo. 1,002,457

Barton, H. 1997. No-till disk opening system and method. U.S. Patent No. 5,609,114

Barton, H. 1995. No-till disk opening system. European Patent No. 0,677,239

Bigbee, M. L., Ridgely, M. L., Snyder, M. D. 1988. Conservation opener. U.S. Patent No. 4,760,806

Brajas, M. D. 2008. Advanced Soil Mechanics. Third edition. New York, N. Y.: Taylor & Francis.

Breaux, N. J. and J. K. Keska. 2002. Application of a pin-on –disk test to determine abrasive wear. In Processings of the 2002 ASEE Gulf Southwest Annual Conderence. Lafayett, LO: American Society for Engineering Education.

Bogachev, V. D., Bogachev, K. D., Bogachyova, V. D. 1975. Combined coulter. Soviet Union Patent No. 491,340

Buhr, A. G. 1959. Grain drill dual feed boot structure with separating device. U.S. Patent No. 2,869,489

Burt, R., Reinsch, T. G., Miller, W. P. 2014. Soil survey filed and laboratory methods manual. Soil survey investigations report no. 51. Version 2. Method 3.2.1.2.2. United States Department of Agriculture (USDA) Natural Resources Conservation Services (NRCS).

Callister, W. D. 2007. Materials science and engineering an introduction. Seventh Edition. United State of America, John Wiler & Sons, Inc.

Chandon, K., and Kushwaha, R. L. 2002.Soil Forces on Deep Tillage Tools. In Proc. AIC 2002 Meeting CSAE/SCGR Program, Paper No. 02-210. Saskatoon, Saskatchewan.

Chen, Y., Tessier, S., Irvine, B. 2004.Drill and crop performances as affected by different drill configurations for no-till seeding. Soil & tillage Research. 77: 147-155

Cleary, P. W. 1998. Predicting charge motion, using power draw, segregation and wear in ball mills using discrete element methods. Material Engineering. 11(11): 1061 – 1080.

Cundall, P. A. 1988. Computer Simulations of Dense Sphere Assemblies. In Micromechanics of Granular Materials. pp. 113 – 123. M. Satake and J. T. Jenkins, Eds. Amsterdam: Elsevier Science Publishers B. V.

Cundall, P. A., O. D. L. Strack. 1979. A discrete numerical model for granular assemblies. Géotechnique. 29(1):47 – 65.

Cundall, P. A. 1971. A Computer Model for Simulating Progressive Large Scale Movements in Blocky Rock Systems. In Proceedings of the Symposium of the International Society for Rock Mechanics, vol 1, paper no. II-8, 129-136. Nancy, France. International Society for Rock Mechanics (ISRM).

DEM Solutions. 2015. EDEM 2.7 User Guide. Edinburgh, UK.: DEM Solutions.

DEM Solutions. 2014. EDEM 2.6 Theory Reference Guide. Edinburgh, UK.: DEM Solutions.

EDEM. 2015. Testimonials. EDEM Engineering with Confidence®. DEM Solutions Ltd. Available at: http://www.dem-solutions.com/company/testimonials/. Accessed 09 September 2015.

Engineers Edge. 2015. Poisson's Ratio Metals Materials Chart. Engineers EDGE. Available at: https://www.engineersedge.com/materials/poissons_ratio_metals_materials_chart_13160.htm . Accessed 25 May 2015.

Er, U. and Par, B. 2006. Wear of plowshare components in SAE 950C steel surface hardened by powder boriding. Wear. 261: 251 – 255.

Fielke, J., Ucgul, M., and Saunders, C. 2013. Discrete Element Modeling of Soil-Implement Interaction Considering Soil Plasticity, Cohesion and Adhesion. In Proc. Annual International Meeting Sponsored by ASABE. Paper No. 131618800.Kansas City, MO.: ASABE.

Forsyth, C. H., Walker, D. W. 1965. Furrow opener. U.S. Patent No. 3,213,812

Friesen, D. E. 2009. Furrow Opener. U.S. Patent No. 7,540,246

Geddes, I. 2005. Soil control Mechanism. U.S. Patent No. 6,978,727

Gegas, V. C., Nazari,A., Griffiths, S., Simmonds, J., Fish, L., Orford, S., Sayers, L., Doonan, J. H., Snape, J. W. 2010. A genetic framework for grain size and shape variation in wheat. The Plant Cell, Vol 22: 1046-1056.

George, R. B. 2008. Encyclopedia of Soil Science. Particle density, 504-505. Ward Chesworth, University of Guelph, Canada.: Springer

Geotechdata. 2014. Typical values of soil cohesion for different soils, Soil Cohesion. Geothechdata.info. Available at: http://www.geotechdata.info/parameter/cohesion.html. Accessed 12 May 2015.

Geotechdata. 2013. Typical values of soil friction angle for different soils according to USCS, Soil friction angle. Geothechdata.info. Available at: http://www.geotechdata.info/parameter/angle-of-friction.html. Accessed 13 May 2015.

Gill, W. R., Shafer, R. L., and Wismer, R. D. 1994. Soil dynamics and soil bins. In advances in Soil Dynamics Vol. 1, eds. S.K. Upadhyaya, W.J. Chancellor, J. V. Perumpral, R. L. Shafer, W. R. Gill, and G. E. Vanderbeg, 1 – 19. St. Joseph, MI: American Society of Agricultural Engineers.

Godwin, D., MJ. O'Dogherty, K. Blackburn. 2004. Typical Soil Properties. Soil Engaging Element Force Models. Cranfield University, National College of Agricultural Engineering. Available at: http://public.cranfield.ac.uk/ns35kwb/soiltine/index.htm Accessed 12 May 2015.

Graff, L. 2010. Discrete element method simulation of wear due to soil-tool interaction. MS thesis. Saskatoon, Saskatchewan.: University of Saskatchewan, Department of Agricultural and Bioresource Engineering.

Graff, L. G., Roberge, R. C., Roberge, M. A., Crowe, T. G. 2007. Wear of ripper point hardsurfacings. In Proceedings of the 2007 North Central Intersectional Conference of the ASABE, RRV-07120. Fargo, ND: American Society of Agricultural and Biological Engineers.

Grant, C., J. Heard. 2004. Spring Options for Nitrogen Fertilization. University of Manitoba. Available at: http://umanitoba.ca/faculties/afs/MAC_proceedings/proceedings/2004/grant_spring_options.pdf. Accessed 26 January 2015

Grant, C. A., L. D. Bailey. 1993. Fertility management in canola production. Canadian Journal of Plant Science. 73: 651-670

Greig, J. D., Bailey, A. J. 1970, Seed drill. U.S. Patent No. 3,507,233

Grisso, R. D., J. V. Perumpral. 1985. Review of Models for Predicting Performance of Narrow Tillage Tool. ASAE Paper No. 81-1535. Blacksburg, VA.: ASAE.

Hansson, K. 1991. Agricultural combined drill dispenser. U.S. Patent No. 4,998,488

Hartman, K. 2002. Furrow opener. Canadian Patent No.2,326,204

Hartman, K. 2000. Disc furrow opener. Canadian Patent. No. 2,275,124

Hothorn, T., F. Bretz, P. Westfall, R. M. Heiberger, A. Schuetzenmeister, and A. Sheibe. 2015. Simultaneous Inference in General Parametric Models. CRC Press.Taylor &Francis Group. Available at: https://cran.r-project.org/web/packages/multcomp/multcomp.pdf. Accessed 12 August 2015.

Immesoete, A. J., 1958. Disk fertilizer applicator. U.S. Patent No. 2,842,078

Itasca. 2003. PFC3D User's Manual, Version 2.0. Itasca Consulting Group Inc, Minneapolis, MN, USA.

Jagow, S., Corriveau, D., Colin, R. 2010. Single disc furrow opener with walking beam. U.S. Patent No. 7,681,656

Janelle, L., Tessier, S., Laguë, C., 1995. Seeding tool design for no-tillage conditions in north-eastern America. ASAE Paper No. 93-1561. ASAE, St. Joseph, MI

Kalala, J. T., Bwalya, M. T., and Moys, M. H. 2005. Discrete element method (DEM) modelling of evolving liner profiles due to wear. Part I: DEM validation. Minerals Engineering. 18: 1386 - 1391.

Kalra, Y. P. and Soper, R. J. 1968. Efficiency of rape, oats, soybeans, and flax in absorbing soil and fertilizer phosphorus at seven stages of growth. Agron. J. 60 209-212.

Kavazanjian, E., JR. N. Matasović, T. Hadj-Hamou, and P.J. Sabatini. 1997. Geotechnical Engineering Circular #3, Design Guidance: Geotechnical Earthquake Engineering for Highways, Volume 1 – Design Principles. Publication No. FHWA-SA-97-076. Washington, DC 20590.: Office of Engineering, Office of Technology Application.

Klenin, N. I., Popov, I. F., Sakun, V. A. 1986. Agricultural Machines Theory of Operation, Computation of Controling Parameters and the Conditions of Operation.New Delhi, India.: Rekha Printers Private Limited.

Kushwaha,R.L., A. S. Vaishnav, and G. C. Zoerb. 1983. Shear Strength of wheat straw. Canadian Agricultural Engineering, Vol.25 No.2: 163-166.

Lam, P. S., S. Sokhansanj, X. Bi, S. Mani, C. J. Lim, A. R. Womac, M. Hoque, J. Peng, T. JayaShankar, L. J. Naimi, and S. Nayaran. 2007. Physical characterization of wet and dry wheat straw and switchgrass – bulk and specific density. ASABE Meeting Presentation Paper Number: 076058. Minneapolis, Minn.: ASABE.

Lenth, R. V. 2012. Least-squares means. The Comprehensive R Archive Network. CRAN. Available at: http://127.0.0.1:29463/library/lsmeans/html/lsmeans.html. Accessed 12 August 2015.

McKyes, E. 1989. Agricultural Engineering Soil Mechanics. Netherland.: Elsevier Science Publishers B.V.

McKyes, E. 1985. Soil Cutting and Tillage. Netherlands.: Elsevier Science Publishers B.V.

McKyes, E. and Ali, O. S. 1977. The cutting of soil by narrow blades. J. Terramechanics, Vol. 14, No. 2: pp.43 – 58

McKyes, E., Negi, S.C., Godwin, R. J. and Ogilvie, J. R. 1977. Desing of a tool for injecting organic waste slurries in soil. J. Terramechanics, Vol. 14, No. 3: pp. 127 136

Medernach, A. M. 2010. Drill disc opener. U.S. Patent No. 7,673,571

Metzler, P. M. 1911. Seed and fertilizer drill. U.S. Patent No. 1,006,771

Mindlin, R. D., and Deresiewicz H. 1953. Elastic Spheres in Contact Under Variying Oblique Forces. J. Appl. Mech., 20.: 327 – 344.

MnDOT. 2007. Pavement Material, 2007 MnDot Pavement Design Manual. Pavement Design. Minnesota Department of Transportation. Available at: http://www.dot.state.mn.us/materials/pvmtdesign/docs/2007manual/Chapter_3-2.pdf. Accessed 13 May 2015.

MNZTFA, 1998. Zero Tillage. Manitoba–North Dakota Zero Tillage Farmers Association, Leech Printing Ltd., Brandon, Man., Canada

Mohsenin, N. N. 1986. Physical Properties of Plant and Animal Materials. Second Revised and Updated Edition, Fourth Printing. New York, N. Y..: Gordon and Breach Science Publisher Inc.

Nartov, P. S., 1985. Disk Soil-Working Implements. Rotterdam, Netherlands.: A.A. Balkema

Negi, S C., McKyes, E., Godwin, R. J. and Ogilvie, J. R. (1976). Development of mechanization for efficient injection of liquid slurry waste into agricultural soils. Agr. Canada Report OSW5-0287, Ottawa, ON: pp. 111.

Nickeson, J. L., Walko, J. A. 1986. Conservation no till farming apparatus. U. S. Patent No. 4,611,545

Nyborg, M. and Hennig, A. M. F. 1969. Field experiments with different placements of fertilizers for barley, flax and rapeseed. Can. J. Soil Sci. 49: 79-88.

Nyborg, M. 1961. The effect of fertilizers on emergence of cereal grains, flax and rape. Can. J. Soil Sci. 4l: 89-98.

Ono, I., Nakashima, H., Shimizu, H., Miyasaka. J., and Ohdoi, K. 2013. Investigation of elemental shape for 3D DEM modeling of interation between soil and narrow cutting tool. Journal of Terramechanics. Vol. 50, 265 – 276. Elsevier Ltd.

Owsiak, Z. 1999. Wear of spring tine cultivator points in sandy loam and light clay soils in southern Poland. Soil & Tillage Research 50: 333 – 340.

Owsiak, Z. 1997. Wear of symmetrical wedge-shaped tillage tools. Soil & Tillage Research. 43: 295 – 308.

PAMI, 1995. K-hart double disc direct seeding unit. Evaluation Report 716. Prairie Agricultural Machine Institute, Portage la Prairie, Man., Canada

Parafiniuk, P., Molenda, M., Horabik, J. 2013. Discharge of rapeseeds from a model silo: Physical testing and discrete element method simulations. Computers and Electronics in Agriculture 97, 40-46.: Elsevier.

Parent, G., Tessier, S., Allard, G., Angers, D.A., 1993. Seedbed characteristics for forages and cereals with no-tillage in the northeast. ASAE Paper No. 93-1562. ASAE, St. Joseph, MI.

Patric, C. E. 1918. Furrow-opener for seeding-machines. U.S. Patent No. 1,254,266

Patric, C. E. 1917. Furrow-opener for seeding-machines. U.S. Patent No. 1,229,194

Payton, D.M., Hyde, G.M., Simpson, J.B., 1985. Equipment and methods for no-tillage wheat planting. Trans. ASAE 28, 1419– 1424

Philips, C. S. 1958. Seeding and fertilizing device and hose securing means therefor. U.S. Patent No. 2,861,527

Rosengren, C. M., Ruff, R. S., Schembri, C. J., Wilson, G. B. 2014. A system for variable-ratio blending of multiple agricultural products for delivery via a ported opener. World Intellectual Property Organization Patent No. 2014/183,182

Sargeant, T. C. 1901. Distributor for agricultural purpose. G.B. Patent No. 1900/09,933

Schilling, R. B., Naylor, M. S., Chahley, D. W. 2014. Single-pass, double-shoot opener for agricultural implement. U.S. Patent No. 8,646,395

Schilling, R. B., Naylor, M. S., Chahley, D. W. 2012. Double-shoot single pass implement. U.S. Patent No. 8,272,339

Schilling, R. B., Naylor, M. S., Chahley, D. W. 2011. Apparatus with double-shoot single pass implement. U.S. Patent No. 8,015,933

Schilling, R. B., Naylor, M. S., Chahley, D. W. 2010. Seed boot for double-shoot disc opener. U.S. Patent No. 7,814,847

Shriver, G. H. 1960. Dual disk furrow opener. U.S. Patent No. 2,920,587

Schuring, D. J., Emori. R. I. 1964. Soil deforming processes and dimensional analysis. SAE New York. Paper 897c.

SImetric. 2011. Specific gravity of metals, Density of Metals. SImetric. Available at: http:// www.simetric.co.uk/si_metals.htm#top. Accessed 21 May 2015.

Singh, R. P. 2015. Wheat: varieties and characteristics. Cereal processing. Encyclopedia Britannica. Available at: http://www.britannica.com/EBchecked/topic/103350/cereal-processing/50104/Wheat-varieties-and-characteristics. Accessed 03 March 2015

Sitkei, G. 1986. Mechanics of Agricultural Materials. Amsterdam, the Netherlands: Elsevier.

Smith, D. B., Willcutt, M. H., Diallo, Y. 2005. Uniformity of size and content of granular fertilizer. Applied Engineering in Agriculture. Vol. 21(4): 559-562.

Srivastava, A. K., Goering, C. E., Rohrbach, R. P., and Buckmaster, D. R. 2006. Soil tillage. In Engineering Principles of Agricultural Machines, 2nd Ed. Ed. P. McCann, 169 – 229. St. Joseph, MI: American Society of Agricultural and Biological Engineers.

Subramanian, N. 2008. Design of Steel Structures. USA.: Oxford University Press

Swanson, P. A. 1993. Comparison of laboratory abrasion tests and field tests of materials used in tillage equipment. In tribology: Wear Test Selection for Design and Application, ASTM STP 1199. Ed. A. W. Ruff and R. Bayer, 80 – 99. Philadelphia, PA: American Society for Testing and Materials.

Ucgul, M., Fielke, J. M., and Sauner C. (2015). Three-dimensional discrete element modeling (DEM) of tillage: Accounting for soil cohesion and adhesion. Biosystems Engineering. Vol. 129, 298 – 306. Elsevier Ltd.

Ucgul, M., Fielke, J. M., and Sauner C. (2014a). Three-dimensional discrete element modeling of tillage: Determination of a suitable contact model and parameters for a cohesionless soil. Biosystems Engineering. Vol. 121, 105 – 117. Elsevier Ltd.

Ucgul, M., Fielke, J. M., and Sauner C. (2014b). 3D DEM tillage simulation: Validation of a hysteretic spring (plastic) contact model for a sweep tool operation in a cohesionless soil. Soil & Tillage Research. Vol. 144, 220 – 227. Elsevier B. V.

Uhl, J. B., and Lamp, B. J., 1966. Pneumatic Seperation of Grain and Straw Mixtures. Trans. Of the ASAE 9(2): 244 – 246.

UNIDO and IFDC. 1998. Fertilizer manual. Chapter 18 Physical properties of fertilizers, 471-505. Dordrecht, The Netherlands. Kluwer Academic Publishers

USDA. 2014. Soil Texture. Soil Physical and Chemical Properties. New Jersey.: USDA Natural Resources Conservation Service. Available at: http://www.nrcs.usda.gov/wps/portal/nrcs/detail/nj/home/?cid=nrcs141p2_018993. Accessed 21 May 2015.

Vaishnav, A. S. 1983. Evaluation of disc coulters for a zero till system. Unpublished M. Sc. Thesis. Saskatoon, SK.: University of Saskatchewan, Department of Agricultural and Bioresource Engineering.

Walker, R. 2014. Density of materials Bulk Materials. SImetric. Available at: http://www.simetric.co.uk/si_materials.htm. Accessed 21 May 2015.

Web of Science. 2015. You searched for: Title: (Discrete element method). Web of Science™ Thomson Reuters™. Available at: http://apps.webofknowledge.com.cyber.usask.ca/RAMore.do?product=WOS&search_mode=GeneralSearch&SID=4DsGyzhqBB2tHXYehPJ&qid=18&ra_mode=more&ra_name=JCRCategories&colName=WOS&viewType=raMore&more_sort_order=alpha. Accessed 09 September 2015

Wendling, I., Stephens, L. E. 2000. Grain drill opener with separate placement and a concave disk therefor. U.S. Patent No. 6,032,593

Wendling, I., Stephens, L. E. 1999. Furchenöffner. European Patent No. 0,956,755

Wheeler, P. N. Godwin, R. J. 1996. Soil Dynamics of Single and Multiple Tines at Speeds up to 20km/h. Journal of Agricultural Engineering Research, 63, 243 – 250

Wingate-Hill, R., AUST, M. I. E., Davis, G. R., and Bowditch, H. G. 1979. Wear of Hardfacing treatments applied to shares of tined tillage implements. Transactions of the Institution of Engineers, Australia. ME: 11 – 16.

Wodrich, T. D. 2001. Two piece seed boot for a seeding machine. U.S. Patent No. 6,209,466

Zhu, H. P., Z. Y. Zhou, R. Y. Yang, A. B. Yu. 2007. Discrete particle simulation of particulates systems: Theoretical developments. Chemical Engineering Science 62: 3378-3396.

APPENDIX A

Soils Characterizations Raw Data

Table A. 1. Field Soil Temperature Data Table

Fields	Plots	No.1 (°C)	No.2 (°C)	No.3 (°C)	No.4 (°C)	No.5 (°C)	Average (°C)
Lutheran Loamy Sand Field	Wheat 8.85 kmh^{-1}	N.a.	N.a.	N.a.	N.a.	N.a.	16.4
	Wheat 12.87 kmh^{-1}	N.a.	N.a.	N.a.	N.a.	N.a.	16.6
	Canola 8.85 kmh^{-1}	N.a.	N.a.	N.a.	N.a.	N.a.	16.7
	Canola 12.87 kmh^{-1}	N.a.	N.a.	N.a.	N.a.	N.a.	16.6
Asquith Loamy Sand Field	Wheat 8.85 kmh^{-1}	23.7	21.9	21.9	21.3	22.8	22.3
	Wheat 12.87 kmh^{-1}	26.9	22.8	23.1	22.9	23.4	23.8
	Canola 8.85 kmh^{-1}	19.7	19.7	19.1	19.8	19.4	19.5
	Canola 12.87 kmh^{-1}	23.8	21.8	21.9	21.2	21.0	21.9
Asquith Summer Fallow Loamy Sand Field	Wheat 8.85 kmh^{-1}	25.5	24.8	29.3	28.2	26.5	26.8
	Wheat 12.87 kmh^{-1}	20.5	19.9	18.6	18.3	18.3	19.1
	Canola 8.85 kmh^{-1}	20.0	17.5	18.4	19.5	18.3	18.7
	Canola 12.87 kmh^{-1}	20.8	19.8	19.8	20.3	20.5	20.2
St-Denis Loam Field	Wheat 8.85 kmh^{-1}	16.8	18.9	18.1	18.0	17.8	17.9
	Wheat 12.87 kmh^{-1}	23.8	23.7	20.9	23.5	20.1	22.4
	Canola 8.85 kmh^{-1}	18.7	19.4	18.2	17.6	17.9	18.4
	Canola 12.87 kmh^{-1}	20.3	21.4	20.0	21.8	20.3	20.8
St-Denis Silty Clay Field	Wheat 8.85 kmh^{-1}	24.7	23.1	24.5	21.1	23.7	23.4
	Wheat 12.87 kmh^{-1}	18.0	18.3	18.7	19.2	18.1	18.5
	Canola 8.85 kmh^{-1}	25.4	23.6	23.9	23.6	24.2	24.1
	Canola 12.87 kmh^{-1}	25.8	25.6	25.2	26.0	25.7	25.7

** N.a. = Not Available data*

Table A. 2. Field Soil Compaction Data Table

Fields	Plots	No.1 (kPa)	No.2 (kPa)	No.3 (kPa)	No.4 (kPa)	No.5 (kPa)	Average (kPa)
Lutheran Loamy Sand Field	Wheat 8.85 kmh^{-1}	2068.4	1379.0	1137.6	1585.8	1172.1	1468.6
	Wheat 12.87 kmh^{-1}	1482.4	896.3	1654.7	1999.5	1723.7	1551.3
	Canola 8.85 kmh^{-1}	1792.6	1792.6	2068.4	1965.0	1379.0	1799.5
	Canola 12.87 kmh^{-1}	1723.7	1723.7	1103.2	758.4	1585.8	1379.0
Asquith Loamy Sand Field	Wheat 8.85 kmh^{-1}	1861.6	2068.4	2068.4	2137.4	1896.1	2006.4
	Wheat 12.87 kmh^{-1}	1723.7	1379.0	1310.0	1241.1	1034.2	1337.6
	Canola 8.85 kmh^{-1}	1379.0	2068.4	1896.1	1723.7	2068.4	1827.1
	Canola 12.87 kmh^{-1}	1379.0	1447.9	1379.0	1654.7	1723.7	1516.8
Asquith Summer Fallow Loamy Sand Field	Wheat 8.85 kmh^{-1}	1930.5	1447.9	2137.4	2068.4	2068.4	1930.5
	Wheat 12.87 kmh^{-1}	1585.8	1241.1	1447.9	1723.7	1930.5	1585.8
	Canola 8.85 kmh^{-1}	1447.9	1965.0	1861.6	1379.0	1723.7	1675.4
	Canola 12.87 kmh^{-1}	1861.6	1930.5	2068.4	1896.1	2068.4	1965.0
St-Denis Loam Field	Wheat 8.85 kmh^{-1}	1103.2	1379.0	1930.5	2068.4	1241.1	1544.4
	Wheat 12.87 kmh^{-1}	1379.0	2068.4	1585.8	2068.4	2068.4	1834.0
	Canola 8.85 kmh^{-1}	1172.1	758.4	1241.1	792.9	861.8	965.3
	Canola 12.87 kmh^{-1}	1379.0	1447.9	758.4	896.3	758.4	1048.0
St-Denis Silty Clay Field	Wheat 8.85 kmh^{-1}	1310.0	1447.9	1034.2	1103.2	1310.0	1241.1
	Wheat 12.87 kmh^{-1}	1516.8	758.4	1172.1	999.7	1034.2	1096.3
	Canola 8.85 kmh^{-1}	689.5	758.4	1034.2	930.8	965.3	875.6
	Canola 12.87 kmh^{-1}	1034.2	999.7	1447.9	1206.6	965.3	1130.7

Table A. 3. Stubble Thickness Data Table

Fields	No.1 (mm)	No.2 (mm)	No.3 (mm)	No.4 (mm)	No.5 (mm)	No.6 (mm)	No.7 (mm)	No.8 (mm)	No.9 (mm)	No.10 (mm)	Average (mm)
Lutheran Loamy Sand Field	3.8	8	6	6	5	4	5	9	6	7	5.98
Asquith Loamy Sand Field	6.6	9	10	9	8	8	8	12	10	12	9.26
Asquith Summer Fallow Loamy Sand Field	N.a.	N.a.	N.a.	N.a.	N.a.	N.a.	N.a.	N.a.	N.a.	N.a.	N.a.
St-Denis Loam Field	3	3	4	4	4	3	4	3	4	4	3.6
St-Denis Silty Clay Field	3	4	4	5	4	3	4	3	3	4	3.7

** N.a. = Not Available data*

Table A. 4. Stubble Height Data Table

Fields	No.1 (mm)	No.2 (mm)	No.3 (mm)	No.4 (mm)	No.5 (mm)	No.6 (mm)	No.7 (mm)	No.8 (mm)	No.9 (mm)	No.10 (mm)	Average (mm)
Lutheran Loamy Sand Field	391	221	236	356	254	310	287	272	249	305	288
Asquith Loamy Sand Field	254	373	259	361	348	325	351	351	343	368	333
Asquith Summer Fallow Loamy Sand Field	N.a.	N.a.	N.a.	N.a.	N.a.	N.a.	N.a.	N.a.	N.a.	N.a.	N.a.
St-Denis Loam Field	241	229	183	229	198	183	211	259	236	279	225
St-Denis Silty Clay Field	208	292	279	300	254	216	259	206	241	254	251

** N.a. = Not Available data*

Table A. 5. Field Ground Coverage Values Result Table

Fields	No.1 (%)	No.2 (%)	No.3 (%)	No.4 (%)	No.5 (%)	No.6 (%)	No.7 (%)	No.8 (%)	No.9 (%)	No.10 (%)	Average (%)
Lutheran Loamy Sand Field	55	60	40	65	35	20	60	25	45	65	47.0
Asquith Loamy Sand Field	40	50	75	30	20	70	65	50	40	35	47.5
Asquith Summer Fallow Loamy Sand Field	30	35	55	45	25	35	70	65	40	20	42.0
St-Denis Loam Field	30	30	55	25	25	30	55	60	45	50	40.5
St-Denis Silty Clay Field	35	25	40	70	50	55	70	45	55	50	49.5

Table A. 6. Soil Moisture Data Table

Fields	Plots	Mms (g)	Ms (g)	Mw(g)	w (%)
Lutheran Loamy Sand Field	Wheat 8.85 kmh^{-1}	344.8	293.7	51.1	17.4
	Wheat 12.87 kmh^{-1}	433.3	384.1	49.2	12.8
	Canola 8.85 kmh^{-1}	419.7	363.3	56.2	15.5
	Canola 12.87 kmh^{-1}	366.6	338.2	28.4	8.4
Asquith Loamy Sand Field	Wheat 8.85 kmh^{-1}	304.2	267.2	37	13.8
	Wheat 12.87 kmh^{-1}	343.1	303.7	39.4	13.0
	Canola 8.85 kmh^{-1}	437.4	394.6	42.8	10.8
	Canola 12.87 kmh^{-1}	370.0	316.6	53.4	16.9
Asquith Summer Fallow Loamy Sand Field	Wheat 8.85 kmh^{-1}	294.6	261.8	32.8	12.5
	Wheat 12.87 kmh^{-1}	433.9	362.8	71.1	19.6
	Canola 8.85 kmh^{-1}	288.4	235.3	53.1	22.6
	Canola 12.87 kmh^{-1}	287.3	245.3	42.0	17.1
St-Denis Loam Field	Wheat 8.85 kmh^{-1}	350.2	270.0	80.2	29.7
	Wheat 12.87 kmh^{-1}	378.9	342.0	36.9	10.8
	Canola 8.85 kmh^{-1}	278.7	212.1	66.6	31.4
	Canola 12.87 kmh^{-1}	369.9	308.2	61.7	20.0
St-Denis Silty Clay Field	Wheat 8.85 kmh^{-1}	277.0	217.9	59.1	27.1
	Wheat 12.87 kmh^{-1}	361.4	290.2	71.2	24.5
	Canola 8.85 kmh^{-1}	322.9	264.5	58.4	22.1
	Canola 12.87 kmh^{-1}	295.4	241.3	54.1	22.4

Table A. 7. ALS Environmental Soil Analysis Result Sheet

Sample Details/Parameters	Result	Qualifier*	D.L.	Units	Extracted	Analyzed	Batch
L1462798-1 1421909 0-6"							
Sampled By: CLIENT on 16-MAY-14							
Matrix: SOIL							
Particle Size Analysis:Mini-Pipet Method							
% Sand (2.0mm - 0.05mm)	80.6		0.10	%	02-JUN-14	03-JUN-14	R2851554
% Silt (0.05mm - 2um)	13.4		0.10	%	02-JUN-14	03-JUN-14	R2851554
% Clay (<2um)	5.92		0.10	%	02-JUN-14	03-JUN-14	R2851554
Texture	Loamy sand				02-JUN-14	03-JUN-14	R2851554
L1462798-2 1421910 0-6"							
Sampled By: CLIENT on 16-MAY-14							
Matrix: SOIL							
Particle Size Analysis:Mini-Pipet Method							
% Sand (2.0mm - 0.05mm)	82.5		0.10	%	02-JUN-14	03-JUN-14	R2851554
% Silt (0.05mm - 2um)	13.0		0.10	%	02-JUN-14	03-JUN-14	R2851554
% Clay (<2um)	4.53		0.10	%	02-JUN-14	03-JUN-14	R2851554
Texture	Loamy sand				02-JUN-14	03-JUN-14	R2851554
L1462798-3 1421911 0-6"							
Sampled By: CLIENT on 16-MAY-14							
Matrix: SOIL							
Particle Size Analysis:Mini-Pipet Method							
% Sand (2.0mm - 0.05mm)	82.0		0.10	%	02-JUN-14	03-JUN-14	R2851554
% Silt (0.05mm - 2um)	12.8		0.10	%	02-JUN-14	03-JUN-14	R2851554
% Clay (<2um)	5.24		0.10	%	02-JUN-14	03-JUN-14	R2851554
Texture	Loamy sand				02-JUN-14	03-JUN-14	R2851554
L1462798-4 1421912 0-6"							
Sampled By: CLIENT on 20-MAY-14							
Matrix: SOIL							
Particle Size Analysis:Mini-Pipet Method							
% Sand (2.0mm - 0.05mm)	38.5		0.10	%	02-JUN-14	03-JUN-14	R2851554
% Silt (0.05mm - 2um)	40.7		0.10	%	02-JUN-14	03-JUN-14	R2851554
% Clay (<2um)	20.8		0.10	%	02-JUN-14	03-JUN-14	R2851554
Texture	Loam				02-JUN-14	03-JUN-14	R2851554
L1462798-5 1421837 0-6"							
Sampled By: CLIENT on 20-MAY-14							
Matrix: SOIL							
Particle Size Analysis:Mini-Pipet Method							
% Sand (2.0mm - 0.05mm)	16.2		0.10	%	02-JUN-14	03-JUN-14	R2851554
% Silt (0.05mm - 2um)	41.5		0.10	%	02-JUN-14	03-JUN-14	R2851554
% Clay (<2um)	42.3		0.10	%	02-JUN-14	03-JUN-14	R2851554
Texture	Silty clay				02-JUN-14	03-JUN-14	R2851554

* Refer to Referenced Information for Qualifiers (if any) and Methodology.

APPENDIX B

Seed-to-Fertilizer Statistical Results Direct Measurements

Legend	
	8.85 kmh^{-1} (5.5 mph) Wheat
	12.87 kmh^{-1} (8.0 mph) Wheat
	8.85 kmh^{-1} (5.5 mph) Canola
	12.87 kmh^{-1} (8.0 mph) Canola

Lutheran Loamy Sand Field 8.85 kmh^{-1} (5.5 mph) Wheat

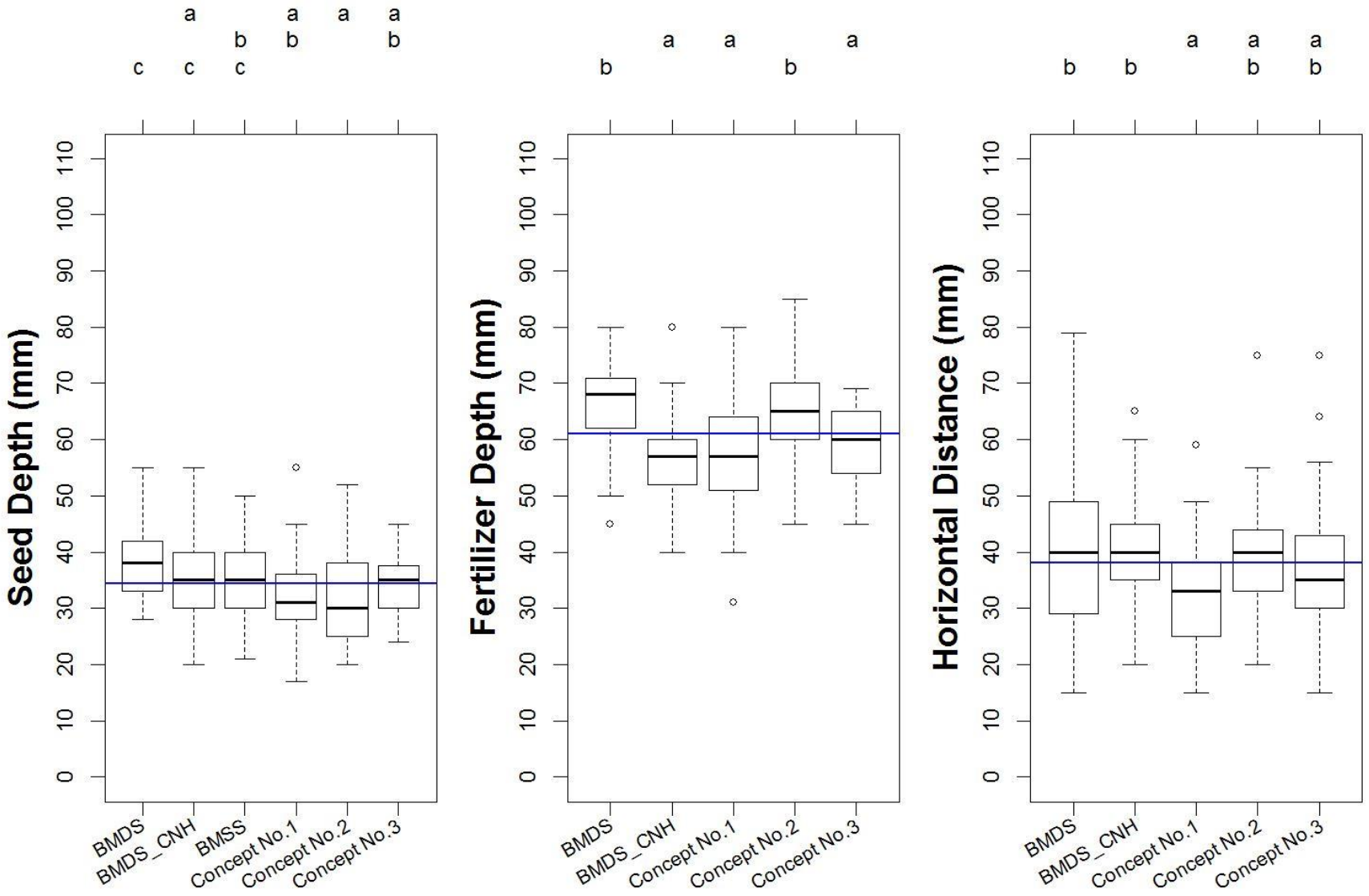

Figure B. 1. Lutheran Loamy Sand Field 8.85 kmh^{-1} Wheat, Seed to Fertilizer Separation Experiment

Lutheran Loamy Sand Field 12.87 kmh^{-1} (8.0 mph) Wheat

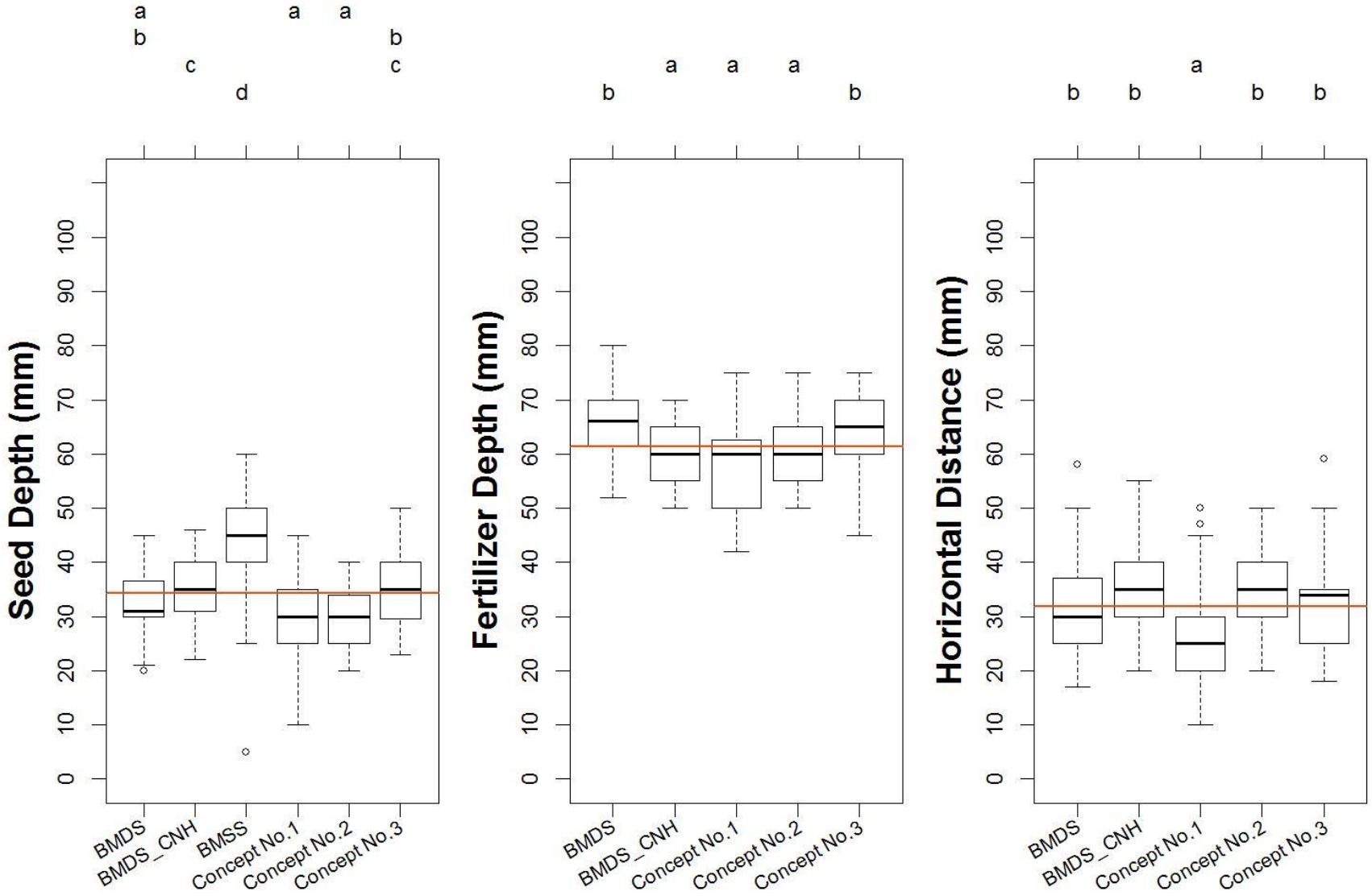

Figure B. 2. Lutheran Loamy Sand Field 12.87 kmh^{-1} Wheat, Seed to Fertilizer Separation Experiment

Lutheran Loamy Sand Field 8.85 kmh^{-1} (5.5 mph) Canola

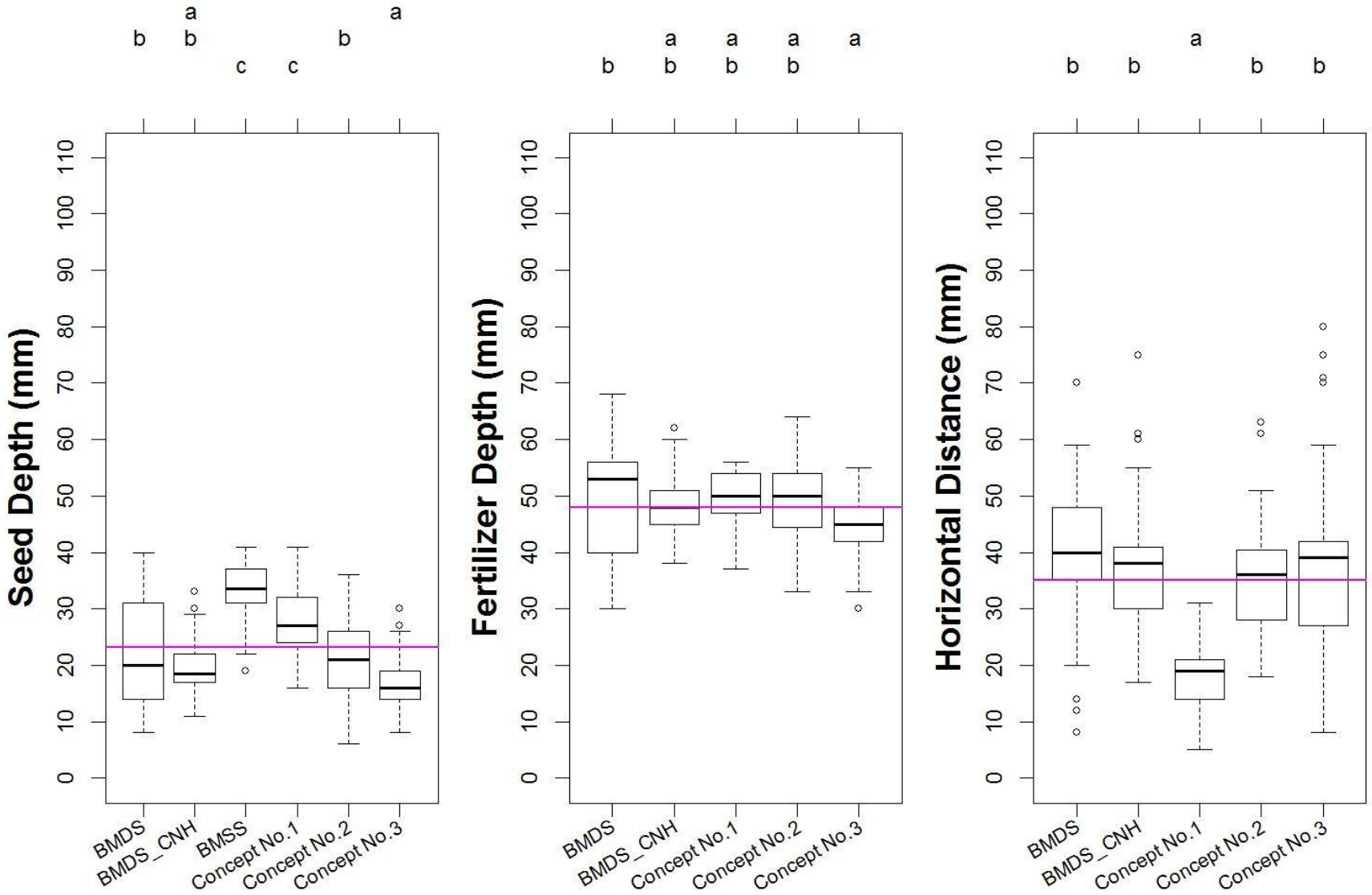

Figure B. 3. Lutheran Loamy Sand Field 8.85 kmh^{-1} Canola, Seed to Fertilizer Separation Experiment

Lutheran Loamy Sand Field 12.87 kmh^{-1} (8.0 mph) Canola

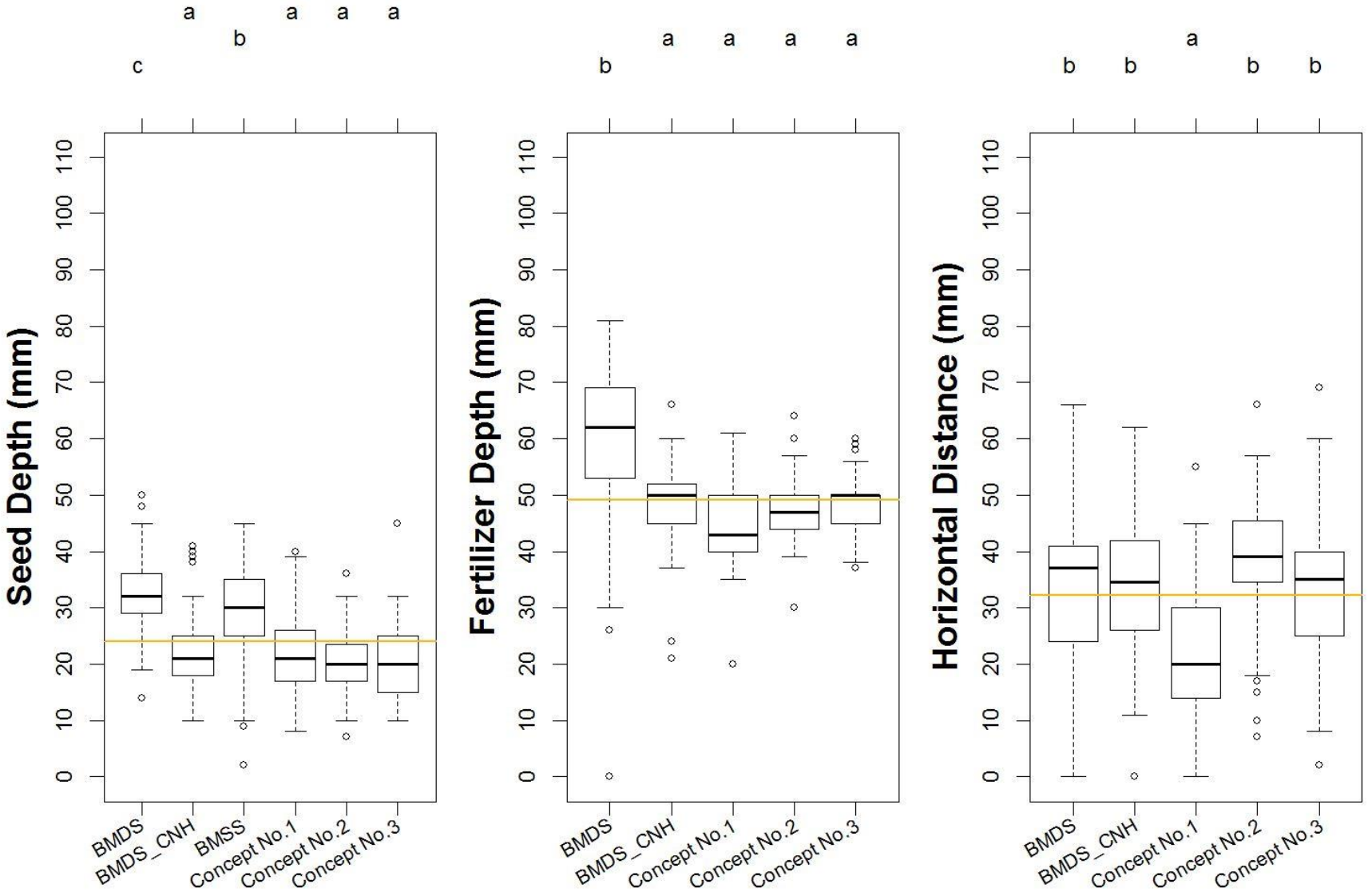

Figure B. 4. Lutheran Loamy Sand Field 12.87 kmh^{-1} Canola, Seed to Fertilizer Separation Experiment

Asquith Loamy Sand Field 8.85 kmh^{-1} (5.5 mph) Wheat

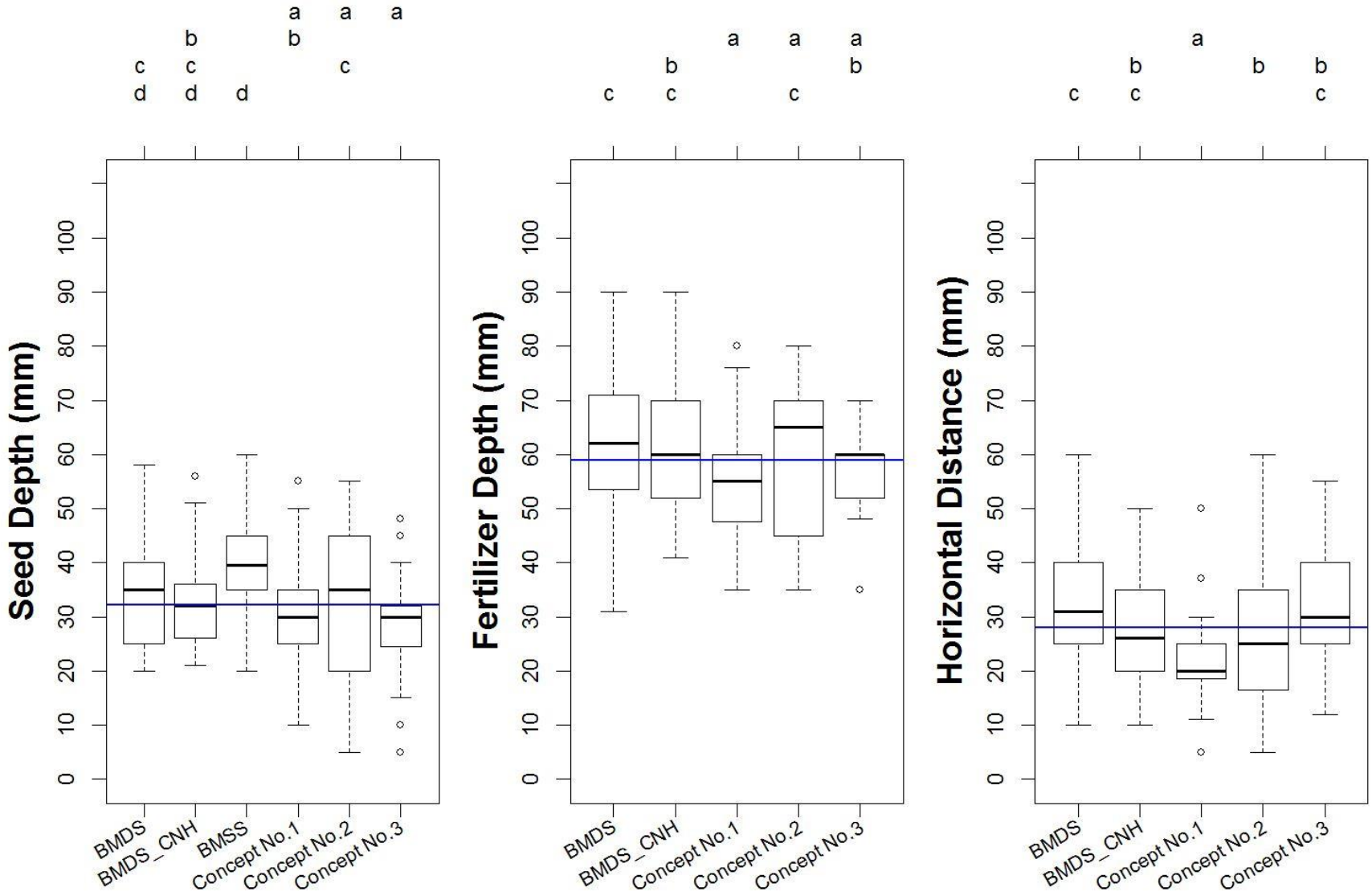

Figure B. 5. Asquith Loamy Sand Field 8.85 kmh^{-1} Wheat, Seed to Fertilizer Separation Experiment

Asquith Loamy Sand Field 12.87 kmh^{-1} (8.0 mph) Wheat

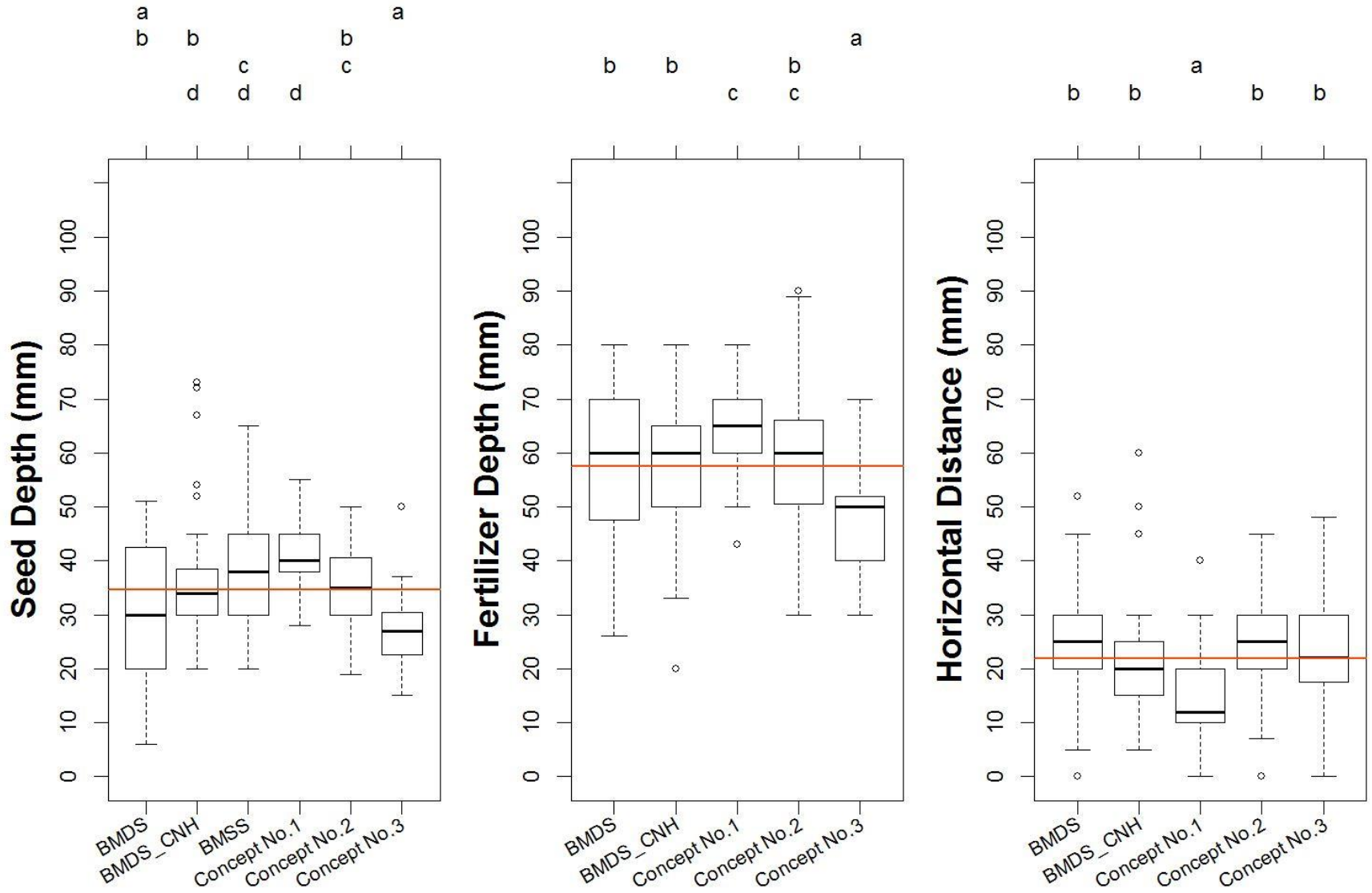

Figure B. 6. Asquith Loamy Sand Field 12.87 kmh^{-1} Wheat, Seed to Fertilizer Separation Experiment

Asquith Loamy Sand Field 8.85 kmh^{-1} (5.5 mph) Canola

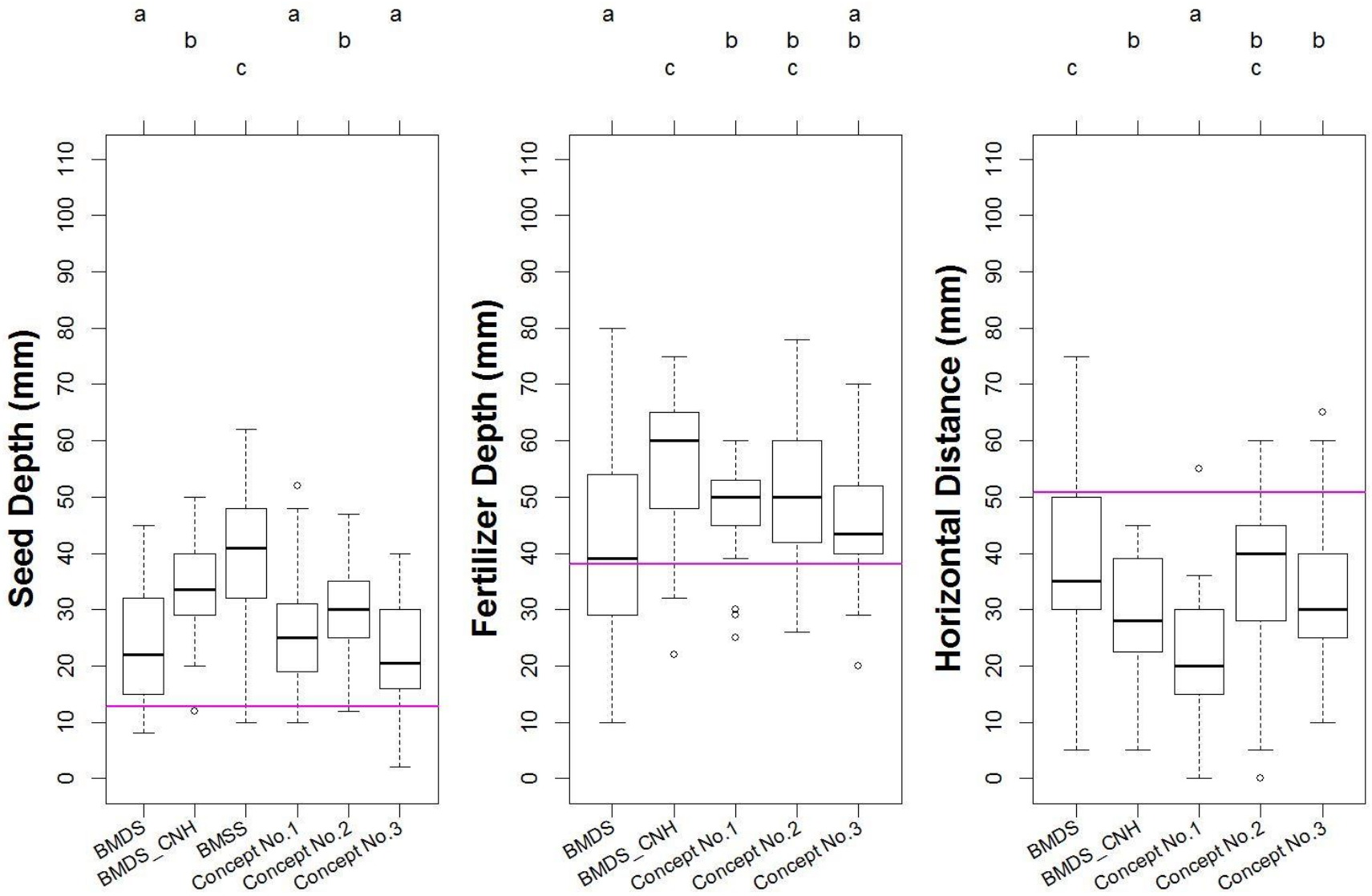

Figure B. 7. Asquith Loamy Sand Field 8.85 kmh^{-1} Canola, Seed to Fertilizer Separation Experiment

Asquith Loamy Sand Field 12.87 kmh^{-1} (8.0 mph) Canola

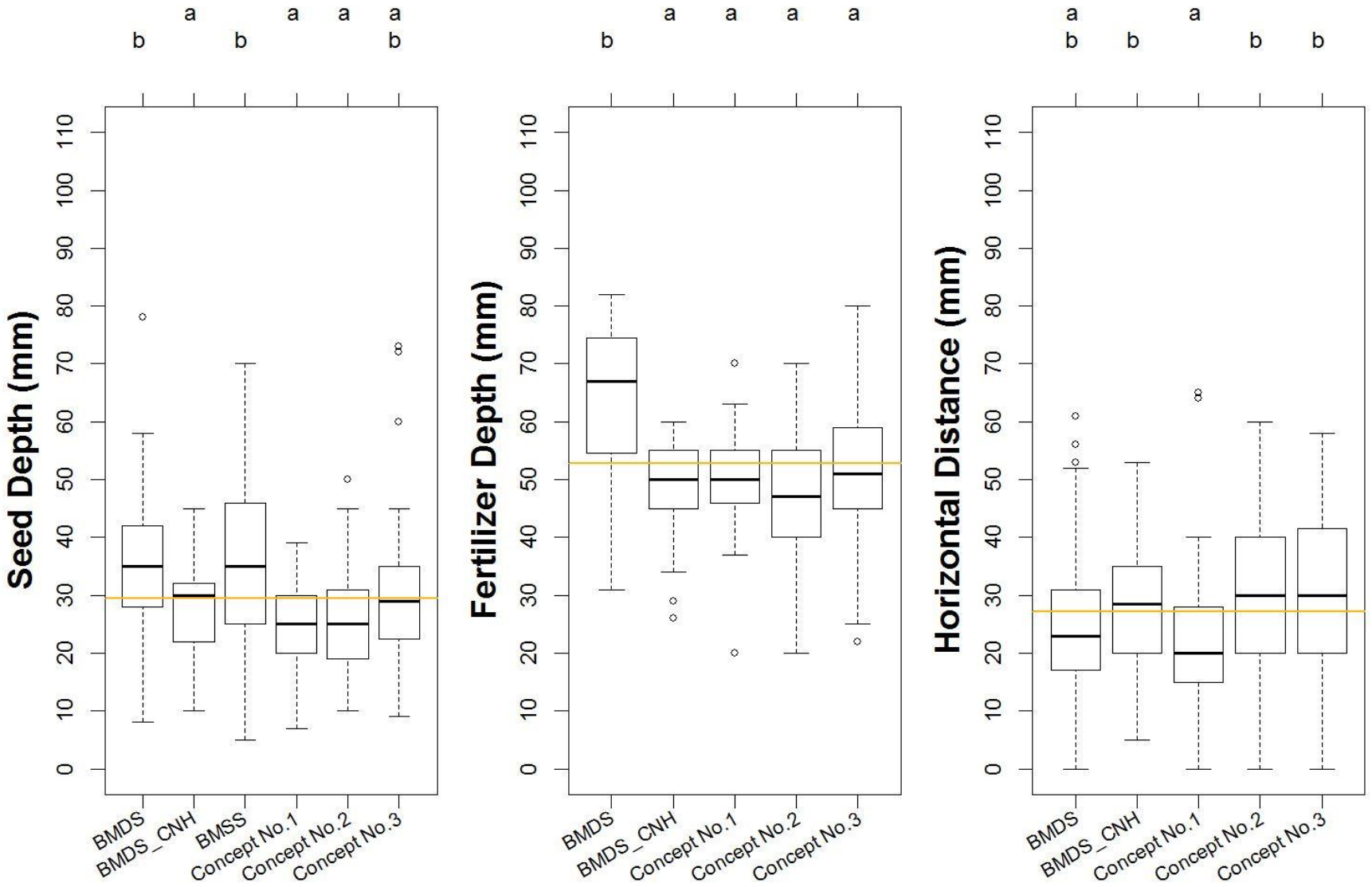

Figure B. 8. Asquith Loamy Sand Field 12.87 kmh^{-1} Canola, Seed to Fertilizer Separation Experiment

Asquith Summer Fallow Loamy Sand Field 8.85 kmh^{-1} (5.5 mph) Wheat

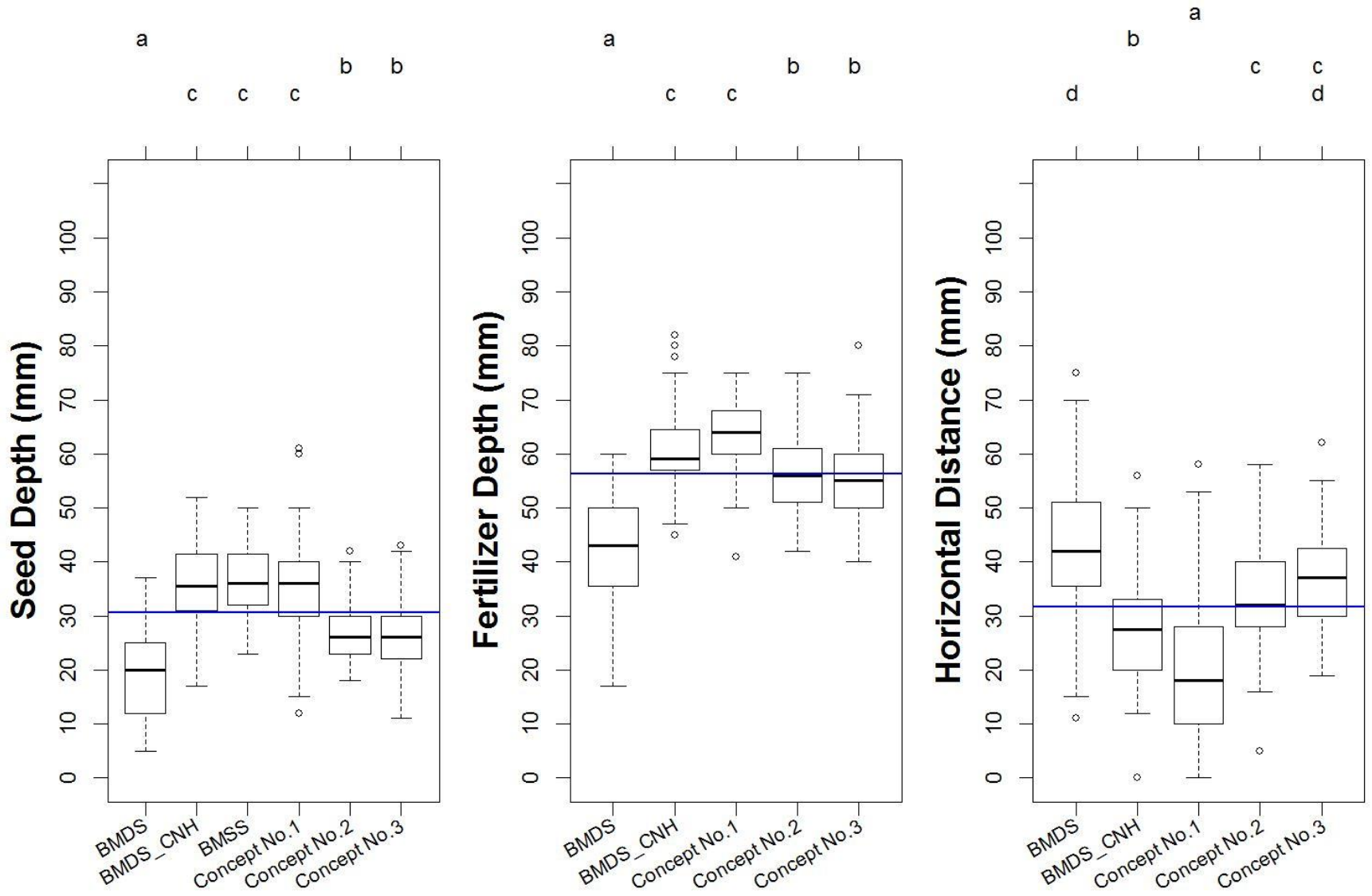

Figure B. 9. Asquith Summer Fallow Loamy Sand Field 8.85 kmh^{-1} Wheat, Seed to Fertilizer Separation Experiment

Asquith Summer Fallow Loamy Sand Field 12.87 kmh^{-1} (8.0 mph) Wheat

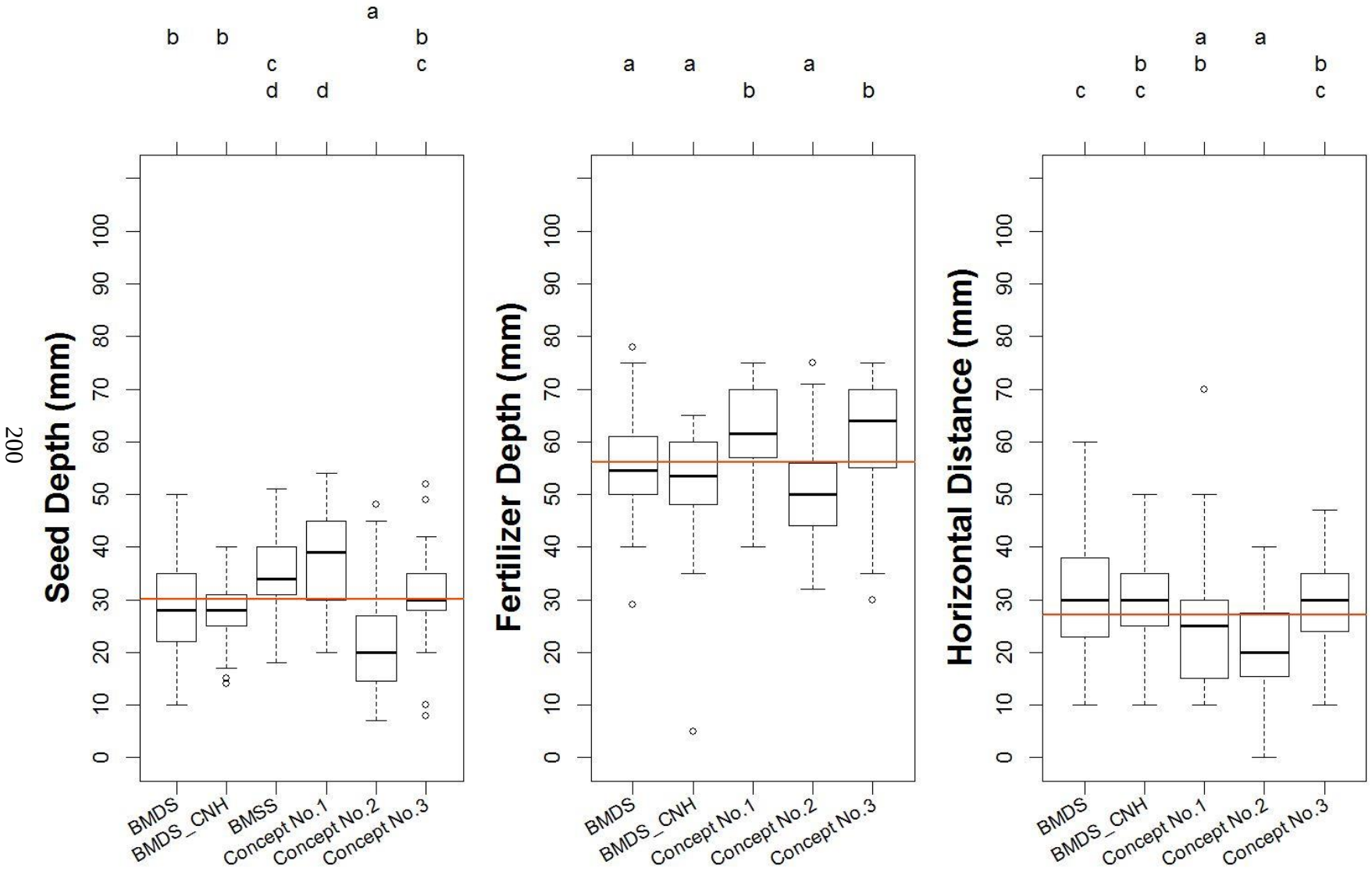

Figure B. 10. Asquith Summer Fallow Loamy Sand Field 12.87 kmh^{-1} Wheat, Seed to Fertilizer Separation Experiment

Asquith Summer Fallow Loamy Sand Field 8.85 kmh^{-1} (5.5 mph) Canola

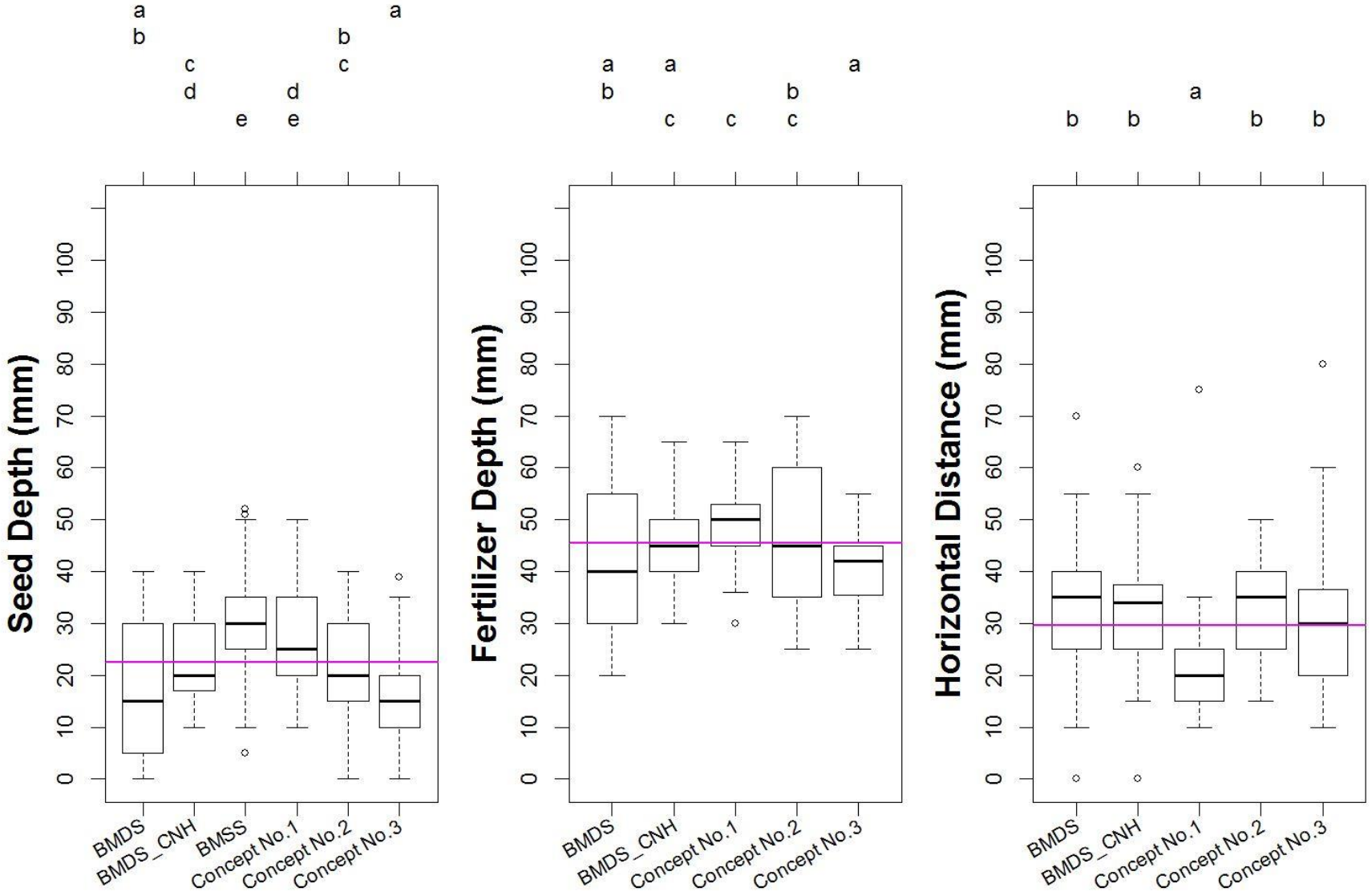

Figure B. 11. Asquith Summer Fallow Loamy Sand Field 8.85 kmh^{-1} Canola, Seed to Fertilizer Separation Experiment

Asquith Summer Fallow Loamy Sand Field 12.87 kmh^{-1} (8.0 mph) Canola

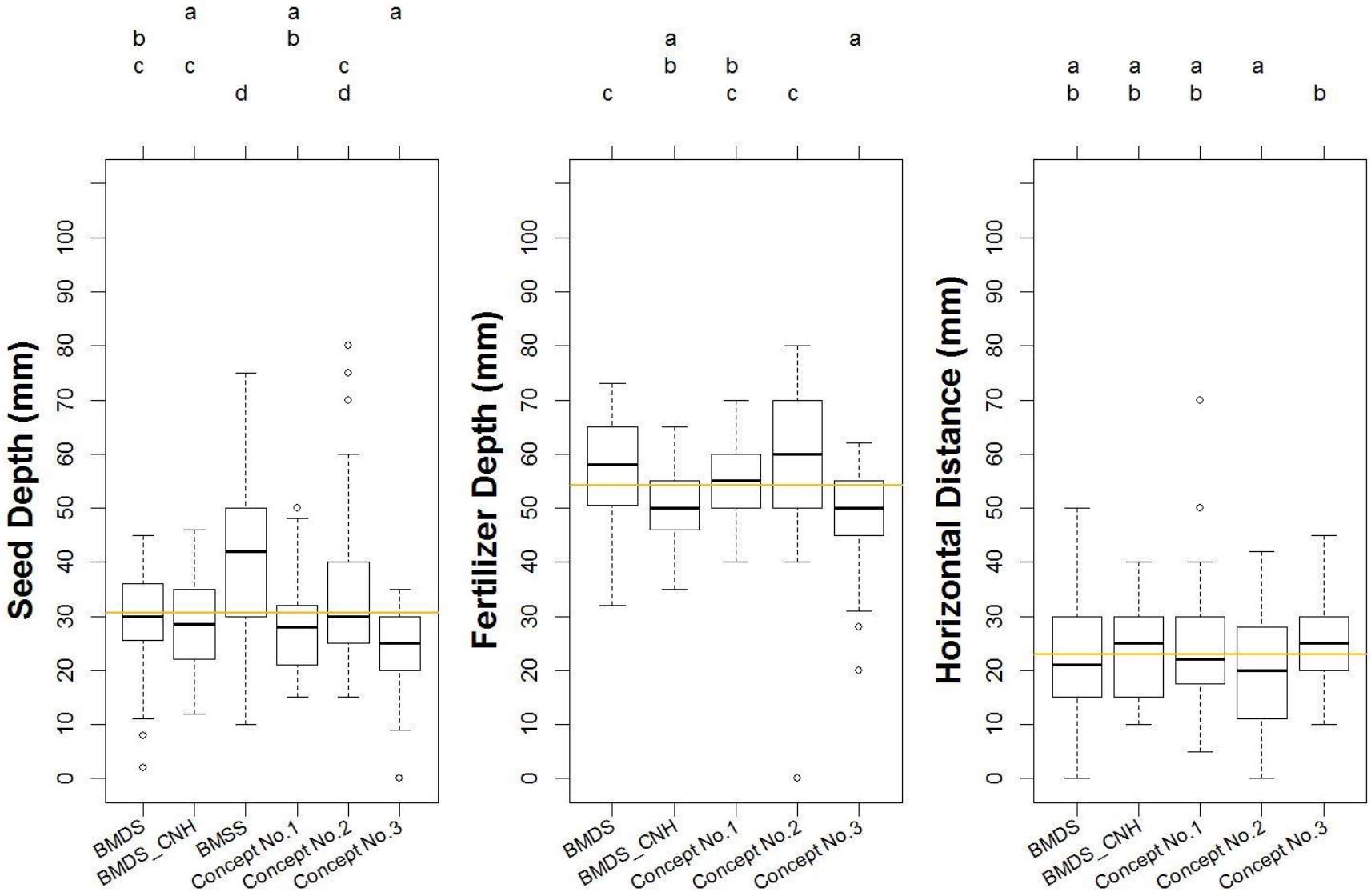

Figure B. 12. Asquith Summer Fallow Loamy Sand Field 12.87 kmh^{-1} Canola, Seed to Fertilizer Separation Experiment

Saint-Denis Loam Field 8.85 kmh^{-1} (5.5 mph) Wheat

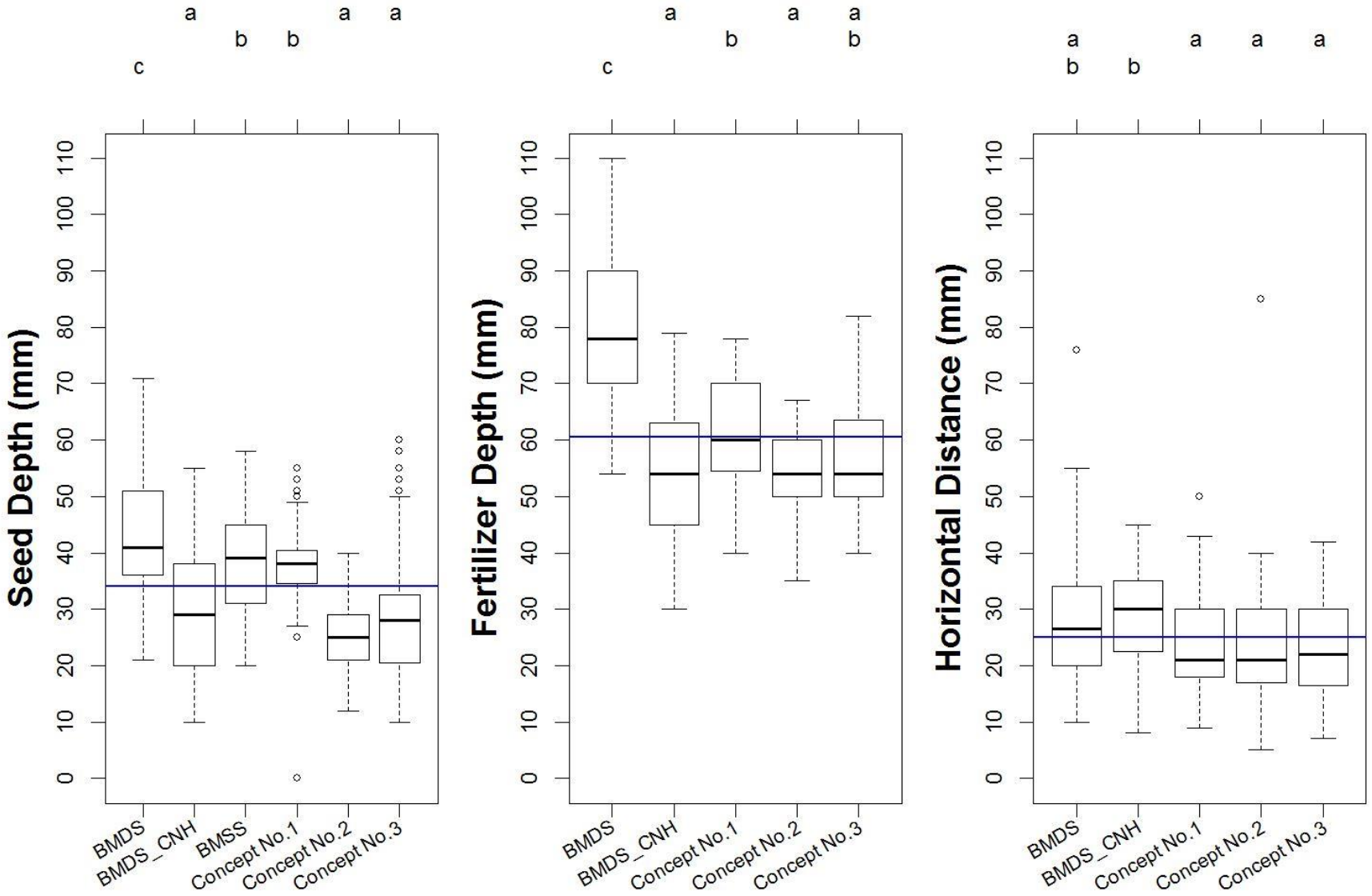

Figure B. 13. Saint-Denis Loam Field 8.85 kmh^{-1} Wheat, Seed to Fertilizer Separation Experiment

Saint-Denis Loam Field 12.87 kmh^{-1} (8.0 mph) Wheat

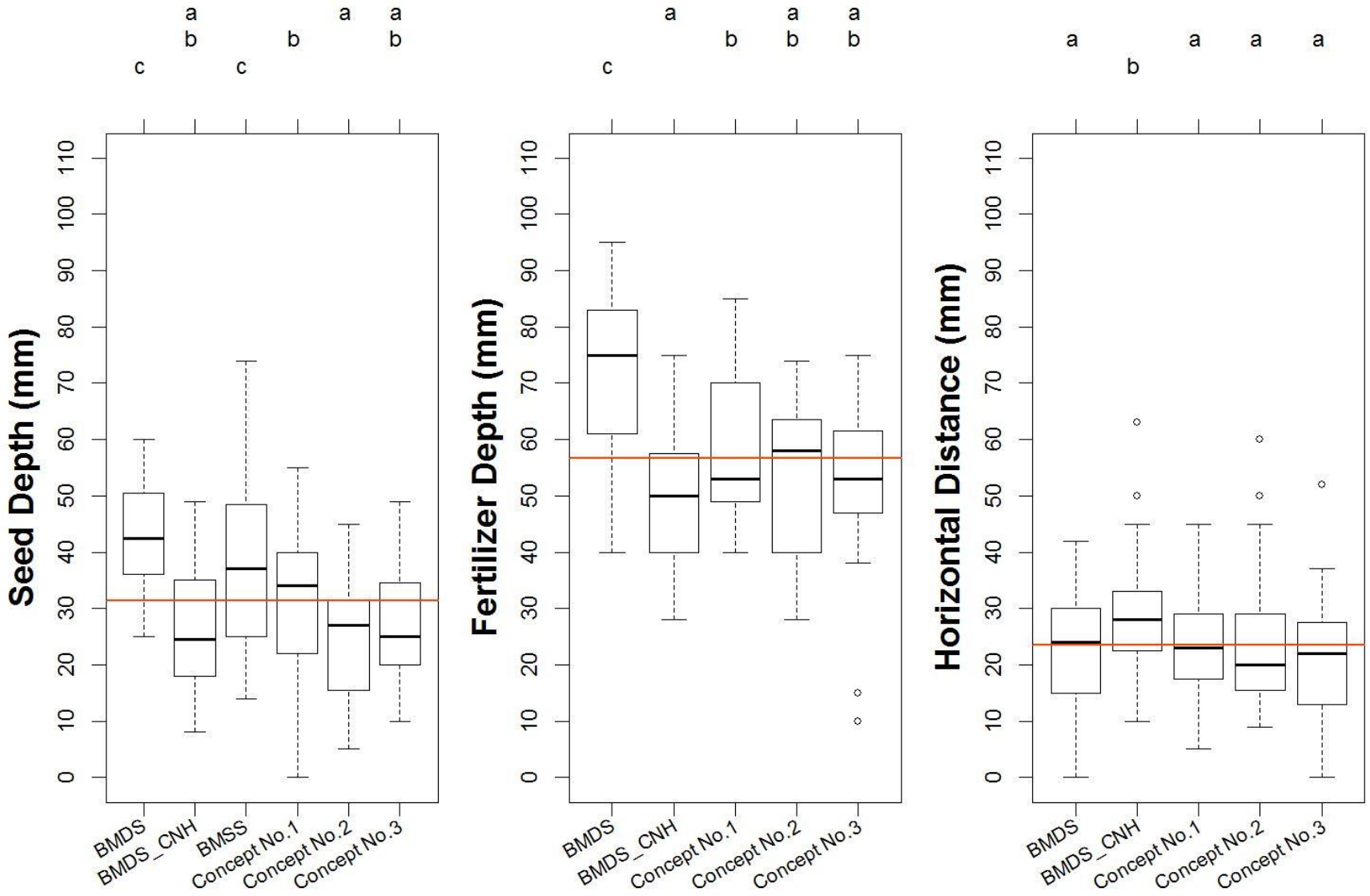

Figure B. 14. Saint-Denis Loam Field 12.87 kmh^{-1} Wheat, Seed to Fertilizer Separation Experiment

Saint-Denis Loam Field 8.85 kmh^{-1} (5.5 mph) Canola

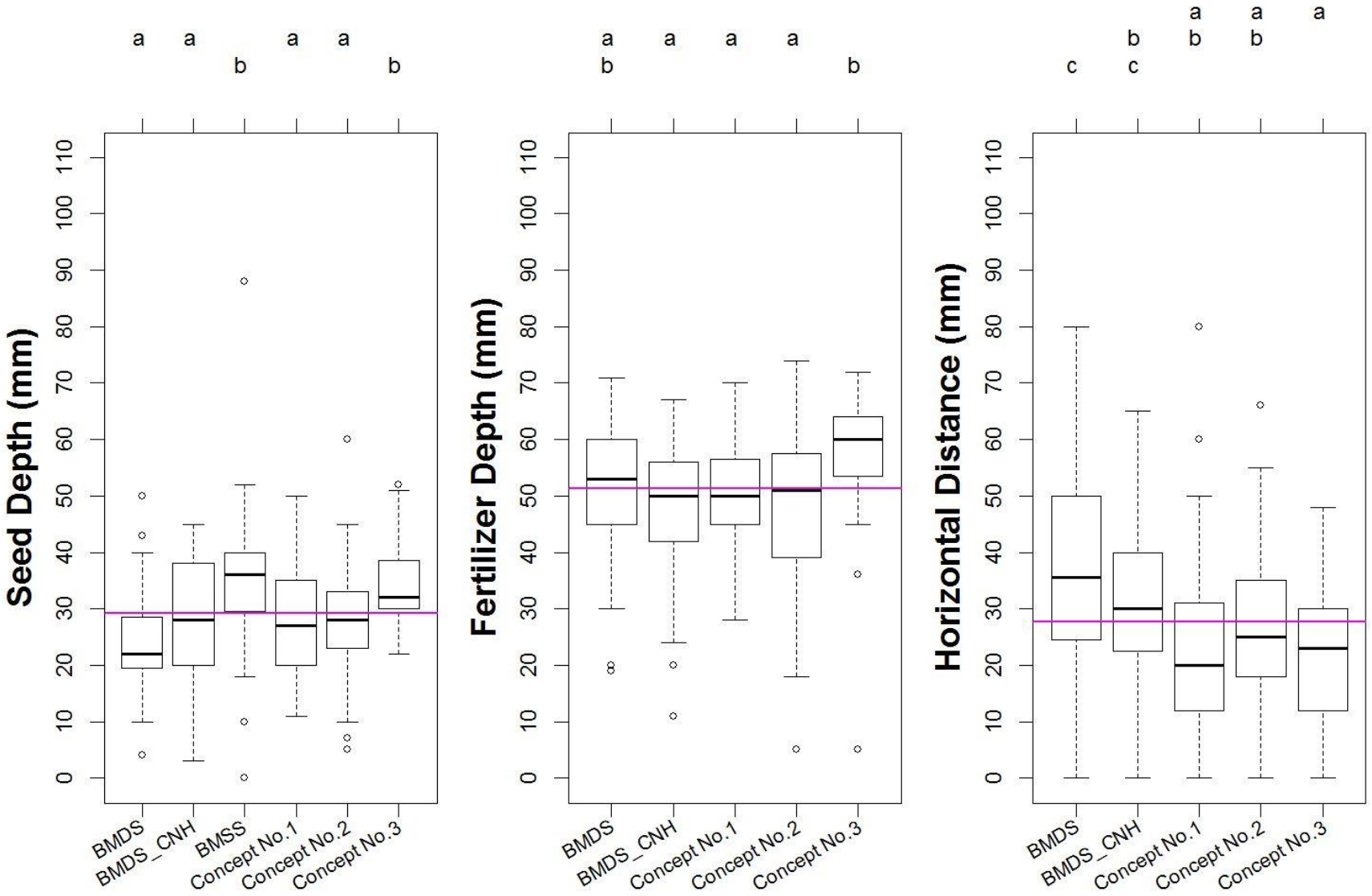

Figure B. 15. Saint-Denis Loam Field 8.85 kmh^{-1} Canola, Seed to Fertilizer Separation Experiment

Saint-Denis Loam Field 12.87 kmh^{-1} (8.0 mph) Canola

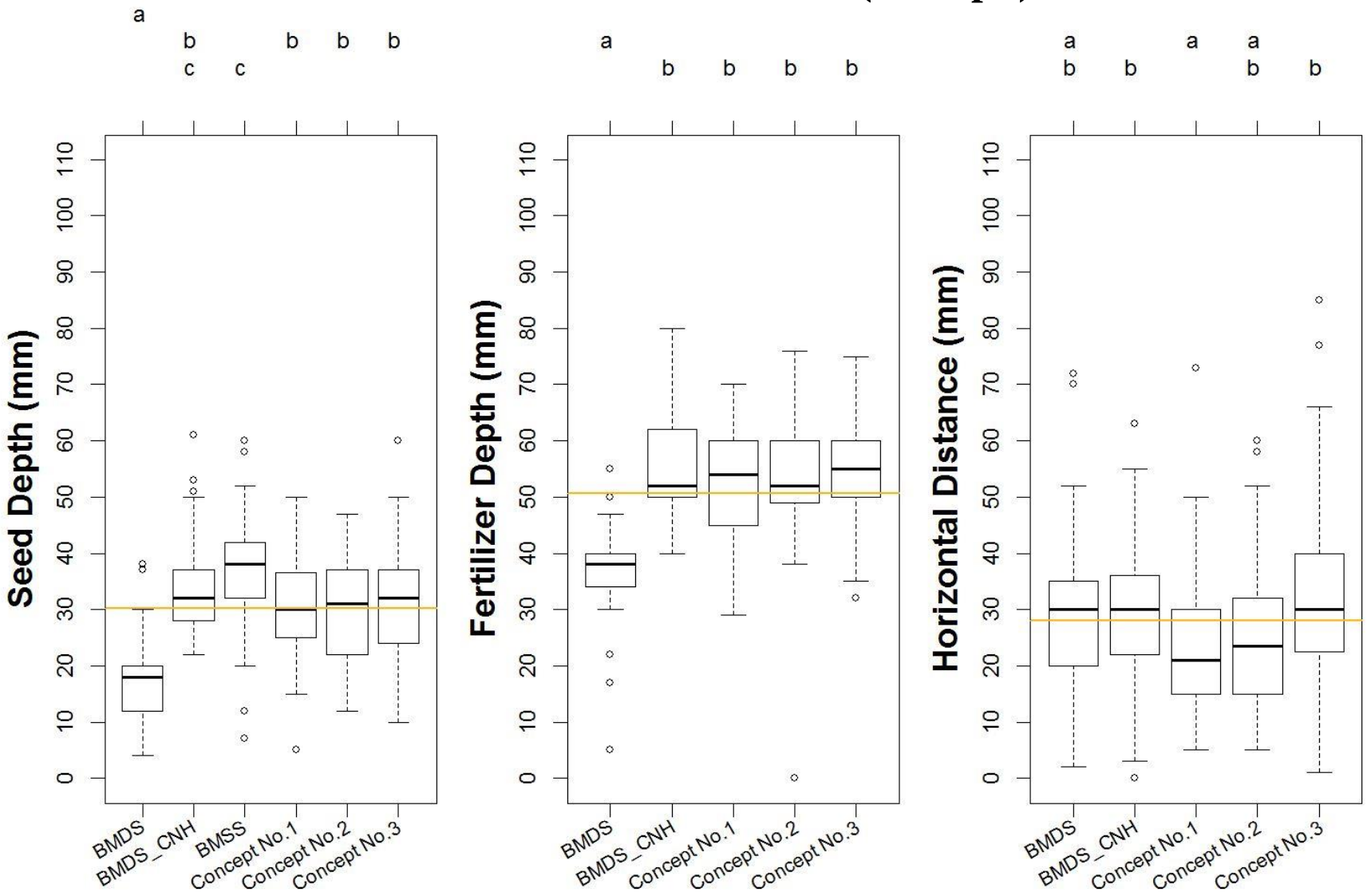

Figure B. 16. Saint-Denis Loam Field 12.87 kmh^{-1} Canola, Seed to Fertilizer Separation Experiment

Saint-Denis Silty Clay Field 8.85 kmh^{-1} (5.5 mph) Wheat

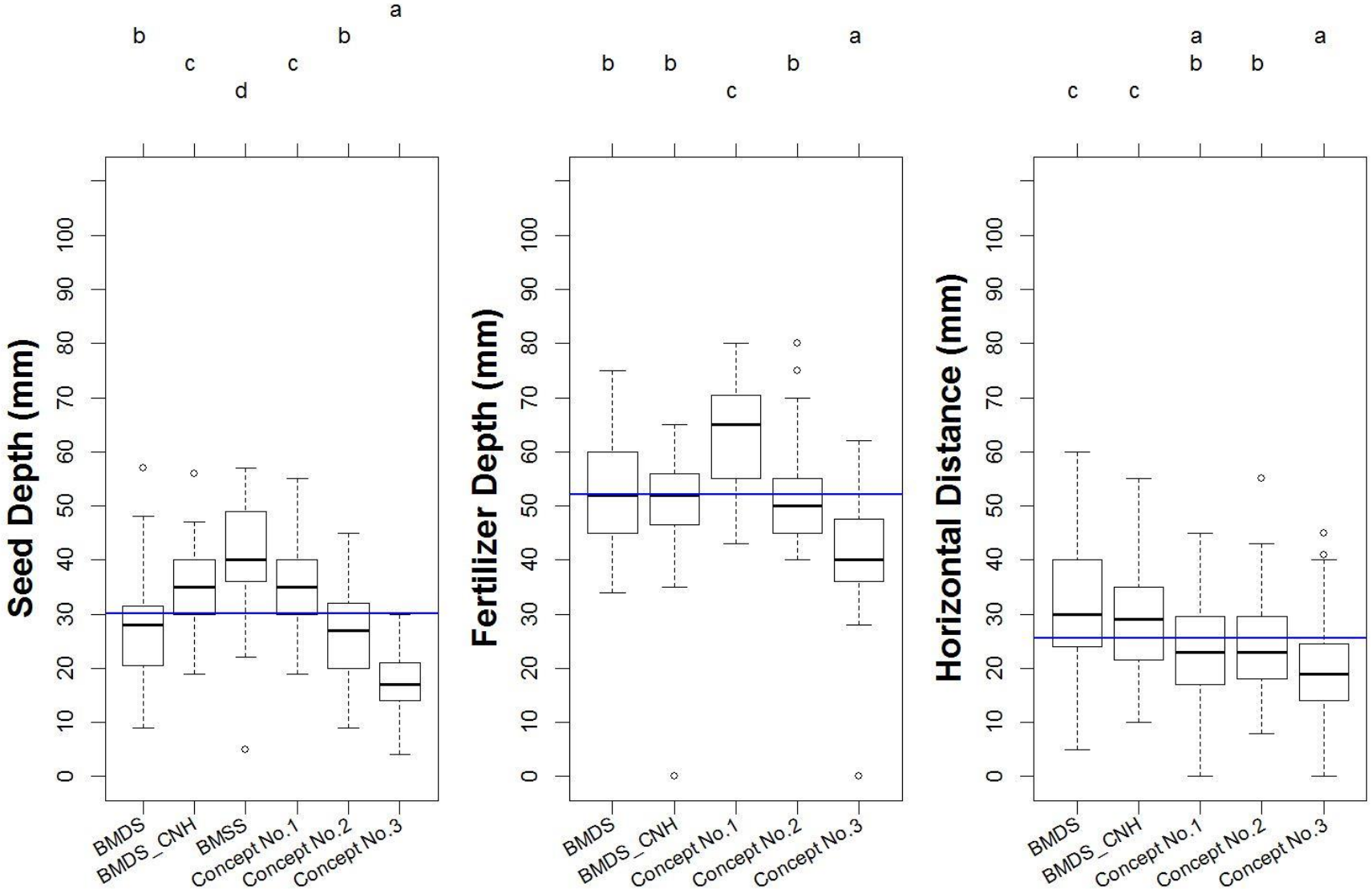

Figure B. 17. Saint-Denis Silty Clay Field 8.85 kmh^{-1} Wheat, Seed to Fertilizer Separation Experiment

Saint-Denis Silty Clay Field 12.87 kmh^{-1} (8.0 mph) Wheat

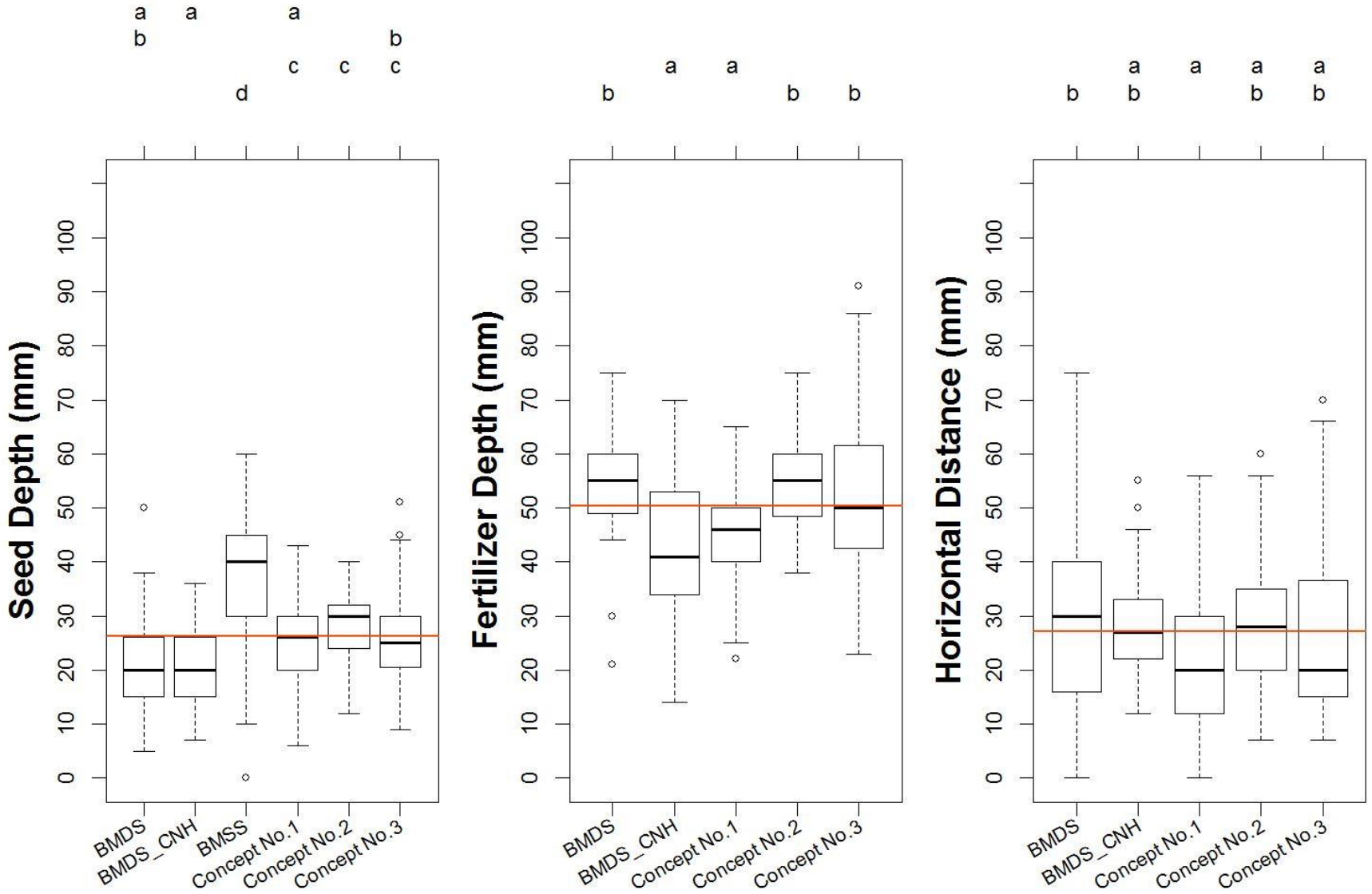

Figure B. 18. Saint-Denis Silty Clay Field 12.87 kmh^{-1} Wheat, Seed to Fertilizer Separation Experiment

Saint-Denis Silty Clay Field 8.85 kmh^{-1} (5.5 mph) Canola

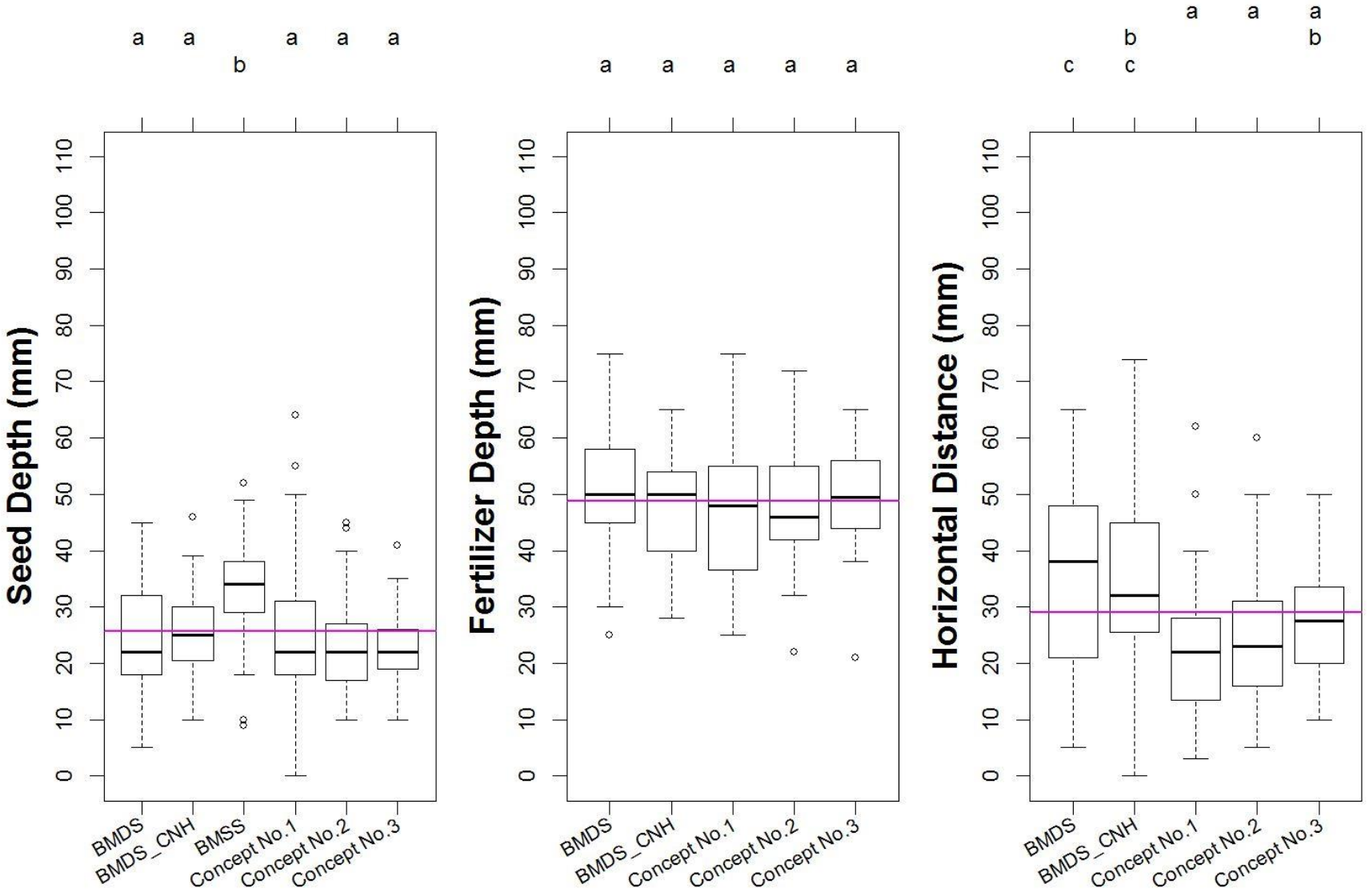

Figure B. 19. Saint-Denis Silty Clay Field 8.85 kmh^{-1} Canola, Seed to Fertilizer Separation Experiment

Saint-Denis Silty Clay Field 12.87 kmh^{-1} (8.0 mph) Canola

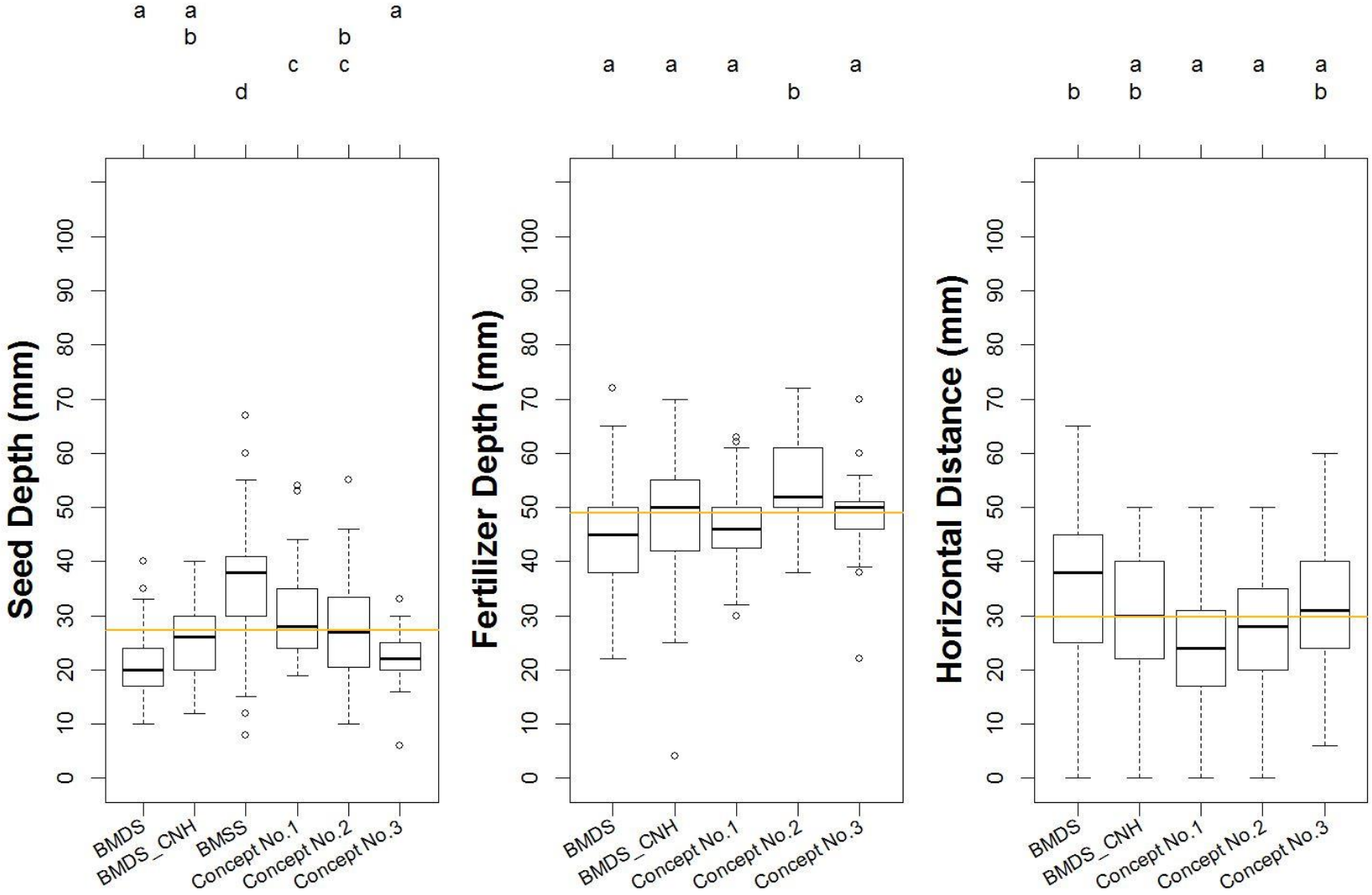

Figure B. 20. Saint-Denis Silty Clay Field 12.87 kmh^{-1} Canola, Seed to Fertilizer Separation Experiment

APPENDIX C

Seed-to-Fertilizer Separation Statistical Results Offset Distances

Legend	
	8.85 kmh^{-1} (5.5 mph) Wheat
	12.87 kmh^{-1} (8.0 mph) Wheat
	8.85 kmh^{-1} (5.5 mph) Canola
	12.87 kmh^{-1} (8.0 mph) Canola

Lutheran Loamy Sand Field 8.85 kmh^{-1} (5.5 mph) Wheat

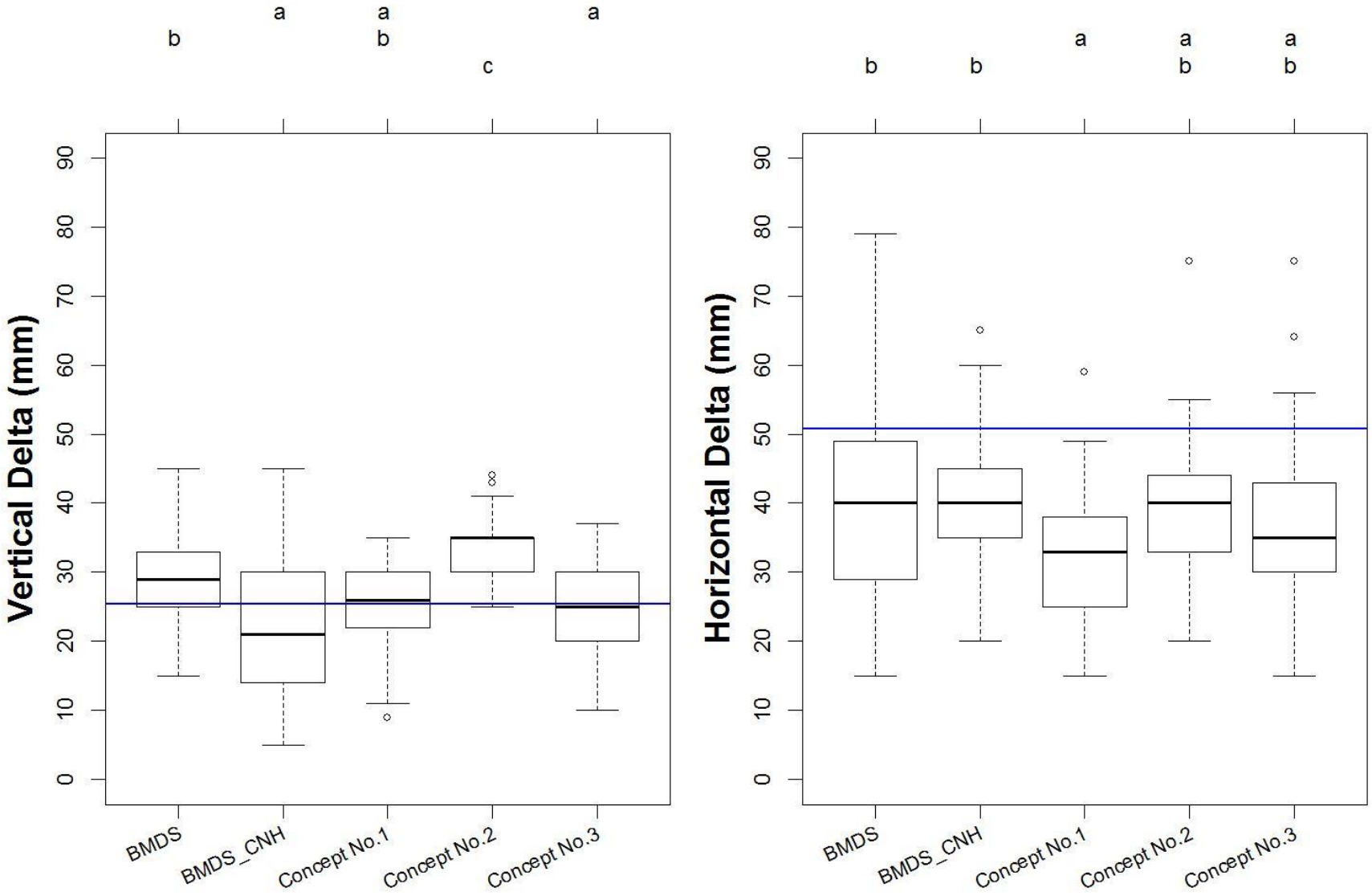

Figure C. 1. Lutheran Loamy Sand Field 8.85 kmh^{-1} Wheat, Delta Measurements

Lutheran Loamy Sand Field 12.87 kmh^{-1} (8.0 mph) Wheat

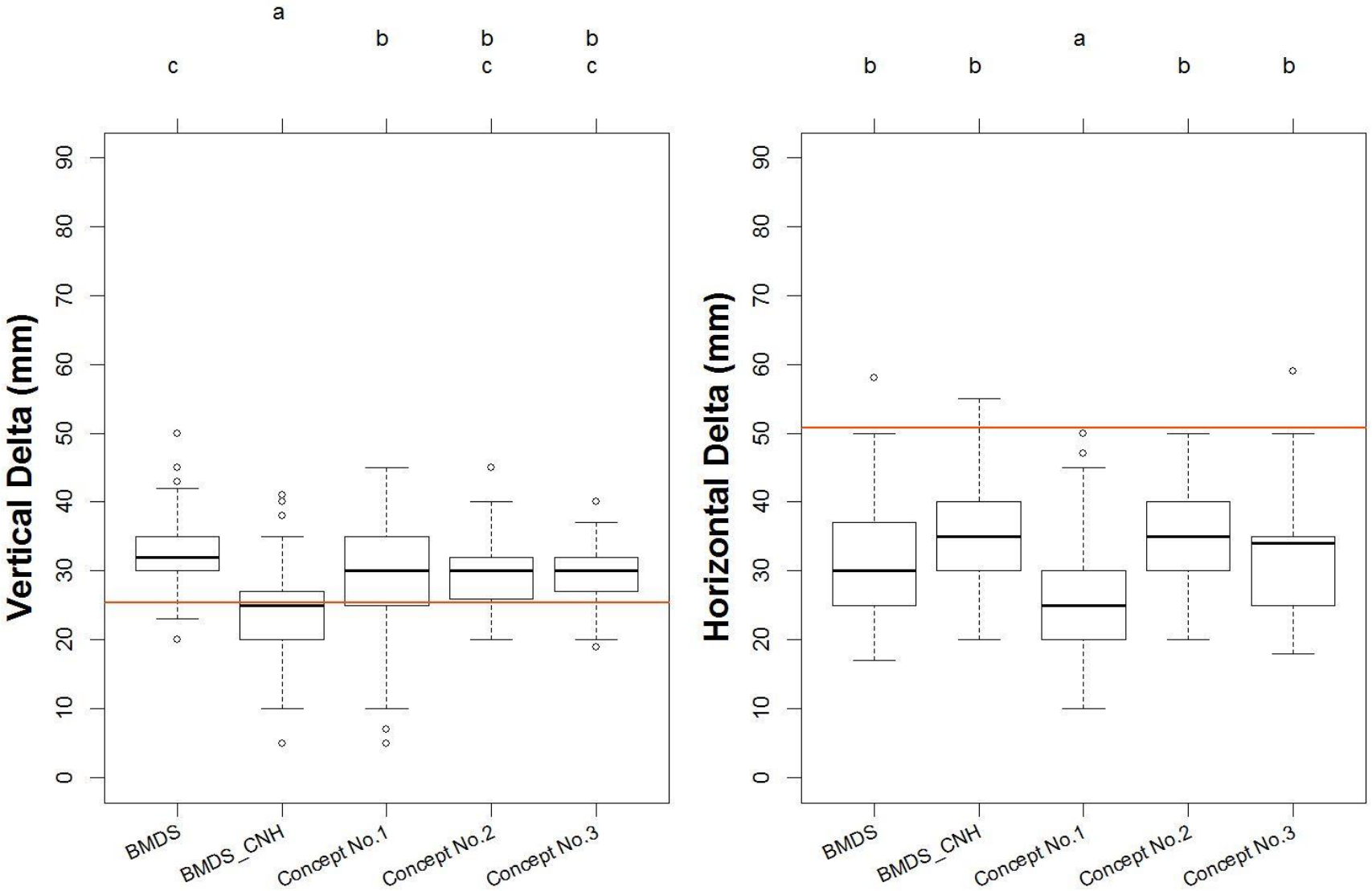

Figure C. 2. Lutheran Loamy Sand Field 12.87 kmh^{-1} Wheat, Delta Measurements

Lutheran Loamy Sand Field 8.85 kmh^{-1} (5.5 mph) Canola

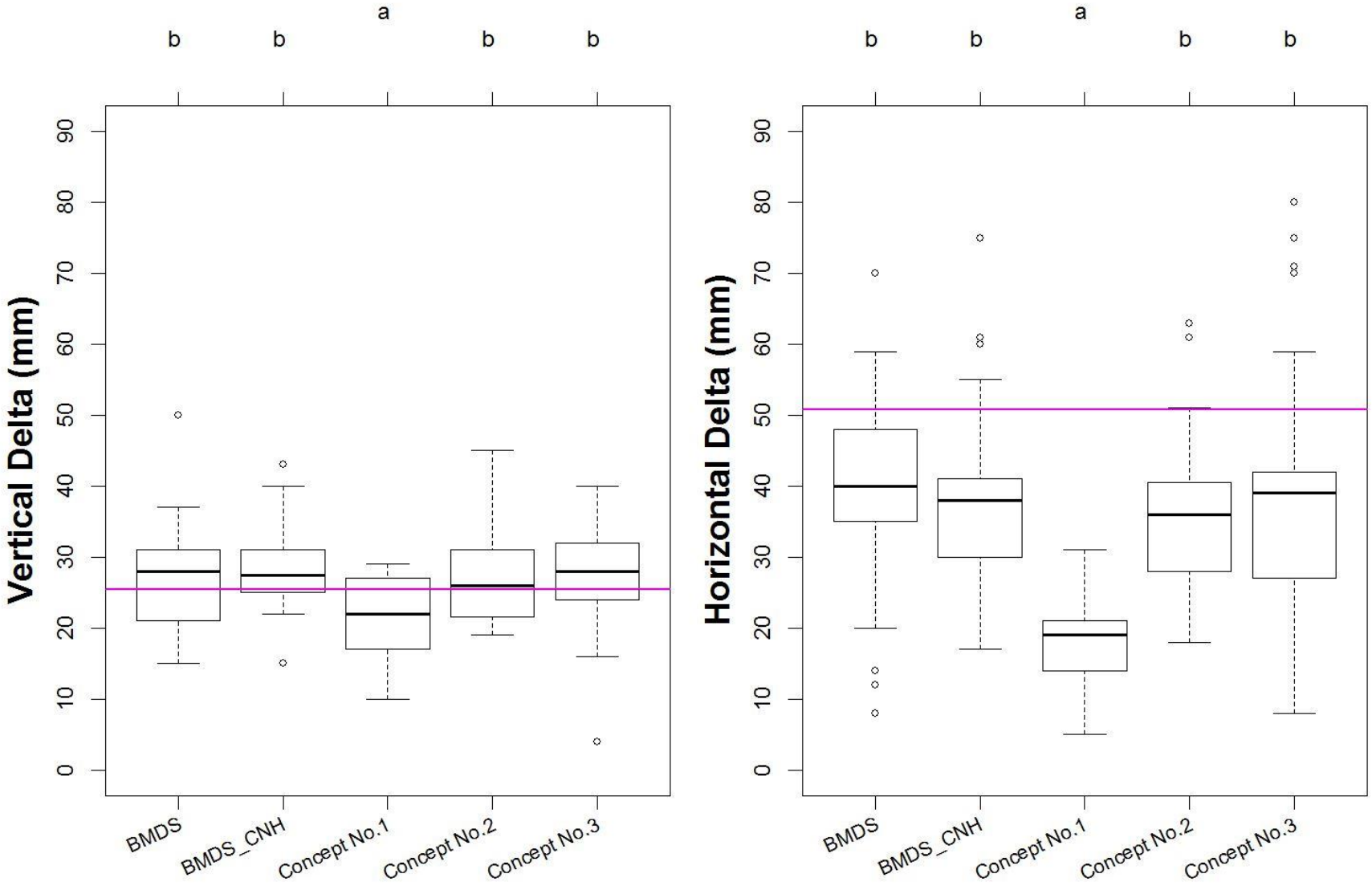

Figure C. 3. Lutheran Loamy Sand Field 8.85 kmh^{-1} Canola, Delta Measurements

Lutheran Loamy Sand Field 12.87 kmh^{-1} (8.0 mph) Canola

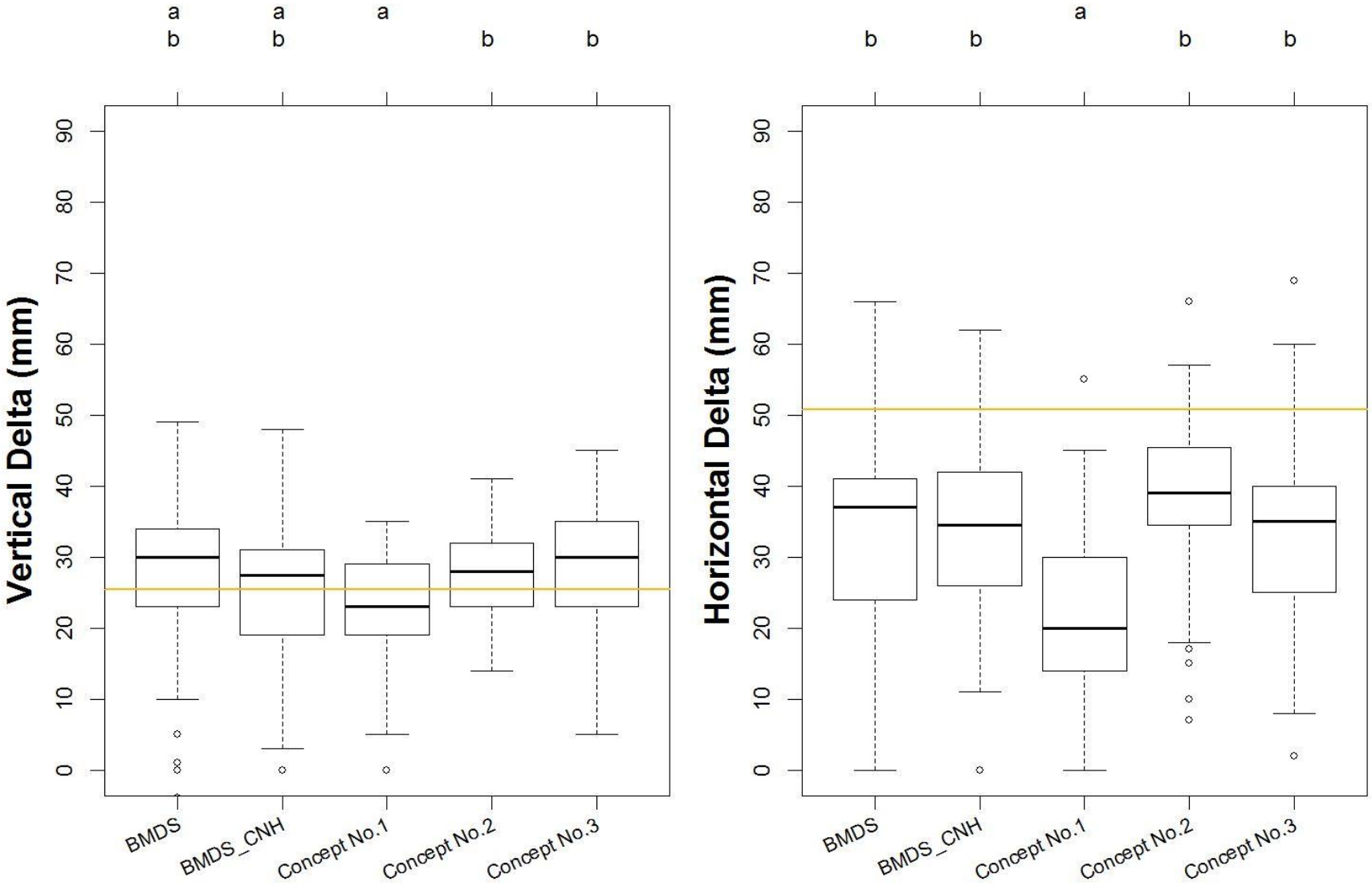

Figure C. 4. Lutheran Loamy Sand Field 12.87 kmh^{-1} Canola, Delta Measurements

Asquith Loamy Sand Field 8.85 kmh^{-1} (5.5 mph) Wheat

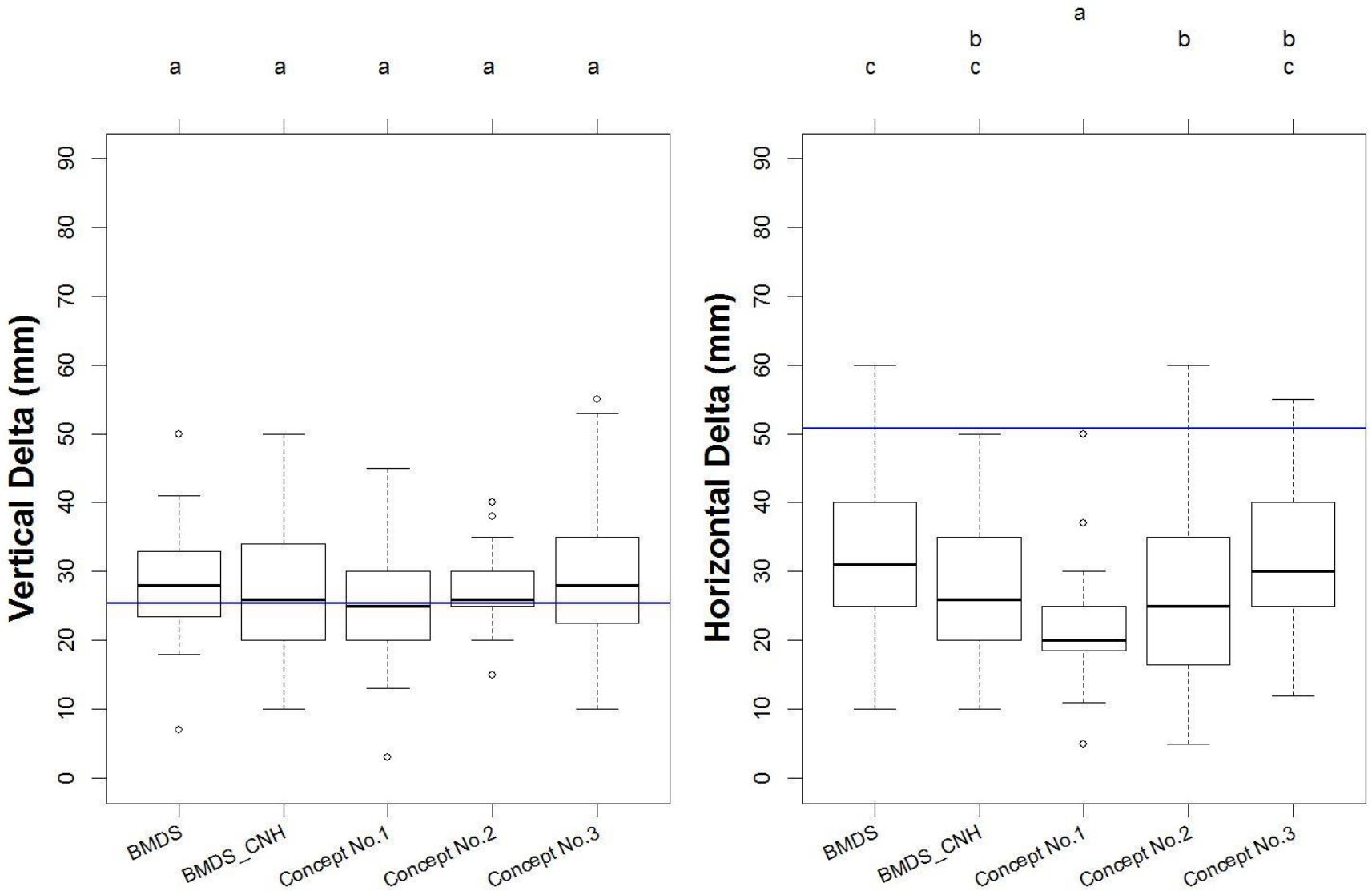

Figure C. 5. Asquith Loamy Sand Field 8.85 kmh^{-1} Wheat, Delta Measurements

Asquith Loamy Sand Field 12.87 kmh^{-1} (8.0 mph) Wheat

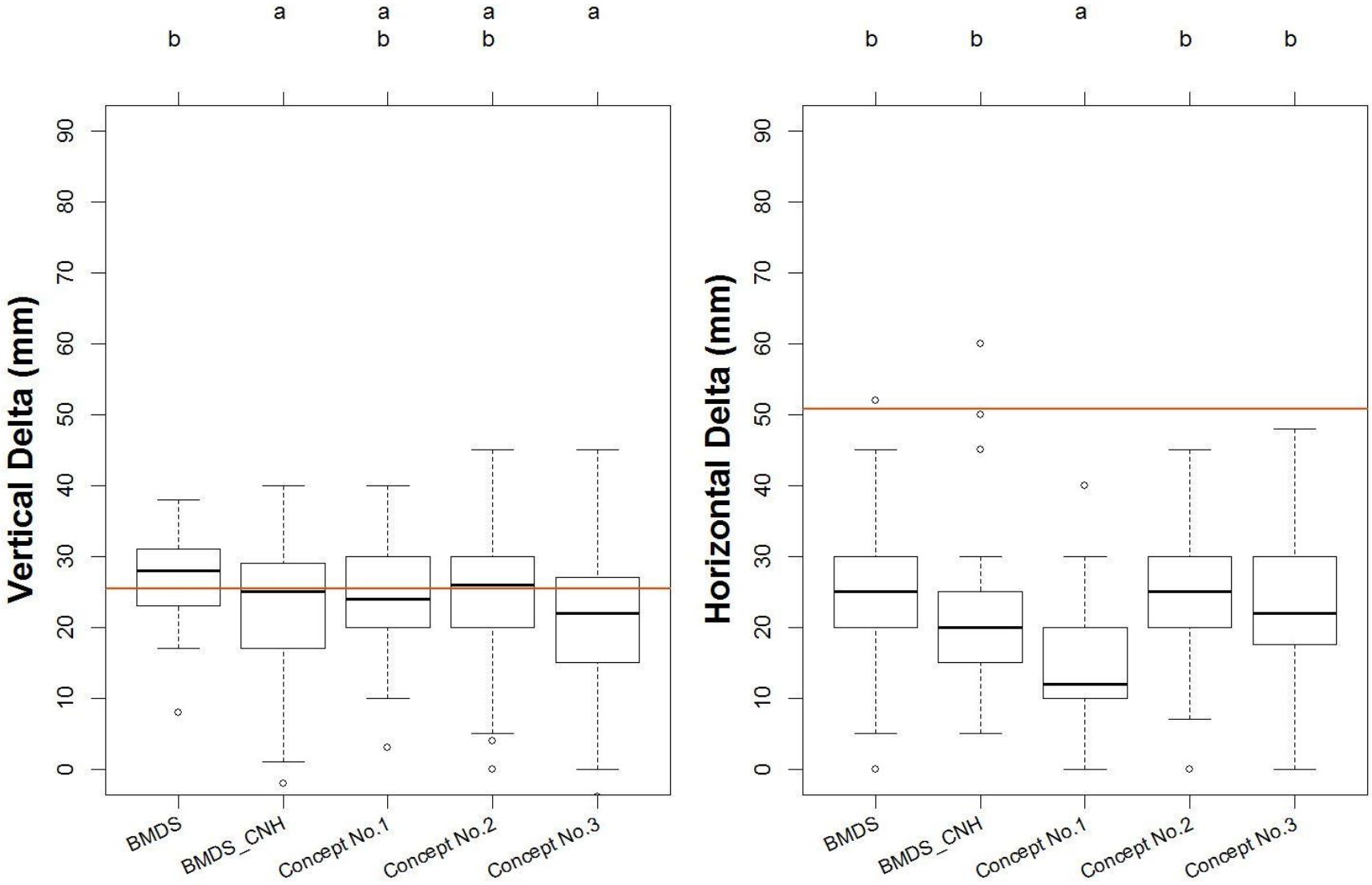

Figure C. 6. Asquith Loamy Sand Field 12.87 kmh^{-1} Wheat, Delta Measurements

Asquith Loamy Sand Field 8.85 kmh^{-1} (5.5 mph) Canola

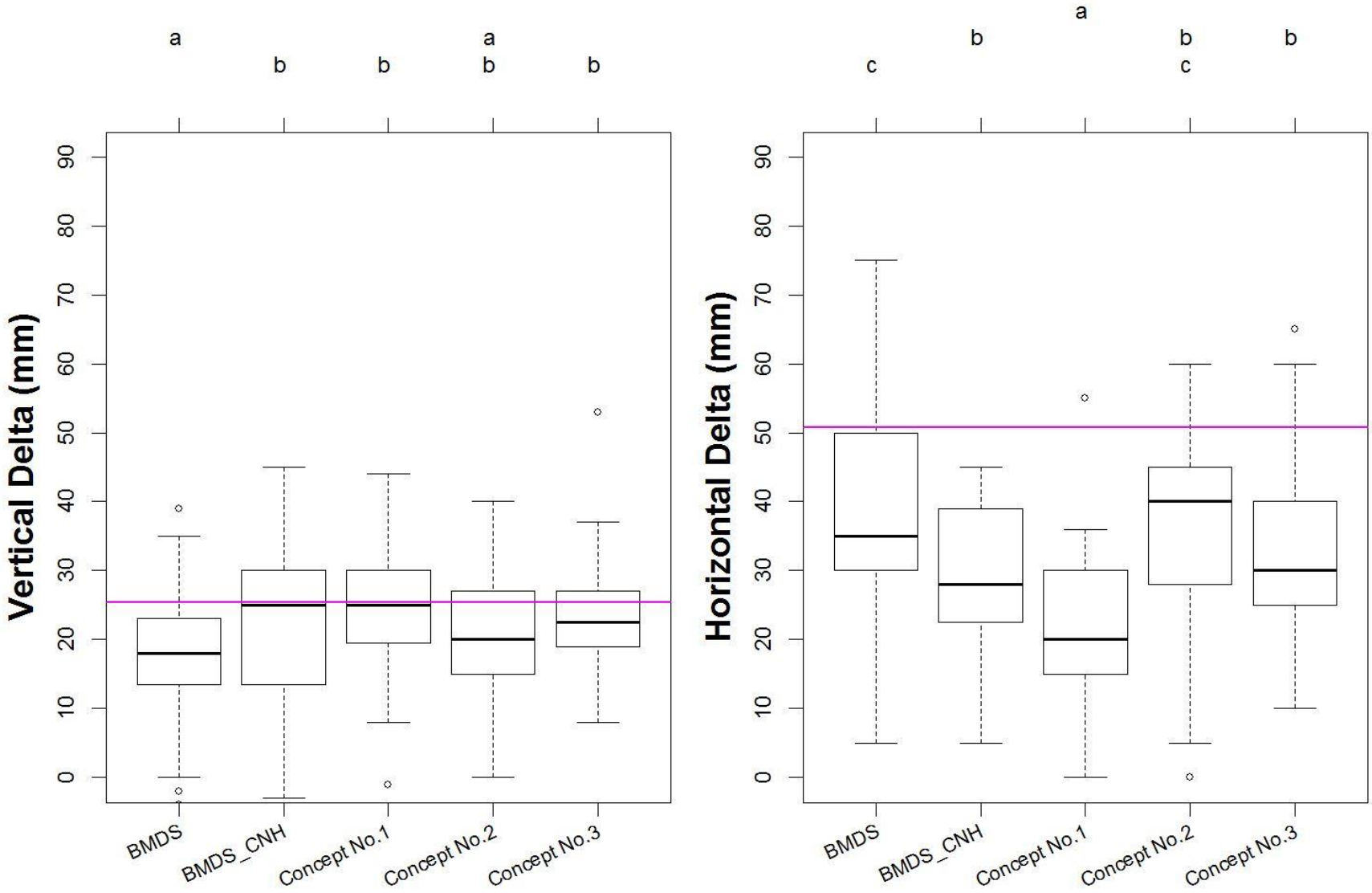

Figure C. 7. Asquith Loamy Sand Field 8.85 kmh^{-1} Canola, Delta Measurements

Asquith Loamy Sand Field 12.87 kmh^{-1} (8.0 mph) Canola

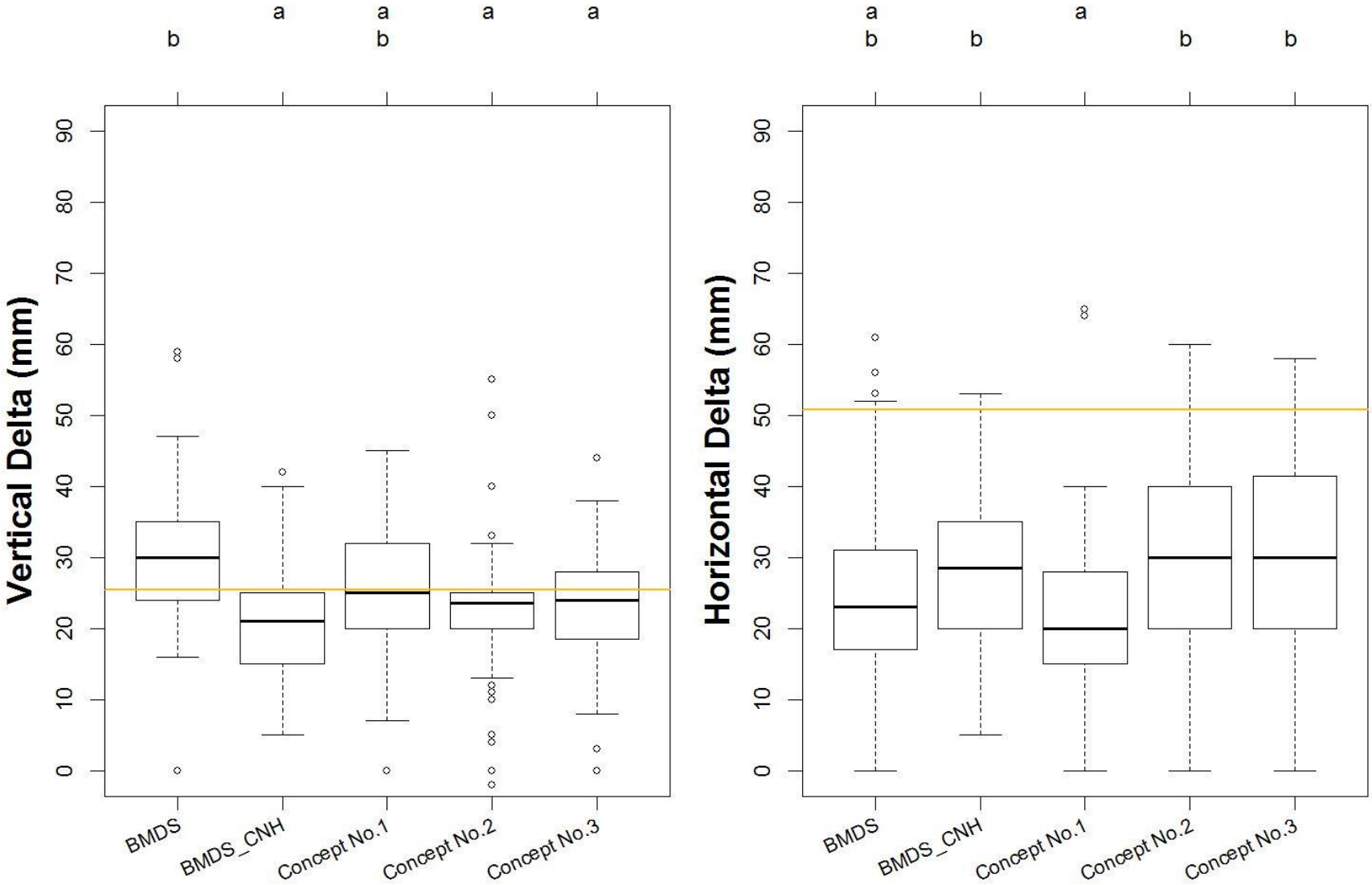

Figure C. 8. Asquith Loamy Sand Field 12.87 kmh^{-1} Canola, Delta Measurements

Asquith Summer Fallow Loamy Sand Field 8.85 kmh^{-1} (5.5 mph) Wheat

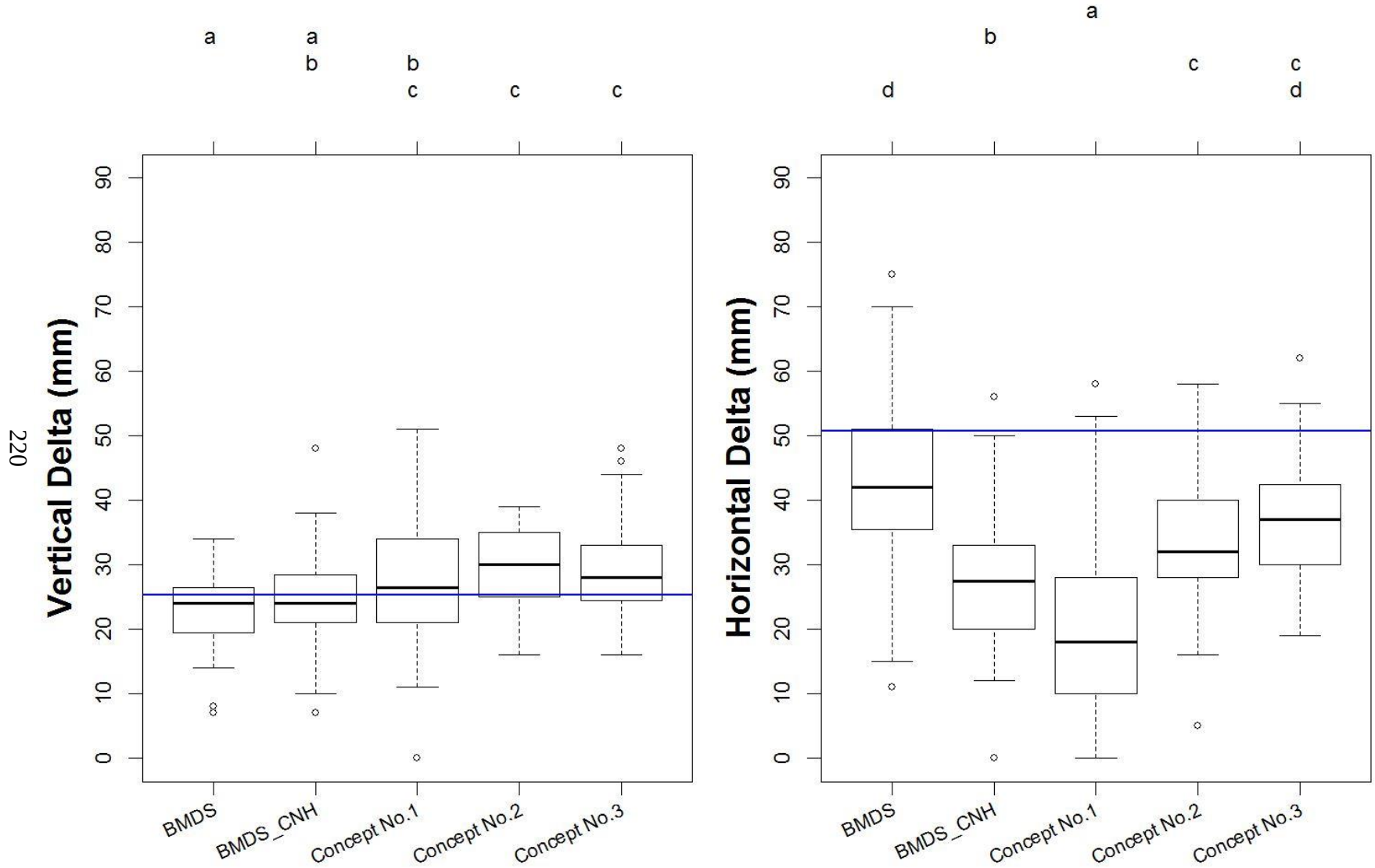

Figure C. 9. Asquith Summer Fallow Loamy Sand Field 8.85 kmh^{-1} Wheat, Delta Measurements

Asquith Summer Fallow Loamy Sand Field 12.87 kmh^{-1} (8.0 mph) Wheat

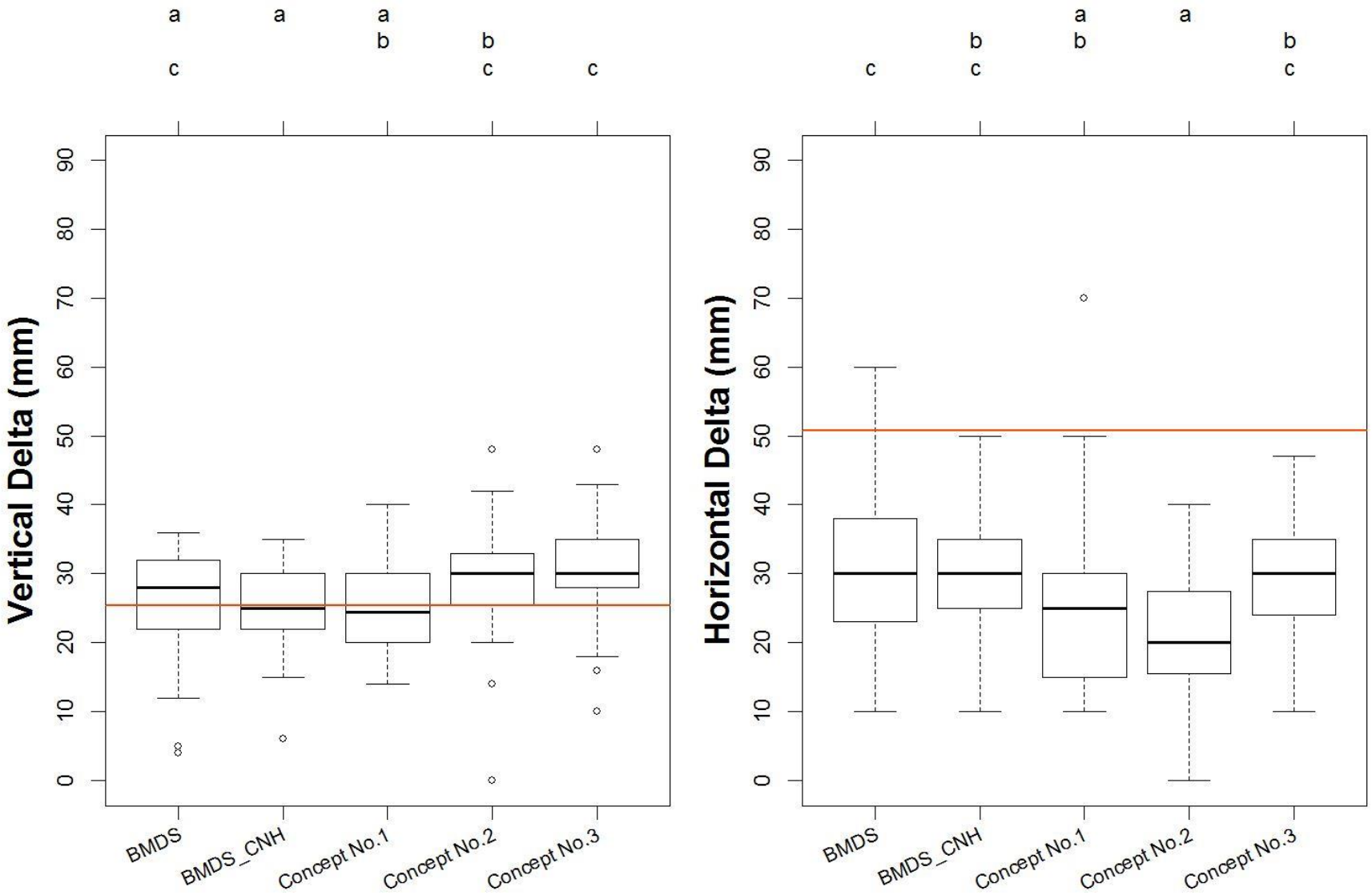

Figure C. 10. Asquith Summer Fallow Loamy Sand Field 12.87 kmh^{-1} Wheat, Delta Measurements

Asquith Summer Fallow Loamy Sand Field 8.85 kmh^{-1} (5.5 mph) Canola

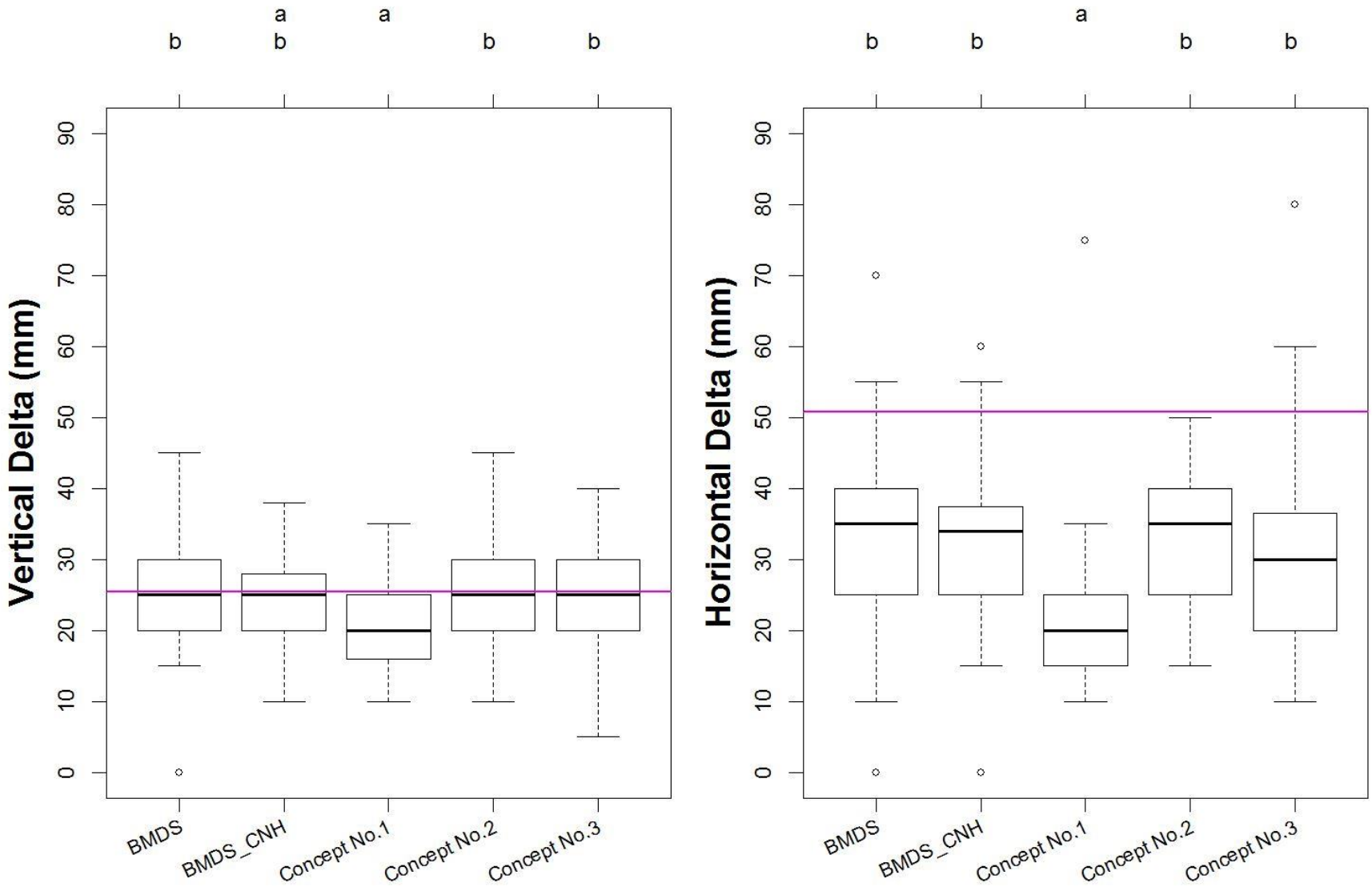

Figure C. 11. Asquith Summer Fallow Loamy Sand Field 8.85 kmh^{-1} Canola, Delta Measurements

Asquith Summer Fallow Loamy Sand Field 12.87 kmh^{-1} (8.0 mph) Canola

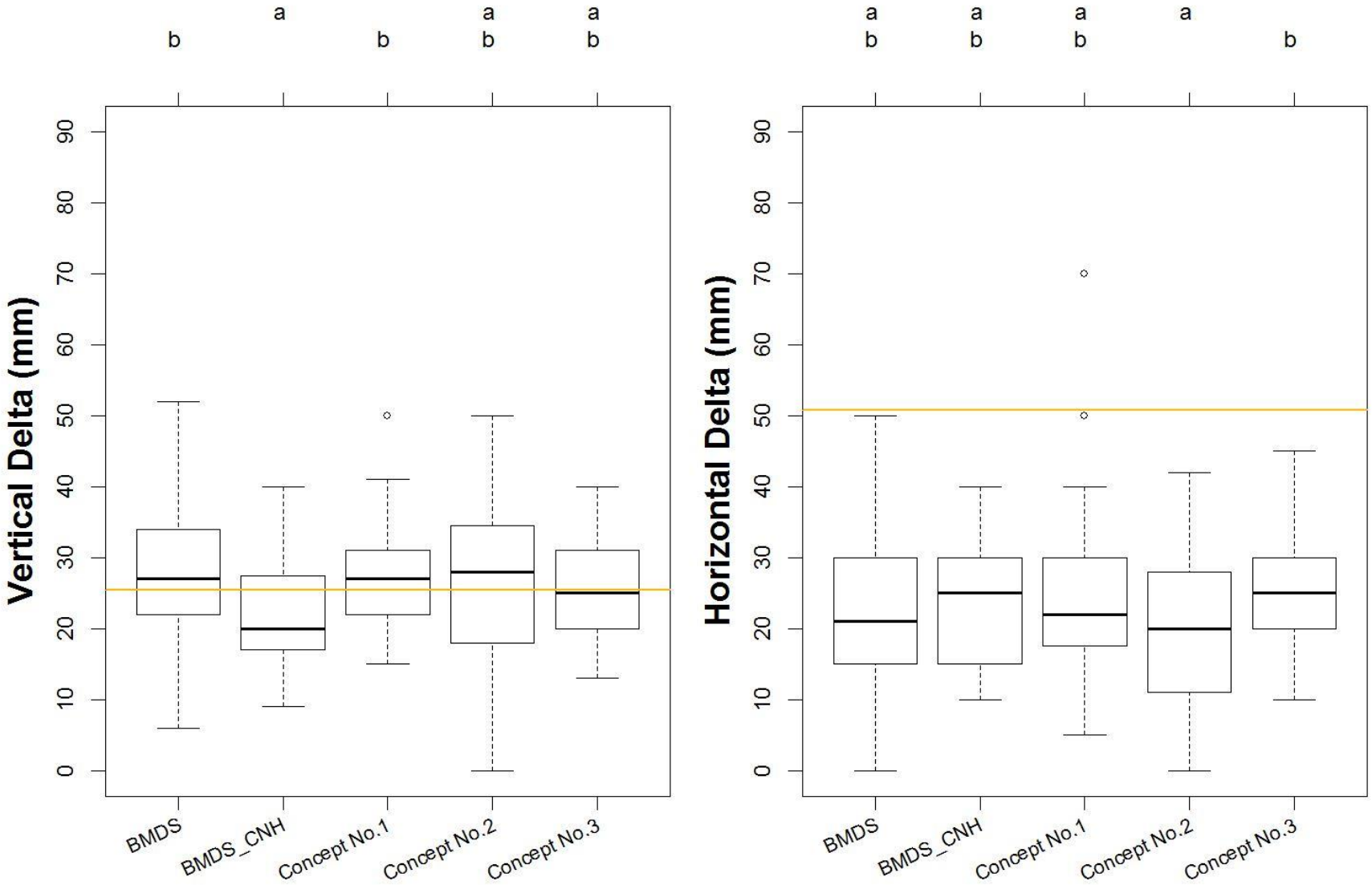

Figure C. 12. Asquith Summer Fallow Loamy Sand Field 12.87 kmh^{-1} Canola, Delta Measurements

Saint-Denis Loam Field 8.85 kmh^{-1} (5.5 mph) Wheat

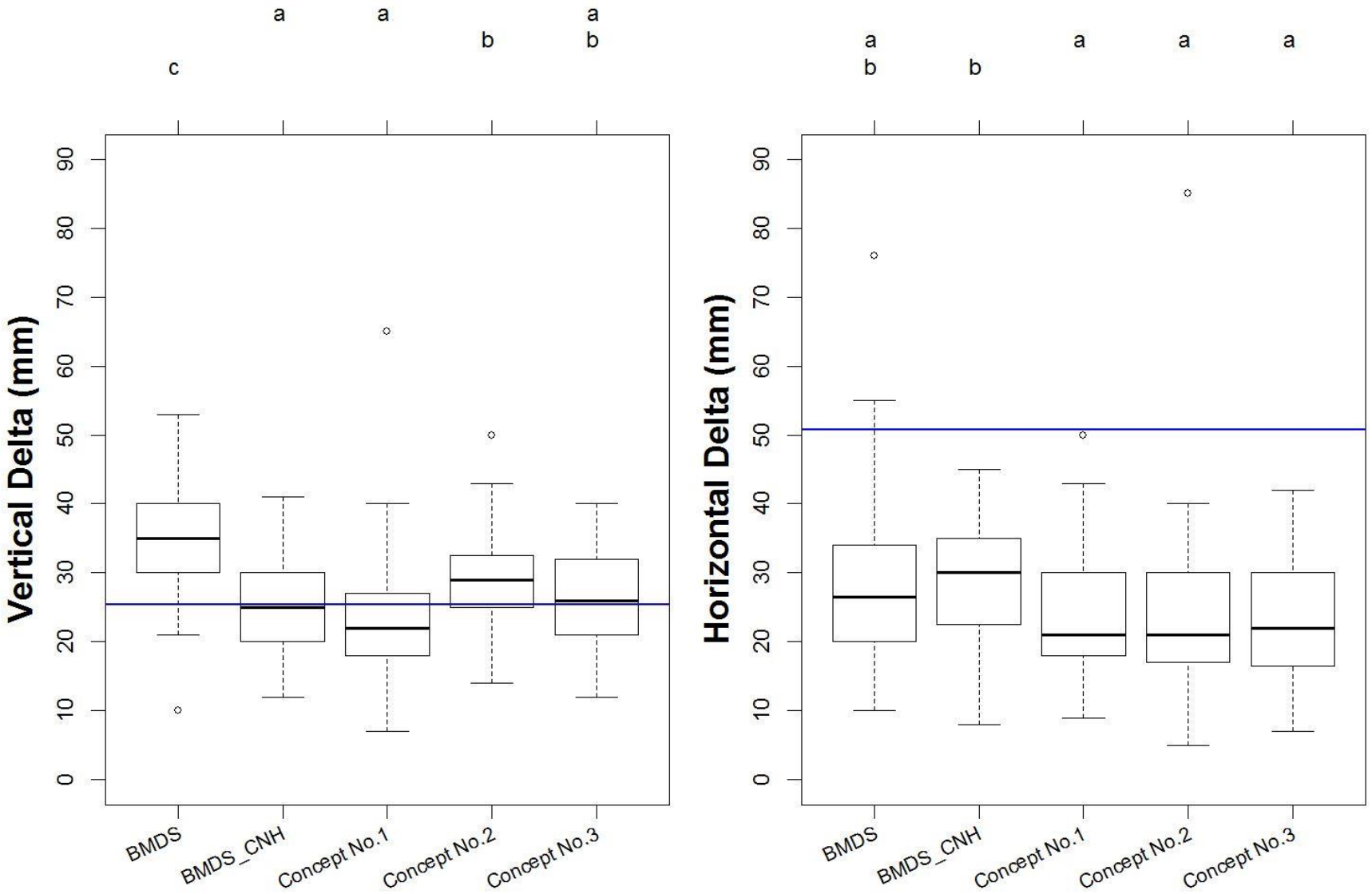

Figure C. 13. Saint-Denis Loam Field 8.85 kmh^{-1} Wheat, Delta Measurements

Saint-Denis Loam Field 12.87 kmh^{-1} (8.0 mph) Wheat

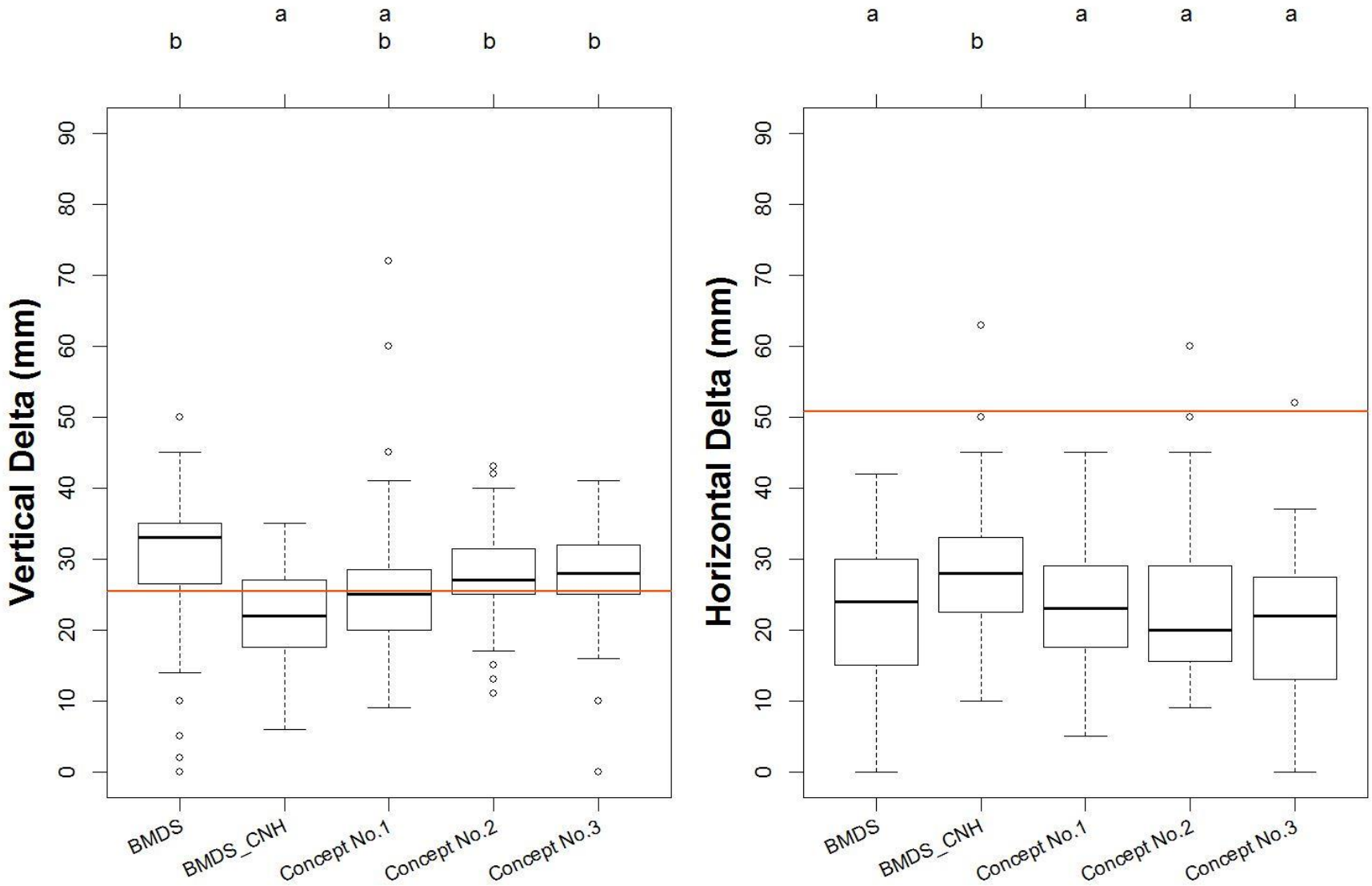

Figure C. 14. Saint-Denis Loam Field 12.87 kmh^{-1} Wheat, Delta Measurements

Saint-Denis Loam Field 8.85 kmh^{-1} (5.5 mph) Canola

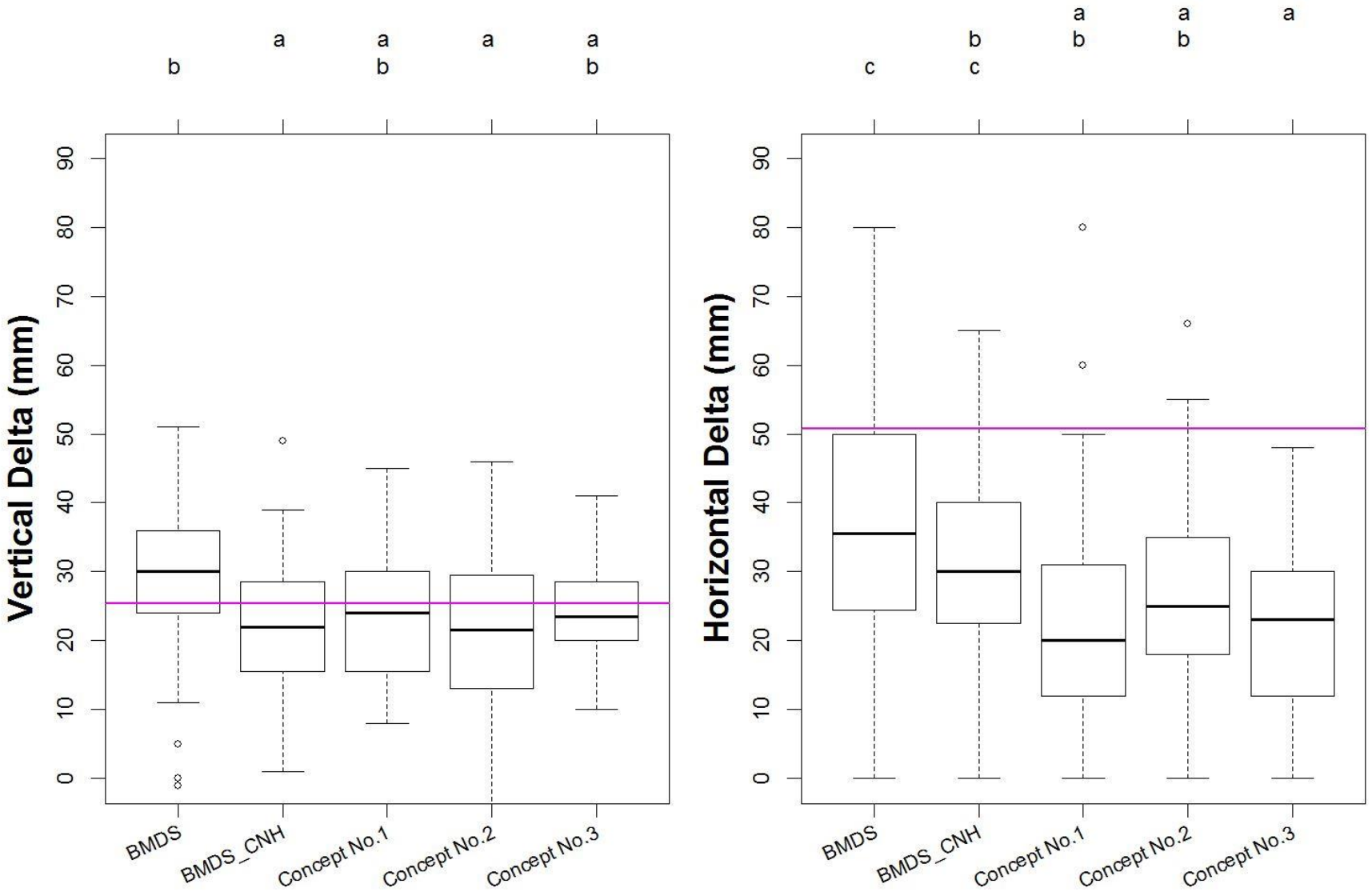

Figure C. 15. Saint-Denis Loam Field 8.85 kmh^{-1} Canola, Delta Measurements

Saint-Denis Loam Field 12.87 kmh^{-1} (8.0 mph) Canola

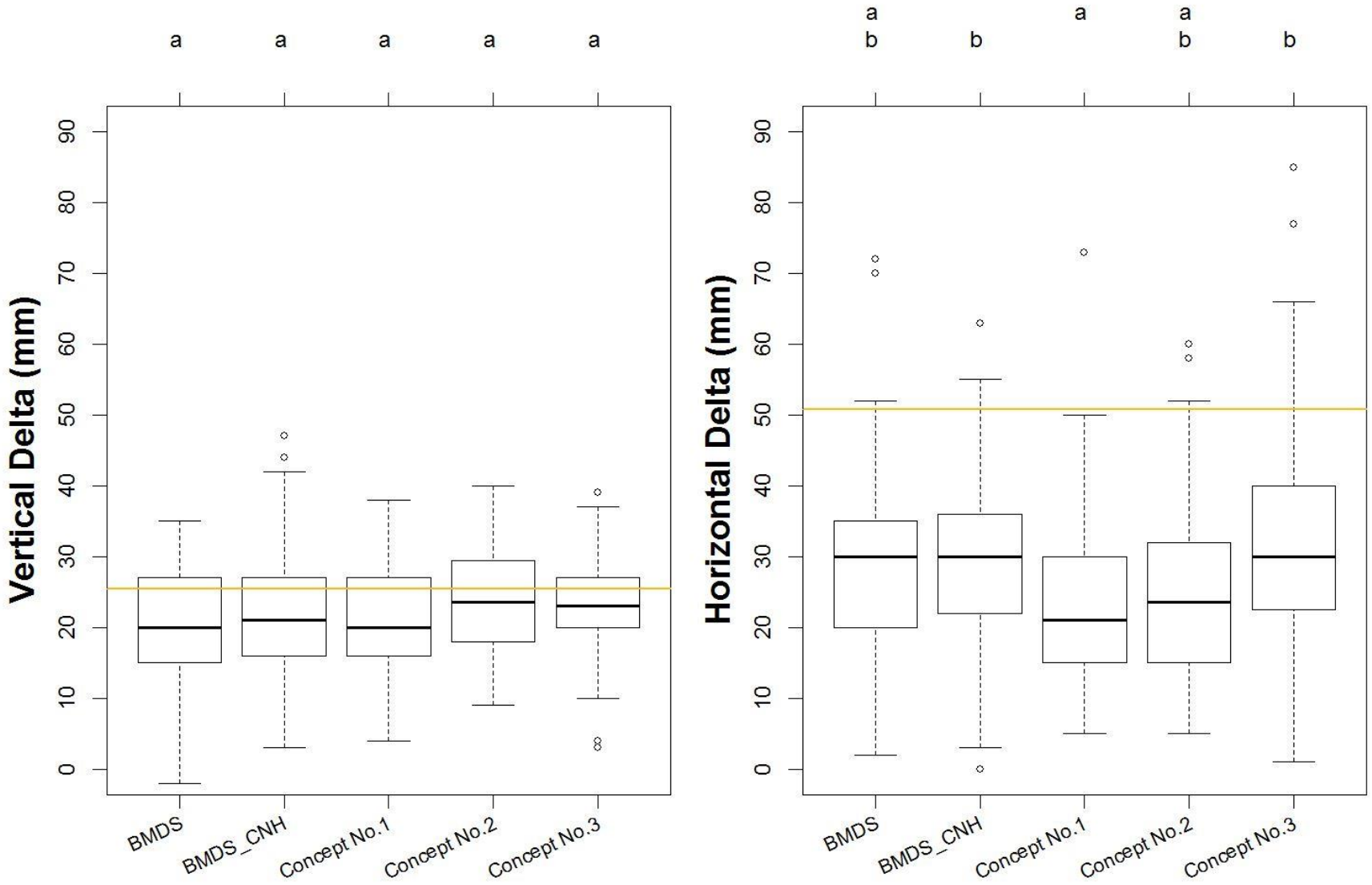

Figure C. 16. Saint-Denis Loam Field 12.87 kmh^{-1} Canola, Delta Measurements

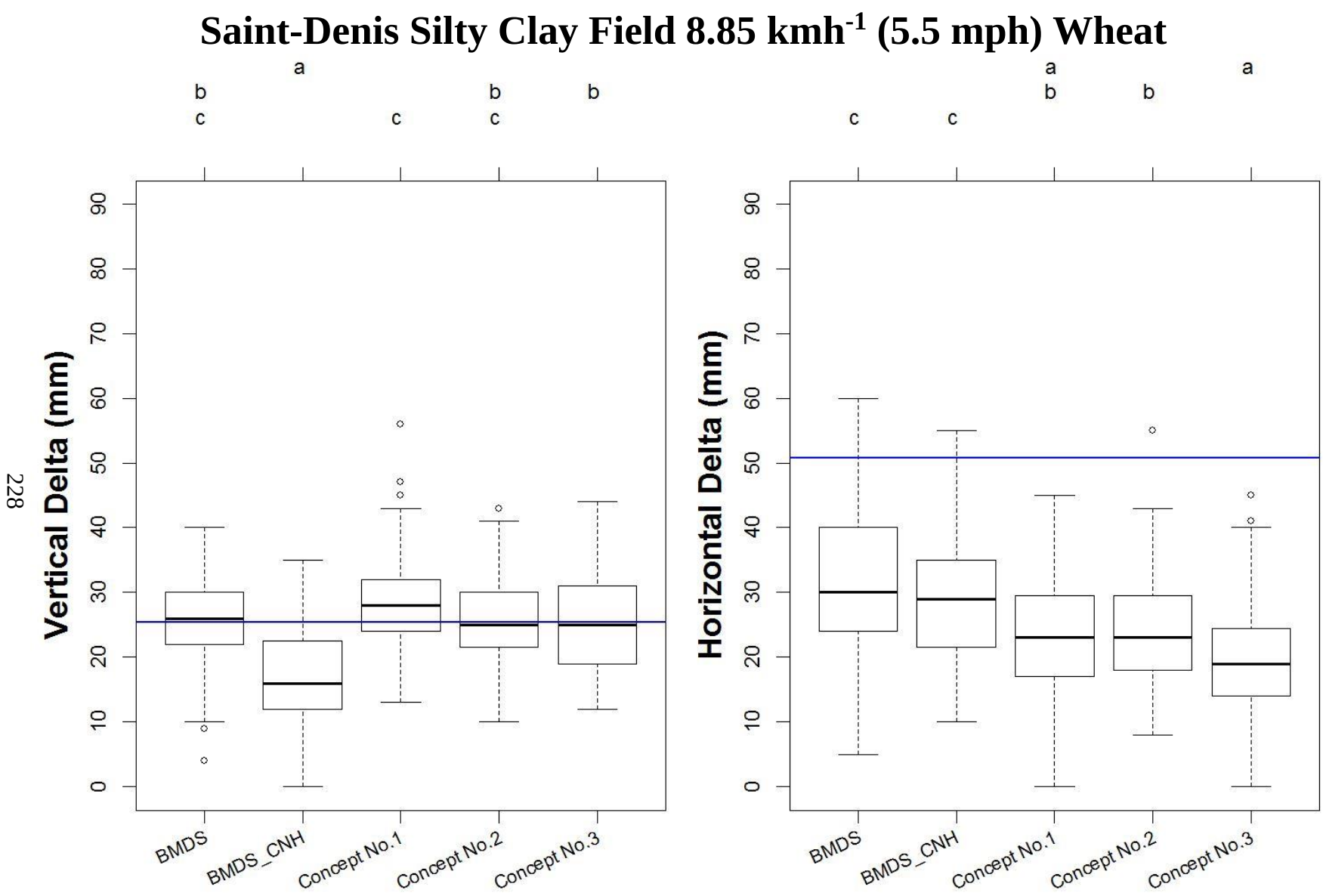

Figure C. 17. Saint-Denis Silty Clay Field 8.85 kmh^{-1} Wheat, Delta Measurements

Saint-Denis Silty Clay Field 12.87 kmh^{-1} (8.0 mph) Wheat

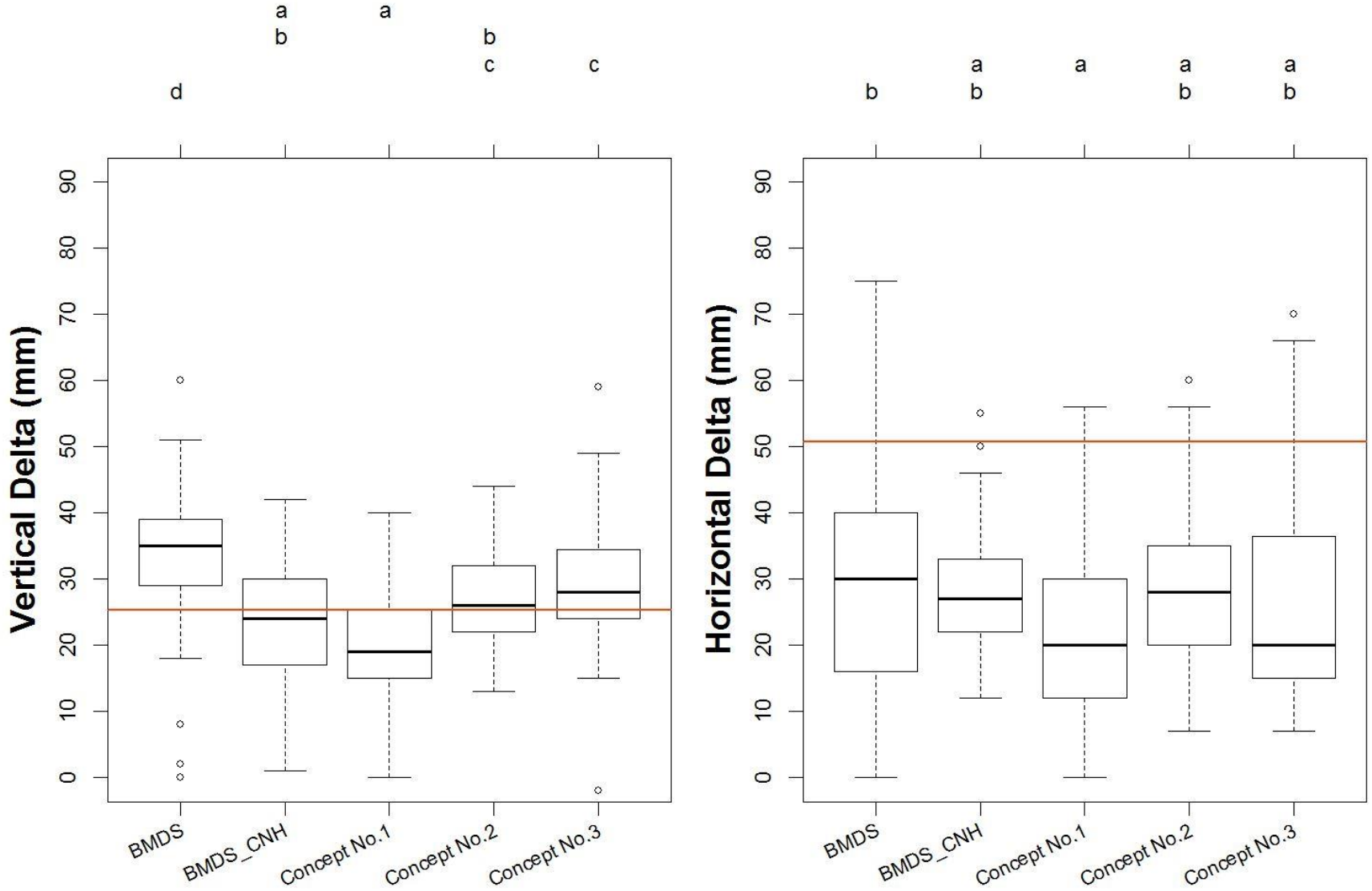

Figure C. 18. Saint-Denis Silty Clay Field 12.87 kmh^{-1} Wheat, Delta Measurements

Saint-Denis Silty Clay Field 8.85 kmh^{-1} (5.5 mph) Canola

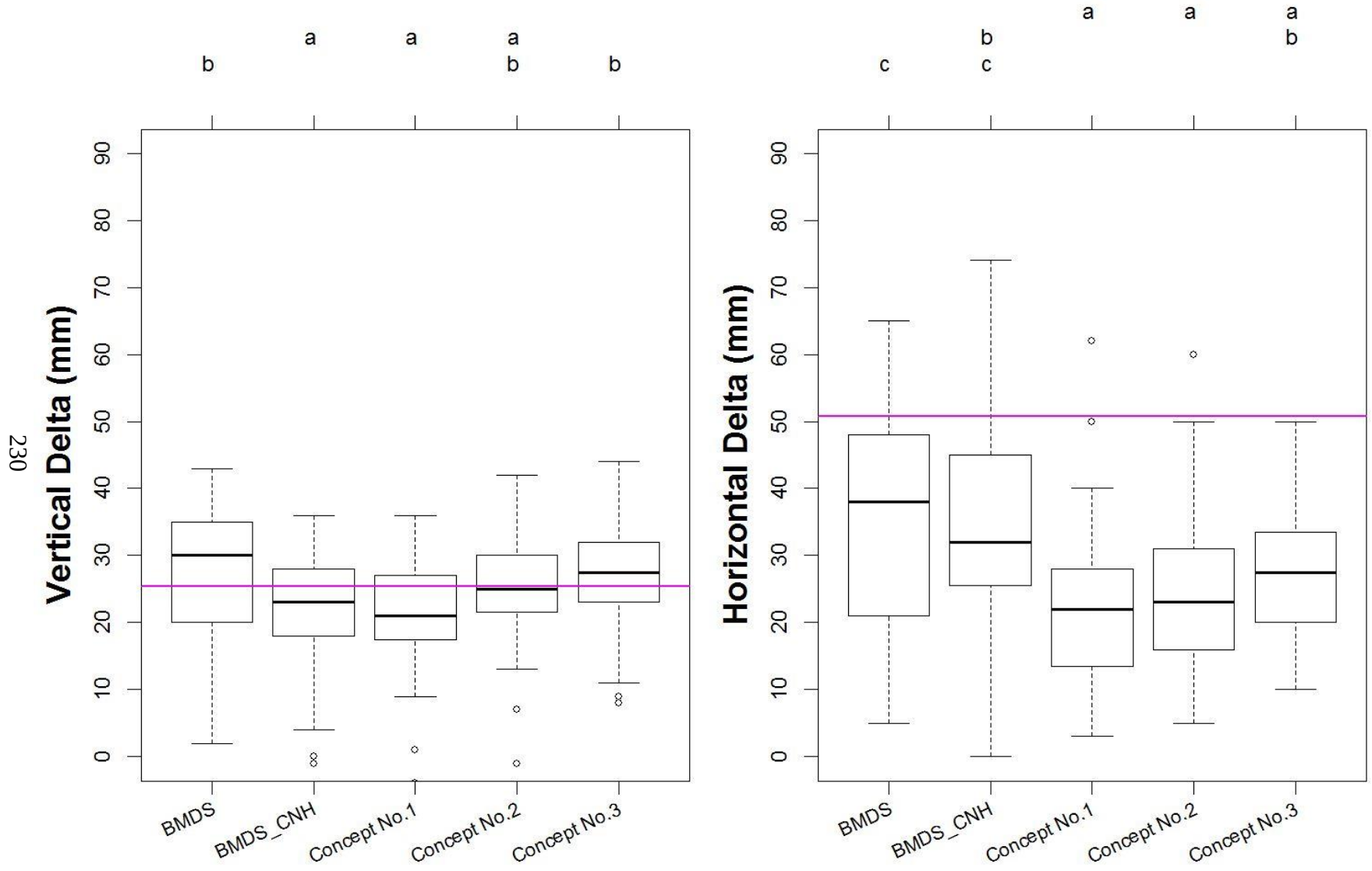

Figure C. 19. Saint-Denis Silty Clay Field 8.85 kmh^{-1} Canola, Delta Measurements

Saint-Denis Silty Clay Field 12.87 kmh^{-1} (8.0 mph) Canola

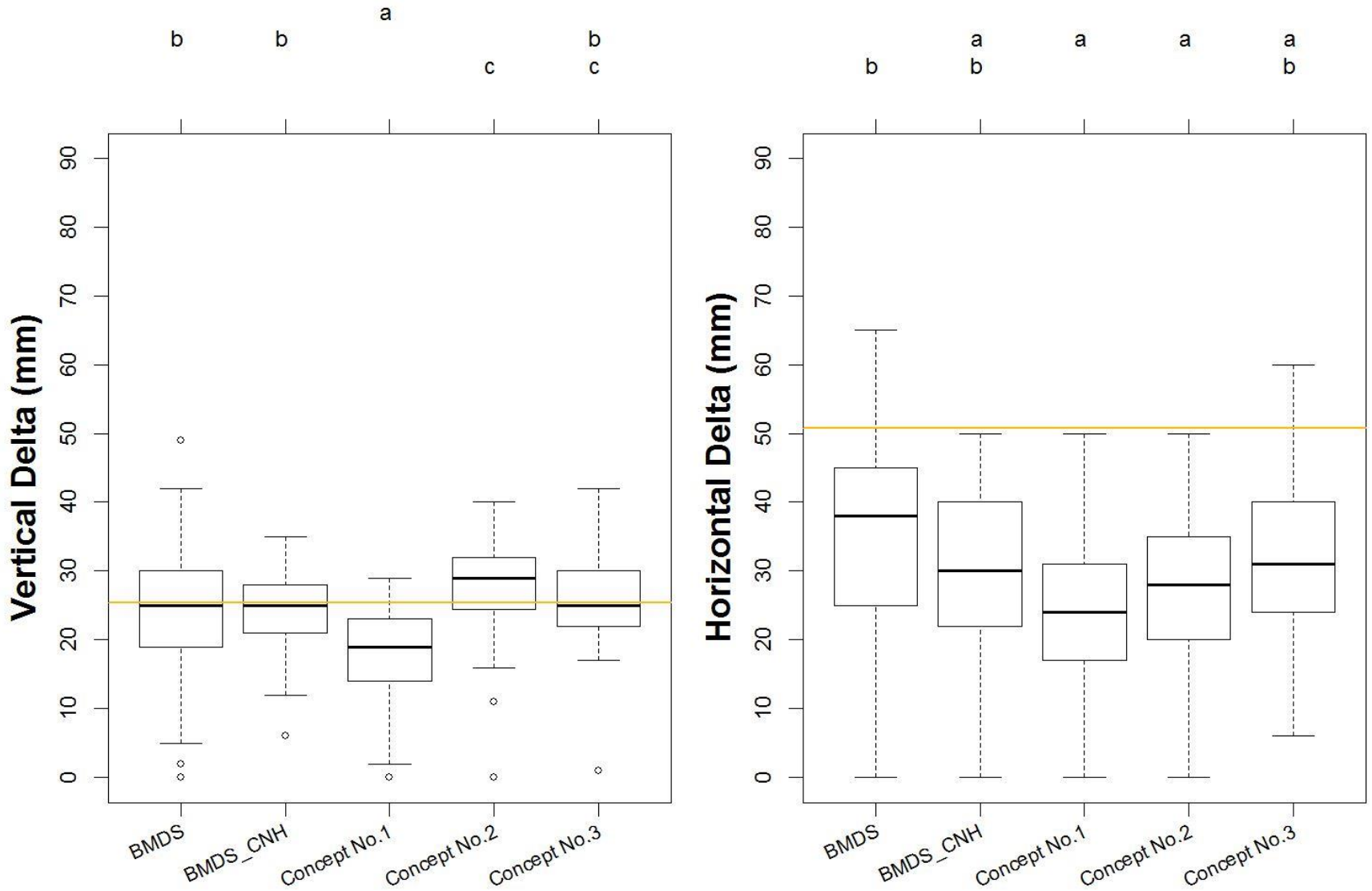

Figure C. 20. Saint-Denis Silty Clay Field 12.87 kmh^{-1} Canola, Delta Measurements

APPENDIX D

Seed to Fertilizer Offset Distances Correlation Tables

Table D. 1. Vertical Delta Interactions Result Table

Vertical Delta																					
Fields	Configurations	Significant Pairwise Comparisons	Openers					Interactions													
			BMDS	BMDS_CNH	Concept No.1	Concept No.2	Concept No.3	BMDS - BMDS_CNH	BMDS - Concept No.1	BMDS - Concept No.2	BMDS - Concept No.3	BMDS_CNH - Concept No.1	BMDS_CNH - Concept No.2	BMDS_CNH - Concept No.3	Concept No.1 - Concept No.2	Concept No.1 - Concept No.3	Concept No.2 - Concept No.3
Lutheran Loamy Sand Field	Wheat 8.85 km/h (5.5 mph)	a		X		X		2	2	3	3	2	2	3	1	2	3
		b	X		X		X										
		c				X											
		d															
	Wheat 12.87 km/h (8.0 mph)	a		X													
		b			X	X	X										
		c	X			X	X										
		d															
	Canola 8.85 km/h (5.5 mph)	a			X												
		b	X	X		X	X										
		c															
		d															
	Canola 12.87 km/h (8.0 mph)	a	X	X	X												
		b	X	X		X	X										
		c															
		d															
Asquith Loamy Sand Field	Wheat 8.85 km/h (5.5 mph)	a	X	X	X	X	X	1	3	3	1	4	4	4	4	4	4
		b															
		c															
		d															
	Wheat 12.87 km/h (8.0 mph)	a		X	X	X	X										
		b	X		X	X											
		c															
		d															
	Canola 8.85 km/h (5.5 mph)	a	X			X											
		b		X	X	X	X										
		c															
		d															
	Canola 12.87 km/h (8.0 mph)	a		X	X	X	X										
		b	X		X												
		c															
		d															
Asquith Summer Fallow Loamy Sand Field	Wheat 8.85 km/h (5.5 mph)	a	X	X				3	2	3	3	3	2	2	3	2	4
		b		X	X												
		c			X	X	X										
		d															
	Wheat 12.87 km/h (8.0 mph)	a	X	X	X												
		b			X	X											
		c	X			X	X										
		d															
	Canola 8.85 km/h (5.5 mph)	a		X	X												
		b	X	X		X	X										
		c															
		d															
	Canola 12.87 km/h (8.0 mph)	a		X		X	X										
		b	X		X	X	X										
		c															
		d															
St-Denis Loam	Wheat 8.85 km/h (5.5 mph)	a		X	X		X	1	3	1	3	4	3	4	3	4	4
		b				X	X										
		c	X														
		d															
	Wheat 12.87 km/h (8.0 mph)	a		X	X	X	X										
		b	X		X		X										
		c															
		d															
	Canola 8.85 km/h (5.5 mph)	a		X	X	X	X										
		b	X		X		X										
		c															
		d															
	Canola 12.87 km/h (8.0 mph)	a	X	X	X	X	X										
		b															
		c															
		d															
St-Denis Silty Clay	Wheat 8.85 km/h (5.5 mph)	a		X				1	1	3	3	2	3	1	2	1	4
		b	X			X	X										
		c	X		X												
		d															
	Wheat 12.87 km/h (8.0 mph)	a		X	X												
		b		X			X										
		c					X										
		d	X														
	Canola 8.85 km/h (5.5 mph)	a		X	X												
		b	X			X	X										
		c															
		d															
	Canola 12.87 km/h (8.0 mph)	a			X		X										
		b	X	X		X	X										
		c															
		d															
							Interactions :	BMDS - BMDS_CNH	BMDS - Concept No.1	BMDS - Concept No.2	BMDS - Concept No.3	BMDS_CNH - Concept No.1	BMDS_CNH - Concept No.2	BMDS_CNH - Concept No.3	Concept No.1 - Concept No.2	Concept No.1 - Concept No.3	Concept No.2 - Concept No.3
							Theoretical Maximum :	20	20	20	20	20	20	20	20	20	20
							Grand Total :	**8**	**11**	**13**	**13**	**15**	**14**	**14**	**13**	**13**	**19**

Table D. 2. Horizontal Delta Interactions Result Table

Horizontal Delta																					
Fields	Configurations	Significant Pairwise Comparisons	Openers					Interactions													
			BMDS	BMDS_CNH	Concept No.1	Concept No.2	Concept No.3	BMDS - BMDS_CNH	BMDS - Concept No.1	BMDS - Concept No.2	BMDS - Concept No.3	BMDS_CNH - Concept No.1	BMDS_CNH - Concept No.2	BMDS_CNH - Concept No.3	Concept No.1 - Concept No.2	Concept No.1 - Concept No.3	Concept No.2 - Concept No.3				
Lutheran Loamy Sand Field	Wheat 8.85 km/h (5.5 mph)	a			X	X	X	4	0	4	4	0	4	4	1	1	4				
		b	X	X		X	X														
		c																			
		d																			
	Wheat 12.87 km/h (8.0 mph)	a			X																
		b	X	X		X	X														
		c																			
		d																			
	Canola 8.85 km/h (5.5 mph)	a			X																
		b	X	X		X	X														
		c																			
		d			X																
	Canola 12.87 km/h (8.0 mph)	a	X	X		X	X														
		b																			
		c																			
		d																			
Asquith Loamy Sand Field	Wheat 8.85 km/h (5.5 mph)	a			X			3	1	3	3	0	4	4	0	0	4				
		b		X		X	X														
		c	X	X			X														
		d																			
	Wheat 12.87 km/h (8.0 mph)	a			X																
		b	X	X		X	X														
		c																			
		d																			
	Canola 8.85 km/h (5.5 mph)	a			X																
		b		X		X	X														
		c	X			X															
		d																			
	Canola 12.87 km/h (8.0 mph)	a	X		X																
		b	X	X		X	X														
		c																			
		d																			
Asquith Summer Fallow Loamy Sand Field	Wheat 8.85 km/h (5.5 mph)	a			X			3	1	2	4	2	2	3	2	2	2				
		b		X			X														
		c				X															
		d	X				X														
	Wheat 12.87 km/h (8.0 mph)	a				X															
		b		X	X		X														
		c	X	X			X														
		d																			
	Canola 8.85 km/h (5.5 mph)	a			X																
		b	X	X		X	X														
		c																			
		d																			
	Canola 12.87 km/h (8.0 mph)	a	X	X	X	X															
		b	X	X	X		X														
		c																			
		d																			
St-Denis Loam	Wheat 8.85 km/h (5.5 mph)	a	X		X	X	X	3	3	3	3	1	2	1	4	3	4				
		b	X	X																	
		c																			
		d																			
	Wheat 12.87 km/h (8.0 mph)	a	X		X	X	X														
		b		X																	
		c																			
		d																			
	Canola 8.85 km/h (5.5 mph)	a			X	X	X														
		b		X	X	X															
		c	X	X																	
		d																			
	Canola 12.87 km/h (8.0 mph)	a	X		X	X															
		b	X	X		X	X														
		c																			
		d																			
St-Denis Silty Clay	Wheat 8.85 km/h (5.5 mph)	a				X	X	4	0	1	2	2	2	3	4	4	3				
		b				X	X														
		c	X	X																	
		d																			
	Wheat 12.87 km/h (8.0 mph)	a		X	X	X	X														
		b	X	X		X	X														
		c																			
		d																			
	Canola 8.85 km/h (5.5 mph)	a			X	X	X														
		b		X			X														
		c	X	X																	
		d																			
	Canola 12.87 km/h (8.0 mph)	a		X	X	X	X														
		b	X	X			X														
		c																			
		d																			
							Interactions :	BMDS - BMDS_CNH	BMDS - Concept No.1	BMDS - Concept No.2	BMDS - Concept No.3	BMDS_CNH - Concept No.1	BMDS_CNH - Concept No.2	BMDS_CNH - Concept No.3	Concept No.1 - Concept No.2	Concept No.1 - Concept No.3	Concept No.2 - Concept No.3				
							Theoretical Maximum :	20	20	20	20	20	20	20	20	20	20				
							Grand Total :	**17**	**5**	**13**	**16**	**5**	**14**	**15**	**11**	**10**	**17**				

APPENDIX E

3-D Forces Statistical Results

Legend	
	8.85 kmh^{-1} (5.5 mph)
	12.87 kmh^{-1} (8.0 mph)

3-D Forces Analyzed Data 8.85 kmh^{-1} (5.5 mph)

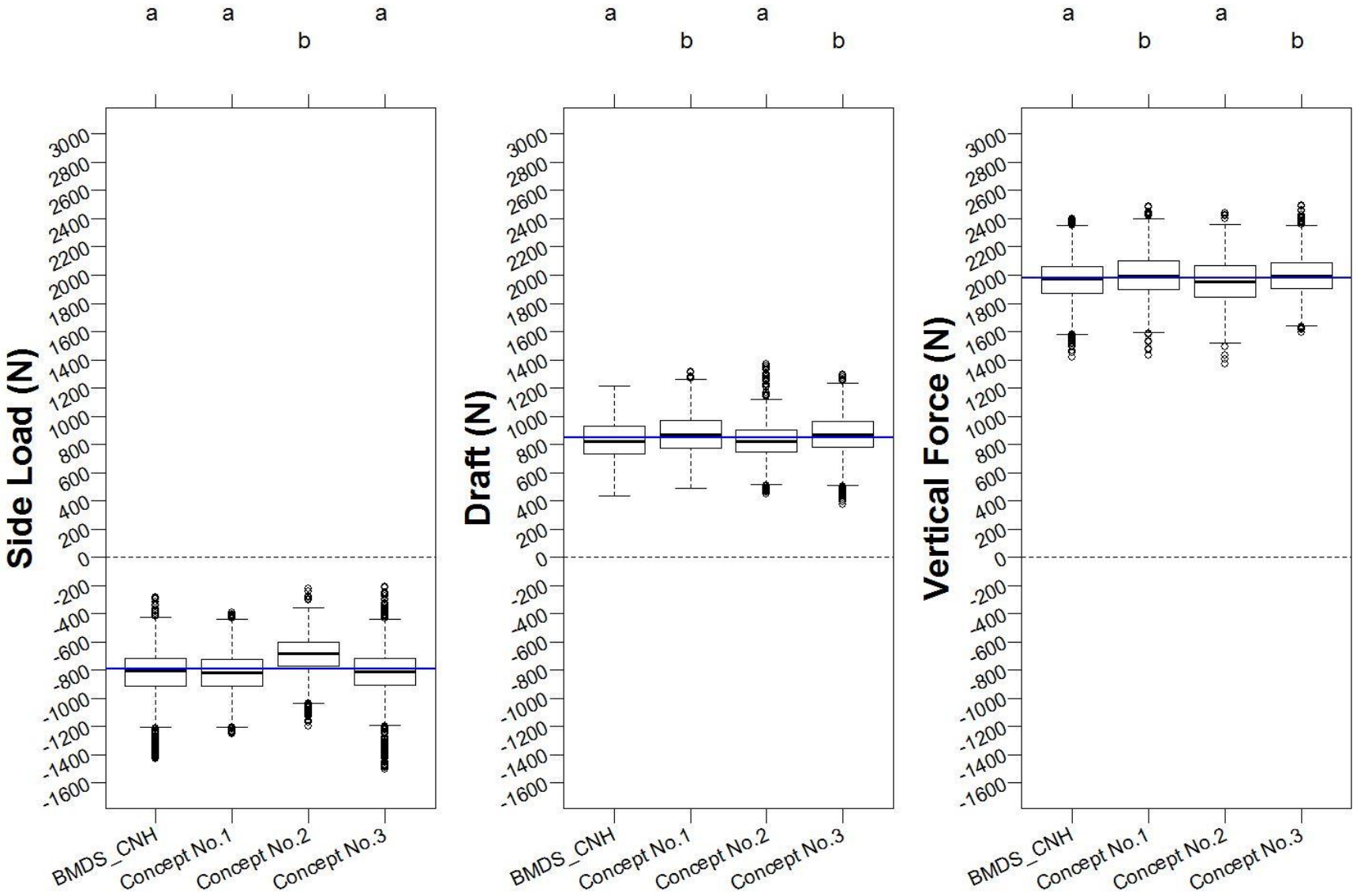

Figure E. 1. 3-D Forces 8.85 kmh^{-1}

3-D Forces Analyzed Data 12.87 kmh^{-1} (8.0 mph)

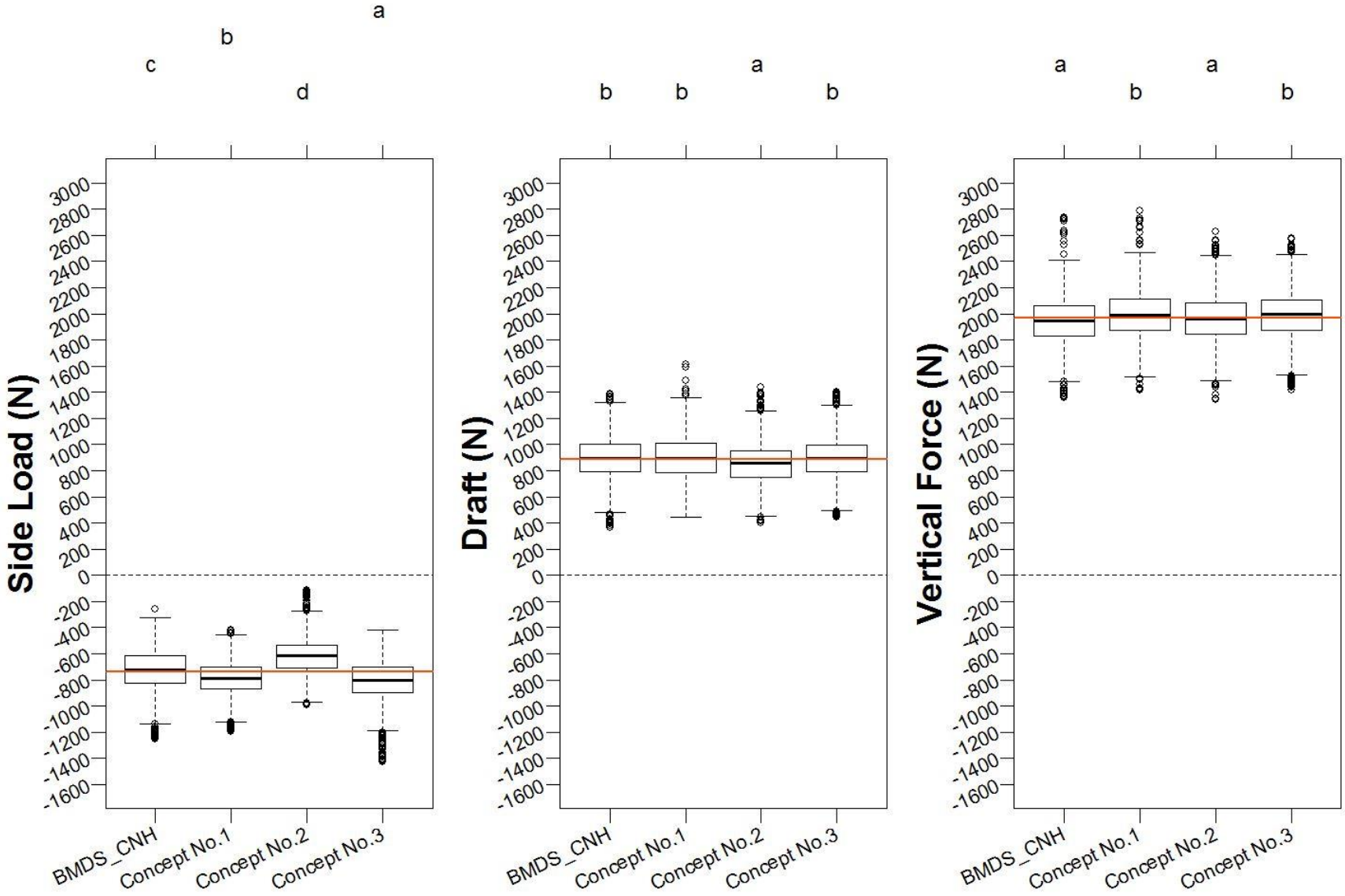

Figure E. 2. 3-D Forces 12.87 kmh^{-1}

APPENDIX F

Table F. 1. The Experimental Field Trials with Crop Residues Result Table

Fields	Openers	Repetition	Yes/No
Lutheran Loamy Sand Field	BMDS	1	Yes
		2	Yes
		3	Yes
	BMD_CNH	1	No
		2	Yes
		3	No
	BMSS	1	Yes
		2	Yes
		3	Yes
	Concept No.1	1	Yes
		2	No
		3	No
	Concept No.2	1	Yes
		2	Yes
		3	Yes
	Concept No.3	1	Yes
		2	Yes
		3	Yes
Lutheran Loamy Sand Field #2	BMDS	1	Yes
		2	Yes
		3	Yes
	BMD_CNH	1	No
		2	No
		3	Yes
	BMSS	1	Yes
		2	Yes
		3	Yes
	Concept No.1	1	Yes
		2	No
		3	Yes
	Concept No.2	1	Yes
		2	Yes
		3	Yes
	Concept No.3	1	Yes
		2	Yes
		3	Yes
Lutheran Loamy Sand Field Extreme Condition	BMDS	1	No
		2	Yes
		3	Yes
	BMD_CNH	1	No
		2	No
		3	No
	BMSS	1	Yes
		2	No
		3	Yes
	Concept No.1	1	No
		2	No
		3	No
	Concept No.2	1	Yes
		2	Yes
		3	Yes
	Concept No.3	1	Yes
		2	Yes
		3	Yes

APPENDIX G

Analytical Knife Draft for Different Speeds, and Soil Bins

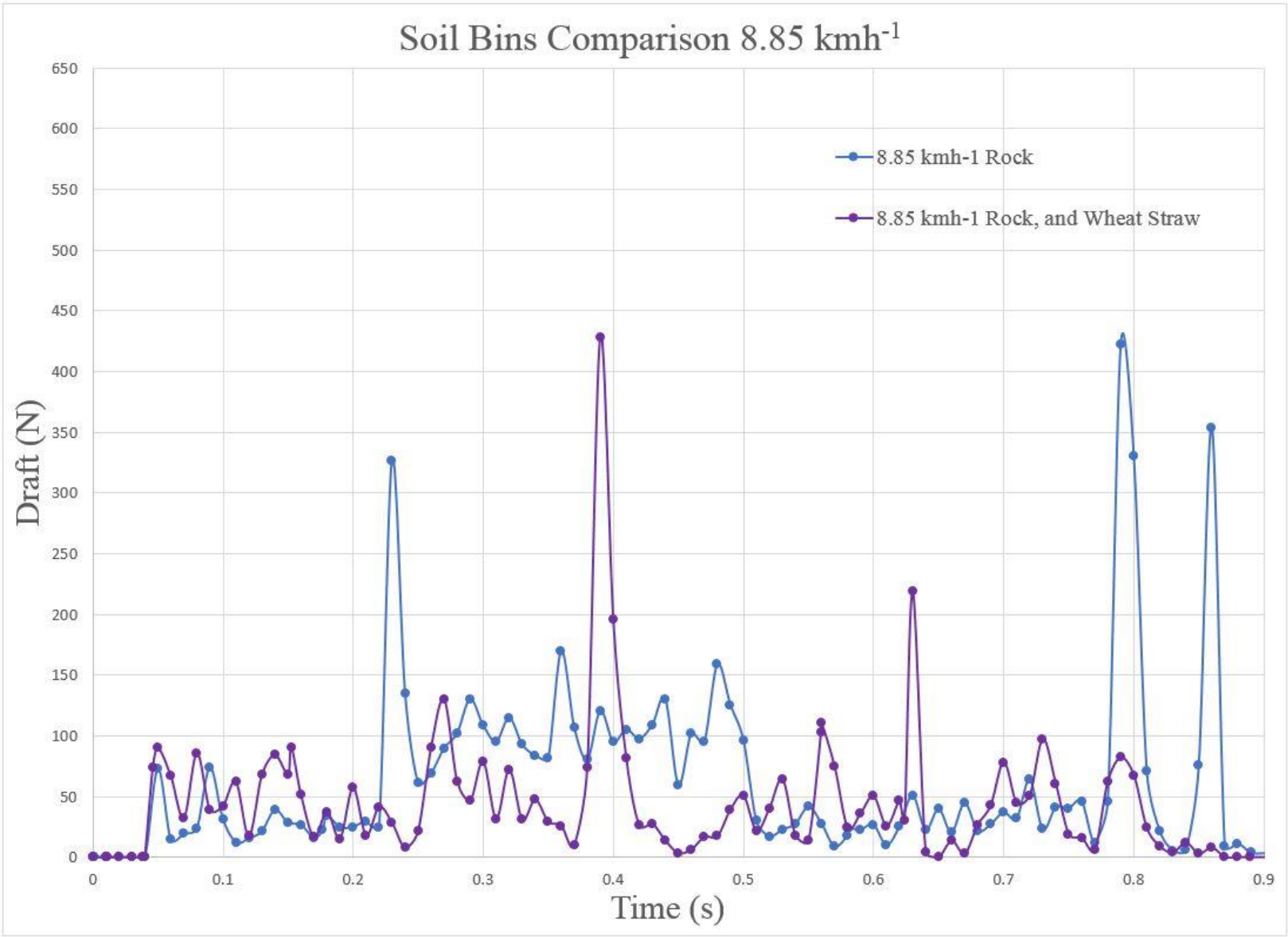

Figure G. 1. Soil Bins Comparison 8.85 kmh^{-1}

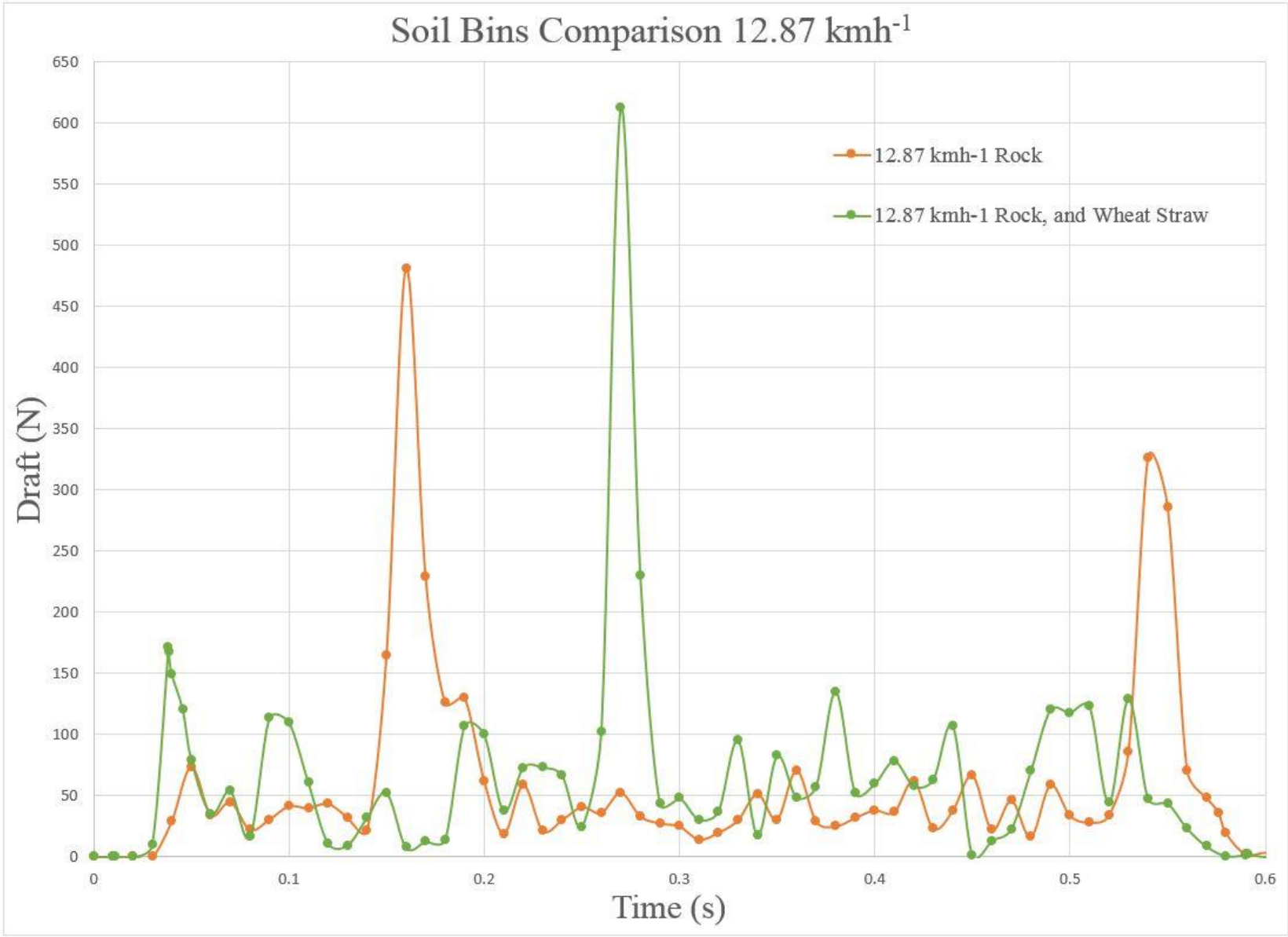

Figure G. 2. Soil Bins Comparison 12.87 kmh^{-1}

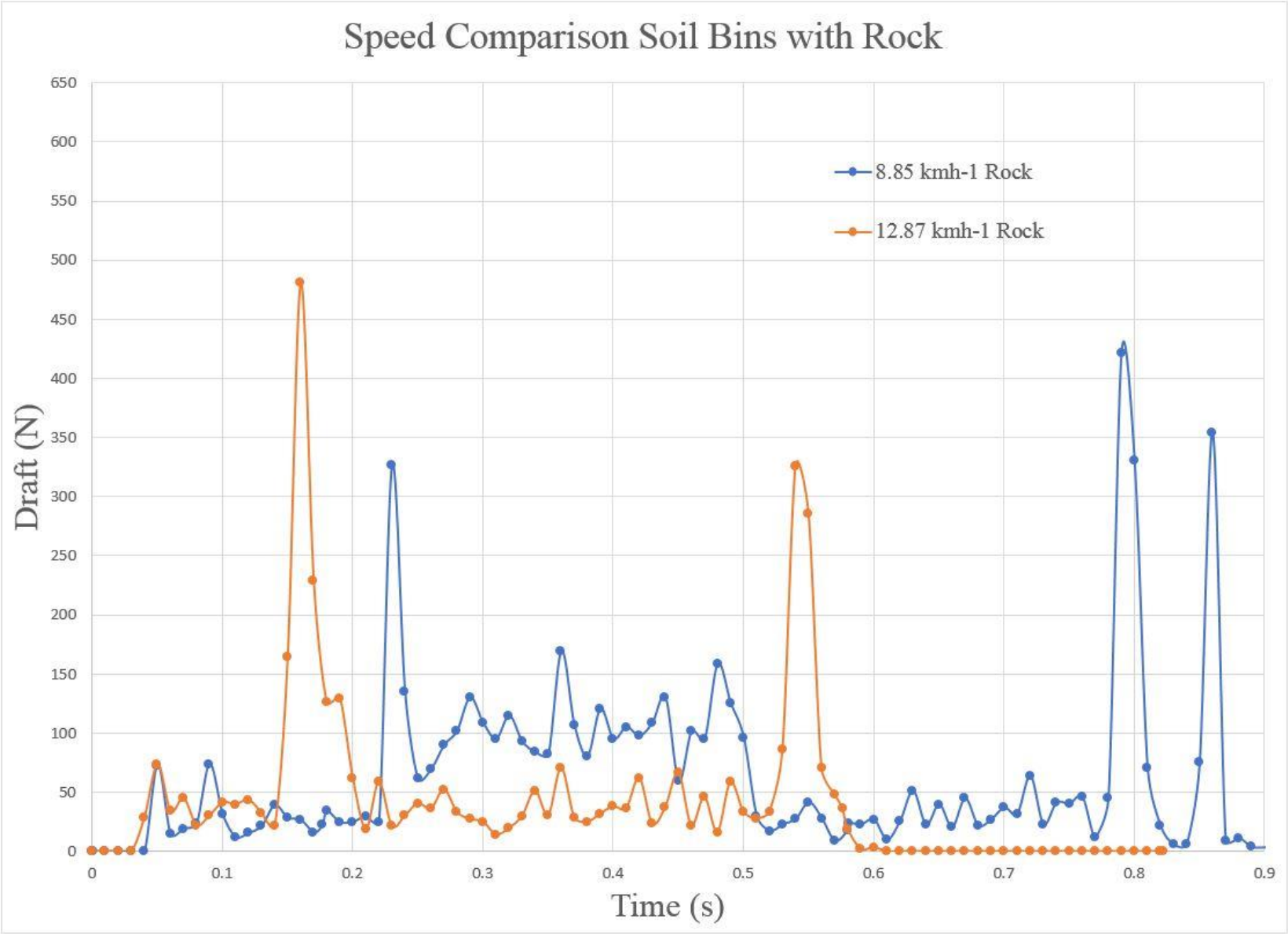

Figure G. 3. Speed Comparison Soil Bins with Rock

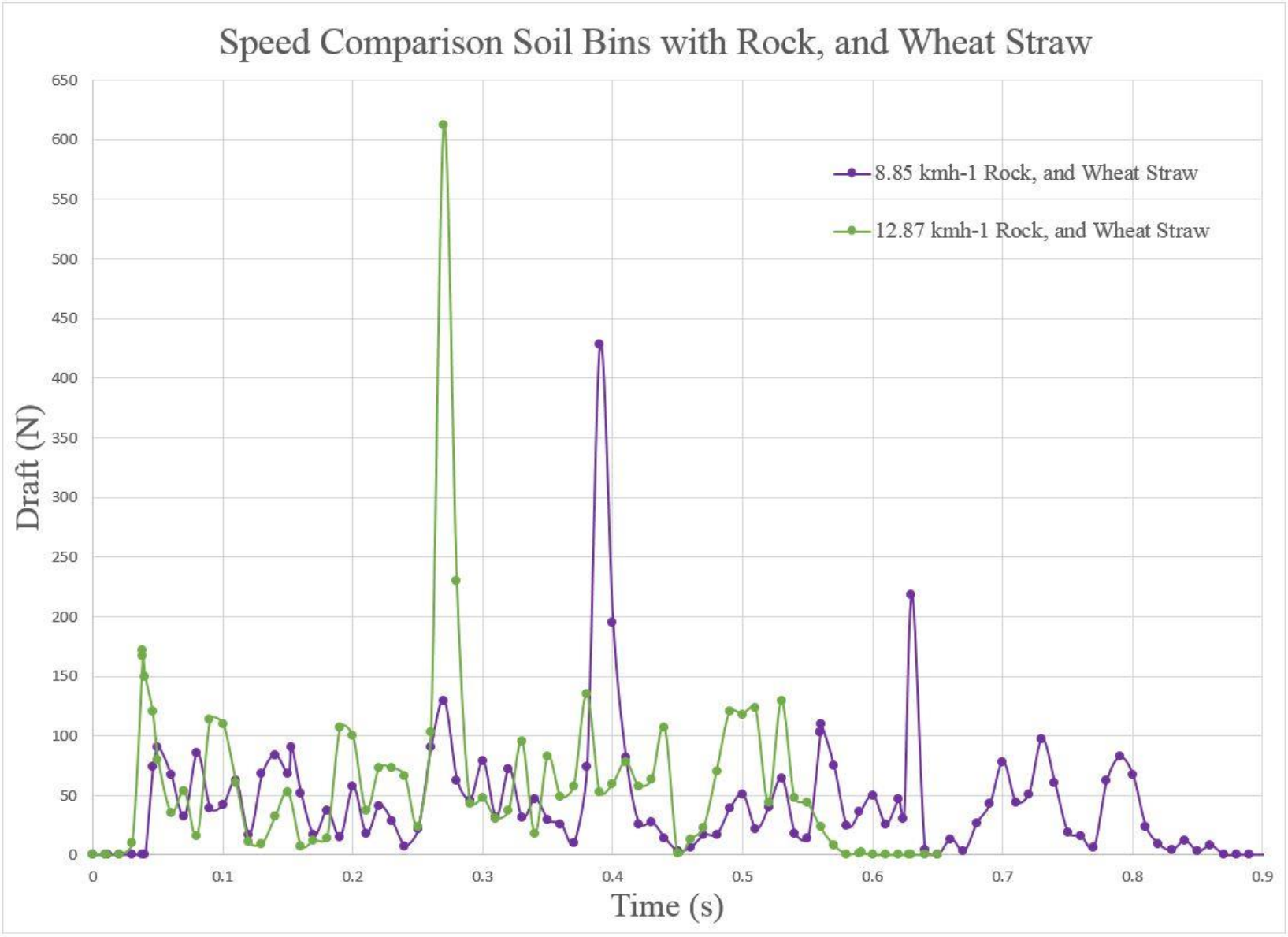

Figure G. 4. Speed Comparison Soil Bins with Rock, and Wheat Straw

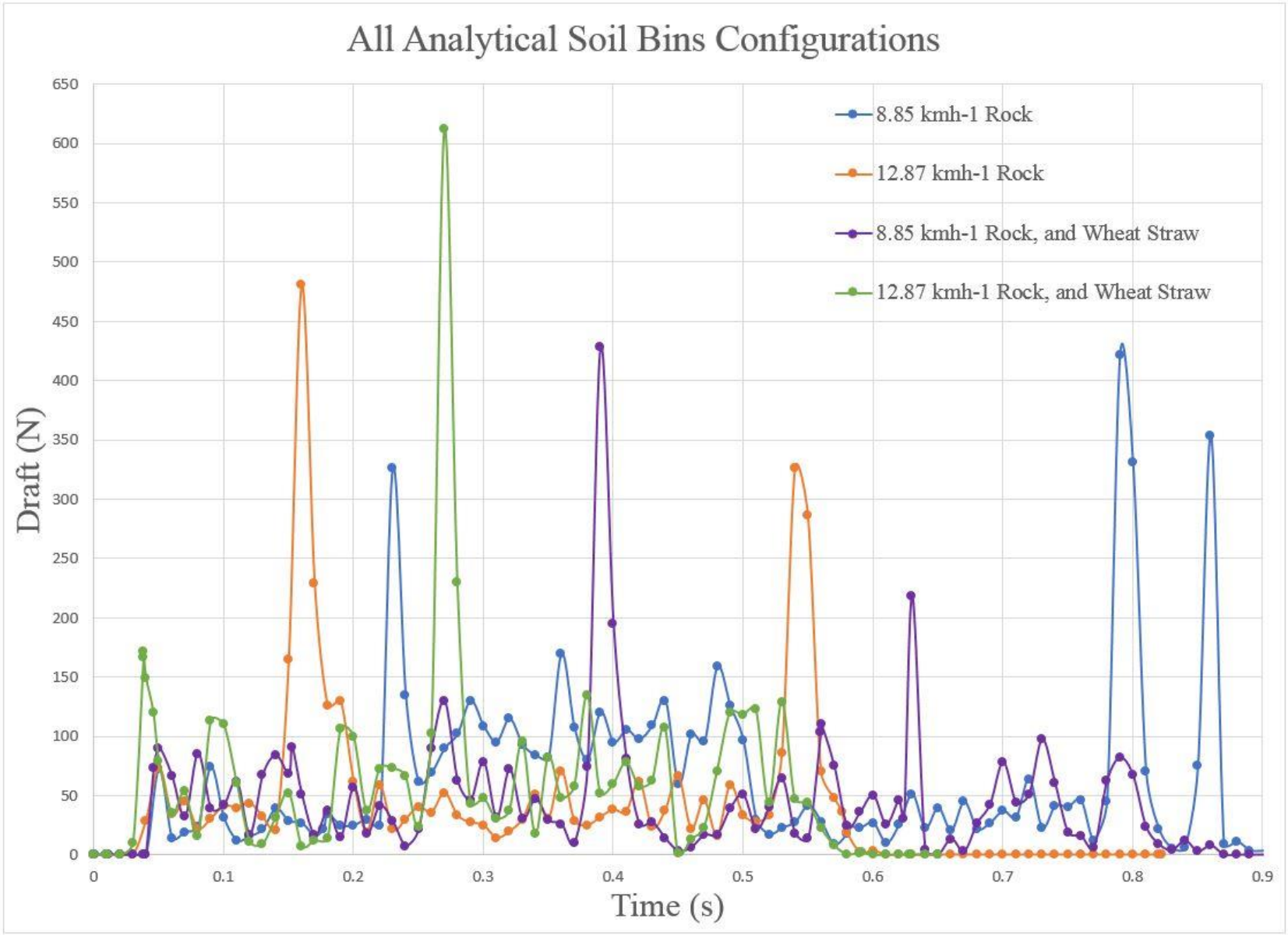

Figure G. 5. All Analytical Soil Bins Configurations

APPENDIX H

Simulate Seed to Fertilizer Placement from the Second-generation Soil Bin

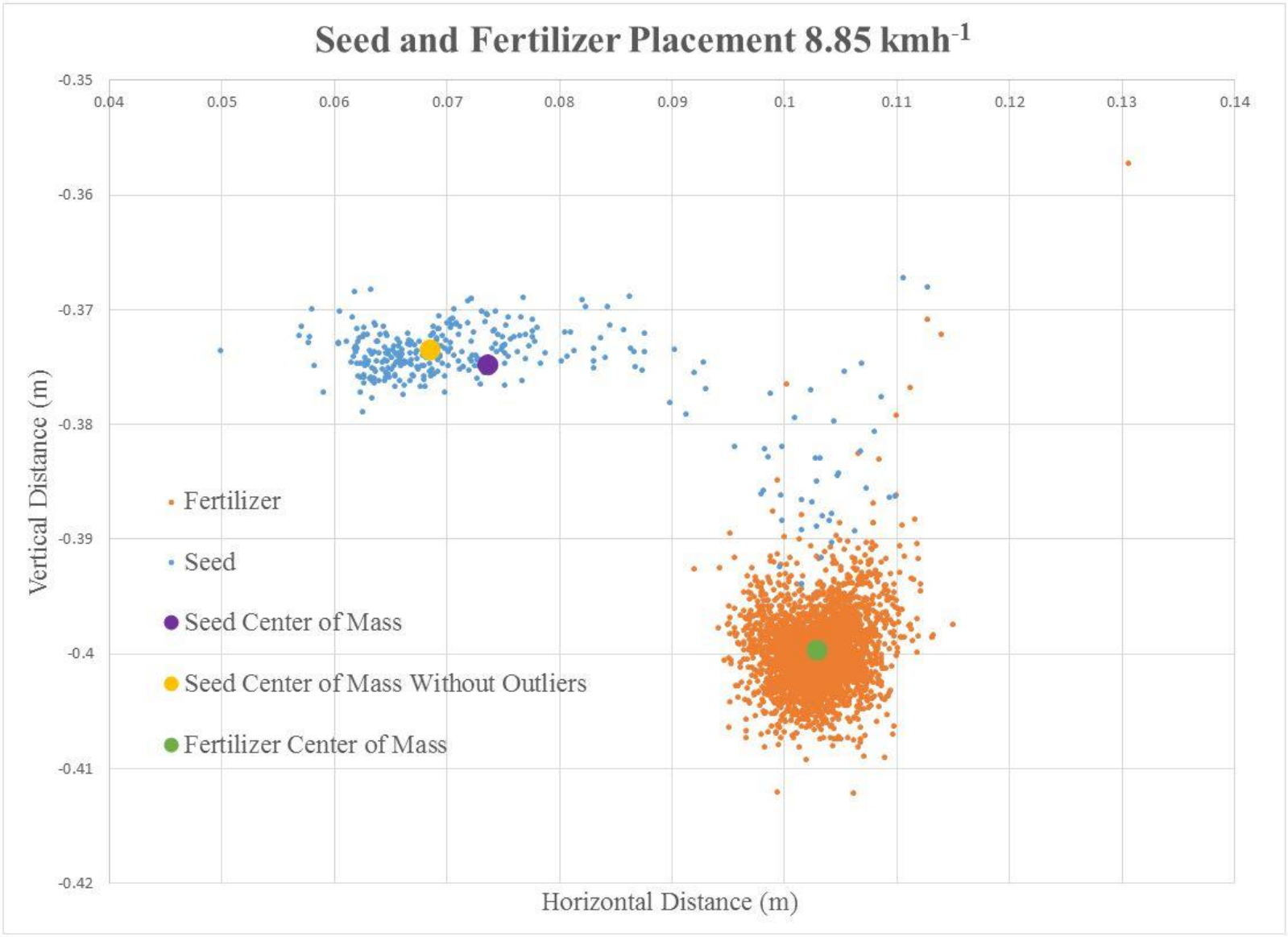

Figure H. 1. Seed and Fertilizer placement 8.85 kmh^{-1}

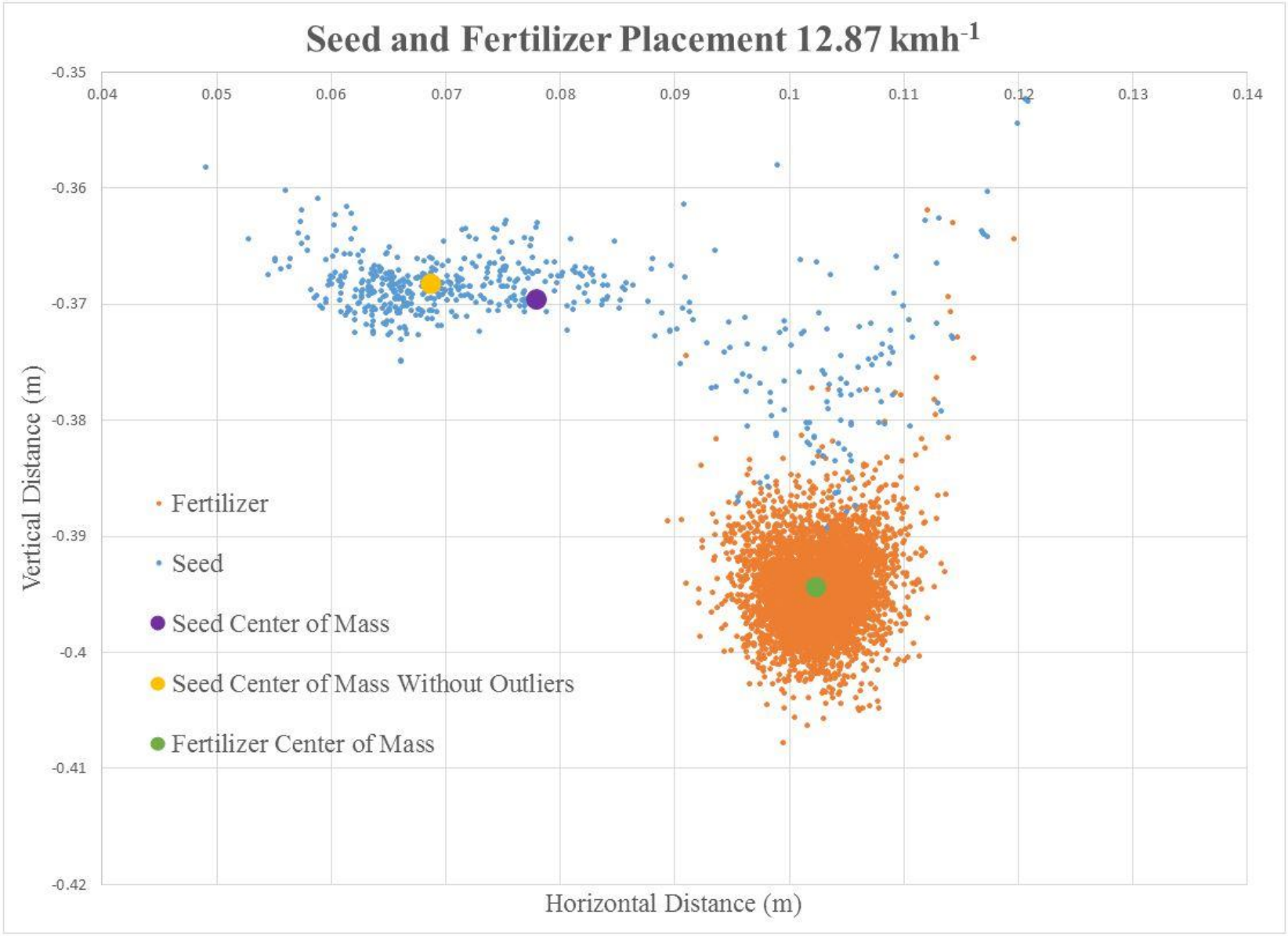

Figure H. 2. Seed and Fertilizer placement 8.85 kmh^{-1}

APPENDIX I

Simulated Wear Pattern

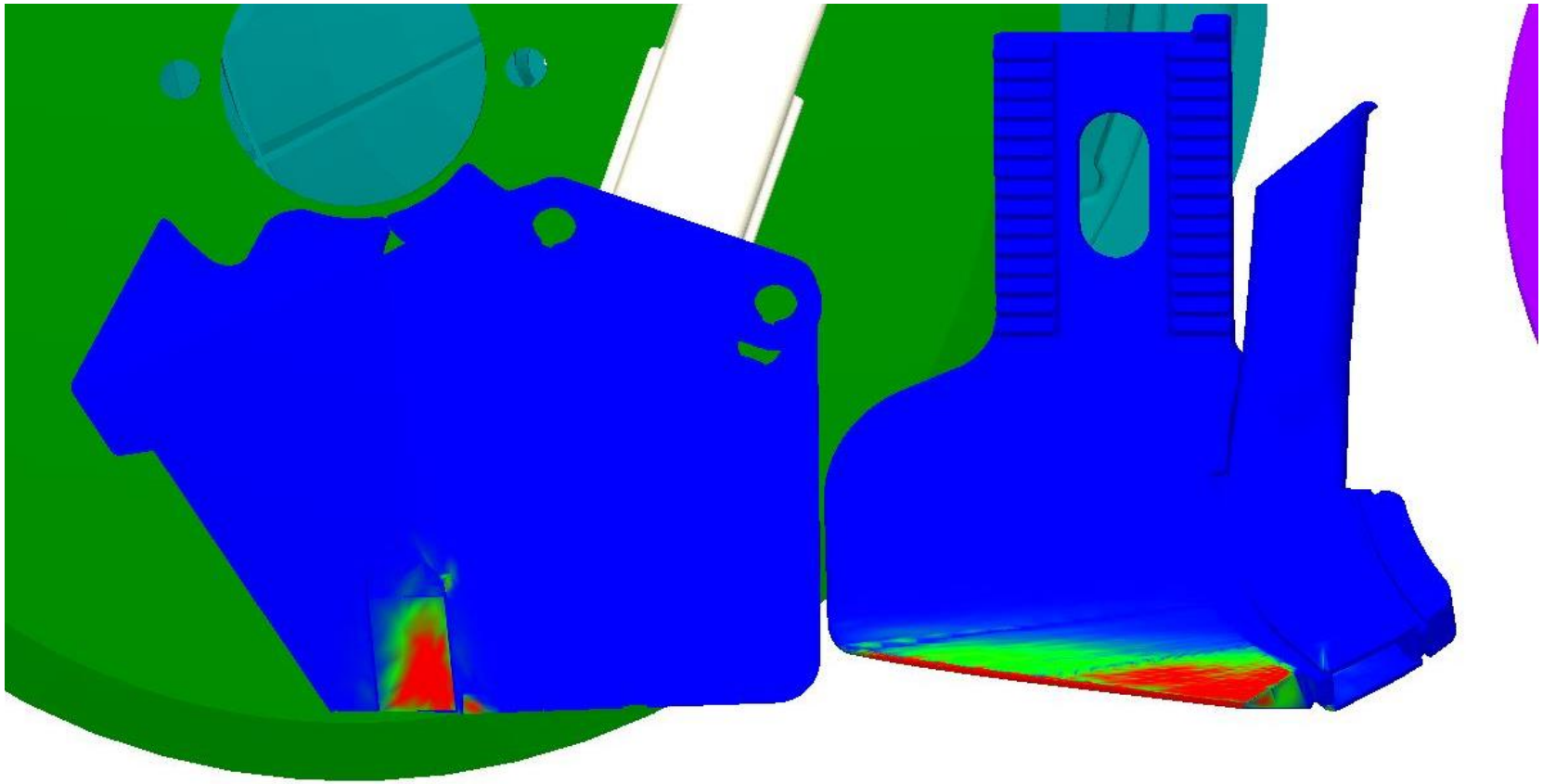

Figure I. 1. 8.85 kmh^{-1} Scraper and Knife Side View

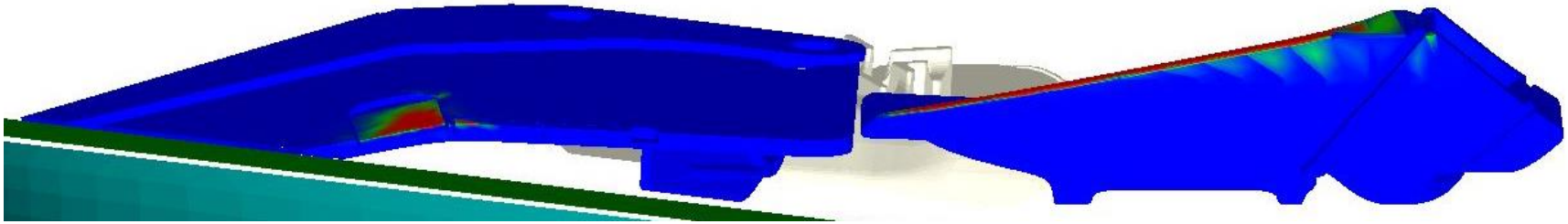

Figure I. 2. 8.85 kmh^{-1} Scraper and Knife Bottom View

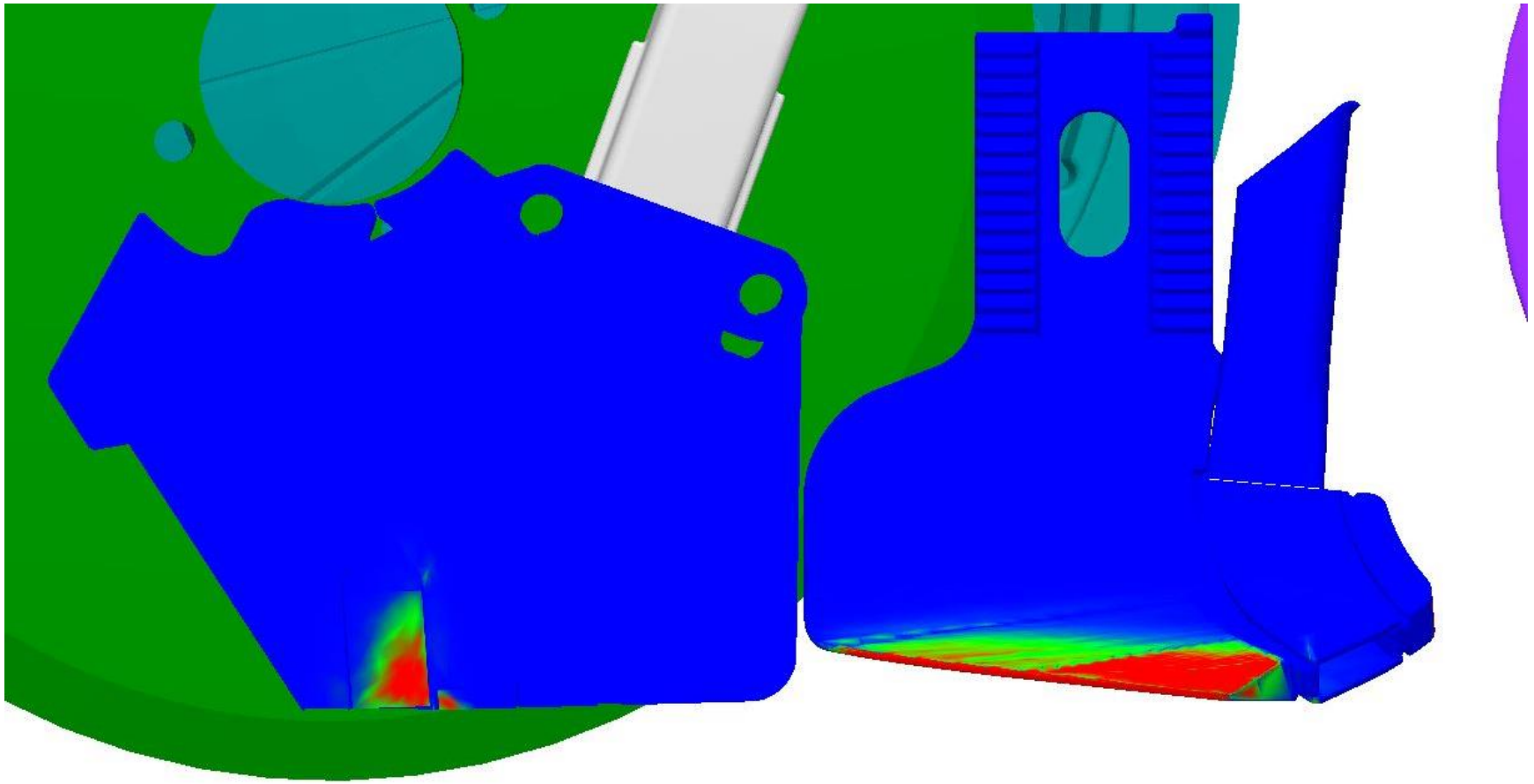

Figure I. 3. 12.87 kmh^{-1} Scraper and Knife Side View

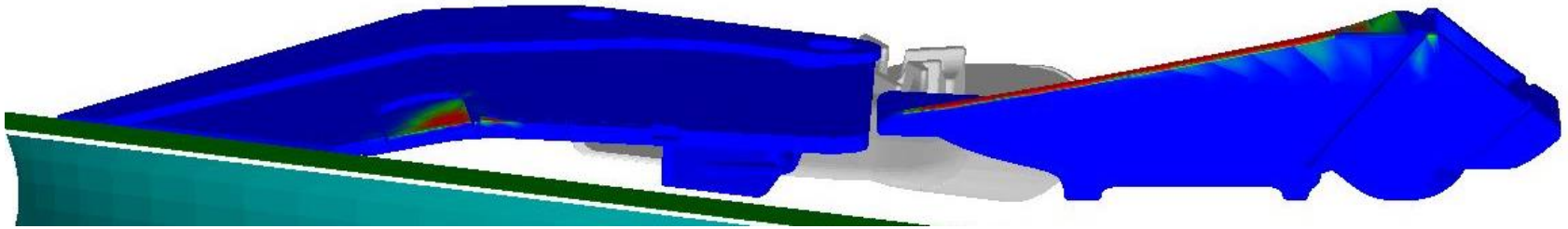

Figure I. 4. 12.87 kmh^{-1} Scraper and Knife Bottom View

APPENDIX J

Simulated Knife Compressive Forces

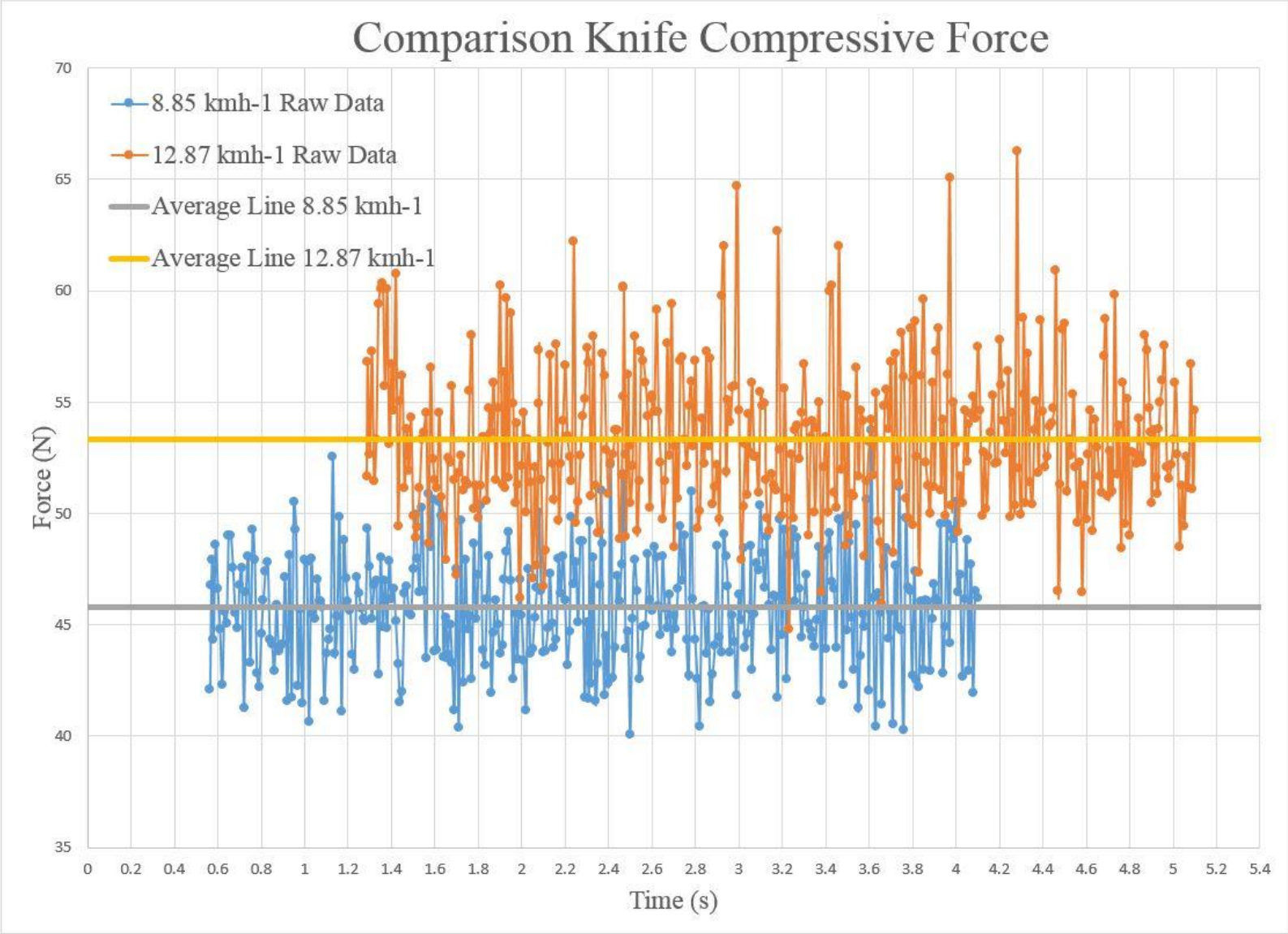

Figure J. 1. Comparison Knife Compressive Force